

GAS HYDRATE TUTORIAL

E. Dendy Sloan, Jr.
Center for Hydrate Research
Colorado School of Mines
Golden, Colorado 80401 USA

Keywords: natural gas hydrates, crystal structures, properties

ABSTRACT

The tutorial provides an overview of time-independent physical/chemical properties as related to crystal structures. Page limitations proscribe only a description of hydrate properties; applications are detailed in other papers in this gas hydrate symposium. The following seven points are illustrated in this tutorial:

1. Gas hydrates are crystalline compounds which form when small (<0.9nm) molecules contact water at temperatures above and below the ice point, with elevated pressures.
2. Properties of sI and sII hydrate crystals are well-defined; measurements have begun on sH.
3. Each volume of hydrate contains as much as 180 volumes (STP) of methane.
4. Physical and chemical properties of hydrates are approximated by three heuristics:
 - Mechanical properties approximate those of ice,
 - Phase equilibrium is set by the size ratio of guest molecules within host cages, and
 - Thermal properties are set by the hydrogen-bonded crystals within a range of guest sizes.
5. Three-phase (L_w -H-V) equilibrium pressure depends exponentially on temperature.
6. There is a need to characterize the hydrate phase directly (via diffraction, NMR, Raman, etc.).
7. No acceptable model exists for hydrate formation kinetics.

The reader may wish to investigate these details further, via references contained in several monographs, (Sloan, 1990; Sloan et al., 1994, Monfort, 1996).

INTRODUCTION

Gas clathrates (commonly called hydrates) are crystalline compounds which occur when water forms a cage-like structure around smaller guest molecules. While they are more commonly called hydrates, a careful distinction should be made between these non-stoichiometric clathrate hydrates of gas and other stoichiometric hydrate compounds which occur for example, when water combines with various salts.

Gas hydrates of current interest are composed of water and the following eight molecules: methane, ethane, propane, isobutane, normal butane, nitrogen, carbon dioxide, and hydrogen sulfide. Yet other apolar components between the sizes of argon (0.35 nm) and ethylcyclohexane (0.9nm) can form hydrates. Hydrate formation is a possibility where water exists in the vicinity of such molecules at temperatures above and below 273 K.

Hydrate discovery is credited in 1810 to Sir Humphrey Davy. Due to their crystalline, non-flowing nature, hydrates became of interest to the hydrocarbon industry in 1934 (Hammerschmidt, 1934), the time of their first observance blocking pipelines. Hydrates act to concentrate hydrocarbons: 1 cubic meter of hydrates may contain as much as 180 SCM of gas. Makogon, (1965) indicated that large natural reserves of hydrocarbons exist in hydrated form, both in deep oceans and in the permafrost. Evaluation of these reserves is highly uncertain, yet even the most conservative estimates concur that there is twice as much energy in hydrated form as in all other hydrocarbon sources combined. While one commercial example exists of gas recovery from hydrates, the problems of *in situ* hydrate dissemination in deepwater/permafrost environments will prevent their cost-effective recovery until the next millennium.

WHAT ARE HYDRATES: HOW DO STRUCTURE RELATE TO PROPERTIES?

Hydrates normally form in one of three repeating crystal structures shown in Figure 1. Structure I (sI), a body-centered cubic structure forms with small natural gas molecules found *in situ* in deep oceans. Structure II (sII), a diamond lattice within a cubic framework, forms when natural gases or oils contain molecules larger than ethane but smaller than pentane. sII represents hydrates which commonly occur in hydrocarbon production and processing conditions, as well as in many cases of gas seeps from faults in ocean environments.

The newest hydrate structure H, named for the hexagonal framework, was discovered and shown by Ripmeester et al. (1987, 1991) to have cavities large enough to contain molecules the size of common components of naphtha and gasoline. Initial physical properties, phase equilibrium data, and models have been advanced (Mehta and Sloan, 1993, 1994a,b, 1996a,b,c; Udachin et al. 1996), and Sassen et al. (1994) have found one instance of *in situ* sH in the Gulf of Mexico. Since information on structure H is in the fledgling stages, most of this tutorial concerns sI and sII.

HYDRATE CRYSTAL STRUCTURES.

Table 1 provides a hydrate structure summary for the three hydrate unit crystals (sI, sII, and sH) shown in Figure 1. The crystals structures are given with reference to the water skeleton, composed of a basic "building block" cavity which has twelve faces with five sides per face, given the abbreviation 5^{12} . By linking the vertices of 5^{12} cavities one obtains sI; linking the faces of 5^{12} cavities results in sII; in sH a layer of linked 5^{12} cavities provide connections.

Interstices between the 5^{12} cavities are larger cavities which contain twelve pentagonal faces and either two, four, or eight hexagonal faces: (denoted as $5^{12}6^2$ in sI, $5^{12}6^4$ in sII, or $5^{12}6^8$ in sH). In addition sH has a cavity with square, pentagonal, and hexagonal faces ($4^25^66^3$). Figure 1 depicts the five cavities of sI, sII, and sH. In Figure 1 a oxygen atom is located at the vertex of each angle in the cavities; the lines represent hydrogen bonds with which one chemically-bonded hydrogen connects to an oxygen on a neighbor water molecule.

Inside each cavity resides a maximum of one of the small, guest molecules, typified by the eight guests associated with 46 water molecules in sI ($2[5^{12}] \bullet 6[5^{12}6^2] \bullet 46\text{H}_2\text{O}$), indicating two guests in the 5^{12} and 6 guests in the $5^{12}6^2$ cavities of sI. Similar formulas for sII and sH are $(16[5^{12}] \bullet 8[5^{12}6^4] \bullet 136\text{H}_2\text{O})$ and $(3[5^{12}] \bullet 2[4^25^66^3] \bullet 1[5^{12}6^8] \bullet 34\text{H}_2\text{O})$ respectively.

Structure I a body-centered cubic structure forms with natural gases containing molecules smaller than propane; consequently sI hydrates are found *in situ* in deep oceans with biogenic gases containing mostly methane, carbon dioxide, and hydrogen sulfide. Structure II a diamond lattice within a cubic framework, forms when natural gases or oils contain molecules larger than ethane but smaller than pentane; sII represents hydrates from thermogenic gases. Finally structure H hydrates must have a small occupant (like methane, nitrogen, or carbon dioxide) for the 5^{12} and $4^25^66^3$ cages but the molecules in the $5^{12}6^8$ cage can be as large as 0.9nm (e.g. ethylcyclohexane).

TIME-INDEPENDENT PROPERTIES FROM HYDRATE CRYSTAL STRUCTURES.

Mechanical Properties of Hydrates. As may be calculated via Table 1, if all the cages of each structure are filled, all three hydrates have the amazing property of being approximately 85% (mol) water and 15% gas. The fact that the water content is so high suggests that the mechanical properties of the three hydrate structures should be similar to those of ice. This conclusion is true to a first approximation as shown in Table 2, with the exception of thermal conductivity and thermal expansivity (Davidson, 1983, Tse, 1994). Many mechanical properties of sH have not been measured to date.

Guest: Cavity Size Ratio: a Basis for Property Understanding. The hydrate cavity occupied is a function of the size ratio of the guest molecule within the cavity. To a first approximation, the concept of "a ball fitting within a ball" is a key to understanding many hydrate properties. Figure 2 (corrected from von Stackelberg, 1949) may be used to illustrate five points regarding the guest:cavity size ratio for hydrates formed of a single guest component in sI or sII.

1. The sizes of stabilizing guest molecules range between 0.35 and 0.75 nm. Below 0.35nm molecules will not stabilize sI and above 0.75 molecules will not stabilize sII.
2. Some molecules are too large to fit the smaller cavities of each structure (e.g. C_2H_6 fits in the $5^{12}6^2$ of sI; or $i\text{-C}_4\text{H}_{10}$ fits the $5^{12}6^4$ of sII).
3. Other molecules such as CH_4 and N_2 are small enough to enter both cavities (labeled as either $5^{12}+5^{12}6^2$ in sI or $5^{12}+5^{12}6^4$ in sII) when hydrate is formed of those single components.
4. The largest molecules of a gas mixture usually determines the structure formed. For example, because propane and *i*-butane are present in many thermogenic natural gases, they will cause sII to form. In such cases, methane will distribute in both cavities of sII and ethane will enter only the $5^{12}6^4$ cavity of sII.
5. Molecules which are very close to the hatched lines separating the cavity sizes appear to exhibit the most non-stoichiometry, due to their inability to fit securely within the cavity.

Table 3 shows the size ratio of several common gas molecules within each of the four cavities of sI and sII. Note that a size ratio (guest molecule: cavity) of approximately 0.9 is necessary for stability of a simple hydrate, given by the superscript "n". When the size ratio exceeds unity, the molecule will not fit within the cavity and the structure will not form. When the ratio is significantly less than 0.9 the molecule cannot lend significant stability to the cavity.

Consider ethane, which forms in the $5^{12}6^2$ cavity in sI, because ethane is too large for the small 5^{12} cavities in either structure and too small to give much stability to the large $5^{12}6^4$ cavity in sII. Similarly propane is too large to fit any cavity except the $5^{12}6^4$ cavity in sII, so that gases of pure propane form sII hydrates from free water. On the other hand, methane's size is sufficient to lend stability to the 5^{12} cavity in either sI or sII, with a preference for sI, because CH_4 lends slightly higher stability to the $5^{12}6^2$ cavity in sI than the $5^{12}6^4$ cavity in sII.

Phase Equilibrium Properties. In Figure 3 pressure is plotted against temperature with gas composition as a parameter, for methane+propane mixtures. Consider a gas of any given composition (marked 0 through 100% propane) on a line in Figure 3. At conditions to the right of the line, a gas of that composition will exist in equilibrium with liquid water. As the temperature is reduced (or as the pressure is increased) hydrates form from gas and liquid water at the line, so three phases (liquid water + hydrates + gas) will be in equilibrium. With further reduction of temperature (or increase in pressure) the fluid phase which is not in excess (gas in ocean environments) will be exhausted, so that to the left of the line the hydrate will exist with the excess phase (water).

All of the conditions given in Figure 3 are for temperatures above 273K and pressures along the lines vary exponentially with temperature. Put explicitly, hydrate stability at the three-phase (L-H-V) condition is always much more sensitive to temperature than to pressure. Figure 3 also illustrates the dramatic effect of gas composition on hydrate stability; as any amount of propane is added to methane the structure changes (sI \rightarrow sII) to a hydrate with much wider stability conditions. Note that a 50% decrease in pressure is needed to form sII hydrates, when as little as 1% propane is in the gas phase.

Any discussion of hydrate dissociation would be incomplete without indicating that hydrates provide the most industrially useful instance of statistical thermodynamics prediction of phase equilibria. The van der Waals and Platteuw (1959) model was formulated after the determination of the crystal structures shown in Figure 1. With the model, one may predict the three-phase pressure or temperature of hydrate formation, by knowing the gas composition. For further discussion of these details the reader is referred to Sloan (1990, Chapter 5).

Heat of Dissociation. The heat of dissociation (ΔH_d) is defined as the enthalpy change to dissociate the hydrate phase to a vapor and aqueous liquid, with values given at temperatures just above the ice point. For sI and sII, Sloan and Fleyfel (1992) show that to a fair engineering approximation ($\pm 10\%$) ΔH_d is a function mostly of crystal hydrogen bonds, but also of the cavity occupied within a wide range of components sizes. Enthalpies of dissociation may be determined via the univariant slopes of phase equilibrium lines ($\ln P$ vs. $1/T$) in the previous paragraphs, using the Clausius-Clapeyron relation [$\Delta H_d = -zR d(\ln P)/d(1/T)$].

As one illustration, simple hydrates of C_3H_8 or $i\text{-C}_4\text{H}_{10}$ have similar ΔH_d of 129 and 133 kJ/mol (Handa, 1986) because the both occupy the $5^{12}6^4$ cavity, although their size:cavity ratios are somewhat different (0.943 and 0.976). As a second illustration, Figure 3 shows that mixtures of $\text{CH}_4 + \text{C}_3\text{H}_8$ have a value of $\Delta H_d = 79$ kJ/mol over a wide range of composition. In such mixtures, C_3H_8 occupies most of the $5^{12}6^4$ cavities while CH_4 occupies a small number of $5^{12}6^4$ and many 5^{12} . In fact, most natural gases (which form sII) have similar values of ΔH_d . Figure 4 shows similar line slopes (and thus ΔH_d values) for binary mixtures of methane when the large guest is changed from C_3H_8 , to $i\text{-C}_4\text{H}_{10}$, to $n\text{-C}_4\text{H}_{10}$. Similarly, over a wide range of composition for mixtures of methane and ethane, ΔH_d values are similar (74 kJ/mol) for components entering both cavities of sI. Identical arguments may be used to explain similar ΔH_d values of $79.5 \pm 7\%$ kJ/mol (Mehta and Sloan, 1996c) for sH mixtures of methane with seventeen larger components.

CHALLENGES FOR FUTURE RESEARCH

A review of the literature suggests that there are two imminent challenges for future research. First we must characterize the hydrate phase both in the laboratory and in the field. Secondly we must characterize the kinetics hydrates formation and dissociation.

Measurements of the Hydrate Phase. For the hydrate phase there are two measurement techniques - diffraction and spectroscopic. Neutron diffraction (typified by Tse, 1994) can detect water atoms and guest molecules, while X-ray diffraction detects oxygen positions. Recently using X-ray diffraction Stern et al. (1996) have been remarkably successful at converting 97% of ice to water, by raising ice grain temperatures above the solidus while under high pressure.

Two types of spectroscopy are useful with hydrates: (1) nuclear magnetic resonance (NMR) with cross polarization (CP) and magic-angle spinning (MAS), and (2) Raman spectroscopy. Virtually all NMR hydrate work to date comes from the Canadian National Research Council. The first comprehensive review of NMR studies of clathrates was written by Davidson and Ripmeester (1984), and a thorough update has been written by Ripmeester and Ratcliffe (1991). Of NMR hydrate compounds Xe has obtained prominence due to its large (ca. 100 ppm) chemical shift.

Recently Sum et al. (1996) have shown that Raman spectroscopy can be used to determine the fraction of filled cages in hydrates, and the fraction of various components in the cages. Since Raman appears to be both more versatile and less resource intensive, it holds substantial

Measurements of Hydrate Kinetics. Most hydrate kinetics research has come from the laboratory of Bishnoi, notably the work of Englezos et al., (1987a,b). They modeled kinetics of methane and ethane hydrate after nucleation, for periods up to 100 minutes. A subsequent model was made by Skovborg and Rasmussen (1994); these workers assumed that the mass transfer of gas to the liquid phase was the rate-controlling step, so that hydrate kinetics and diffusion to the hydrate phase could be ignored.

However, even with these excellent beginnings, quantification of hydrate kinetics still pose substantial challenges to hydrate researchers. For example, no model of hydrate nucleation can acceptably fit all the data of a single experimenter; no universal nucleation model is available. As another example, all models of hydrate growth kinetics are apparatus-dependent. While the growth model may be a satisfactory fit for the apparatus in which the data were generated, the model will not fit data generated in other apparatuses. Determining time-dependent hydrate behavior is one of the most significant challenges for research.

CONCLUSIONS

This tutorial reviews hydrate crystal structures, and shows how properties such as phase equilibria and heat of dissociation relate to molecular structure. While many time-independent properties of sI and sII hydrates are determined, those for newer structures (e.g. sH) are just beginning to be explored. The time-dependent characteristics of all three hydrate structures are largely unspecified and kinetic models to date appear to be apparatus-dependent. Characterization of the hydrate phase constitutes a current challenge.

LITERATURE CITED

- Davidson, D.W., in Natural Gas Hydrates: Properties, Occurrence and Recovery, J.L. Cox, ed., pg 1. Butterworths, Boston (1983)
- Davidson, D.W., Ripmeester, J.A., in Inclusion Compounds, Vol 3 Chapter 3, J.L. Atwood, J.E.D. Davies, and D.D. MacNichol, eds, Academic Press (1984)
- Englezos, P., Kalogerakis, N., Dholabhai, P., Bishnoi, P., Chem. Eng. Sci., **42**(11), 2647 (1987a)
- Englezos, P., Kalogerakis, N., Dholabhai, P., Bishnoi, P., Chem. Eng. Sci., **42**(11), 2659 (1987b)
- Hammerschmidt, E.G., Ind. Eng. Chem. **26** 851 (1934)
- Handa, Y.P., J. Chem. Thermo., **18**, 891 (1986)
- Makogon, Y.F., Gazov. Promst. **14** (1965)
- Mehta, A.P., A Thermodynamic Investigation of Structure H Clathrate Hydrates, Ph.D. Thesis, Colorado School of Mines, Golden, CO (1996)
- Mehta, A.P., Sloan, E.D., J. Chem. Eng. Data, **38**, 580 (1993)
- Mehta, A.P., Sloan, E.D., J. Chem. Eng. Data, **39**, 887 (1994a)
- Mehta, A.P., Sloan, E.D., AIChE Journal, **40**, 312 (1994b)
- Mehta, A.P., Sloan, E.D., AIChE Journal, **42**, 2036 (1996a)
- Mehta, A.P., Sloan, E.D., in Proc. 2nd Internl. Conf. on Natural Gas Hydrates, pl. Monfort, J.P., ed., Toulouse, 2-6 June (1996b)
- Mehta, A.P., Sloan, E.D., "Structure H Hydrates: Implications for the Petroleum Industry," Proc. 1996 Annual Tech Conf., SPE 36742, 607 Denver, CO., 6-9 October (1996c)
- Monfort, J.P., ed, Proc. 2nd Internl. Conf. on Natural Gas Hydrates, F. Foucaud, Secretariat, 18 Chemin de la Loge, 31078 Toulouse Cedex, France 2-6 June (1996)

- Ripmeester, J.A., Tse, J.A., Ratcliffe, C.I., Powell, B.M., Nature, **325**, 135 (1987)
- Ripmeester, J.A., Ratcliffe, C.I., Solid State NMR Studies of Inclusion Compounds, National Research Council of Canada, Report C1181-89S, August 17 (1989)
- Ripmeester, J.A., "The Role of Heavier Hydrocarbons in Hydrate Formation," presented at 1991 AIChE Spring Meeting, Houston, April 10 (1991)
- Ripmeester, J.A., Ratcliffe, C.I., Klug, D.D., Tse, J.A., , in (First) International Conference on Natural Gas Hydrates, Annals of New York Academy of Sciences, Sloan, E.D., Happel, J., Hnatow, M.A., eds., **715**, p161, (1994)
- Sassen, R., MacDonald, I.R., Org. Geochem. **22(6)** 1029 (1994)
- Skovborg, P., Rasmussen, P., Chem. Eng. Sci., **49**, 1131 (1994)
- Sloan, E.D., Clathrate Hydrates of Natural Gases, Marcel Dekker, Inc., New York (1990)
- Sloan, E.D., Fleyfel, F., Fluid Phase Equil., **76**, 123 (1992)
- Sloan, E.D., Happel, J., Hnatow, M.A., eds, (First) International Conference on Natural Gas Hydrates, Annals of New York Academy of Sciences,., **715**, (1994)
- Stern, L.A., Kirby, S.H., Durham, W.B., Science, **273**, 1843 (1996)
- Sum, A., Burruss, R., Sloan, E.D., in Proc. 2nd Intl. Conf. on Natural Gas Hydrates, p51. Monfort, J.P., ed., Toulouse, 2-6 June (1996b)
- Tse, J.S., in (First) International Conference on Natural Gas Hydrates, Annals of New York Academy of Sciences, Sloan, E.D., Happel, J., Hnatow, M.A., eds., **715**, p187, (1994)
- van der Waals, J.H., and Platteuw, J.C., "Clathrate Solutions," Adv. Chem. Phys., vol 2,1,(1959)
- von Stackelberg, M., Naturwiss **36** 327, 359 (1949)

Table 1 Geometry of Cages in Three Hydrate Crystal Structures

Hydrate Crystal Structure	I		II		H		
	Small	Large	Small	Large	Small	Medium	Large
Cavity	5 ¹²	5 ¹² 6 ²	5 ¹²	5 ¹² 6 ⁴	5 ¹²	4 ³ 5 ⁶ 6 ³	5 ¹² 6 ⁸
Description							
Number of Cavities/Unit Cell	2	6	16	8	3	2	1
Average Cavity Radius, Å	3.95	4.33	3.91	4.73	3.91 ³	4.06 ³	5.71 ³
Variation in Radius ¹ , %	3.4	14.4	5.5	1.73	Not Available		
Coordination Number ²	20	24	20	28	20	20	36
Number of Waters/Unit Cell	46		136		34		

1. Variation in distance of oxygen atoms from center of cage.

2. Number of oxygens at the periphery of each cavity.

3. Estimates of structure H cavities from geometric models

Table 2 Comparison of Properties of Ice and sI and sII Hydrates¹

Property	Ice	Structure I	Structure II
<u>Spectroscopic</u>			
<u>Crystallographic Unit Cell</u>			
Space Group	P6 ₃ /mmc	Pm3n	Fd3m
No. H ₂ O molecules	4	46	136
Lattice Parameters at 273K	a =4.52 c =7.36	12.0	17.3
Dielectric Constant at 273 K	94	~58	58
Far infrared spectrum	Peak at 229 cm ⁻¹ .	Peak at 229 cm ⁻¹ with others	
H ₂ O Diffusion Correl Time, (µsec)	220	240	25
H ₂ O Diffusion Activ. Energy(kJ/m)	58.1	50	50
<u>Mechanical Property</u>			
Isothermal Young's modulus at 268 K (10 ⁹ Pa)	9.5	8.4 ^{est}	8.2 ^{est}
Poisson's Ratio	0.33	-0.33	-0.33
Bulk Modulus (272 K)	8.8	5.6	NA
Shear Modulus (272 K)	3.9	2.4	NA
VelocityRatio(Comp/Shear):272K	1.88	1.95	NA
<u>Thermodynamic Property</u>			
Linear. Therm. Exprn: 200K (K ⁻¹)	56x10 ⁻⁶	77x10 ⁻⁶	52x10 ⁻⁶
AdiabBulkCompress:273K(10 ⁻¹¹ Pa)	12	14 ^{est}	14 ^{est}
Speed Long Sound:273K(km/sec)	3.8	3.3	3.6
<u>Transport</u>			
Thermal Conductivity:263K(W/m-K)	2.23	0.49±.02	0.51±.02

1. Modified from Davidson (1983) and from Ripmeester et al. (1994)

Table 3 Ratios of Molecular Diameters to Cavity Diameters¹ for Some Molecules Including Natural Gas Hydrate Formers

Molecule	Cavity Type=> Guest Dmtr (Å)	(Molecular Diameter) / (Cavity Diameter)			
		Structure I		Structure II	
		5 ¹²	5 ¹² 6 ²	5 ¹²	5 ¹² 6 ⁴
N ₂	4.1	0.804	0.700	0.817 [†]	0.616 [†]
CH ₄	4.36	0.855 [†]	0.744 [†]	0.868	0.655
H ₂ S	4.58	0.898 [†]	0.782 [†]	0.912	0.687
CO ₂	5.12	1.00	0.834 [†]	1.02	0.769
C ₂ H ₆	5.5	1.08	0.939 [†]	1.10	0.826
C ₃ H ₈	6.28	1.23	1.07	1.25	0.943 [†]
i-C ₄ H ₁₀	6.5	1.27	1.11	1.29	0.976 [†]
n-C ₄ H ₁₀	7.1	1.39	1.21	1.41	1.07

[†] indicates the cavity occupied by the simple hydrate former

1. cavity radii from Table 2-1 minus 1.4Å water radii

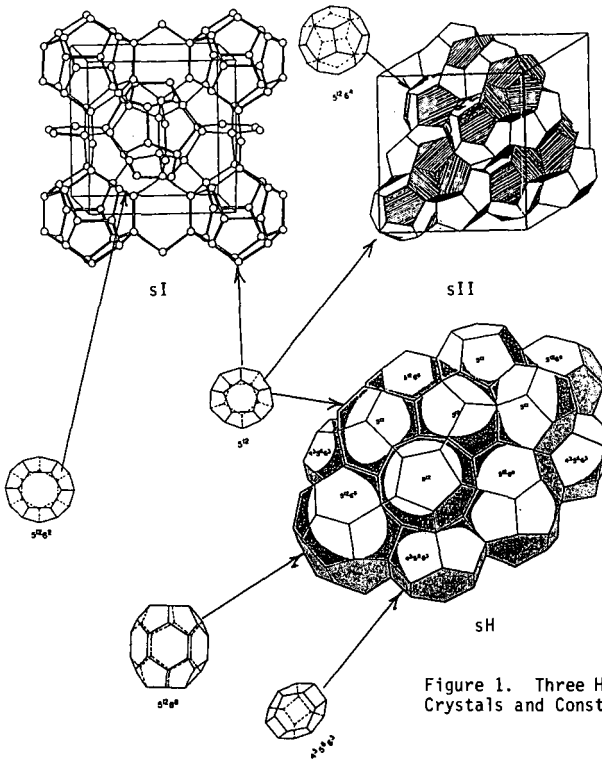


Figure 1. Three Hydrate Unit Crystals and Constituent Cavities

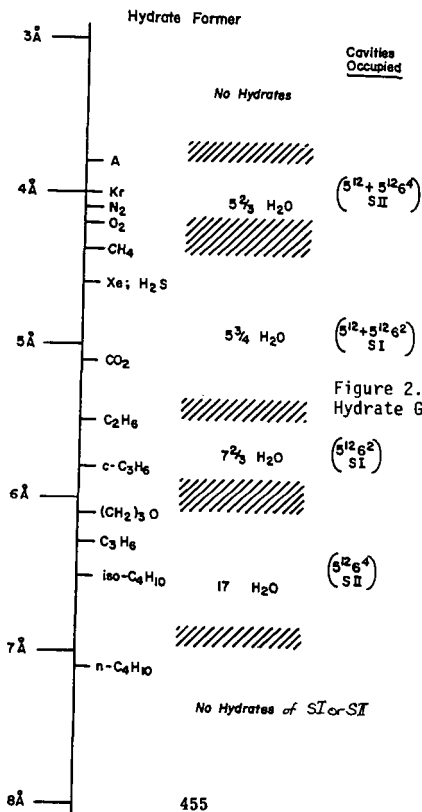


Figure 2. Relative Sizes of Hydrate Guest and Host Cavities

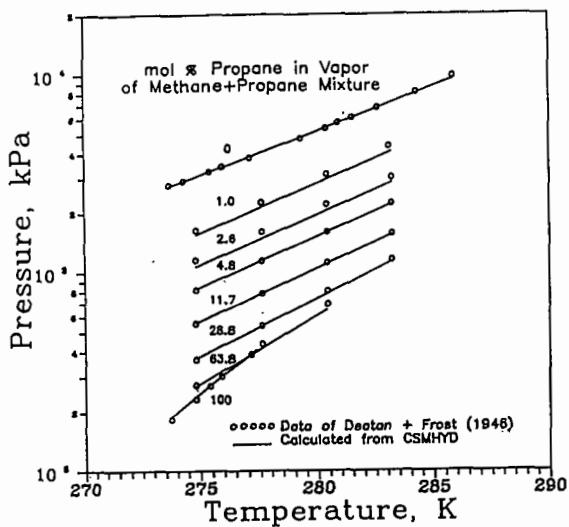
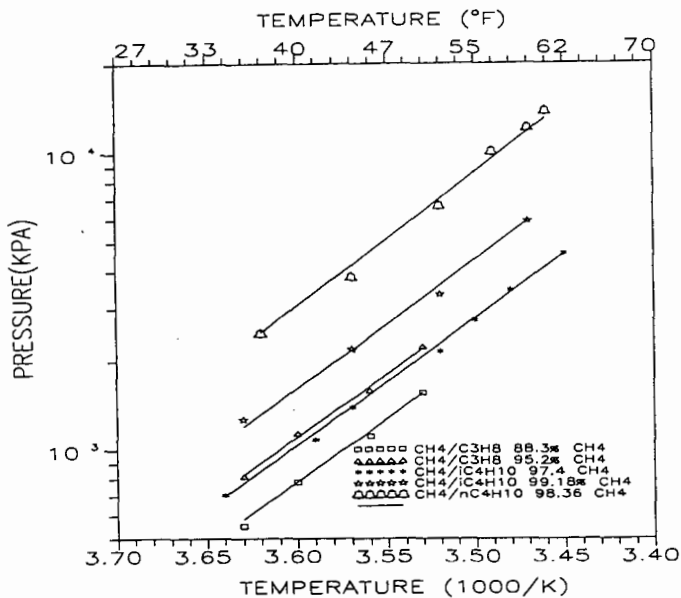


Figure 3. Three-Phase (Lw-H-V) Equilibria of Methane+Propane Mixtures

Figure 4. Three-Phase Equilibria of Methane +(Propane and Two Butanes)



ASSESSMENT OF UNITED STATES GAS HYDRATE RESOURCES

Timothy S. Collett
U.S. Geological Survey, Denver Federal Center
Box 25046, MS-939, Denver, CO 80225

Keywords: gas hydrates, energy resources, natural gas

I. INTRODUCTION

Gas hydrates are crystalline substances composed of water and gas, in which a solid water-lattice accommodates gas molecules in a cage-like structure, or clathrate. Gas hydrates are widespread in permafrost regions and beneath the sea in sediment of outer continental margins. While methane, propane, and other gases can be included in the clathrate structure, methane hydrates appear to be the most common in nature¹. The amount of methane sequestered in gas hydrates is probably enormous, but World estimates of the amounts are speculative and range over three orders-of-magnitude, from about 100,000 to 270,000,000 trillion cubic feet². The estimated amount of gas in hydrate reservoirs of the world greatly exceeds the volume of known conventional gas reserves. The production history of the Russian Messoyakha gas hydrate field demonstrates that gas hydrates are an immediate source of natural gas that can be produced by conventional methods^{3,4}. Gas hydrates also represent a significant drilling and production hazard. Russian, Canadian, and American researchers have described numerous problems associated with gas hydrates, including blowouts and casing failures^{3,5,6}. As exploration and development activity moves into deeper water (>300 m) and high latitude arctic environments, the frequency of gas hydrate induced problems will likely increase.

One of the fundamental problems that links the gas hydrate resource and hazard issues is the need for accurate assessments of the gas volumes within a gas hydrate occurrence. Most of the published gas hydrate resource estimates have by necessity been made by broad extrapolation of only general knowledge of local geologic conditions². The primary objectives of our gas hydrate research efforts in the U.S. Geological Survey are to document the geologic parameters that control the occurrence of gas hydrates and to assess the volume of natural gas stored within the onshore and offshore gas hydrate accumulations of the United States. This paper begins with a discussion of the geologic parameters that affect the stability and formation of gas hydrates, which is followed by a description of the methodology used to assess gas hydrate resources. This paper ends with a cumulative estimate of the *in-place* gas hydrate resources of the United States onshore and offshore regions.

II. GAS HYDRATE TECHNICAL REVIEW

Under appropriate conditions of temperature and pressure (figs. 1A, 1B, and 1C), gas hydrates usually form one of two basic crystal structures known as Structure I and Structure II. Each unit cell of Structure I gas hydrate consists of 46 water molecules that form two small dodecahedral voids and six large tetradecahedral voids. Structure I gas hydrates can only hold small gas molecules such as methane and ethane, with molecular diameters not exceeding 5.2 angstroms. The unit cell of Structure II gas hydrate consists of 16 small dodecahedral and 8 large hexakaidecahedral voids formed by 136 water molecules. Structure II gas hydrates may contain gases with molecular dimensions in the range of 5.9 to 6.9 angstroms, such as propane and isobutane. At conditions of standard temperature and pressure (STP), one volume of saturated methane hydrate (Structure I) will contain as much as 164 volumes of methane gas -- because of this large gas-storage capacity, gas hydrates are thought to represent an important source of natural gas. For a complete description of the structure and properties of hydrates see the summary by Sloan⁷.

II.A. Permafrost Gas Hydrates

Onshore gas hydrates are known to be present in the West Siberian Basin⁸ and are believed to occur in other permafrost areas of northern Russia, including the Timan-Pechora province, the eastern Siberian Craton, and the northeastern Siberia and Kamchatka areas⁹. Permafrost-associated gas hydrates are also present in the North American Arctic. Direct evidence for gas hydrates on the North Slope of Alaska comes from a core-test, and indirect evidence comes from drilling and open-hole industry well logs which suggest the presence of numerous gas hydrate layers in the area of the Prudhoe Bay and Kuparuk River oil fields^{10,11}. Well-log responses attributed to the presence of gas hydrates have been obtained in about one-fifth of the wells drilled in the Mackenzie Delta, and more than half of the wells in the Arctic Islands are inferred to contain gas hydrates^{12,13}. The combined information from Arctic gas-hydrate studies shows that, in permafrost regions, hydrates may exist at subsurface depths ranging from about 130 to 2,000 m¹.

II.B. Marine Gas Hydrates

The presence of gas hydrates in offshore continental margins has been inferred mainly from anomalous seismic reflectors that coincide with the predicted phase boundary at the base of the gas-hydrate stability zone. This reflector is commonly called a bottom-simulating reflector or BSR. BSRs have been mapped at depths below the sea floor ranging from about 100 to 1,100 m¹. Gas hydrates have been recovered in gravity cores within 10 m of the sea floor in sediment of the Gulf of Mexico¹⁴, the offshore portion of the Eel River Basin of California¹⁵, the Black Sea¹⁶, the Caspian Sea¹⁷, and the Sea of Okhotsk¹⁸. Also, gas hydrates have been recovered at greater sub-bottom depths during research coring along the southeastern coast of the United States on the Blake Outer Ridge¹⁹, in the Gulf of Mexico²⁰, in the Cascadia Basin near Oregon²¹, the Middle America Trench^{22,23}, offshore Peru²⁴, and on both the eastern and western margins of Japan^{25,26}.

Because gas hydrates are widespread in permafrost regions and in offshore marine sediments, they may be a potential energy resource. In-place World estimates for the amount of natural gas in gas hydrate deposits range from 5.0×10^{12} to 1.2×10^{16} trillion cubic feet for permafrost areas and from 1.1×10^{15} to 2.7×10^{18} trillion cubic feet for oceanic sediments². The published gas hydrate resource estimates show considerable variation, but oceanic sediments seem to be a much greater resource of natural gas than continental sediments. Current estimates of the amount of methane in the world gas hydrate accumulations are in rough accord at about 7×10^{15} trillion cubic feet². If these estimates are valid, then the amount of methane in gas hydrates is almost two orders of magnitude larger than the estimated total remaining recoverable conventional methane resources, estimated to be about 9×10^{13} trillion cubic feet²⁷.

III. GEOLOGIC CONTROLS ON GAS HYDRATE DISTRIBUTION

Review of previous gas hydrate studies indicates that the formation and occurrence of gas hydrates is controlled by formation temperature, formation pore-pressure, gas chemistry, pore-water salinity, availability of gas and water, gas and water migration pathways, and the presence of reservoir rocks and seals. In the following section, these geologic controls on the stability and formation of gas hydrates will be reviewed and assessed.

III.A. Formation-Temperature, Formation Pore-Pressure, Gas Chemistry

Gas hydrates exist under a limited range of temperature and pressure conditions such that the depth and thickness of the zone of potential gas-hydrate stability can be calculated. Depicted in the temperature/depth plots of figures 1A, 1B, and 1C are a series subsurface temperature profiles from an onshore permafrost area and two laboratory-derived gas-hydrate stability curves for different natural gases²⁸. These gas-hydrate phase-diagrams (figs. 1A, 1B, and 1C) illustrate how variations in formation-temperature, pore-pressure, and gas composition can affect the thickness of the gas-hydrate stability zone. In each phase-diagram, the mean-annual surface temperature is assumed to be -10°C; however, the depth to the base of permafrost (0°C isotherm) is varied for each temperature profile (assumed permafrost depths of 305 m, 610 m, and 914 m). Below permafrost, three different geothermal gradients (4.0°C/100 m, 3.2°C/100 m, and 2.0°C/100 m) are used to project the sub-permafrost temperature profiles. The two gas-hydrate stability curves represent gas hydrates with different gas chemistries. One of the stability curves is for a 100 percent methane hydrate, and the other is for a hydrate that contains 98 percent methane, 1.5 percent ethane, and 0.5 percent propane. The only difference among the three phase-diagrams (figs. 1A, 1B, and 1C) is the assumed pore-pressure gradient. Each phase diagram is constructed assuming different pore-pressure gradient; 9.048 kPa/m [0.400 psi/ft] (fig. 1A), 9.795 kPa/m [0.433 psi/ft] (fig. 1B), and 11.311 kPa/m [0.500 psi/ft] (fig. 1C).

The zone of potential gas-hydrate stability in each phase-diagram (figs. 1A, 1B, and 1C) lies in the area between the intersections of the geothermal gradient and the gas-hydrate stability curve. For example, in figure 1B, which assumes a hydrostatic pore-pressure gradient, the temperature profile projected to an assumed permafrost base of 610 m intersects the 100 percent methane-hydrate stability curve at about 200 m, thus marking the upper boundary of the methane-hydrate stability zone. A geothermal gradient of 4.0°C/100 m projected from the base of permafrost at 610 m intersects the 100 percent methane-hydrate stability curve at about 1,100 m; thus, the zone of potential methane-hydrate stability is approximately 900 m thick. However, if permafrost extended to a depth of 914 m and if the geothermal gradient below permafrost is 2.0°C/100 m, the zone of potential methane-hydrate stability would be approximately 2,100 m thick.

Most gas-hydrate stability studies assume that the pore-pressure gradient is hydrostatic (9.795 kPa/m; 0.433 psi/ft). Pore-pressure gradients greater than hydrostatic will correspond to higher pore-pressures with depth and a thicker gas-hydrate stability zone. A pore-pressure gradient less than hydrostatic will correspond to a thinner gas-hydrate stability zone. The effect of pore-pressure variations on the thickness of the gas-hydrate stability zone can be quantified by comparing each of the phase diagrams in figures 1A, 1B, and 1C. For example, in figure 1A,

which assumes a 9.048 kPa/m (0.400 psi/ft) pore-pressure gradient, the thickness of the 100 percent methane-hydrate stability zone with a 610 m permafrost depth and a sub-permafrost geothermal gradient of 2.0°C/100 m would be about 1,600 m. However, if a pore-pressure gradient of 11.311 kPa/m (0.500 psi/ft) is assumed (fig. 1C) the thickness of the methane-hydrate stability zone would be increased to about 1,850 m.

The gas-hydrate stability curves in figures 1A, 1B, and 1C were obtained from laboratory data published in Holder and others²⁸. The addition of 1.5 percent ethane and 0.5 percent propane to the pure methane gas system shifts the stability curve to the right, thus deepening the zone of potential gas-hydrate stability. For example, assuming a hydrostatic pore-pressure gradient (fig. 1B), a permafrost depth of 610 m, and a sub-permafrost geothermal gradient of 4.0°C/100 m, the zone of potential methane (100 percent methane) hydrate stability would be about 900 m thick; however, the addition of ethane (1.5 percent) and propane (0.5 percent) would thicken the potential gas-hydrate stability zone to 1,100 m.

III.B. Pore-Water Salinity

It is well known that dissolved salt can depress the freezing-point of water. For example, the base of the ice-bearing permafrost on the North Slope of Alaska does not coincide with the 0°C isotherm but with a lower temperature¹⁰. This freezing-point depression has been attributed in part to the presence of salt in the unfrozen pore-waters. Salt, such as NaCl, when added to a gas-hydrate system, also lowers the temperature at which gas hydrates form. Pore-water salts in contact with the gas during gas hydrate formation can reduce the crystallization temperature by about 0.06°C for each part per thousand of salt²⁸. Therefore, a pore-water salinity similar to that of seawater (32 ppt) would shift the gas-hydrate stability curves in figures 1A, 1B, and 1C to the left about 2°C and reduce the thickness of the gas-hydrate stability zone.

III.C. Availability of Gas and Water

Most naturally occurring gas hydrates are characterized by two crystal structures known as Structure I and Structure II⁷. The ideal gas/water ratio of Structure I gas hydrate is 8/46, whereas the ideal gas/water ratio of Structure II gas hydrate is 24/136. These ideal ratios confirm the observation that gas hydrates contain a substantial volume of gas. For example, if all the cages of Structure I gas hydrate are occupied, each volume of gas hydrate will contain 189 volumes of gas at standard temperature and pressure. The ideal hydrate gas/water ratios also indicate that there is a substantial amount of water stored in the gas-hydrate structure. These high gas and water concentrations demonstrate that the formation of gas hydrate requires a large source of both gas and water. Thus, it becomes necessary to quantify the potential sources of gas and water when assessing a potential gas-hydrate accumulation.

III.D. Gas and Water Migration Pathways

Other factors controlling the availability of gas and water are the geologic controls on fluid migration. As previously shown, gas hydrates contain a substantial volume of gas and water that must be supplied to a developing gas-hydrate accumulation. If effective migration pathways are not available, it is unlikely that a significant volume of gas hydrates would accumulate. Therefore, geologic parameters such as rock permeability and the nature of faulting must be evaluated to determine if the required gas and water can be delivered to the potential hydrate reservoir.

III.E. Presence of Reservoir Rocks and Seals

The study of gas-hydrate samples recovered during research coring operations in oceanic sediments suggests that the physical nature of in-situ gas hydrates may be highly variable⁷. Gas hydrates were observed to be (1) occupying pores of coarse-grained rocks; (2) nodules disseminated within fine-grained rocks; (3) a solid, filling fractures; or (4) a massive unit composed mainly of solid gas hydrate with minor amounts of sediment. Because of the limited number of gas-hydrate samples, it is not known if gas hydrates are usually pore-filling material or occur as massive units. A study of well logs from northern Alaska indicate that gas hydrates occur there as pore-filling constituents within coarse-grained reservoir rocks¹⁰. This study suggests that porous rock intervals serve as reservoir rocks in which gas and water can be concentrated in the amounts necessary for gas-hydrate formation. Therefore, the presence of reservoir rocks may play a role in gas-hydrate formation, particularly in well-consolidated rock intervals. It is also speculated that the presence of effective reservoir seals or traps may play a role in gas-hydrate formation. Gas generated at depth moves upward, generally along tilted permeable carrier beds, until it either seeps at the surface or meets an impermeable barrier (trap) that stops or impedes its flow. As migrating gas accumulates below an effective seal, the total gas concentrations may reach the critical amounts necessary for the formation of gas hydrates. Thus, impermeable seals can provide a mechanism by which the required gas can be concentrated within reservoir rocks. Besides conventional reservoirs and trapping mechanisms, it is possible for gas hydrate to form its own reservoir and trap. As gas migrates into the zone of gas-hydrate stability, it may interact with the available pore water to generate gas hydrate. With the appropriate volumes

of gas and water, the pore space within the reservoir rock could be completely filled, thus making the rock impermeable to further hydrocarbon migration. The plugging of gas pipelines and production tubing by gas hydrates is testimony to the sealing potential of gas hydrates⁷. It has also been shown that, in marine environments, gas hydrates can mechanically displace sediments to form their own reservoir. Thus, the availability of reservoir quality rocks may not always be a limiting factor.

IV. GAS HYDRATE RESOURCE ASSESSMENT

The major goal of this resource assessment is to estimate the gas hydrate resources in the United States, both onshore and offshore. Similar to the assessment of the conventional resources in the 1995 U.S. Geological Survey (USGS) Oil and Gas Assessment²⁹, this assessment of gas hydrates is based on a play-analysis scheme, which was conducted on a province-by-province basis. We have defined, described, and assessed all the gas-hydrate plays in the United States regardless of their current economic or technological status. Therefore, this assessment is concerned with the *in-place* gas hydrate resources—that is, the amount of gas that may exist within the gas hydrates without reference to its recoverability. In a play analysis method, prospects (potential hydrocarbon accumulations) are grouped according to their geologic characteristics into plays. The geologic settings of the hydrocarbon occurrences in the play are then modeled. Probabilities are assigned to the geologic attributes of the model necessary for generation and accumulation of hydrocarbons. In this assessment method, geologists make judgments about the geologic factors necessary for the formation of a hydrocarbon accumulation and quantitatively assess the geologic factors that determine its size.

In this assessment, 11 gas-hydrate plays were identified within four offshore and one onshore petroleum provinces (figure 2); for each play, *in-place* gas hydrate resources were estimated. Estimates for each of the 11 plays were aggregated to produce the estimate of total gas-hydrate resources in the United States. The offshore petroleum provinces assessed consist of the U.S. Exclusive Economic Zone (EEZ) adjacent to the lower 48 States and Alaska. The only onshore province assessed was the North Slope of Alaska, which included State water areas and some offshore Federal waters. The provinces shown in figure 2 are geographic in character; however, their formation represents an attempt to group the individual petroleum provinces along broad geologic lines. Maps depicting the geologic data required for this hydrate assessment have been included in the U.S. Geological Survey 1995 National Oil and Gas Assessment CD-ROM²⁹. Maps of bathymetry, sedimentary thickness, total organic carbon (TOC) content of the sediments, seabed temperature, geothermal gradient, and hydrate stability zone thickness have been published for all four offshore provinces assessed in the U.S. Geological Survey 1995 National Oil and Gas Assessment CD-ROM²⁹. Maps depicting the thickness of the onshore gas-hydrate stability zone in northern Alaska are also included in the Assessment CD-ROM²⁹.

The estimates of *in-place* gas-hydrate resources included in this report are presented in the form of complementary cumulative probability distributions (fig. 3). These distributions summarize the range of estimates generated by the FASPU computer program²⁹ as a single probability curve in a "greater than" format (fig. 3). Our estimates are reported at the mean and at the 95th, 75th, 50th, 25th, and 5th fractiles. We consider the 95th and 5th fractiles to be "reasonable" minimum and maximum values, respectively. *In-place* gas resources within the gas hydrates of the United States are estimated to range from 112,765 to 676,110 trillion cubic feet of gas (TCFG) [3,193 to 19,142 trillion cubic meters of gas (TCMG)], at the 0.95 and 0.05 probability levels, respectively (fig. 3). Although these ranges of values show a high degree of uncertainty, they do indicate the potential for enormous quantities of gas stored as gas hydrates. The mean *in-place* value for the entire United States is calculated to be 320,222 trillion cubic feet of gas (TCFG) [9,066 trillion cubic meters of gas (TCMG)]. This assessment of *in-place* gas hydrates represents those deposits that constitute the resource base *without reference to recoverability*.

V. REFERENCES CITED

1. Kvenvolden, K.A., 1988, Methane hydrate--A major reservoir of carbon in the shallow geosphere?: *Chemical Geology*, v. 71, p. 41-51.
2. Kvenvolden, K.A., 1993, Gas hydrates as a potential energy resource -- A review of their methane content, *in* Howell, D.G., ed., *The Future of Energy Gases: U.S. Geological Survey Professional Paper 1570*, p. 555-561.
3. Makogon, Y.F., 1981, *Hydrates of natural gas*: Tulsa, Penn Well Publishing Company, 237 p.
4. Collett, T.S., 1993, Natural gas production from Arctic gas hydrates, *in* Howell, D.G., ed., *The Future of Energy Gases: U.S. Geological Survey Professional Paper 1570*, p. 299-312.
5. Franklin, L.J., 1981, Hydrates in Arctic Islands, *in* Bowsher, A.L., ed., *Proceedings of a Workshop on Clathrates (gas Hydrates) in the National Petroleum Reserve in Alaska*, July 16-17, 1979, Menlo Park, California: U.S. Geological Survey Open-File Report 81-1298, p. 18-21.

6. Yakushev, V.S., and Collett, T.S., 1992, Gas hydrates in Arctic regions: risk to drilling and production: Second International Offshore and Polar Engineering Conference, June 14-19, 1992, San Francisco, California, Proceedings, p. 669-673.
7. Sloan, E.D., 1990, Clathrate hydrates of natural gases: New York, Marcel Dekker, Inc., 641 p.
8. Makogon, Y.F., Trebin, F.A., Trofimuk, A.A., Tsarev, V.P., and Cherskiy, N.V., 1972, Detection of a pool of natural gas in a solid (hydrate gas) state: Doklady Academy of Sciences U.S.S.R., Earth Science Section, v. 196, p. 197-200.
9. Cherskiy, N.V., Tsarev, V.P., and Nikitin, S.P., 1985, Investigation and prediction of conditions of accumulation of gas resources in gas-hydrate pools: Petroleum Geology, v. 21, p. 65-89.
10. Collett, T.S., 1993, Natural gas hydrates of the Prudhoe Bay and Kuparuk River area, North Slope, Alaska: American Association of Petroleum Geologists Bulletin, v. 77, no. 5, p. 793-812.
11. Collett, T.S., 1983, Detection and evaluation of natural gas hydrates from well logs, Prudhoe Bay, Alaska, in Proceedings of the Fourth International Conference on Permafrost, Fairbanks, Alaska: Washington D.C., National Academy of Sciences, p. 169-174.
12. Judge, A.S., 1988, Mapping the distribution and properties of natural gas hydrates in Canada: Proceedings of the American Chemical Society Third Chemical Congress of the North American Continent, June 6-7, Toronto, Ontario, Abstract no. 29.
13. Judge, A.S., and Majorowicz, J.A., 1992, Geothermal conditions for gas hydrate stability in the Beaufort-Mackenzie area: The global change aspect: Global and Planetary Change, v. 98, no. 2/3, p. 251-263.
14. Brooks, J.M., Cox, B.H., Bryant, W.R., Kennicutt, M.C., Mann, R.G., McDonald, T.J., 1986, Association of gas hydrates and oil seepage in the Gulf of Mexico: Organic Geochemistry, v. 10, p. 221-234.
15. Brooks, J.M., Field, M.E., and Kennicutt, M.C., 1991, Observations of gas hydrates in marine sediments, offshore northern California: Marine Geology, v. 96, p. 103-109.
16. Yefremova, A.G., and Zhizhchenko, B.P., 1974, Occurrence of crystal hydrates of gas in sediments of modern marine basins: Doklady Akademii Nauk SSSR, v. 214, p. 1179-1181.
17. Ginsburg, G.D., Guseinov, R.A., Dadashev, A.A., Ivanova, G.A., Kazantsev, S.A., Soloviev, V.A., Telepnev, Ye.V., Askery-Nasirov, R.E., Yesikov, A.D., Mal'tseva, V.I., Mashirov, Yu.G., and Shabayeva, I.Yu., 1992, Gas hydrates in the southern Caspian Sea: Izvestiya Akademii Nauk Serya Geologicheskaya, v. 7, p. 5-20.
18. Ginsburg, G.D., Soloviev, V.A., Cranston, R.E., Lorensen, T.D., and Kvenvolden, K.A., 1993, Gas hydrates from the continental slope, offshore from Sakhalin Island, Okhotsk Sea: Geo-Marine Letters, v. 13, p. 41-48.
19. Kvenvolden, K.A., and Barnard, L.A., 1983, Hydrates of natural gas in continental margins, in Watkins, J.S., and Drake, C.L., eds., Studies in Continental Margin Geology: American Association of Petroleum Geologists Memoir 34, p. 631-641.
20. Shipboard Scientific Party, 1986, Sites 614-624, in Bouma, A.H., and others, Proceedings, Deep Sea Drilling Project, Initial Reports, Washington D.C., U.S. Government Printing Office, v. 96, p. 3-424.
21. Shipboard Scientific Party, 1994, Site 892, in Westbrook, G.K., and others, Proceedings, Ocean Drilling Program, Initial Reports, College Station, Texas, v. 146, p. 301-375.
22. Kvenvolden, K.A., McDonald, T.J., 1985, Gas hydrates of the Middle America Trench, Deep Sea Drilling Project Leg 84, in von Huene, R., Aubouin, J., and others, Initial Reports Deep Sea Drilling Project, Washington, D.C., U.S. Government Printing Office, v. 84, p. 667-682.
23. Shipley, T.H., and Diddy, B.M., 1982, Occurrence of methane hydrates offshore Mexico, in Watkins, J.S., Moore, J.C., and others, Initial Reports, Deep Sea Drilling Project: Washington D.C., U.S. Government Printing Office, v. 66, p. 547-555.
24. Kvenvolden, K.A., and Kastner, M., 1990, Gas hydrates of the Peruvian outer continental margin, in Suess, E., von Huene, R., and others, Proceedings, Ocean Drilling Program, Scientific Results, College Station, Texas, v. 112, p. 517-526.
25. Shipboard Scientific Party, 1990, Site 796, in Tamake, K., and others, Proceedings, Ocean Drilling Program, Initial Reports, College Station, Texas, v. 127, p. 247-322.
26. Shipboard Scientific Party, 1991, Site 808, in Taira, A., and others, Proceedings, Ocean Drilling Program, Initial Reports, College Station, Texas, v. 131, p. 71-269.
27. Masters, C.D., Root, D.H., and Attanasi, E.D., 1991, Resource constraints in petroleum production potential: Science, v. 253, p. 146-152.
28. Holder, G.D., Malone, R.D., Lawson, W.F., 1987, Effects of gas composition and geothermal properties on the thickness and depth of natural-gas-hydrate zone: Journal of Petroleum Technology, September, p.1147-1152.
29. Gautier, D.L., Dolton, G.L., Takahashi, K.I., and Varnes, K.L., 1995, National assessment of United States oil and gas resources on CD-ROM: U.S. Geological Survey Digital Data Series 30.

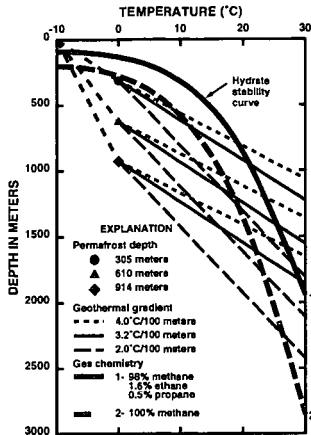


Figure 1A. Graph showing the depth-temperature zone in which gas hydrates are stable in a permafrost region [9.048 kPa/m pore-pressure gradient].²⁸

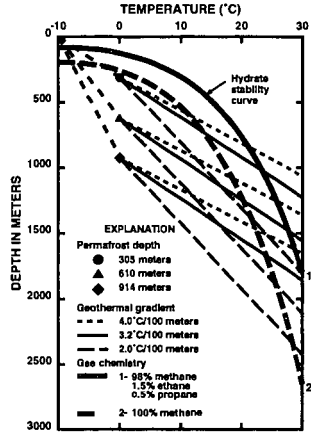


Figure 1B. Graph showing the depth-temperature zone in which gas hydrates are stable in a permafrost region [9.795 kPa/m pore-pressure gradient].²⁸

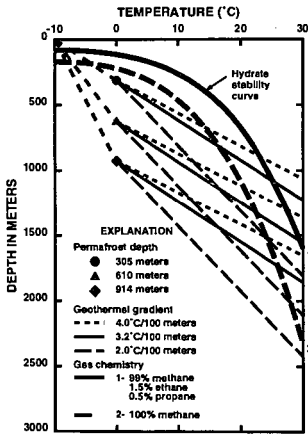


Figure 1C. Graph showing the depth-temperature zone in which gas hydrates are stable in a permafrost region [11.311 kPa/m pore-pressure gradient].²⁸

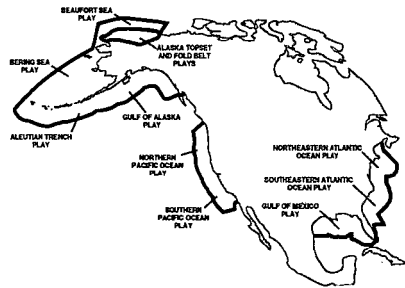


Figure 2. Gas hydrate play map of the United States.²⁹

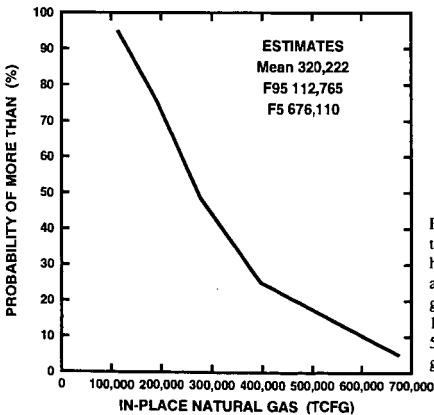


Figure 3. Cumulative probability curve showing the estimated in-place resources within the gas hydrates of the United States. The curve is read as follows: there is a 95 percent chance that the gas hydrate resource potential is greater than 112,765 trillion cubic feet of gas, and there is a 5 percent chance that the gas hydrate resource is greater than 676,110 trillion cubic feet of gas.²⁹

CLATHRATE-BASED FUEL STORAGE AND TRANSPORT MEDIA: POTENTIAL IMPACT

M. D. Max, Code 7420, R. E. Pellenberg, Code 6101, Naval Research Laboratory, Washington, D.C. 20375

Synthetic hydrate fuel, methane, gas

INTRODUCTION

Clathrates, particularly methane and other hydrocarbon gas hydrates, have been known as laboratory curiosities since chlorine hydrate ($\text{Cl}_2 \cdot 6\text{H}_2\text{O}$), was reported (Faraday, 1823). In the 1930's and 1940's the natural gas industry had problems with the formation of a crystalline, wax-like substance in natural gas transport pipes. This material clogged the lines and research was focused on understanding the origin and physical chemistry of the material so that its appearance in pipelines could be minimized. Methane hydrates are now recognized as being very widespread in marine sediments and in permafrost regions, and may constitute the largest store of fixed carbon on earth (Kvenvolden, 1993). Our present knowledge about methane hydrate physical chemistry, and the potential large volumes of recoverable methane from naturally occurring sources argues strongly that methane is likely to be the fuel of the future, especially if the aspect of compressing methane within a clathrate crystal lattice can be utilized on an industrial scale.

There is currently an increasing interest in methane as a fuel because the technology for handling it as a fuel, and the direct (e.g., on-site combustion for heating) and indirect (electricity generation) energy conversion technologies are well understood and cost effective. Additionally, because methane contains more hydrogen atoms for each carbon atom in its molecule than any other hydrocarbon fuel, less carbon dioxide is produced upon combustion. Also, gas field methane is usually relatively pure and relatively easy to purify. Its use as a fuel is thus more environmentally benign than other more complex hydrocarbon fuels or coal. Methane also produces much less carbon dioxide per mole than alcohols, where OH substitutes for one molecule of H, and much less than in liquid petroleum and oil based fuels.

Methane ("natural gas") produced from conventional gas deposits is plentiful, easily delivered (as a gas) to the user by an in-place domestic distribution system, and as a fuel, methane is clean burning and has a respectable heat content. The prospect of methane recovery from vast oceanic gas hydrate deposits, however, argues for an almost indefinite supply of methane, the recovery of which will probably speed the development of the gas-energy economy to replace the current oil-based economy. In addition to this development being ecologically sound, oil may be viewed better as an industrial feedstock than as a direct fuel, so long as a convenient, alternate source of energy such as methane is made available.

Methane is particularly amenable to transport and handling as a gas in pipelines and transport to point use in pipes within contiguous land areas. In fact, most of the early work into the chemistry of methane hydrates was undertaken by the gas transport industry because hydrates were forming and clogging gas pipelines even at relatively high temperatures and moderate pressures. Current technology frequently requires that methane fuel be moved as either compressed gas or as liquefied gas, as when natural gas is imported to the U.S. distribution grid from foreign gas fields. Of course, many fixed-site utilizations for natural gas (e.g. space heating, electrical power generation, or cooking) rely exclusively on gaseous methane as a fuel stock. Where technical or geographic difficulties prohibit the use of piped distribution, however, other means of distributing gas must be developed for use. Storage of methane (e.g., compressed gas) at the point of use may also be a problem so long as a continuous piped supply is not available.

Both compressed gas and liquefied gas, as transport media, possess serious safety concerns associated with the flammability of the material (compressed natural gas) or the cold temperatures and ultimate flammability/potentially explosive nature of the liquefied medium. This paper suggests and examines a new application of clathrate chemistry, which could have a significant impact on methane fuel use and distribution if implemented. We call attention to a potential third alternative for bulk gas transport and point-of-use storage, which would be energy dense, fairly stable, non-flammable in bulk, easy to transport, and potentially useable as-is for motor fuels.

SYNTHETIC METHANE CLATHRATE FUEL (SMCF)

Naturally occurring methane hydrates are not stable at sea level ambient temperatures and pressures. However, it is not intended to use pure methane hydrate as the basis for the new fuel transport and storage media. Current experimental results show that hydrates can be fabricated both from natural gas more dense than methane (de Boer et al, 1985) with variable physical property ranges that are stable well above the normal methane hydrate P-T stability field (Sloan, 1990). Also, in the course of producing synthetic methane hydrate, metastabilities about the liquidus line exist (Stern et al., 1996), which may point toward controlling metastability ranges of methane hydrate rather than expanding the methane hydrate stability field. This broader stability of naturally occurring multiple gas clathrates, poorly understood metastability, and relative ease with which synthetic methane (based) hydrate can be formed, leads us to suggest that research fabricating special property methane clathrates is feasible and that research should be undertaken to fabricate a new methane fuel storage and transport media.

The gas to be transported would be carried as a stabilized water-gas hydrate, or as a clathrate utilizing selected (probably gaseous) additives which could expand the stability field for pure methane-pure water clathrates well beyond that of natural methane hydrate or even some of the other natural hydrates that are stable nearer standard T-P (Fig. 1). It is clear that development and adoption of a clathrate-based fuel transportation/distribution system, to augment the in-place domestic gaseous-state fuel distribution complex, would offer many advantages above and beyond those associated with safety.

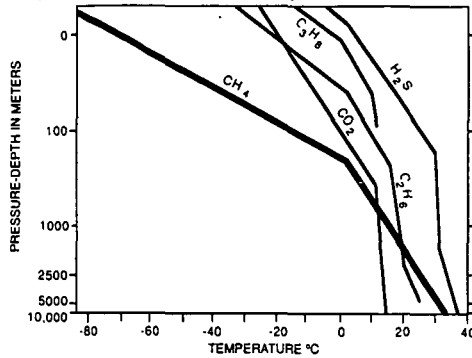


Figure 1. Natural hydrate phase boundaries for different common gases. From Makogon (1988). Replotted with temperature in normal scale and pressure-depth in meters seawater. 0 is atmospheric pressure at sea level. CH₄, methane; C₂H₆, ethane; C₃H₈, propane; C₄H₁₀, butane, the highest molecular weight of the paraffin gases, which most easily forms clathrates. CO₂, carbon Dioxide; H₂S, hydrogen sulphide.

Although the energy density of methane clathrate is low compared with common liquid fuels (Table 1), its potential energy density is actually greater than a similar volume of liquid methane, and up to 164 times (Kvenvolden, 1993) the same volume of methane gas (at STP). The compression factor is obtained because methane molecules are forced closer together in the crystalline solid methane hydrate than is obtained by any other form of methane compression. For our energy conversion factor we use 160 X compression factor, although it is unlikely that the industrial synthetic fuel will actually have a compression factor that high, because it is conservatively less than the maximum anticipated and results in even numbers appropriate for preliminary estimation.

Fuel or form of methane	Formula	Density g/cc	Energy Content Btu/lb	Energy Content Btu/ft ³
Methane Gas	CH ₄	7x10 ⁻⁴	160 * ³	1,150 * ³
Methane Liquid	CH ₄	0.42 * ²	1,500 * ⁴	152,000 * ⁴
Methane-water solid (natural hydrate energy conversion equivalent)	CH ₄ (H ₂ O) ₆	~ 1.0	277 * ⁴	15,800 * ⁴ * ⁵
Methane-water solid (natural hydrate potential)	CH ₄ (H ₂ O) ₆	~ 1.0	277 * ⁴	184,000 * ⁴ * ⁶
Octane (gasoline)	C ₈ H ₁₈	0.70	19,000 * ³	840,000 * ³
JP-5 * ¹	C ₁₄ H ₃₀	0.77	18,500 * ³	930,000 * ³

Table 1. Energy content of various Hydrocarbon Fuels. *¹, Less volatile jet fuel used by Navy, mandated for use on carriers to reduce danger of explosion. *², boiling point -161 C. *³, STP Conditions, gas phase. *⁴, Energy may be consumed producing gaseous methane from these forms or in containing them. *⁵, Combustion products are H₂O and CO₂. Energy content takes into account energy required to decompose hydrate to H₂ and CH₄; this figure represents energy content after conversion at 150 volumes of methane in hydrate per

volume of methane at STP. *6. Total potential energy content with no account taken of dissociation energy requirements based on 160 volumes of methane in hydrate per 1 volume of methane at STP (engineering may reduce the energy requirements for dissociation from specially fabricated clathrate or natural heat sinks may be used as an energy source).

It must be pointed out that the precise nature of SMCF is not known because it has yet to be designed and fabricated. Thus, the energy density, energy losses upon fabrication and subsequent gasification, and the equivalent energy of methane after conversion, in addition to the cost of the conversion and other engineering necessary for an SMCF system need to be known before a commercial value can be placed on the SMCF media. The potential energy content of naturally occurring methane hydrate is high enough to allow for some system or usage diminution and still remain an attractive new fuel storage and transport media. Thus, if an energy efficient means for gasifying synthetic methane clathrate fuel (SMCF), can be found, it may prove to be a more efficient means of compressing methane than liquification.

Because it is unlikely that the energy density of a clathrate-based fuel media will ever significantly approach that of liquid petroleum fuels, the clathrate fuel is clearly not appropriate for all vehicles. For instance, vehicles with small volumes capacity for fuel storage, such as private motor vehicles and aircraft, where weight/volume is a major factor, are not likely end-point users. Larger platforms, however, such as ships and possibly high-speed trains which could be made environmentally benign (with respect to noise of energy generation and exhaust), might be possible end-users, especially when the other attributes of clathrate based fuel media, such as inhibiting uncontrolled fires and explosions in commercial applications and explosion damping and deflecting in military applications, are taken into consideration.

The proposed safer transport system utilizes gas hydrates (clathrates) which are physical associations of water ice and low molecular weight gas molecules (e.g. methane, ethane, propane or butane). These clathrates form spontaneously when water and a suitable low molecular weight gas (e.g. methane, carbon dioxide, hydrogen sulfide, chlorine) are mixed at suitable temperatures (generally low) and pressures (generally moderate). Indeed, the older literature contains many references to gas hydrates forming spontaneously in natural gas transmission pipelines, and often blocking them; this potential situation requires the drying of gas prior to pipeline transportation (DoE, 1987).

Research into the low pressure species has mainly concerned developing techniques that will allow for industrial capability to efficiently dissolve, or gasify hydrates. Where bonding interaction between guest and host molecules might be enhanced somewhat, gas that normally does not hydrate, such as hydrogen, may be bound into specially formulated hydrates. If host cavities were to be lined with groups having a high hydrogen bonding character, such as hydroxyl or amino groups, other factors, such as the solubility parameter of the host, would be of less importance. Increased hydrogen bonding power might also be induced by charging guest molecules prior to exposure to hydrate lattice, or through the use of magnetic field charging (moving the fuel in a field, pulsing a field, or moving a field with respect to the orientation of the hydrate). Release of gas could be induced through heating, lowering of pressure, or electronic stimulation that would produce effects similar to that of microwaving food (where the frequency of the microwave is specific to water molecules).

FUEL SYSTEM REQUIREMENTS

The proposed SMCF storage and transport system would consist of three separate components: (1) Formation Module, (2) Transport Vessels, and (3) Gas Separation Unit.

(1). Hydrate Formation Module (HFM). Methane hydrates are stable under moderate pressures, and low temperatures (Fig. 1). The HFM will consist of a pressure vessel into which are pumped stabilizer, water spray, and methane; the P-T conditions of formation are presently uncertain but may be different from those needed for stability of the special hydrate during storage. Recent research shows that the methane hydrate forms immediately upon mixing water with the gas, when the system is within the stability field of the clathrate (Peter Brewer, MBARI, pers. comm., November, 1996). Once the hydrate is formed, the material would be removed from the HFM, and transferred to the transport vessel for movement to point of use or distribution.

(2) Hydrate Transport Vessel (HTV). The HTV would consist of a insulated container which could contain the stable special hydrate at ambient to moderate pressures. The insulation would more than likely consist of plastic foam such as is used by the refrigeration industry; vacuum jackets would be avoided because of cost and safety concerns. The HTV could be fabricated in any desired shape, and might evolve to be conformal to the hull or some interior structural members of the platform using the stored gas as a fuel, for example, in the double hull space of a ship.

(3) Gas Separation Unit (GSU). The GSU could be integral to the HTV, or separate, as mandated by the ultimate use of the released fuel gas. The clathrates are unstable in the presence of elevated heat; the hydrate could be decomposed by direct heating (e.g. a clathrate slush would be transferred to a heated vessel: gas evolves from the slush and escapes for use, and the water

from the hydrate is discarded or retained for use in making more hydrate later). Alternatively, the hydrate slush could be sprayed with water, the heat in which would be sufficient to decompose the hydrate. In either case, the evolved gas would be routed to a device (e.g. engine) which could use the combustible gas as a fuel.

It must be noted that there is no inherent reason why the units listed above would necessarily be separate components. For example, the storage vessel could contain integral sub-sections which would allow both formation of and decomposition of the gas hydrate right in the HTV. Further, it is technically possible to design and build an internal combustion engine which would use hydrate as the only, or majority, fuel; such a system would be similar to water-injection technology as applied to internal combustion engines, as in some experimental fighter plane engines and race cars.

CONCLUSIONS AND DISCUSSION

We have considered the feasibility of forming gas hydrates on demand, the utility of doing so (safe transportation of methane as a fuel), and potential end uses of gas moved as a hydrate (decomposition into gas for combustion, or design of engines to operate on hydrate itself). It is appropriate to examine the effects of adding a clathrate-based fuel on the current energy economy of a developed society.

Where would the SMCF system be applied and how would it develop? These questions cannot be fully answered because: 1. the engineering possibilities have yet to be explored, 2. the effect on market forces cannot be assessed beyond observing that the technology and potential fuel handling systems largely exist or can be developed at low cost, and, 3. government regulations that would apply (but do not yet exist) could either inhibit or promote development of both the SMCF itself and a world gas economy.

In the broadest sense, a SMCF-based fuel economy would be akin to the system based on liquid hydrocarbons. Specially formulated clathrates would be transported in the form of slush in much the same way as present liquid hydrocarbons. Transportation in solid form could utilize much of the present container-handling equipment and facilities including much of the sea, rail, and road equipment already in existence. Production as slush (Najafi and Schaetzle, 1989) would also allow pumped distribution. Moreover, where safety concerns are paramount, the SMCF might be used because of could greatly enhance safety; even in the presence of open flames, methane is evolved slowly from hydrates through breakdown of the crystal structure. This means that all of the gas or liquid methane available as an explosive component in present conventional methane storage media can only be evolved at a rate at which it could feed a fire, but not an explosion without first collecting evolved gas. In addition, upon gas evolution, substantial quantities of water are also produced, whose presence could be engineered to inhibit accidental ignition attributes of the system.

A dedicated clathrate-based methane fuel economy, in existence and developing, would drive exploration and development to utilize the vast quantities of methane that are only now being recognized as present on the planet (Max and Lowrie, 1996). Current conservative estimates indicate that naturally occurring methane hydrates contain at least twice the amount of fixed carbon as do conventional methane, liquid hydrocarbons, and coal, combined, on Earth (Kvenvolden, 1993), and it is unlikely that this fuel source will remain untapped, especially if an SMCF system can be developed at a reasonable cost.

References

- De Boer, R.B., Houbolt, J.J.H.C. & Lagrand, J. 1985. Formation of gas hydrates in a permeable medium. *Geologie en Mijnbouw*, **64**, 245-249.
- DoE, 1987. Gas hydrates Technology Status Report. Department of Energy DOE/METC-870246 (DE8700127) 54pp.
- Faraday, M. 1823. On fluid chlorine. *Philosophical Transactions Royal Society of London* **22A**, 160-189.
- Kvenvolden, K.A. 1993. A primer on gas hydrate. In: Howell, D.G. et al. (eds). *The future of energy gases*. USGS Professional Paper 1570, 279-291.
- Makogon, Yu.F. 1988. Gas-hydrate accumulations and permafrost development. In: Senneset, K. (ed). *Permafrost*. Fifth International Conference Proceedings, 95-101.
- Max, M.D. & Lowrie, A. 1996. Methane hydrate: A frontier for exploration of new gas resources. *Journal of Petroleum Geology*, **19**, 41-56.
- Najafi, M. & Schaetzle, W.J. 1989. Analysis of clathrate solidification. *IEEE CH2781-3/89/0000*, 1839-1844.
- Sloan, E.D., Jr. 1990. *Clathrate Hydrates of Natural Gases*. Marcel Dekker, Inc., New York and Basel. 641pp.
- Stern, L.A., Kirby, S.H. & Durham, W.B. 1996. Peculiarities of methane clathrate hydrate formation and solid-state deformation, including possible superheating of water ice. *Science*, **273**, 1843-1848.

CLATHRATE HYDRATES: SOME NEW STRUCTURAL INFORMATION*

Konstantin A. Udachin^a, Gary D. Enright, Christopher I. Ratcliffe and John A. Ripmeester¹

Steacie Institute for Molecular Sciences
National Research Council of Canada
Ottawa, Ontario, Canada K1A 0R6

Keywords: clathrate hydrates, crystal structure, structure H hydrate, CO₂ as small cage guest, bromine hydrate

INTRODUCTION

The accurate prediction of conditions for hydrate formation depends strongly on the availability of good structural information¹. For clathrate hydrates, a complete description of structure involves not only the unit cell parameters and average atomic positions, but also the cage occupancies. In order to provide this kind of information, it is necessary to use techniques such as diffraction, which is sensitive to long range order, in combination with techniques such as NMR which are sensitive to local order². Previously we have demonstrated the use of NMR methods for the determination of relative cage occupancies for structure I and II hydrates³.

Although the crystal structures of Str. I and II hydrates have been known for a considerable length of time⁴, the detailed lattice information on Str. H hydrate has remained unknown until recently⁵. It is also remarkable that a number of other apparently simple clathrate hydrate structures remain unsolved. Examples are the low hydrate of dimethyl ether⁶ and bromine hydrate. The latter is especially intriguing as the hydrate was first reported in 1829⁷, and it has been studied on and off for over 160 years⁸. A crystal space group and a set of lattice parameters were reported by Allen and Jeffrey⁹, although atomic coordinates were not obtained. More recently, Dyadin and co-workers⁹ have claimed that on the basis of hydration numbers which range from ~ 7 to 12, and the different crystal morphologies reported that there is evidence for as many as four different structures. We have now shown that a single crystal structure accounts for all of the different hydration numbers and crystal morphologies.

Another factor that is relatively unappreciated is the fact that although the small 5¹² (D) cage is common to all 3 structures, I, II and H, the symmetry and size of these small cages is different¹⁰, and hence their behaviour towards guest molecules should also be quite different. This is very directly evident from the chemical shift parameters of xenon trapped in the small cages which suggest that the structure II and H small cages are significantly larger and less symmetric than the Structure I small cage. Experiments with CO₂ have confirmed this idea.

Experimental

Bromine hydrate single crystals suitable for diffraction were grown from solutions of different concentrations to give material of different morphologies and hydration numbers see table 1. The crystal structures were determined on a Siemens diffractometer equipped with a CCD detector using Mo K_α radiation. In all, 16 different crystals were examined. The structures were solved with the Shextl software package.

Double hydrates of xenon or ¹³CO₂ were made by sealing into 10mm pyrex tubes measured quantities of powdered ice, along with the appropriate large cage and small cage guests. Samples were conditioned for times lasting from ~ 1 day to several weeks. NMR spectra were measured on an Bruker MSL 200 spectrometer equipped with a double-tuned solenoid probe suitable for cross-polarization and dipolar decoupling⁷. Temperature variation was achieved with a cold gas-flow system and a temperature controller. Spectral simulations were carried out with the Bruker Xedplot package.

RESULTS AND DISCUSSION

a) The structure of bromine hydrate

As was pointed out in the introduction, bromine hydrate can be made with different hydration numbers and vastly different morphologies⁸. Hydration numbers have been reported by at least 13 different authors and vary from 7 to 12⁸. For the crystals used in this study, the composition of the crystals was controlled by changing the concentration of the starting solutions from (Br:H₂O) 1:20 to 1:5. (table 1). The morphology of the different crystals is shown in fig. 1. Six crystals were studied in detail in order to come to a satisfactory solution of the structure, the space group and cell parameters for ten

other crystals were determined to cover the different crystal morphologies. For all of the crystals studied, the space group turned out to be the one reported by Allen and Jeffrey⁹: $P4_2/mnm$. At -100°C the lattice parameters are $a=23.044$, $c=12.075$ Å.

One view of the structure is shown in fig.2. The unit cell can be represented¹¹ as follows: $2D_A, 8D_B, 8T_A, 8T_B, 4P, 172H_2O$ with a $5^{12}6^3$ (P) cage, two distinct $5^{12}6^6$ (T_A , T_B) cages similar to those in str. I, and two kinds of 5^{12} (D_A , D_B) cages. The reason for the difficulty in finding a good structural solution becomes apparent when examining the guest positions in fig. 2. As opposed to structures with hydrocarbon guests, in the bromine hydrate case the scattering is dominated by the highly disordered bromine guest: the P cage has as many as 12 possible positions for bromine; the T cages each have 14 (T_A) or 15 (T_B), with the site occupancies varying from 20 down to 2 %. The highly anisotropic site distribution is evident especially for the T cages, where the centre of the cavity can be seen to be clear as the bromine atoms are confined to be near to the equatorial plane of the cage. The variable hydration numbers observed for bromine hydrate arise from the variable degree of filling of the large cages (table 1). The minimum hydration number possible is 8.6.

It will be another challenge to work out a thermodynamic model for bromine hydrate, as the clathrate has 3 types of large cage (P, T_A , T_B) suitable for bromine, and two small cages (D_A , D_B) which may contain oxygen or nitrogen from the air (some electron density in the small cages was indeed observed). The bromine hydrate structure is the only one of its type, as all other molecules of this size form str. II hydrate. Attempts to form a different hydrate with xenon as helpgas initially gave a structure II hydrate, but with time this was seen to revert back to the bromine hydrate structure. The fact that the large cages do not need to be full seems to be unique as well. This suggests that guest - guest interactions may play an important role in dictating structure type. Significant guest - guest interactions are likely for the electron-rich bromine molecule which should have a sizable molecular quadrupole moment. Another challenge is the understanding of the reasons for the different crystal morphologies. It appears that some kind of "self-inhibition " takes place to suppress the growth of certain crystal faces when the bromine concentration varies in the growth solution.

b) NMR Chemical Shifts and Cage Size

One of the first applications of ^{129}Xe NMR spectroscopy was the chemical shift resolution of the distinct sites in str. I hydrate². It was also noted that the chemical shifts for the 5^{12} cages in str. I and II were quite different¹⁰. According to the empirical chemical shift - cage size relationship, the D cage in str. II is larger than that in str. I. Since little is known about potential helpgases for str. H, it was thought that the Xe NMR parameters could give some guidance for the prediction of the suitability of CO_2 as such a helpgas for the two small cages. ^{129}Xe chemical shift for different hydrate cages are summarized in table 2 along with the point symmetry of the cages.

We note that str. I has the only pseudospherical D cage. From the chemical shift data, the other D cages are not only less symmetric, as indicated by non-zero chemical shift anisotropies, but also somewhat larger, as seen from the smaller shifts. This is likely to be of some importance for all small cage guests, since in str. I the fact that the small cage occupancy decreases with increasing guest size suggests that it is the repulsive interactions that limit the cage occupancy. Also, especially for non-spherical guests small departures from spherical symmetry are likely to be important. CO_2 is a good test molecule, as it appears to be a marginal guest for the 5^{12} cages. An indirectly determined hydration number from thermodynamic measurements is 7.0^{12} , which leads to an occupancy ratio $\theta_g/\theta_c \sim 0.3$ through the relationship between hydration number and guest occupancy ratio once the free energy difference between the hypothetical empty lattice and ice is known³. In a previous NMR study¹³, small cage CO_2 guests were not observed, as the central region of the spectrum is dominated by contributions from liquid and/or gaseous CO_2 . By using the appropriate polarization transfer pulse technique, these contributions can be eliminated from the spectrum, leaving the small cage contribution visible (fig. 3 (top)). On the other hand, for a double hydrate of propane and CO_2 , the ^{13}C spectrum indicates that nearly all of the CO_2 molecules are now located in the 5^{12} cage, that, from the Xe spectrum, is slightly larger and shaped like an oblate spheroid. The very weak central line indicates that there is almost no CO_2 in the large cage of the hydrate. The two propane ^{13}C resonance lines aren't resolved and occur as a single peak at ~ 18 ppm.

Based on these observations, what would one expect for the Str. H small cages ? From the ^{129}Xe spectra, the D and D' cages should be as large as the str. II D cage and

also quite asymmetric. An attempt was made to produce a hydrate sample of neohexane with CO₂ as small cage guest. The product gave the ¹³C spectrum shown in fig. 4. Indeed, contributions can be found from CO₂ in both D and D' cages with NMR lineshapes characteristic of axial and non-axial symmetry. We can conclude that CO₂ is indeed suitable as a small cage guest in str. H hydrate.

CONCLUSIONS

The long outstanding problem of the structure(s) of bromine hydrate has been solved successfully by examining 16 crystals of different morphologies and hydration numbers. There is just one structure, now solved in detail, and it is the tetragonal form originally suggested by Jeffrey.

By using the Xe NMR spectrum observed for xenon trapped in the small cages in str. I, II and H, it was predicted that the small cages in str. II and H should be good sites for CO₂. This was confirmed by using ¹³C NMR spectroscopy to examine a number of CO₂-containing hydrates. CO₂ is now also confirmed as a possible helppgas molecule for the structure H hydrate. The fact that all of the small cages (D and D' in str I, II and H) have different shapes and sizes (especially as defined by ¹²⁹Xe NMR) suggests that the Langmuir constants which define the affinity of small guests for these cages should also be different.

Acknowledgments: KAU and CIR thank the NATO Science Program for a Research Visit Grant.

* Published as NRCC no:39129

* Permanent address: Institute of Inorganic Chemistry, Russian Academy of Sciences, Novosibirsk, Russia

[†] Author for correspondence

¹ Davidson, D. W. in " Water. A Comprehensive Treatise. Franks, F. Ed., Plenum, New York, N. Y., 1973, Vol. 2; Sloan, Jr., E. D. " Hydrates of Natural Gas ", Marcel Dekker, New York, N. Y., 1991

² Davidson, D. W, Handa, Y. P., Ripmeester, J. A., J. Phys. Chem. 1986 **90**, 6549

³ Collins, M., Ratcliffe, C. I., Ripmeester, J. A., J. Phys. Chem. 1990 **94**, 157

⁴ Ripmeester, J. A., Tse, J. S., Ratcliffe, C. I., Powell, B. S., Nature 1987 **325**, 135

⁵ Udachin, K. A., Enright, G. A., Ratcliffe, C. I., Ripmeester, J. A., Supramol. Chem. (in press)

⁶ Miller, S. L., Gough, S. R., Davidson, D. W., J. Phys. Chem., 1977 **81**, 2154

⁷ Lowig, Ann. Pogg., 1829 **16**, 376

⁸ Dyadin, Y. A., Belosludov, V. R., in Comprehensive Supramolecular Chemistry, Atwood, J. L., Davies, J. E. D., MacNicol, D. D., Vogtle, F., Ed., Pergamon, 1996 **6**, 789

⁹ Allen, K. W., Jeffrey, G. A., J. Chem. Phys. 1963 **38**, 2304

¹⁰ Ripmeester, J. A., Ratcliffe, C. I., Tse, J. S., J. Chem. Soc. Faraday Trans. I 1988, 3731

¹¹ Jeffrey, G. A., in Inclusion Compounds, Atwood, J. L., Davies, J. E. D., MacNicol, D. D., Ed., Pergamon, 1982, Vol. 1

¹² Bozzo, A. T., Chen, H-S., Kass, J. R., Barduhn, A., Desalination, 1975 **16**, 303

¹³ Ratcliffe, C. I., Ripmeester, J. A. J. Phys. Chem. 1986 **90**, 1259

Table 1. Some details on the crystals of bromine hydrate studied

Initial composition of solution (Br ₂ :H ₂ O)	Average degree of filling of large cavities* (P, T _A , T _B)	Crystal Stoichiometry* (Br ₂ :H ₂ O)
1:20	0.805	1:10.68
1:14	0.914	1:9.41
1:10	0.946	1:9.09
1:7	0.962	1:8.94
1:5	0.998	1:8.62

* from analysis of crystal structure data

Table 2. Hydrate cages, cage sizes and ¹³⁵Xe chemical shift data

Structure	cage type	symmetry	radius/Å ^a	σ _{iso} (iso) ^b (ppm)	δ ^c (ppm)	η ^d
I	5 ¹² (D)	m3	2.50	-242	0	
I	5 ¹² 6 ¹ (T)	42m	2.93	-152	-21	
II	5 ¹² (D)	3m	2.50	-231	-16	
II	5 ¹² 6 ⁴ (H)	43m	3.28	-80	0	
H	5 ¹² (D)	mmm	2.50	-231	-13.6	0.8
H	4 ⁵ 5 ⁶ 6 ¹ (D')	62m	2.50	-212.4	-31.8	
H	5 ¹² 6 ³ (E)	6/mm	4.1	-----	-----	

^a estimate from X-ray diffraction data; ^b isotropic chemical shift; ^c δ=(2/3)Δσ - chemical shift anisotropy; ^d asymmetry parameter - departure of cage geometry from axial symmetry

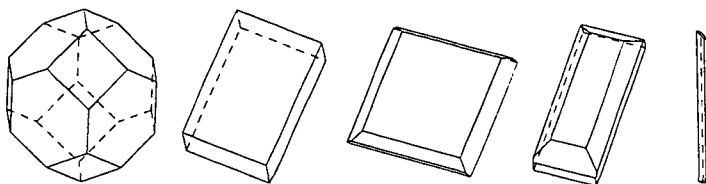


Figure 1. Morphology of different bromine hydrate crystals studied. In general, the massive form is seen most readily in dilute solutions, the needles in concentrated solutions.

Figure 2. General view of the bromine hydrate structure with the view approximately along the z direction; hydrogen atoms are omitted for clarity; the bromine atoms are shown in their many possible disordered positions in the cages, the maximum occupancy being one molecule per cage

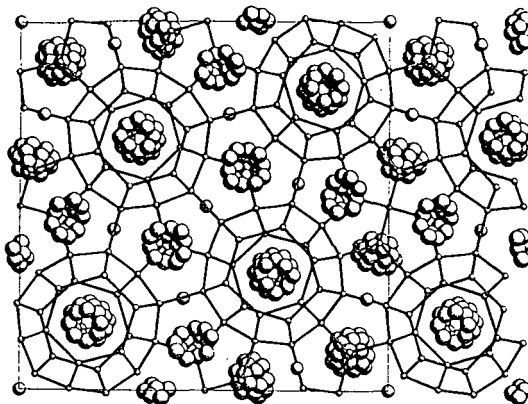


Figure 3. ^{13}C NMR powder patterns obtained for a) CO_2 hydrate b) double hydrate of CO_2 and propane. Note that the symmetry rather than the cage size determine the chemical shift patterns which reflect the nature of the guest motion (isotropic vs anisotropic). Pseudo-spherical cages give the sharp central lines (since cross-polarization methods were used, the liquid and gaseous CO_2 are not visible).

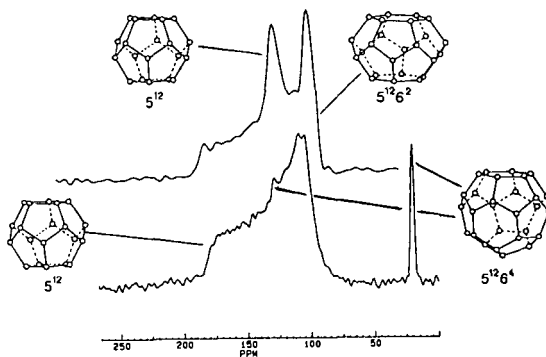
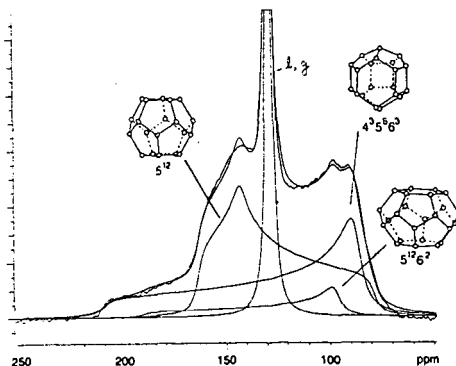


Figure 4. ^{13}C NMR spectrum for a str.H hydrate of CO_2 and 2,2 dimethyl butane. There is a small amount of str. I CO_2 hydrate present also. This spectrum does show liquid and gaseous CO_2 as a sharp line in the centre of the spectrum, as it was not recorded with a cross-polarization technique. The ^{13}C tensor pattern is axially symmetric for the $4^3 5^6 3$ (D') cage, and is a general tensor pattern for the low symmetry 5^{12} (D) cage.



THERMOGENIC GAS HYDRATES, GULF OF MEXICO CONTINENTAL SLOPE

Roger Sassen and Ian R. MacDonald

Geochemical and Environmental Research Group, Texas A&M University, College Station, Texas 77845

Keywords: gas hydrates, thermogenic hydrocarbons, Gulf of Mexico

INTRODUCTION

The Gulf of Mexico continental slope is a natural laboratory for gas hydrates that contain hydrocarbons from deeply buried thermogenic sources. Thermogenic hydrocarbons (oil and gas) from actively generating Mesozoic source rocks (>6 km burial depth) migrate vertically along conduits associated with actively-moving salt structures and faults to subsurface reservoirs (2-4 km) of Tertiary age¹. The hydrocarbon trapping system is so "leaky" that large volumes of thermogenic hydrocarbons reach the sea floor¹, and enter the water column².

Although biogenic gas hydrates are abundant on the Gulf slope³, oil and gas from deep source rocks create a geochemically complex and physically dynamic environment for thermogenic gas hydrates at the sea floor. Structure II gas hydrate containing C₁-C₄ thermogenic hydrocarbon gases was first sampled in 1984 by piston cores in 530-560 m water depths on the Gulf slope offshore Louisiana⁴. Identification of the hydrate as structure II was based on the relative abundance of the C₃ and *i*-C₄ hydrocarbons⁴. The structural assignment was corroborated using solid-state nuclear magnetic resonance (NMR)⁵. Research on gas hydrates of the Gulf slope, however, has advanced rapidly in the last few years, and our objective here is to summarize new results.

THE BUSH HILL STUDY AREA

The Bush Hill site in the Green Canyon area of the Gulf slope offshore Louisiana is a well-documented site for study of thermogenic gas hydrates (27°47.5' N and 91°15.0' W). Bush Hill is a fault-related sea-floor mound about 500 m wide, with relief of about 40 m⁶. Water depth of the mound crest is about 540 m, where mean water temperature is about 7° C (range = 6 to 11° C). Phase equilibria models indicate that Bush Hill is within the stability zone of thermogenic gas hydrates (Sloan, E.D., pers. communication).

Sea-floor sediments contain crude oil and related free hydrocarbon gases. Bacterial oxidation of these hydrocarbons produces CO₂ which precipitates as authigenic carbonate rock with isotopically-light δ¹³C values⁷. The crest of the mound is colonized by seep-dependent chemosynthetic organisms including bacterial mats, vestimentiferan tube worms, and methanotrophic mussels⁸. Persistent natural oil slicks appear on satellite remote sensing images of the sea surface over Bush Hill².

Thermogenic gas hydrates and gases that vent to the water column at the mound crest are readily sampled by research submarines. Copious streams of gas vent continuously to the water column where subsurface migration conduits intersect the sea floor^{9,10}. Thermogenic gas hydrates form around the orifices of gas vents. The gas hydrates at vents are not dispersed in sediments as nodules or thin seams, but instead occur as continuous masses. Lens-shaped masses of yellow to orange gas hydrates breach the sea-floor at numerous locations on the crest of Bush Hill^{9,10}. The hydrates form sediment-draped mounds 30-50 cm high and up to several m in width, with exposed gas hydrate visible at the edges of mounds¹⁰.

Vent Gases

The C₁-C₅ hydrocarbons of the vent gases are dominated by methane (C₁ = 91.1-94.7%), and δ¹³C values of C₁ are within the narrow range of -42.4 to -45.6 ‰ PDB (Table 1). The C₁-C₅ distributions and δ¹³C of C₁ of the vent gases (Table 1) correlate to gases from underlying subsurface reservoirs of Joliet Field¹¹.

Table 1. Normalized C₁-C₅ hydrocarbon compositions and methane δ¹³C of vent gases and thermogenic gas hydrates (Structure II and Structure H) at Bush Hill. Number in superscript indicates the citation to the data.

Sample	C ₁	δ ¹³ C	C ₂	C ₃	<i>i</i> -C ₄	<i>n</i> -C ₄	<i>i</i> -C ₅
Vent Gas ¹⁰	93.2	-43.3	4.3	1.5	0.3	0.6	0.3
Vent Gas ¹⁰	93.5	-42.5	4.3	1.4	0.2	0.4	0.2
Vent Gas ¹⁰	94.7	-45.6	3.9	0.7	0.1	0.5	0.2
Vent Gas ¹⁰	94.6	-43.8	3.8	0.7	0.1	0.5	0.3
Vent Gas ¹⁰	91.1	-42.4	4.8	1.8	0.4	1.2	0.8
Hydrate (II) ¹⁰	71.7	-36.3	10.6	12.6	2.6	1.7	0.8
Hydrate (II) ¹⁰	80.2	-38.5	9.4	7.3	1.6	1.2	0.3
Hydrate (II) ¹⁰	72.1	-39.9	12.4	11.4	2.3	1.6	0.3
Hydrate (H) ⁶	21.2	-29.3	9.5	7.5	2.5	17.5	41.1

Structure II hydrate

Hydrocarbon compositions of massive hydrate lenses of Bush Hill are shown in Table 1. The C₁-C₅ hydrocarbons of the hydrate gases are dominated by C₁ (71.7-80.2%). The δ¹³C values of C₁ are in the range of -36.3 to -39.9 ‰ PDB, somewhat heavier than vent gases, possibly because of bacterial activity¹⁰. The C₂ and C₃ hydrocarbons are both present in similar but relatively high percentages compared with the vent gas (Table 1). Preliminary NMR of an intact hydrate sample preserved in liquid nitrogen is consistent with structure II hydrate (Ripmeester, J., pers. communication).

Structure H gas hydrate

Structure H hydrates produced in the laboratory can enclose larger molecules than structure I or II hydrates, including common thermogenic hydrocarbons such as *i*-C₅. Given the widespread occurrence of petroleum, it was postulated in 1993 that structure H hydrate could co-exist in nature with structure II hydrate¹².

Evidence for the natural occurrence of structure H gas hydrate at the Bush Hill locality was first reported in 1994⁶. Massive amber-colored gas hydrate breached the sea-floor. It had been exposed when a buoyant lobe of hydrate broke free of the sediment and floated upwards into the water column. Identification of structure H hydrate was based on abundant *i*-C₅, which represented 41.1% of the total C₁-C₅ hydrocarbon distribution of the sample (Table 1). The δ¹³C of C₁ from the sample is heavy (-29.3 ‰ PDB), possibly because of bacterial activity⁶.

Experimentally-Precipitated gas hydrate

Gas hydrate was experimentally precipitated at the crest of Bush Hill in 1995 using natural vent gases as the starting material¹⁰. Water temperatures during experiments were 9.0-9.2°C. Precipitation of white to yellow gas hydrate was noted to occur within minutes.

The hydrocarbon compositions of experimentally precipitated gas hydrates are similar to vent gas compositions¹⁰. The C₁-C₅ hydrocarbons of the experimentally precipitated gas hydrates are dominated by methane (C₁ = 87.7-93.9%), and the δ¹³C values of C₁ are within the -40.5 to -45.3 ‰ PDB range.

CONCLUSIONS

Thermogenic gas hydrates occur on the Gulf of Mexico continental slope because of active vertical migration of oil and gas to the sea floor within their stability zone. The Bush Hill seep site on the Gulf slope is an important case history. Massive thermogenic gas hydrates occur in association with the orifices of hydrocarbon vents. Both structure II and structure H hydrates appear to co-exist in this

environment. Gas hydrate is also rapidly precipitated in sea-floor experiments using natural vent gas as the starting material. More sophisticated sampling and experiments from research submarine platforms could significantly enhance our understanding of thermogenic gas hydrate formation in the deep sea.

ACKNOWLEDGEMENTS

Support for research was provided by the NOAA National Undersea Research Center, University of North Carolina at Wilmington, and the Minerals Management Service, New Orleans.

REFERENCES

1. R. Sassen; J.M. Brooks; I.R. MacDonald; M.C. Kennicutt II; N.L. Guinasso; A. G. Requejo Trans. Gulf Coast Assoc. Geol. Soc. 1993 **43** 349-355.
2. MacDonald, I.R.; N.L. Guinasso, Jr.; S.G. Ackleson; J.F. Amos; R. Duckworth; R. Sassen; J.M. Brooks J. Geophys. Res. 1993 **98** 16,351-16,364.
3. J.S. Booth; M. M. Rowe; K. Fischer U.S. Geological Survey Open-File Report 96-272, June 1966.
4. Brooks J.M.; M.C. Kennicutt II; R.R. Fay; T.J. McDonald; Sassen R. Science 1984 **225** 409-411.
5. Davidson, D.W.; S.K. Garg, S.R. Gough, Y.P. Handa; C.I. Ratcliffe; J.A. Ripmeester; J.S. Tse; W.F. Lawson Geochim. Cosmochim. Acta. 1986 **50** 619-623.
6. Sassen, R.; I.R. MacDonald Org. Geochem. 1994 **22** 1029-1032.
7. Sassen R.; H.H. Roberts; P. Aharon; J. Larkin; E.W. Chinn; R. Carney Org. Geochem. 1993 **20** 77-89.
8. MacDonald I.R.; G.S. Boland; J.S. Baker; J.M. Brooks; M.C. Kennicutt II; R.R. Bidigare R.R. Marine Biol. 1989 **101** 235-247.
9. MacDonald, I.R.; N.L. Guinasso; R. Sassen; J.M. Brooks; L. Lee; K.T. Scott Geology 1994 **22** 699-702.
10. Sassen, R.; I.R. MacDonald. Org. Geochem. 1996, in press.
11. Kennicutt II, M.C.; J.M. Brooks; G.J. Denoux Mar. Chem. 1988 **24** 39-59.
12. Mehta, A.P.; Sloan, E.D. J. Chem. Eng. Data 1993 **38** 580-582.

HYDRATE FORMATION DURING CONTROLLED RELEASE OF CH₄ AND CO₂ IN MONTEREY BAY

Peter G. Brewer*, Franklin M. Orr⁺, Jr., G. Friederich*, K.A. Kvenvolden#, and D.L. Orange*

* Monterey Bay Aquarium Research Institute, P.O. Box 628, Moss Landing CA 95039

⁺ School of Earth Sciences, Stanford University, Stanford CA 94305

U.S. Geological Survey, 345 Middlefield Road, Menlo Park CA 94025

Keywords: Methane hydrate, CO₂ hydrate, ocean chemistry

INTRODUCTION

We have initiated a program of research into gas hydrate formation in the deep sea by controlled release of gas into natural sea water and marine sediments with the object of investigating the formation rates and growth patterns in natural systems, and the geochemical stability of the reaction products over time. Here we present a brief account of the experiments we have performed to date, we describe the novel experimental apparatus and procedures developed by our group for *in situ* oceanic work, and comment briefly on the significance of our results.

Laboratory experiments on the formation of hydrates are well known (1,2,3) and the techniques typically involve rocking or shaking the reactants in a pressure vessel, and initiation of the reaction with ice crystals or by supercooling. The experience of laboratory researchers is that significant (> 24 hours for methane) induction times delay the onset of hydrate formation (4), and several mechanistic theories have arisen to explain this lag in terms of the activation barrier associated with cluster formation. The growth of hydrates in nature does not involve shaking the reactants, nor is supercooling or the presence of ice crystals part of the deep sea natural environment, and therefore we approached our first *in situ* experiment with genuine curiosity as to whether the reaction would proceed via simple injection of the gas within the time frame of a few hours available to us for observation. We report here that we have repeatedly observed the formation of hydrates in a few seconds from methane, methane+ethane+propane, and CO₂, under various oceanic conditions, and have begun a program of time series observations of material left in place in our natural laboratory on the sea floor for an extended period of time.

EXPERIMENTAL METHODS

We have made use of Remotely Operated Vehicle (ROV) technology, and specifically the ROV *Ventana* (5,6) operated by the Monterey Bay Aquarium Research Institute from the research vessel *Point Lobos*, to carry out our experiments. The basic vehicle has a depth rating of 1,850 m and is powered by a 40 hp electro/hydraulic power pack. The vehicle is linked to the surface by a Kevlar armored tether with five copper conductors and an optical fiber core of ten elements which carry all control and telemetry signals. Imaging is provided by a Sony DXC-3000 three-chip color video camera with a Fujinon 5.5 to 40 mm zoom lens through which we observed and recorded the experiment. A Conductivity - Temperature - Pressure sensor (CTD; Sea Bird Instruments) is mounted on the vehicle and data is telemetered in real time to the control room.

Below the main frame of the vehicle is an open tool sled structure which housed the gas tank for the methane, and mixed gas experiments. The basic system is similar to that described earlier by us (7). A pressure regulator set to 0.7 Mpa above ambient pressure and a needle valve that limited the flow rate to about 125 ml per minute were in line. Gas was distributed to the reaction chambers by four hydraulically actuated pistons (Allenair) operating quarter turn valves that were controlled directly by us through the *Point Lobos* control room interface. The valves and reaction tubes were mounted on an aluminum box frame carried on the front of the vehicle and positioned for optimum viewing. The reaction tubes were vented to the outside ocean by an overflow tube at the top of the cylinder, arranged so as to trap a small gas bubble at all times while allowing for pressure equalization. A peristaltic pump was attached to all reaction cylinders to flush sea water at the local temperature and salinity through the apparatus prior to gas injection. The gas flow schematics are illustrated in Fig. 1.

For CO₂ release we faced the problem of dispensing a liquid at the pressures and temperatures encountered. Two systems were used: overpressuring the liquid CO₂ with a bubble of He gas to expel the fluid from a vertically mounted tank; and use of a hydraulically activated piston to expel the liquid CO₂ from a pressured reservoir. Once the CO₂ was expelled the gas flow, valving and reaction vessel were identical to that for methane.

The gas was expelled into acrylic reaction cylinders (60 x 4.5 cm; volume 954 cm³) mounted vertically on the frame; a second reaction chamber with a plane viewing surface, and large enough to contain a temperature probe of five thermistors was also constructed and used in the later experiments. The chambers contained either sea water alone, or were partially filled with sediments of varying grain sizes. No provision was made for sample recovery on board ship at this time, and

the observations were purely visual, although the environmental conditions for the experiment are well defined by the CTD sensor.

OBSERVATIONS

Methane Hydrate Formation

In our first experiment (January, 1996) we used pure methane gas (Linde); the thermodynamic boundary for methane hydrate formation posed by the local hydrographic (P,T,S) conditions in Monterey Bay is close to 525 m water depth. We paused at about 500m to inject a small amount of gas as a precaution to clear the lines, then drove *Ventana* to a depth of about 910m and switched on the peristaltic pump to flush the system of trapped sea water and achieve T,S equilibrium with the external medium (approximately 3.9°C; 34.42‰). Once the system had flushed we injected methane gas by bubble stream through a 10 µm porous frit at the bottom of the reaction cylinders. Methane hydrate formation occurred within a few seconds, seen easily as a bright reflective bubbly mass at the gas/water interface at the top of the tube. The hydrate formed as a white rind on the gas bubble surface that appeared to separate the water and gas from further rapid reaction unless some mechanical disturbance occurred. The reaction was reproducible; an injection into a second reaction cylinder produced an identical result. No significant induction period was observed, nor was anything other than gas and natural sea water present.

Of the two remaining reaction cylinders one contained about 20 cm of coarse sand, and the other a similar amount of fine grained mud. Here the hydrate formation was again first seen at the top of the tube. But the pores of the coarse sand matrix were soon observed to be flooded with hydrate, which sealed off further gas flow. The effect was to create cracking and then lifting of a major piece of the solidified sand column. Gas flow through the fine mud caused channels to open up since the capillary pressure for the gas to enter the pore spaces was higher than that required to displace the sediment. White hydrate masses quickly formed on the walls of the channels and gas created void spaces with an appearance and effect quite different from the coarse sand matrix. On recovery of the vehicle the hydrates formed in our experiment dissociated during transit to the surface, and we were not able to recover specimens for analysis.

CO₂ Hydrate Formation

In a second dive with an almost identical experimental arrangement (water, and sediment containing, reaction cylinders) we observed hydrate formation with CO₂. Here the local thermodynamic boundary for CO₂ hydrate formation occurs at about 350m water depth. We added a small amount of helium gas to the CO₂ cylinder prior to the dive so as to create an overpressure to drive the liquid CO₂ out of the primary reservoir. *Ventana* was then driven to about 568 m, and gas injected as before. White hydrate "whiskers" appeared at the frit within a few seconds, and a mass of hydrate coated bubbles formed quickly at the upper gas/water interface. Any induction period for hydrate formation was so short as to be negligible.

Our inspection of the performance of the apparatus at depth, and leakage of gas around valves, lead us to believe that our stratagem of using He to overpressure the CO₂ had in fact created a CO₂/He gas mixture, and that this particular experiment cannot therefore be strictly interpreted as pure CO₂ hydrate formation. Since He does not form a hydrate under any conditions the overall effect is likely to be small. Interestingly all CO₂ hydrates formed were buoyant, and rose rapidly through the sea water to rest at the interface between gas and water. The density of CO₂ hydrate is substantially greater than sea water, and the buoyancy is an indication of trapped unreacted liquid CO₂ (plus a small amount of dissolved He) in the formed product. Visual inspection, by close camera focus, of the bubbles of hydrate confirmed the presence of a liquid layer inside the hydrate sheath. Injection of CO₂ into the sediment containing cylinders produced a sequence of results very close to that observed for methane.

Mixed Gas Experiment

An experiment with a methane (90%) ethane (5%) and propane (5%) mixture was also carried out. Here the presence of propane as a hydrate Structure II former significantly shifts the hydrate boundary to shallower depths than that for methane alone; moreover the presence of propane is widely regarded as acting to reduce any induction period for hydrate formation. Since we have observed a very short formation time for CH₄ hydrate, the differential effect of using this gas mixture was insignificant and equally rapid hydrate formation on bubble surfaces was seen.

Liquid CO₂ injection

In an effort to create pure CO₂ hydrate without the complexity of probable He contamination in the mixture, we rebuilt the gas release apparatus so as to contain liquid CO₂ in a piston actuated cylinder. Care was taken to apply pressure from ROV system hydraulics to the open side of the cylinder throughout the dive so as to maintain a positive pressure over ambient and thus avoid pressures in the incorrect sense on the gas regulator. Here we dove to about 910m, and released CO₂ into the apparatus. At this depth only the liquid CO₂ phase is present. No fine pore frit, but a simple

small bore tube, was used for sample introduction in this experiment for fear of plugging the apparatus completely. The effect was to create globules of liquid CO_2 which, after sticking temporarily to the release port, rose slowly to the upper interface. There it appeared that a fine film of accreting hydrate gave a pearly appearance to the external surface of the globules, which did not coalesce but remained as separated units.

Thermal Signatures

In a modification of our apparatus we replaced one of the cylindrical reaction tubes with a plane faced larger unit for better viewing. In this unit we placed a heat flow probe constructed by the Woods Hole Oceanographic Institution's Alvin group. This consists of a metal rod about 1 m long with five thermistors each separated by about 10 cm. Readout from the probe was fed directly to the control room for real time monitoring of the experiment. Working with pure CH_4 gas in sea water we observed the temperature rise from the heat of formation during hydrate creation on bubble surfaces at the gas/water interface. Disturbance of the upper boundary by bubble flow created a mixed layer several centimeters deep which served to dissipate the heat, and it was not possible to gain a more quantitative estimate of the amount of hydrate formed.

On termination of the experiment and on raising *Ventana* to shallower depths we immediately observed a temperature drop due to quasi-adiabatic expansion cooling of the unreacted gas in the head space. Adiabatic cooling of the sea water itself is much smaller, but can be evaluated since the equation of state for sea water is well known (8). The temperature drop associated with gas expansion continued on raising until the hydrate decomposition point was reached. This point was not identical with the external oceanic boundary condition for dissociation due to the lower temperature at equal pressure within the apparatus, but it was clearly defined by a sharp break in the temperature trend due to cooling from the heat of dissociation.

Longer Term Observations

We intend to make longer term studies of the *in situ* stability of the hydrates we form than can be afforded within the confines of a one day dive schedule. This has meant devising a means to leave the apparatus on the sea floor for an extended period, and to return to it periodically for inspection and sampling of the trends. We have begun this process by constructing a square frame designed to sit above the sea floor and to hold the reaction tubes in place at a level where they can be viewed by the vehicle camera on return visits. This requires some means to first form the hydrate, then sever the connecting gas lines, pick up the frame with the vehicle robotic arm, and place it away from *Ventana* so that we can exit the site. Return to the location is provided for by deploying an interrogatable acoustic beacon nearby.

We have completed the first step and have left in place both CH_4 and CO_2 hydrate containing reaction cylinders at about 905 m depth at the "Clamfield" site in Monterey Bay. Revisits to this site after approximately 3 days, and 3 weeks, showed very little change in the hydrate structures we first formed. The cylinder containing CH_4 hydrate, unreacted gas, and sea water, was characterized by a bright white bubbly appearance. The bubbles with hydrate rind had not significantly coalesced or changed dimensions in the 3 week period. The CO_2 hydrate system, again containing liquid CO_2 , hydrate and sea water, had the aforementioned appearance of pearly globules that remained as distinct entities separated by their hydrate sheath for the full observation period to date.

DISCUSSION

From the experiments we have carried out to date we can make some interesting conclusions about the manner and characteristics of hydrate formation in the deep sea, where the reaction medium contains the normal assemblage of suspended particles, bacteria, and trace gases which characterize the natural environment. Firstly we have repeatedly made hydrates of several gases, each within the period of a very few minutes or seconds, by the simple technique of direct gas injection with no shaking or ice nucleation step whatsoever. The initial manifestation of this was the creation of hydrate coated bubbles at the gas/water interface; but hydrate also formed in seconds to minutes within the pore spaces of marine sediments where no provision was made for gas trapping. We surmise that passage of the gas bubbles around the sediment grains caused sufficient surface renewal that hydrate formed in a similar manner to the more easily visualized upper boundary, but with smaller unit size granules. No significant induction or lag period was observed for hydrate formation for any gas yet injected in this manner.

Once formed the hydrate structures appeared quite stable. That behavior is consistent with the idea that the hydrate rind on bubble surfaces separates the inside gas from the outside water well enough that further growth must occur only slowly by diffusion of the reactants through the hydrate skin. Unless some defect or fracturing of the hydrate rind occurs, this appears to be the rate limiting step.

Growth of hydrate in marine sediments is critically dependent on the grain size of the material. In a coarse material (sand) flooding of the pores results in cementing of the sediment into a massy unified

structure within seconds, yet yields no hydrate nodules of the kind often reported in nature (9). These nodular structures were observed in the process of forming in the flow channels carved by gas in experiments in fine grained mud, and the contrast between hydrate formation in the coarse and fine matrices was dramatic.

Our work with CO₂ hydrate has yielded results relevant to the proposed disposal of CO₂ in the deep ocean (10). For instance the ease with which CO₂ hydrate forms will pose a challenge to deep injection facilities concerned with plugging of the system; and the observation of the relative stability of the hydrate coated globules restricts interaction between disposed CO₂ and the surrounding ocean water. Furthermore, CO₂ hydrate did not separate spontaneously from unreacted CO₂; instead it formed a mass of intermediate density between sea water and liquid CO₂. Our observations were consistent with the description by Sakai et al. (11) of the natural venting of CO₂ rich fluids on the ocean floor.

Our experience with CO₂ hydrate formation is that the liquid CO₂ used experimentally requires excellent technique to handle. Post cruise analysis of our experiment carried out with He overpressure indicated by formal calculation (using the Peng-Robinson (12) equation of state) that the gas injected was indeed a CO₂/He mixture, since under the conditions we used (about 4.4⁰ C, 1800 psia) to prepare the gas reservoir then about 10 mol% He will dissolve in the liquid CO₂. Release of this at our *in situ* experimental conditions will form a mixture of about 20 volume % liquid phase, and 80 volume % vapor, accounting for our observations.

Once formed from sea water/gas (or liquid) contact, the hydrates are stable over a period of several weeks, and quite possibly very much longer indeed, even though sea water and unreacted gas or liquid are separated only by a thin hydrate film. The initial attempt we made to study this was successful in separating the experimental apparatus from the vehicle, and leaving it in place. In future experiments we will leave hydrates within sediment matrices for later recovery, and arrange for greater sea water/hydrate contact, since water flow around the hydrates was quite restricted in the present system.

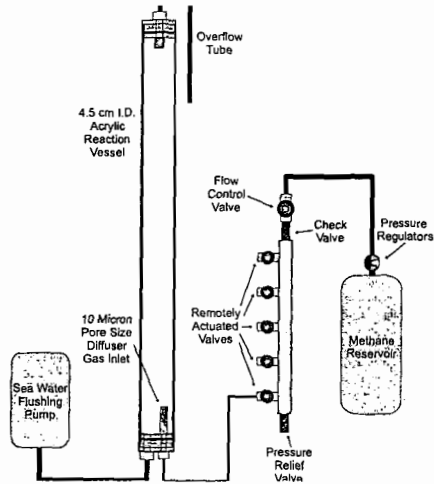
Finally we are devising means for surface recovery of the experimental material for laboratory investigation, and wish to apply the knowledge we have gained to a variety of important geochemical and gas disposal problems.

REFERENCES

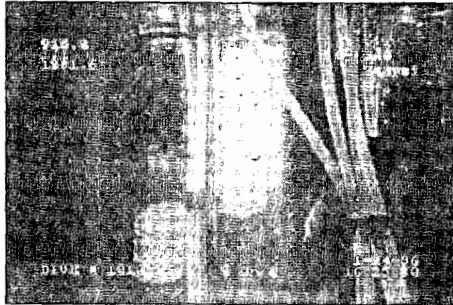
1. Sloan, E.D. Jr. *Clathrate Hydrates of Natural Gases*. Marcel Dekker. 1990 pp 641.
2. Stern, L.A.; Kirby, S.H.; Durham, W.B. *Science* 1996, 273, 1843-1848.
3. Dickens, G.R.; Quinby Hunt, M.S. *Geophys. Res. Lett.* 1994, 8, 2115-2118.
4. Sloan, E.D. In: *Gas Hydrates: Relevance to World Margin Stability and Climatic Change* 1996, pp. 1-38.
5. Robison, B.H. *Mar. Tech. Soc. J.* 1993, 26, 45-53.
6. Newman, J.B.; Robison, B.H. *Mar. Tech. Soc. J.* 1993, 26, 45-53.
7. Brewer, P.G.; Orr, F.M., Jr.; Friederich, G.; Kvenvolden, K.A.; Orange, D.L.; McFarlane, J.; Kirkwood, W. *Geology* 1996 submitted.
8. Millero, F.J.; Chen, C.T.; Bradshaw, A.L.; Schleicher, K. *Deep-Sea Res.* 1980, 27, 255-264.
9. Brooks, J.M.; Field, M.E.; Kennicutt, M.C. *Mar. Geol.* 1991, 96, 103-109.
10. Golomb, D. *Energy Convers. Manage.* 1993, 34, 967-976.
11. Sakai, H.; Gamo, T.; Kim, Es.; Tsutumi, T.; Tanaka, T.; Ishibashi, J.; Wakita, H.; Yamano, M.; Oomori, T. *Science* 1990, 248, 1093-1096.
12. Peng, D.Y.; Robinson, D.B. *Ind. Eng. Chem. Fundam.* 1976, 15, 59-64.

ACKNOWLEDGEMENTS

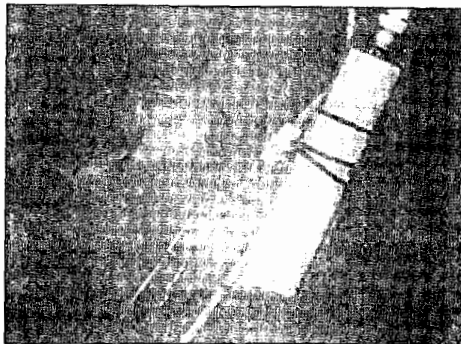
We wish to thank the Captain and crew of the RV *Point Lobos*, and the pilots of the ROV *Ventana* for their outstanding work in making these experiments possible. Support was provided by the David and Lucile Packard Foundation, and by Stanford University (F.M.O.) and the United States Geological Survey (K.A.K.)



1. Line diagram of the experimental apparatus used for hydrate generation from the ROV *Ventana*; the various pieces are not to scale.



2. Image of methane hydrate formed at the upper gas/water interface. The hydrate rind on bubble surfaces is plainly seen. The digital information on the screen gives (top, upper left) depth, and date and time (lower right). The reaction cylinders are 4.5 cm. diameter.



3. Image of both methane (right, white) and carbon dioxide (left, gray) hydrates approximately 3 weeks after initial formation in experimental apparatus left on the sea floor. The granular appearance of the methane hydrate is retained; the less rounded blobs of liquid carbon dioxide have a thin veneer of hydrate that apparently prevents surrounding sea water from further reaction.

ACCUMULATION OF SUBMARINE GAS HYDRATES

Gabriel D. Ginsburg and Valery A. Soloviev
Research Institute for Geology and Mineral Resources of the Ocean
1, Angliyskiy prospekt, St.Petersburg, 190121 Russia

Keywords: submarine gas hydrates, accumulation mechanisms, fluid migration

INTRODUCTION

During last fifteen years the authors have been studying the generation and accumulation of submarine gas hydrates. In particular, expeditions have been carried out in the Caspian, Black, and Okhotsk seas (Ginsburg et al., 1990, 1992, 1993), and the Norwegian Sea (1996, unpublished). The results of our investigations have been summarized in a monograph (Ginsburg and Soloviev, 1994). That is the basis of this presentation.

RESULTS AND DISCUSSION

The analysis of the worldwide observational data suggests that submarine hydrates largely occur in local accumulations (Ginsburg and Soloviev, 1994, 1995). All observed submarine gas hydrates are readily divisible into two groups: associated and non-associated with fluid vents. Hydrates of the first group, which have been observed close to the sea floor in the Caspian, Black, Okhotsk and Norwegian seas, the Gulf of Mexico, and in several other sites (altogether in 11 regions, Fig.1) are controlled by fluid conduits: mud volcanoes, diapirs, and faults. As for the second group of gas-hydrates (deep-seated), their control by fluid flow may be usually deduced from an association with indirect borehole indications of fluid flows, such as relatively coarse-grained sediments and anomalies of pore water chlorinity (Figs.2, 3).

The generation, accumulation and disappearance of any water-soluble naturally occurring compound in terms of water availability are governed by solubility variations of this compound. This is true also in regard to gas hydrates. It is extremely important for natural gas hydrate formation that the solubility of methane (which is the major component of natural hydrates) in water in terms of hydrate stability is little affected by the general (hydrostatic) pressure (contrary to "normal" conditions of hydrate instability) but is dictated essentially by the equilibrium pressure of hydrate formation, which is temperature-dependent. Since the equilibrium pressure of hydrate stability is diminished with decreasing temperature, methane solubility in water also decreases (Fig.4, solid line). Because of this, the solubility of methane in pore waters generally decreases towards the sea floor within the submarine gas hydrate stability zone (Fig.5). The higher the geothermal gradient, accordingly the thinner the hydrate stability zone, the sharper is the methane solubility decrease.

Three major mechanisms of methane transport in sediments can be distinguished: dissolved in pore water flows, as free gas flows, and molecular diffusion. Hydrate precipitation from ascending methane-saturated water is thought to be the most straightforward (Ginsburg, 1990; Ginsburg and Soloviev, 1994). The hydrate zone forms a gas-geochemical barrier for methane-saturated water which rises either from below or from within this zone: as the water cools it should precipitate hydrate. The amount of precipitated hydrate obviously corresponds to the excess of dissolved methane (i.e., over the solubility). Clearly the effectiveness of this process depends, in particular, on the rate of water flow and the water temperature; in the case of focused flow of warm water, the thickness of the submarine hydrate zone can decrease to zero. Gas hydrates being precipitated from infiltrated waters are progressively filling the sediment pore space and/or fracture porosity and eventually cement them, producing massive and vein hydrate sediment structures.

Gas hydrates associated with free gas flows discharging on the sea floor were observed in the Gulf of Mexico (Brooks et al., 1994) and in the Okhotsk Sea (Ginsburg et al., 1993). Clearly, the gas seeping through the hydrate stability zone has no time to crystallize as a hydrate. After a hydrate film forms at the gas-water interface, each succeeding portion of free gas, prior to hydration, has to penetrate this film. Thus the rate of hydrate formation in the vicinity of free gas flows is limited by the rate of this penetration (i.e., the rate of molecular diffusion), and hydrates are accumulated primarily from the water-dissolved gas: a solid (hydrate) phase grows at a distance from free gas. The lateral outward diffusion of methane of the ascending gas flow appears to be governed by the difference between chemical potentials of gaseous and dissolved methane at common depths. The above difference is deduced from the difference between the pressure of a free methane close to the hydrostatic pressure and the vapour pressure of dissolved methane, which in terms of pore water saturation should be close to the equilibrium pressure of gas hydrate formation (compare P_h and P_{eq} on Fig.6). Since this difference decreases with increasing subbottom depth, hydrate accumulations associated with ascending free gas flows are assumed to taper off downward. Accumulations of this type at great water depths should be more extensive than shallow ones (other factors being equal) because the considered difference increases with deepening water. It is self-evident that this model simplifies the matter. In fact, the heat release caused by hydrate formation enhances the outward methane transport and extends the diffusion aureole around ascending gas flow. Within this aureole the hydrates are thought to result not only from outward diffusing methane

but also from upward diffusion, the intensity of which is controlled by high gradients of concentration and vapor pressure of water-dissolved methane in the hydrate zone (in terms of methane-saturated water); these gradients greatly exceed values outside the hydrate zone (Figs.5 and 6).

A similar pattern of methane diffusion and gas hydrate accumulation should also characterize the vicinity of ascending flows of gas-saturated water. In particular this is possible around the water flows which are too warm for hydrate precipitation. High gradient of temperature nearby these flows provides favorable conditions for rapid gas hydrate accumulation.

It is generally believed that diffusion plays only a destructive role in the history of hydrocarbon accumulations. In contrast, Egorov (1988) has put forward the concept of "directional diffusion recondensation". This implies the diffusional transfer of hydrocarbons which saturate water in the presence of a temperature-controlled solubility gradient. According to this concept, the formation and accumulation of a hydrocarbon phase in the region of lower temperature results from such a transfer. We suggest that directional diffusion recondensation is just the process which governs gas hydrate accumulation in the vicinity of free gas and gas-saturated water flows, as well as within and above the sediment sections where biochemical methane is intensively generated. Relatively impervious sediments may act as a cap in this process. DSDP-ODP data offer examples of gas hydrate occurrences close to the boundary between relatively coarse- and fine-grained sediments (Ginsburg and Soloviev, 1994).

Thus, gas hydrates accumulate from water solutions, no matter whether methane is delivered into the reaction zone, by infiltration or diffusion. The important distinction between two modes of hydrate accumulation in sediments (aside from the process rate) lies in the source of hydrate water. In the case of hydrate precipitation from infiltrated gas-saturated water this source is flow itself; in the case of diffusional methane delivery the hydrate water is extracted from sediment pore water in-situ.

We have proposed the term segregation to designate the mechanism of hydrate accumulation from diffusing gas and from water being extracted from sediments (Ginsburg and Soloviev, 1994). A continuous delivery of methane and the associated formation of hydrate generates a migration of pure water into the reaction zone from the adjacent sediments or sea water. This mechanism of water migration is thought to be diffusion-osmotic. Hydrate inclusions of a different shape are formed during this process due to the dewatering of surrounding sediments if the latter are compacted. The shape of inclusions is obviously caused by the factors controlling the fields of gas and water chemical potentials. In particular the subhorizontal lenticular-bedded hydrate sediment structure observed in association with submarine gas vents in the Okhotsk Sea (Ginsburg et al., 1993) may result from the subhorizontal extension of isotherms.

As a result of water redistribution during segregational gas hydrate accumulation, the total water content of hydrate-bearing sediments may turn out to be higher than that of the adjacent nonhydrated ones, as has been observed in the Okhotsk Sea (Ginsburg et al., 1993). A water content of sediments directly proportional to their hydrate content has been demonstrated in the Caspian Sea (Ginsburg et al., 1992). Hence the hydrate accumulation in sediments may imply not only gathering of gas but also of water. Due to hydrate water abundance, a sediment may become fluidized upon decomposition of hydrate.

Diffusion is known to be an ubiquitous process in marine sediments. Since a hydrate of any origin is subject to subsequent decomposition and possible diffusional recondensation of the released hydrate methane, segregational hydrates are thought to be more common than those precipitated by infiltrated water.

We mentioned two kinds of inhomogeneity of the geological medium exerting influence upon gas hydrate accumulation: permeability variations, which control fluid conduits and gas hydrate caps, and geothermal inhomogeneity (geothermal gradient), which predominantly governs gas solubility in water. In addition two other kinds of inhomogeneity - hydrochemical and lithological can have a pronounced effect on this process. It is well-known that water-dissolved salts inhibit (prevent) gas hydrate formation, i.e. hydrates form more readily from fresh water. Therefore, a gradient of water salinity within the hydrate zone under gas-saturation conditions must provoke a diffusional flux of methane into fresh water, where this arriving methane should be hydrated. Such a situation may occur near boundaries of water flows. It is necessary to emphasize here that the solubility of methane in the fresh gas-saturated water is known to be higher than in saline water, whereas the corresponding methane fugacity, which actually should be considered as a driving force of diffusion, is higher in saline water (Handa, 1990).

A lithological (or in more exact terms, a porometric) inhomogeneity implies, in particular, a distinction of sediment pore size (we do not consider here a shape of sediment pores and their specific properties, which of course also affect gas hydrate accumulation). The pore medium influences the hydrate equilibrium (thermodynamic effect) and the kinetics of hydrate formation. The thermodynamic effect essentially is as follows: a pore surface is hydrophilic and

therefore lowers the pore water chemical potential. As a result, a higher thermodynamic concentration of methane is required for the formation of hydrate. In principle, this effect is similar to the influence of salts dissolved in water. This surface effect was studied by many authors and had been found negligible in terms of natural sediment water content. The kinetic effect lies in the fact that a pore size may be less than a gas hydrate critical nucleus size at a given temperature. In this case, for hydrate formation to start, more significant overcooling or oversaturation is required (Chersky and Mikhailov, 1990). We suggest that the essence of both effects (thermodynamic and kinetic) can be understood by examination of hydrate formation in adjacent sediments having different pore sizes. It is evident that the hydrate formation in coarse-pored sediments has an advantage over fine-pored ones - the same gas concentration in water may turn out to be sufficient to form hydrates in the former case and insufficient in the latter. What this means is hydrate can accumulate rather in relatively large pores in the course of sediment compaction and/or biochemical gas generation.

CONCLUSIONS

Submarine gas hydrates mostly occur locally and are linked to fluid flows. They accumulate from methane-saturated water, in the course of pore water infiltration and methane diffusion. Apart from the methane availability the accumulation of hydrates is controlled by physical factors such as temperature gradient, pore water salinity gradient and lithological variability. The hydrates precipitate at lower temperatures and from less saline water; relatively coarse-grained sediments make better hydrate reservoirs than fine-grained sediments.

REFERENCES

Brooks, J.M., Anderson, A.L., Sassen, R., MacDonald, I.R., Kennicutt II, M.C. and Guinasso, N.L., Jr., 1994. Hydrate occurrences in shallow subsurface cores from continental slope sediments. In: E.D. Sloan, Jr., J. Happel and M.A. Hnatow (Eds.), *Int. Conf. on Natural Gas Hydrates*. *Annals of the New York Acad. Sci.*, 715: 381-391.

Cherskiy, N.V. and Mikhailov, N.E., 1990. Size of equilibrium critical nuclei of gas hydrates. *Doklady Akademii Nauk SSSR*, 312(4): 968-971 (in Russian).

Egorov, A.V., 1988. *Diffusional Mechanisms of Hydrocarbons Primary Migration and Accumulation in Offshore Sedimentary Basins*, Thesis. Institut Okeanologii Akademii Nauk SSSR, Moscow, 218pp. (in Russian).

Gieskes, J.M., Johnston, K., Boehm, M., 1985. Appendix. Interstitial water studies. Leg 66. In: von Huene, R., Aubouin, J. et al. *Init. Repts. DSDP, 84: Washington, D.C.*: 961-967.

Ginsburg, G.D., 1990. Submarine gas hydrate formation from seeping gas-saturated underground waters. *Doklady Akademii Nauk SSSR*, 313(2): 410-412 (in Russian).

Ginsburg, G.D. and Soloviev, V.A., 1994. *Submarine Gas Hydrates*. VNIIOkeangeologia, St.Petersburg, 199 pp. (in Russian, with English abstract).

Ginsburg, G.D. and Soloviev, V.A., 1995. Submarine gas hydrate estimation: theoretical and empirical approaches. *Proc. 27th Annu. OTC., Houston, Texas, USA, 1-4 May 1995*: 513-518.

Ginsburg, G.D., Kremlev, A.N., Grigor'ev, M.N., Larkin, G.V., Pavlenkin, A.D. and Saltykova, N.A., 1990. Nitrogenic gas hydrates in the Black Sea (twenty-first voyage of the research vessel "Evpatoriya"). *Soviet Geology and Geophysics (Geologia i Geofizika)*, 31(3): 8-16.

Ginsburg, G.D., Guseynov, R.A., Dadashev, G.A., Ivanova, G.A., Kazantsev, S.A., Solov'yev, V.A., Telepnev, E.V., Askeri-Nasirov, R.Ye., Yesikov, A.D., Mal'tseva, V.I., Mashirov, Yu.G. and Shabayeva, I.Yu., 1992. Gas hydrates of the Southern Caspian. *Int. Geol. Rev.*, 34(8): 765-782.

Ginsburg, G.D., Soloviev, V.A., Cranston, R.E., Lorenson, T.D., Kvenvolden, K.A., 1993. Gas hydrates from continental slope offshore from Sakhalin Island, Okhotsk Sea. *Geo-Marine Letters*, 13: 41-48.

Handa, Y.P., 1990. Effect of hydrostatic pressure and salinity on the stability of gas hydrates. *Journ. Phys. Chem.*, 94(6): 2652-2657.

Makogon, Yu.F. and Davidson, D.W., 1983. Influence of excessive pressure on methane hydrate stability. *Gazovaya promyshlennost'*, 4: 37-40 (in Russian).

Namiot, A.Yu., 1991. *Solubility of Gases in Water*. Reference Textbook. Nedra, Moscow, 167 pp. (in Russian).

von Huene, R., Aubouin, J. et al., 1985. *Init. Repts. DSDP, 84: Washington, D.C.*

Watkins, J.S., Moore, J.C. et al., 1981. *Init. Repts. DSDP, 66: Washington, D.C.*

FIGURES

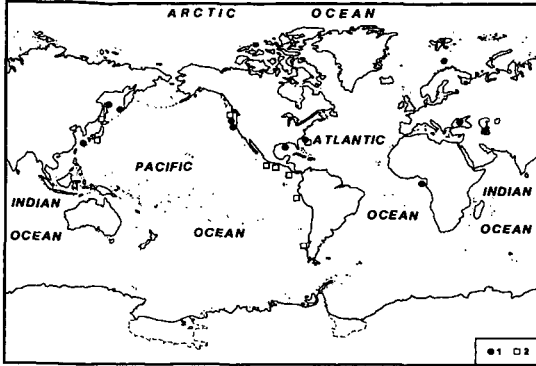


Fig.1. Worldwide locations of observed submarine gas hydrates. Updated after Ginsburg and Soloviev, 1994. 1, 2 - sea floor seepage-associated and non-associated gas hydrates, respectively.

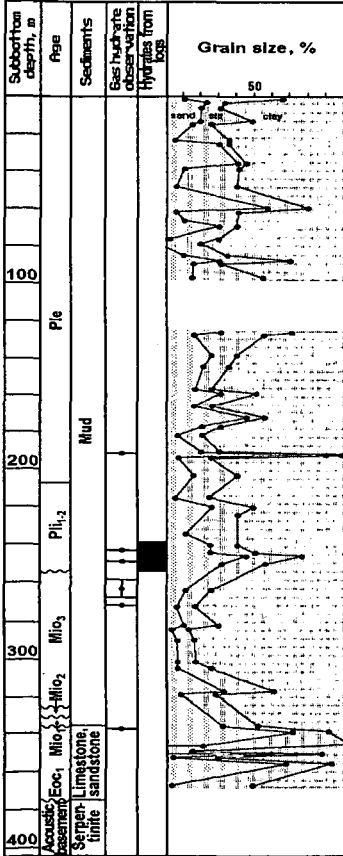


Fig.2. Gas hydrate shows and sediment grain size in geological section at DSDP Site 570, Middle America Trench. Compiled from von Huene, Aubouin et al., 1985.

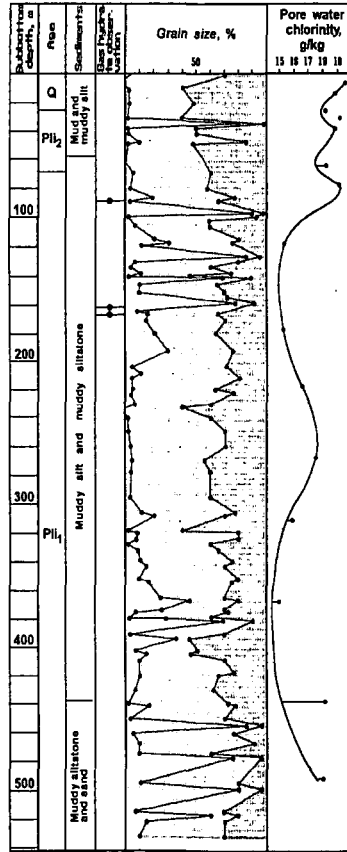


Fig.3. Gas hydrate shows, sediment grain size, and pore water chlorinity in geological section at DSDP Site 491, Middle America Trench. Compiled from Watkins, Moore et al., 1981, and Gieskes et al., 1985. The chlorinity curve is drawn using sulfate as a measure of sample contamination with the sea water. For symbols of sediment grain size see Fig.2.

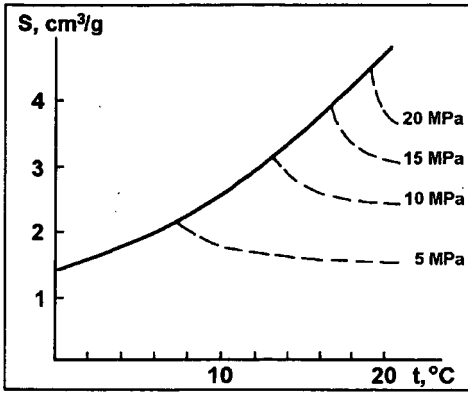


Fig. 4. Solubility of methane (S) in pure water plotted against temperature (t): isobars of instability in terms of gas hydrate instability (set of dashed lines), and solubility in equilibrium with hydrate (solid line). Compiled using the data of Makogon and Davidson (1983) and Namiot (1991).

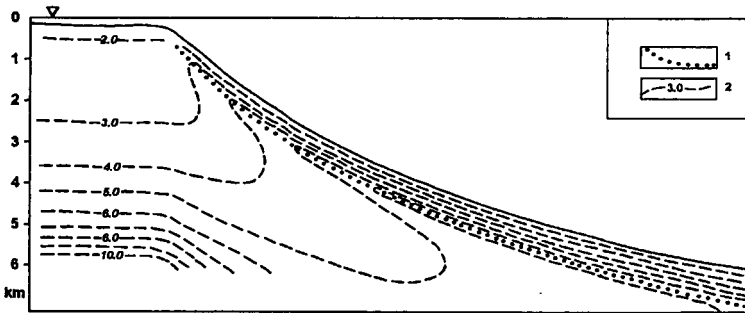


Fig. 5. Vertical cross-section demonstrating solubility of methane in water under thermobaric conditions of continental margins (after Ginsburg and Soloviev, 1994). The dashed lines are isolines of solubility numbered in STP cm³/g. Dotted line is the base of thermobaric gas hydrate stability zone. Compiled using the data of Makogon and Davidson (1983) and Namiot (1991). Accepted assumptions: water is pure; bottom water temperature is 5°C for water depths down to 500 m, and 2°C at greater depths; geothermal gradient is 30°C/km; hydrobaric gradient is 10 MPa/km.

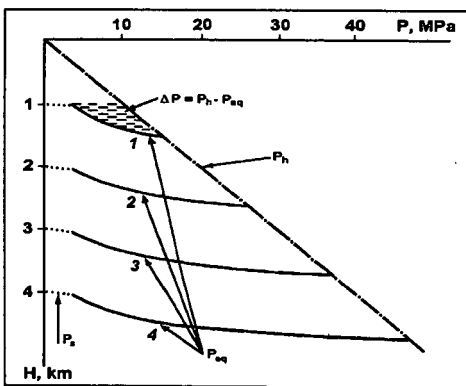


Fig. 6. Relationship between different kinds of pressure (P) affecting diffusion of methane in subbottom conditions. H is total depth = water depth + subbottom depth. P_h is conventional hydrostatic pressure. P_{eq} is equilibrium pressure of methane hydrate; curves 1-4 relate to water depths 1, 2, 3, 4 km, respectively. P_s is saturation pressure of dissolved methane within sulfate reduction zone. Accepted assumptions: water is pure, gas is pure methane (see also Fig. 5). The P_{eq} curves are the usual PT gas hydrate equilibrium curves but the temperature axis is replaced by the depth axis based on the accepted assumptions.

ON THE MECHANISM OF GAS HYDRATE FORMATION IN SUBSEA SEDIMENTS

B. Tohidi, A. Danesh, and A.C. Todd
Department of Petroleum Engineering, Heriot-Watt University
Edinburgh EH14 4AS, Scotland.

Keywords: Gas Hydrates, Gas Solubility, Subsea Sediments

INTRODUCTION

Gas hydrates are crystalline molecular complexes formed from mixtures of water and suitably sized gas molecules. Based on hydrogen bonding, water molecules form unstable lattice structures with several interstitial cavities. The gas molecules can occupy the lattice cavities and, when a minimum number of cavities are occupied, the crystalline structure becomes stable and solid gas hydrates are formed, even at temperatures well above the ice point^[1]. The known gas hydrate structures are; structure-I, structure-II, and the recently discovered structure-H^[2].

The necessary condition for hydrate formation is the presence of water or ice, suitably sized non-polar or slightly polar molecules, together with appropriate pressure and temperature conditions. In subsea environments, the sediments are normally saturated with sea water and a combination of the geothermal gradient and the weight of the column of water (which causes a hydrostatic pressure) could provide the right conditions for hydrate formation. Under these conditions, gas released from biogenic activities (or seepage from oil and gas reservoirs) could form gas hydrates. Current estimates show that the amount of energy in the gas hydrates is twice that of the total fossil fuel reserves, indicating a huge source of energy which could be exploited in the right economical conditions^[1].

Although most scientists agree on the process of hydrate formation in subsea sediments, the mechanism of gas hydrate formation is the subject of some debate. Some researchers suggest that the presence of the free gas phase is necessary and gas hydrates form in the gas-water interface. Others believe that at least a local supersaturation of gas with respect to gas-water equilibria is required. Some propose that this supersaturation will result in the evolution of micro-bubbles and hence formation of gas hydrates. While others suggest that there is no need for the presence of gas bubbles for the hydrates to be stable^[1,3-5].

In this presentation, a thermodynamic model, validated against experimental data, is used to predict the solubility of methane in pure or saline water. The results show that gas hydrates could form from dissolved gas as well as from free gas. Based on the above findings, two mechanisms for hydrate formation in subsea sediments have been suggested and discussed.

It should be noted that, the hydrate forming gas is assumed to be pure methane to simplify the argument. Obviously for multi-component systems, upon hydrate formation, some compositional variation will occur which will result in changes in equilibrium conditions. Also, any effect due to capillary forces and the type of rock has been ignored in this work.

THERMODYNAMIC MODEL

The fugacity of each component in all fluid phases, including the salt free water-rich phase, have been calculated by an equation of state (EoS). The saline water phase has been modelled by combining the EoS with the modified Debye-Hückel electrostatic term, using only one interaction parameter. In optimising the water-salt interaction parameters, water vapour pressure depression data at 373.15 K and freezing point depression data have been used. For the gas-salt interaction coefficient, gas solubility data in single electrolyte solutions at different temperatures and salt concentrations have been used. The model has been extended to mixed electrolyte solutions with nine salts in its library. A detailed

description of modelling vapour, liquid hydrocarbon, salt free water phase, hydrate phases, ice phase, and saline water phase is given elsewhere[6, 7].

Figure-1 shows methane solubility in distilled water at different temperatures. There is a good agreement between experimental[8] data and predictions which demonstrates the success of the EoS in representing highly polar systems.

Methane solubility in distilled water and in 1 and 4 molar NaCl solutions are presented in Figure-2. The agreement between experimental[9] data and predictions is very good, which indicates the reliability of the thermodynamic model. (There are some deviations for pure water at higher pressures, which could be due to the inaccuracy of experimental data, as Figure-1 shows better agreement for the case of pure water).

RESULTS AND DISCUSSIONS

Figure-3 shows the predicted methane solubility in the water-rich phase in a wide temperature range (i.e., 275 to 400 K), at different isobars. This figure indicates that methane solubility passes through a minimum. The dashed lines show the methane solubility in metastable conditions. Also in the above figure, the concentration of methane in the water-rich phase at water-hydrate and water-hydrate-methane phase equilibria are presented.

For simplicity, the sea water in subsea sediments is represented by 3.5 Wt% NaCl aqueous solution. Methane solubility in the water-rich phase in the presence of sea water, is depicted in Figure-4. Constant pressure lines are replaced by depth, taking into account the density of the sea water. Again the dashed lines, which are the extension of methane solubility in water-gas equilibria, show the methane solubility in the water-rich phase at metastable conditions. For simplicity, pressure (or depth) is assumed to be constant; by cooling and moving along the constant pressure line, the system will approach the water-hydrate-methane equilibrium point, i.e. the potential hydrate formation temperature. Assuming no subcooling is required, methane hydrates could form at this point. In the absence of a free gas phase, a further reduction in temperature will cause more hydrates to form and the methane concentration in equilibrium with hydrates to reduce. Nevertheless, for hydrate formation, a certain degree of subcooling is required. Therefore, the methane concentration in the water rich phase could be as high as those presented by the dash lines. However, when hydrate formation is initiated the equilibrium methane concentration in the water-rich phase is much lower. This means that gas hydrates could form without the presence of a free gas phase.

In the presence of a free gas phase and under the above conditions (constant pressure, temperature, and composition), hydrate formation would cease only when one of the phases (i.e., water or the free gas phase) disappears. However, in the presence of sea water the increase in the concentration of salts (due to hydrate formation) could inhibit the further formation of hydrates, as discussed later.

The effect of salt(s) on the equilibrium concentration of methane in the water-rich phase is presented in Figure-5. As shown, the presence of salt(s) will reduce the methane solubility, and inhibit hydrate formation, as the hydrate-water-methane point for 3.5 Wt% NaCl solution is at a lower temperature compared to pure water.

Figure-6a shows the mole% hydrates formed from dissolved gas in 3.5 Wt% NaCl solution at 280 K. The x-axis is pressure (or depth). As an example, at 20 MPa (1993 m depth), the dissolved gas in the metastable condition is enough to form 1% hydrates. However, the amount of hydrates could be as high as 2.2% for 60 MPa pressure (5980 m depth).

As shown in Figure-6b, the 1% hydrates will increase the salt concentration by 0.03 Wt%, i.e., the salt concentration will increase from 3.5 to 3.53 Wt%. However, the effect on phase equilibria conditions is insignificant (an inhibition of 0.013 K). This means that for further hydrate formation, the controlling factor is

most likely to be the supply of gas. As the gas concentration in the hydrate stability zone is significantly lower, the gas could be transported by diffusion. Convection is also another means of supplying gas to the hydrate stability zone.

Based on the above results the following two mechanisms are proposed for hydrate formation in subsea sediments:

1. Hydrate formation from dissolved gas:

- Gas released from biogenic and thermogenic sources are dissolved in sea water.
- The dissolved gas reaches the hydrate stability zone by diffusion, or the water containing the dissolved gas reaches the hydrate stability zone by convection/advection.
- Hydrate formation initiates at a certain degree of subcooling and the concentration of gas in the water-rich phase is reduced, as shown in Figure-4. Therefore, the gas concentration (in the water-rich phase) outside the hydrate stability zone would be higher than that inside the hydrate stability zone.
- More gas is provided to the hydrate stability zone by diffusion (due to the concentration gradient) for further hydrate formation.

As mentioned previously, the increase in salt concentration due to hydrate formation is very small. Therefore, the diffusion of gas from the high concentration region to the hydrate stability zone is likely to be the controlling factor.

2. Hydrate formation from free gas:

- Free gas is generated in-situ, or reaches the hydrate stability zone by convection.
- Large amounts of hydrates could be formed which could result in the consumption of all the free gas, or a significant increase in the salt concentration in the pores.
- The increase in salt concentration could inhibit further hydrate formation (Figure-5), unless the salt concentration is reduced by diffusion.
- More free gas is converted into hydrates. This process will terminate when all the gas (or water) is converted into hydrates.

In the above mechanism, the transfer of salts by diffusion is likely to be the controlling factor.

ACKNOWLEDGEMENTS

The authors would like to thank Professor Westbrook and Dr Minshull for very useful discussions.

REFERENCES

1. Sloan, E. D., Clathrate Hydrates of Natural Gases, Marcel Dekker Inc., New York, (1990).
2. Ripmeester, J.A., Tse, J.S, Ratcliffe, C.I., and Powell, B.M., "A New Clathrate Hydrate Structure", *Nature*, Vol. 325, No. 135, pp. 135-136, (1987).
3. Miller, S.L., "The Nature and Occurrence of Clathrate Hydrates", *Natural gases in Marine Sediments*, Ed. Kaplan, I.R., Plenum Press, New York, (1974).
4. Makogon, Y., "Gas Hydrate Formation in Porous Media", *Proceed. of the 2nd International Conference on Natural Gas Hydrates*, pp. 275-289, (1996).
5. Brown, K.M., Bangs, N.L., Froelich, Kvenolden, K.A., "The Nature, Distribution, and Origin of Gas Hydrate in the Chile Triple Junction Region", *Earth and Planetary Science Letter*, Vol. 139, pp. 471-483, (1996).
6. Tohidi, B., Danesh, A., and Todd, A.C., "Modelling Single and Mixed Electrolyte Solutions and its Applications to Gas Hydrates", *Chem. Eng. Res. and Des.*, Vol. 73 (May), Part A, pp. 464-472, (1995).
7. Tohidi, B., Danesh, A., Burgass, R.W., and Todd, A.C., "Gas Solubility in Saline Water and Its Effect on Hydrate Equilibria", *Proceedings of the 5th International Offshore and Polar Engineering Conference (ISOPE-95)*, Vol. 1, pp. 263-268, (1995).
8. Culberson, O.L., and McKetta, J.J., *Petrol. Trans. AIME*, Vol. 192, P. 223, (1951).
O'Sullivan, T.D., and Smith, N.O., "The Solubility and Partial Molar Volume of Nitrogen and Methane in Water and in Aqueous Sodium Chloride from 50 to 125 ° and 100 to 600 Atm", *J Phys Chem*, Vol 74, No 7, pp. 1460-1466, (1970).

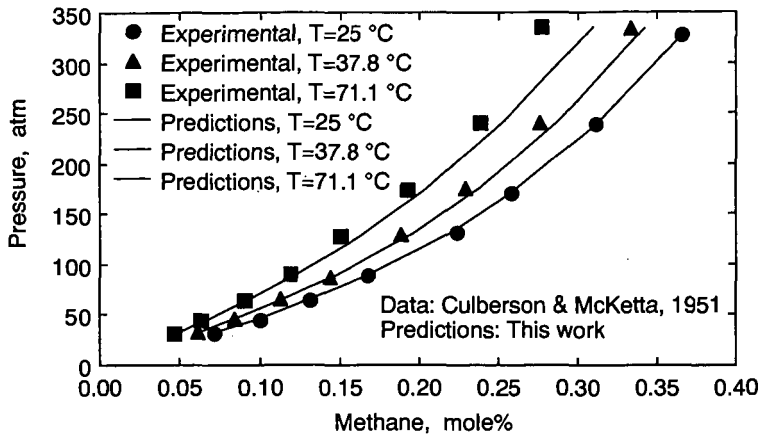


Figure-1 Experimental and predicted methane solubilities in distilled water.

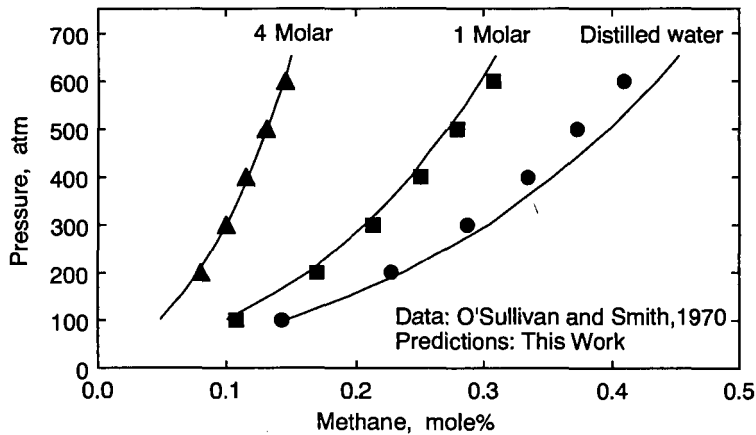


Figure-2 Experimental and predicted methane solubilities in distilled water and NaCl aqueous solutions.

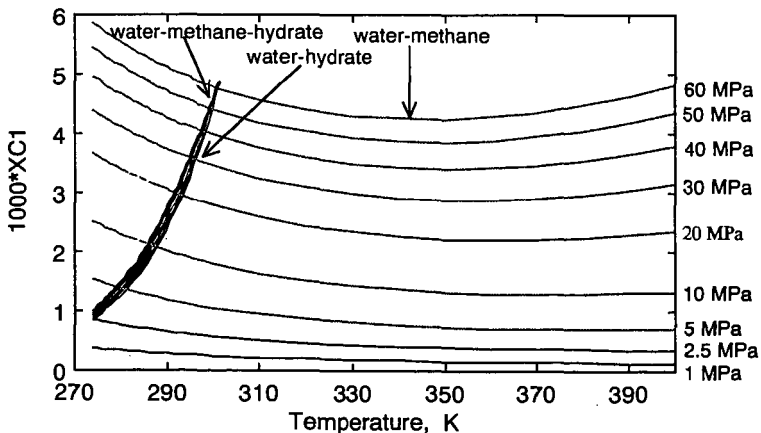


Figure-3 Predicted methane concentrations in the water-rich phases (Salt free) of water-methane, water-methane-hydrate, and water-hydrate equilibria.

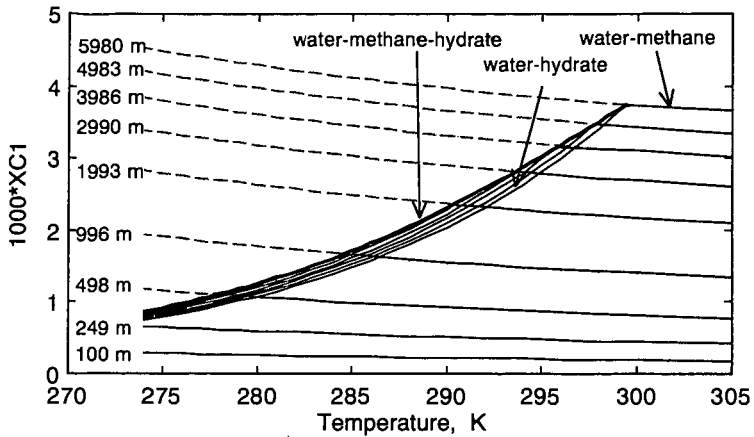


Figure-4 Predicted methane concentrations in the water-rich phases (3.5 Wt% NaCl) of water-methane, water-methane-hydrate, and water-hydrate equilibria.

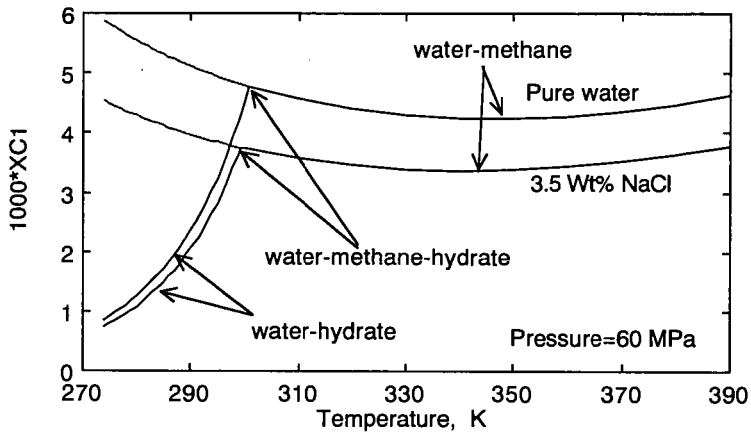


Figure-5 Effect of water salinity on methane concentration.

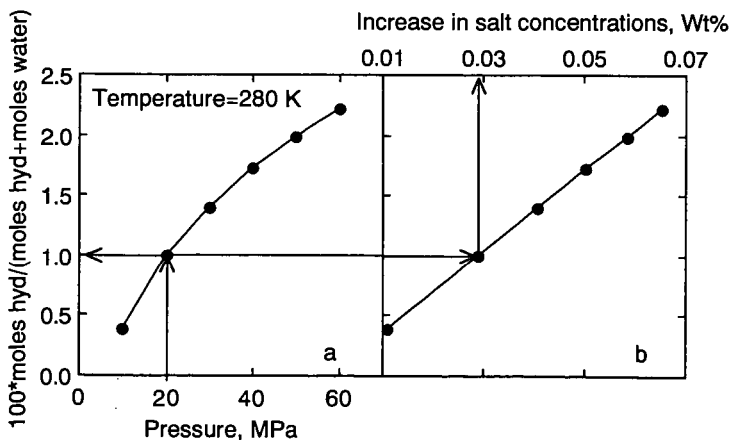


Figure-6 Percent hydrates formed from the dissolved methane and the increase in salt concentration.

KINETICS OF METHANE HYDRATE FORMATION IN PURE WATER AND INHIBITOR CONTAINING SYSTEMS

Tian-Min Guo and Jun-Hong Qiu
High Pressure Fluid Phase Behavior & Property Research Laboratory
University of Petroleum
Beijing, P.R. China 100083

Keywords: Kinetics, Methane hydrate formation, Brines

INTRODUCTION

The discovery of huge deposits of methane hydrate *in situ* (a possible energy source in the future), the production problems associated with the offshore oil/gas exploitation/transportation, and the new applications of hydrate technology have renewed interest in hydrate research in the past decade.

The two basic problems to be studied are the hydrate equilibrium thermodynamics and the hydrate formation/dissociation kinetics. Most of the papers published previously have been related to the former topic, a number of engineering applicable thermodynamic models has been developed, including recent models for salt-containing systems (Zuo et al., 1996; etc.). Compared to hydrate equilibrium thermodynamics, our knowledge on the kinetics of hydrate formation are far from mature. Due to the complexity of the dynamic process of hydrate formation, and the lack of consistent experimental data, a generalized kinetic model is not yet available. Since knowledge of the kinetics of hydrate formation is of critical importance in the transportation pipeline design, effective utilization of the methane hydrate resource *in situ*, and the various applications of hydrate technology, it has received increasing attention in recent years. Comprehensive reviews on the progress are available (Sloan, 1990; Makogon, 1981; Englezos, 1993; and Qiu and Guo, 1995).

The major objectives of this work are: (1) Measure the kinetic data of methane hydrate formation in the presence of pure water, brines containing single salt and mixed salts, and aqueous solutions of ethylene glycol (EG)/(salt + EG). (2) Develop a new kinetic model of hydrate formation for the methane + pure water systems based on a four-step formation mechanism and reaction kinetics approach. (3) Explore the feasibility of extending the proposed kinetic model to salt(s) and EG containing systems.

EXPERIMENTAL SECTION

Apparatus. It is well known that the specific equipment used in the study of hydrate formation kinetics has significant influence on the experimental results. There are basically two types of equipment, fixed boundary type and turbulent boundary type. The former is more suitable for simulating the hydrate formation/dissociation *in situ*, and the latter is closer to the conditions in the transportation pipelines and natural gas processing equipment. The apparatus used in this work belongs to the latter type. The schematic diagram of the experimental system is shown in Fig. 1, and the major parts are briefly described as follows:

Transparent sapphire cell: The 2.5 cm i.d. sapphire cell was purchased from the DB Robinson Design & Manufacturing Ltd. (Canada), the total volume and the effective volume (excluding the piston and stirrer volume) are 78 and 59 mL, respectively. The working volume of the cell can be adjusted by a floating piston driven by a positive displacement pump. The maximum working pressure and temperature are 20 MPa and 423 K, respectively.

Air bath: The air bath was manufactured by Shanghai Instruments Corp., the working temperature range is 263 ~ 373 K and can be controlled to within ± 0.2 K by a digital programmable temperature controller.

Agitation system: The agitation system consists of a magnetic stirrer coupled with a permanent magnet mounted outside of the cell. A variable speed DC motor equipped with an rpm-controller provides up and down reciprocating motion of the magnet.

Pressure measurement: The pressure in the cell was measured through pressure transducer and pressure gauge simultaneously. A differential pressure transducer (Honeywell Inc.) was connected with the data acquisition system. The precision of the DP transducer at the working span (0 ~ 10 MPa) is ± 0.1 %. A 0 ~ 25 MPa Heise pressure gauge was also installed for taking parallel pressure readings. The pressure measurement system was calibrated against a Ruska standard dead-weight gauge, and the precision of the pressure measurements is estimated at ± 0.015 MPa.

Experimental Procedure. The kinetics of hydrate formation can be studied in two modes: the constant temperature-constant pressure mode and the constant temperature-constant volume mode. In the former mode, to maintain constant system pressure, the hydrate former gas consumed in the hydrate formation process is continuously supplemented from outside. In the latter mode, the system is closed, with its volume kept constant, and the system pressure is lowered gradually in the hydrate formation process. The latter mode was applied in this study.

Prior to performing the experiment, the floating piston was lowered to the bottom of the sapphire cell and its position was unchanged during the measuring process. About 12 mL liquid sample was charged into the evacuated sapphire cell. When the system temperature stabilized at the preset value, methane was introduced into the cell until the pressure was raised to about 4.0 MPa. The gas was then discharged to eliminate the trace amounts of residual air in the cell. Methane was again charged until the preset initial

system pressure was attained, then the DC motor to actuate the magnetic stirrer was started with the stirrer was moving up and down at a rate of four strokes per minute. The system temperature and the change of system pressure were recorded through the data acquisition system every 30 seconds, and displayed on the monitor screen.

Experiments Performed. The systems studied and the corresponding operating conditions are summarized in Table 1. A total of 30 sets of kinetic data were measured for the following systems: methane + water, methane + water + salt(s), methane + water + EG, and methane + water + salt + EG.

Experimental Results. A typical pressure vs. time ($P \sim t$) curve measured for the methane hydrate formation process is shown in Fig. 2. The curve can be roughly divided into three zones. The first zone (from t_0 to t_s) is called the "gas dissolution zone", P_s stands for the system pressure when saturation of the dissolved gas is established. The second zone (from t_s to t_r) is called the "nucleation zone", system pressure remains nearly at constant in this zone. The time interval from t_0 to t_r is the so called induction period. The third zone, from t_r to t_d , is called the "crystal growth zone", in this zone the system pressure falls gradually from P_r to P_d and remains stabilized after time t_d . The three zones are divided rather arbitrarily, as in fact, nucleation could proceed simultaneously with the gas dissolution process. The relative time distribution of the three zones in the 30 experiments performed are also listed in Table 1. The detailed $P \sim t$ data for typical experiments are given in Table 3 and Figs. 3 ~ 5 along with the calculated results which are discussed below.

Analysis of the Experimental Results. From Table 1, it can be seen that the time interval of the gas dissolution period is, in general, 1 ~ 2 hours, however, the time interval of nucleation period differs appreciably for the experiments performed, from ~ 25 minutes (E04, E08, and E25) to ~ 5 hours (E16), and for some experiments (E01 and E20) no crystal nucleus was formed even after 10 hours. Since during the nucleation period, the liquid phase is in the metastable state, the nucleation process is sensitive to very small perturbations to the system. This caused difficulty in obtaining repeatable results even when the experiments were run under identical temperature and initial pressure conditions (E09a ~ E09c). The time period for crystal growth also differed significantly for experiments run under different operating conditions, from 80 minutes (E04) to more than 5 hours (E28).

Under the same operating temperatures, the initial pressure has little effect on the time interval of gas dissolution period (E01 ~ E04 and E05 ~ E09), however, its influence on the nucleation period is significant. In general, the lower the initial pressure, the longer of the nucleation period. Similar initial pressure effect was observed in the crystal growth period (E02 ~ E04 and E07 ~ E09).

The temperature effect on the time interval of gas dissolution and nucleation periods (under same initial pressure) is, in general, the higher the temperature, the longer the time period (E10 and E12, E08 and E11). The effect increases with the lowering of the initial pressure. Significant temperature effect was also observed in the crystal growth period; the time interval increase almost linearly with the increase of temperature, however, the temperature effect seemed not as sensitive to the initial pressure in this period.

The effects of inhibitors (salt/ethylene glycol) on the hydrate formation process are quite complex. When the concentration of the inhibitor is less than 1.0 mass%, the effect of concentration is not obvious on the time distribution of the three periods (E13 and E14, E17 and E18, E21 and E22).

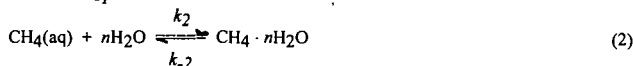
For concentrations greater than 1.0 mass%, the time interval of gas dissolution period is little effected by the inhibitor concentration, however, the concentration has significant effect on the time interval of nucleation period, the higher the concentration the longer the time interval (E15 and E16, E19 and E20, E23 and E24, E26 and E28). The order of inhibition effect is as follows (when concentration of inhibitor > 1.0 mass%): EG > NaHCO₃ > NaCl > (NaCl + NaHCO₃) > (NaHCO₃ + EG) > (NaCl + EG).

An interesting phenomenon observed in the experiments is that when the concentration of inhibitor is less than 1.0 mass% (E13, E14, E17, E18 and E25), the induction time (gas dissolution period + nucleation period) is significantly shorter as compared with the methane + pure water systems (run under similar temperature and initial pressure conditions). It is in consistency with the observation of Yousif et al. (1994), that the hydrate formation could be enhanced at low inhibitor concentration.

MECHANISM OF METHANE HYDRATE FORMATION

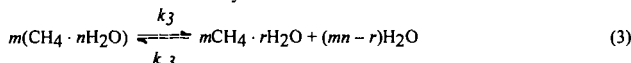
In this work, the mechanism of methane hydrate formation in pure water was described by the following four steps.

Step 1: A portion of the methane molecules in the gas phase dissolve into the aqueous phase, and the dissolved methane molecules are clathrated by n water molecules to form a metastable cluster (i.e. the water molecules comprising the clusters may be replaced by other water molecules in the bulk),



Following Long and Sloan (1993), the coordination number n was taken as 20. Since the structure of this labile cluster is similar to the 5^{12} hydrate cavity (Christiansen and Sloan, 1994), we assume their size is also similar, i.e. ~ 0.5 nm.

Step 2: The link of clusters to form a crystal unit.



It has been well established that methane forms structure I hydrate, the structure I hydrate crystal unit cell contains 46 water molecules, and consists of two 5^{12} and six $5^{12}6^2$ crystal cavities. The maximum number of methane molecules per unit cell is 8. Assume the crystal unit in Eq. (3), $m\text{CH}_4 \cdot r\text{H}_2\text{O}$, is an ideal crystal unit cell (with its cavities fully occupied), thus $m = 8$, and $r = 46$. It is also assumed that the size of the crystal unit cell $m\text{CH}_4 \cdot r\text{H}_2\text{O}$ is the same as the crystal unit cell of structure I hydrate, and is thus taken as 1.2 nm (van der Waals and Platteeuw, 1959). Since the size of the crystal unit is smaller than the critical size, some of the crystal units could be dissociated back to individual labile molecular clusters, and the others will be further linked to form a stable *crystal nucleus*, its size exceeding a certain critical size.

Step 3: Crystal units linked to form crystal nucleus N,



Englezos et al. (1987) proposed an equation for calculating the critical size of hydrate crystal nucleus. Based on the proposed equation, Natarajan et al. (1994) calculated the critical size of the methane hydrate crystal nucleus to be approximately 10–30 nm. That means, about 8–25 unit cells with a size of 1.2 nm are required to form a crystal nucleus of the critical size, i.e. $l = 8$ –25. Thus, approximately 64–200 methane molecules and 368–1150 water molecules are required to form a crystal nucleus of critical size.

Step 4: Crystal nucleus growing to form hydrate crystal H,



During the crystal nucleus growing period, hydrate crystals H with different sizes could be formed. Graauw and Rutten (1970) has measured the size distribution of propane hydrate crystals (structure II) in a continuous stirred tank crystallizer, the results showed that the crystal size is within 10–35 μm , the average being about 20 μm . Bylov and Rasmussen (1996), Monfort and Nzihou (1993) have also studied the crystal size distribution. Based on the size distribution data available, we can conclude that the size of the methane hydrate crystal is at least three times in magnitude larger than the size of the critical crystal nucleus. The magnitude of p and q in Eq. (5) should be 10^5 and 10^6 , respectively.

KINETIC EQUATIONS

For simplifying the derivation of the rate equations involved in the hydrate formation process, the following assumptions were made:

(1) The rate of concentration change of each component (r_i) in the reactions shown in Eqs. (1) to (5) can be expressed in the following polynomial form,

$$r_i = -\frac{dC_i}{dt} = kC_i^\alpha C_j^\beta \dots \quad (6)$$

where C_i and C_j represent the concentration (mol/L) of components i and j , α and β denote the order of concentration change.

(2) The order of concentration change is unity for all components ($\alpha = \beta = 1.0$).

(3) The water content in the aqueous phase is constant during the hydrate formation process.

(4) The volume of gas phase and liquid phase remain unchanged during the hydrate formation process.

Based on the above assumptions, the following rate equations can be derived:

$$\frac{dC_G}{dt} = -k_1 C_G + k_{-1} C_A \quad (7)$$

$$\frac{dC_A}{dt} = k_1 C_G - k_{-1} C_A - k_2 C_A + k_{-2} C_B - pk_5 C_A C_N \quad (8)$$

$$\frac{dC_B}{dt} = k_2 C_A - k_{-2} C_B - mk_3 C_B + mk_{-3} C_D \quad (9)$$

$$\frac{dC_D}{dt} = k_3 C_B - k_{-3} C_D - lk_4 C_D \quad (10)$$

$$\frac{dC_N}{dt} = k_4 C_D - k_5 C_A C_N \quad (11)$$

$$\frac{dC_H}{dt} = k_5 C_A C_N \quad (12)$$

where C_G stands for the apparent mole concentration of methane in the gas phase (mole of methane in gas phase per liter of liquid phase), C_A , C_B , C_D , C_N and C_H denote the concentrations (mol/L) of $\text{CH}_4(\text{aq})$, $\text{CH}_4 \cdot n\text{H}_2\text{O}$, $m\text{CH}_4 \cdot r\text{H}_2\text{O}$, N and H, respectively. Based on assumption (3), the concentration of water in the liquid phase does not appear in the rate equations. At initial conditions: $t = 0$, $C_G = C_G^0$, $C_A = C_B = C_D = C_N = C_H = 0$, from mass balance of methane we have:

$$C_G^0 = C_G + C_A + C_B + mC_D + lmC_N + (p + lm)C_H \quad (13)$$

Since C_G , C_A , C_B , C_D , C_N and C_H are restrained by Eq. (13), only five of the above six concentration variables are independent. The concentration of the metastable molecular cluster C_B was chosen as a dependent variable. From Eq. (13) we have:

$$C_B = C_G^0 - C_G - C_A - mC_D - lmC_N - (p + lm)C_H \quad (14)$$

Eq. (9) can then be removed from the rate equation set. Substituting Eq. (14) into Eqs. (8) and (10) yields:

$$\frac{dC_A}{dt} = k_{-2}C_G^0 + (k_1 - k_{-2})C_G - (k_{-1} + k_2 + k_{-2})C_A - mk_{-2}C_D - lm_{k_{-2}}C_N - (p + lm)k_{-2}C_H - pk_5C_A C_N \quad (15)$$

$$\frac{dC_D}{dt} = k_3(C_G^0 - C_G) - k_3C_A - (mk_3 + k_{-3} + lk_4)C_D - lm_{k_3}C_N - (p + lm)k_3C_H \quad (16)$$

The initial conditions are changed to: $t = 0$, $C_G = C_G^0$, $C_A = C_D = C_N = C_H = 0$.

Eqs. (7), (11), (12), (15) and (16) coupled with the corresponding initial conditions constitute the mathematical model of the kinetic behavior of methane hydrate formation in pure water.

THE LEAST SQUARE ESTIMATION OF THE KINETIC PARAMETERS

In the rate equations established in the previous section, there are eight unknown parameters: k_1 , k_{-1} , k_2 , k_{-2} , k_3 , k_{-3} , k_4 and k_5 . As k_1 and k_{-1} are restrained by the following expression of equilibrium constant K_c (derivation is referred to the expanded manuscript):

$$K_c = \frac{k_1}{k_{-1}} = \frac{C_w^0 Z R T V_l}{C_w^0 Z R T V_l} \quad (17)$$

where C_w^0 , Z and H denote the initial water concentration, compressibility of methane and Henry's constant of methane, respectively. k_{-1} can be calculated through k_1 as follows:

$$k_{-1} = \frac{k_1}{K_c} = \frac{k_1 H V_g}{C_w^0 Z R T V_l} \quad (18)$$

Thus, only seven unknown parameters (k_1 , k_2 , k_{-2} , k_3 , k_{-3} , k_4 and k_5) in the kinetic equations needed to be determined.

The damped nonlinear least square method was used for parameter estimation, the details of the algorithm are also given in the expanded manuscript (which is available on request). The regressed parameter values for the methane + water systems are tabulated in Table 2, and a typical comparison between experimental and calculated $P \sim t$ data for Experiment E09b is shown in Fig. 3.

TEST ON THE PROPOSED KINETIC MODEL

Sensitivity on Initial Pressure. Experiments E01 ~ E04 were run under the same temperature (273.65 K) and different initial pressures. Tests were performed on the prediction of the $P \sim t$ data of E01 ~ E03 based on the parameter values determined from E04. The test results show that, in the gas dissolution zone the deviations between experimental and calculated gas phase pressure are in the range of $-0.11\% \sim -0.50\%$; in the nucleation zone, the maximum relative deviations are -0.37% for E02 and E03, and 0.74% for E01 (no hydrate finally formed); and in the hydrate growth zone, the maximum relative deviation is -0.29% for E02 and E03. Typical comparison between the experimental and predicted $P \sim t$ curves for E01 is shown in Fig. 4.

Experiments E05 ~ E09 were also run at the same temperature (274.15 K) and different initial pressures. The $P \sim t$ data of Experiments E08, E09b and E09c were predicted by using the parameter values determined from E07. In the gas dissolution zone, the measured and calculated gas phase pressures are close, the maximum relative deviation is 0.38% . In the nucleation zone, the maximum deviations are -0.059% for E08, and 0.54% for E09b and E09c. In the crystal growth zone, the maximum deviations for E08, E09b and E09c are 0.78% , 1.01% and 0.52% , respectively.

The test results indicate that although the kinetic data of hydrate formation depend on the initial pressure, the model parameters determined from a specific run are capable of predicting the $P \sim t$ data of runs carried out at different initial pressures (under same temperature) with good accuracy.

Prediction of the $P \sim t$ Data for Salt/EG Containing Systems. The prediction of the kinetic data of methane hydrate formation in brines and aqueous solution of EG are of particular interest in real production processes and has not been previously reported. It is well known that the presence of salt(s) and alcohol in the aqueous phase can inhibit the hydrate formation (similar to the freezing point depression), as the solubility of methane will be significantly lowered, and the physical properties (viscosity, density, diffusivity, interfacial tension, etc.) of the aqueous phase will in turn be significantly changed. As a preliminary attempt to extend the proposed kinetic model to the salt/ethylene glycol containing systems, we assumed the solubility of methane in the aqueous phase (expressed in terms of the Henry's constant of methane) is the critical factor affecting the inhibition of methane hydrate formation. The larger the Henry's constant, the greater the inhibition effect.

Among the eight parameters in the proposed kinetic model, k_{-1} is the only parameter related to Henry's constant, hence, the other model parameters determined from methane + pure water system can be applied directly to the salt/ethylene glycol containing systems. For illustration purposes, the $P \sim t$ data of methane hydrate formation in 5.0 mass% NaCl solution (Experiment E16) were predicted by using the kinetic parameters determined from Experiment E09b performed on methane + pure water system (E16 and E09b were run at the same temperature and initial pressure conditions). The Henry's constant of methane in the 5.0 mass% NaCl solution at 274.15 K was taken from Cramer (1984), $H = 3.642 \times 10^3$. The comparison between the predicted and experimental results is presented in Fig. 5. Fairly good prediction results were observed, the maximum deviations of the predicted gas phase pressure are -0.13 % in the gas dissolution zone, and 0.31 % in the nucleation and crystal growth zones.

CONCLUSIONS

- (1) The new kinetic model developed from a four-step hydrate formation mechanism and reaction kinetics approach is capable of describing the $P \sim t$ data measured in this work.
- (2) Under identical temperature condition, the kinetic parameters determined for a specific initial pressure can be applied to estimate the $P \sim t$ data run at other initial pressures (within the pressure range of this study), the maximum deviation is within 0.3%.
- (3) The kinetic model developed for methane + water systems can be extended to inhibitor containing systems by replacing the Henry's constant of methane in corresponding aqueous phase.
- (4) As the dynamic behavior of hydrate formation is strongly dependent on the type of equipment and agitation intensity, the kinetic data measured in this work can only be considered as typical for a mildly agitated non-flowing system.

ACKNOWLEDGMENT

Financial support received from the China National Science Foundation, Postdoctoral Research Foundation and the China National Petroleum & Natural Gas Corporation are gratefully acknowledged.

REFERENCES

- M. Bylov and P. Rasmussen, A new technique for measuring gas hydrate kinetics, Proceedings of the 2nd International Conference on Natural Gas Hydrates, June 2-6, 1996, Toulouse, France, 259-266.
- R. L. Christiansen and E. D. Sloan, Mechanisms and kinetics of hydrate formation, Annals of the New York Academy of Sciences, Vol. 715 (1994) 283-305.
- S. D. Cramer, Solubility of methane in brines from 0 to 300 °C, Ind. Eng. Chem. Proc. Des. Dev., 23 (1984) 533-538.
- J. de Graauw and J. J. Rutten, The mechanism and the rate of hydrate formation, Proceedings 3rd Int. Symp. on Fresh Water from the Sea, 1970, Athens, 103-116.
- P. Englezos, N. Kalogerakis, P. D. Dholabhai and P. R. Bishnoi, Kinetics of formation of methane and ethane gas hydrates, Chem. Eng. Sci., 42 (1987) 2647-2658.
- P. Englezos, Clathrate hydrates, Ind. Eng. Chem. Res., 32 (1993) 1251-1274.
- J. Long and E. D. Sloan, Quantized water clusters around apolar molecules, J. Mol. Simul., 11 (1993) 145-161.
- Y. F. Makogon, Hydrates of Natural Gas (translated from Russian by W. J. Cieslewicz), PennWell, Tulsa, 1983.
- J. P. Monfort and A. Nzihou, Light scattering kinetics study of cyclopropane hydrate growth J. Crystal Growth, 128 (1994) 1182-1186.
- V. Natarajan, P. R. Bishnoi and N. Kalogerakis, Induction phenomena in gas hydrate nucleation, Chem. Eng. Sci., 49 (1994) 2075-2087.
- J.-H. Qiu and T.-M. Guo, Status of the kinetic studies on the hydrate formation/dissociation, J. Ind. & Eng. Chem. (China), 46 (1996) 741-756.
- P. Skovborg, H. J. Ng, P. Rasmussen and U. Mohn, Measurement of induction times for the formation of methane and ethane hydrates, Chem. Eng. Sci., 48 (1993) 445-453.
- E. D. Sloan, Clathrate Hydrates of Natural Gas, Marcel Dekker, New York, 1990.
- J. A. van der Waals and J. C. Platteeuw, Clathrate solutions, Adv. Chem. Phys., 2 (1959) 2-57.
- M. H. Yousif, R. B. Dorshow and D. B. Young, Testing of hydrate kinetic inhibitors using laser scattering technique, Annals of the New York Academy of Sciences, Vol. 715 (1994) 330-340.
- Y.-X. Zuo, S. Gommessen and T.-M. Guo, Equation of state based hydrate model for natural gas systems containing brine and polar inhibitor, Chinese J. Chem. Eng. (in English), 4 (1996) 189-202.

Table 1. Summary of the methane hydrate systems studied and the time distribution of three zones

Exp. No.	Aqueous phase*	Temp. (K)	Initial Press. (MPa)	Gas dissolution zone (min)	Nucleation zone (min)	Crystal growth zone (min)
E01	H ₂ O	273.65	4.47	100	645*	-
E02	H ₂ O	273.65	5.46	100	80	150
E03	H ₂ O	273.65	7.45	100	100	125
E04	H ₂ O	273.65	8.47	95	25	80
E05	H ₂ O	274.15	4.49	100	575*	-
E06	H ₂ O	274.15	5.10	105	510*	-
E07	H ₂ O	274.15	5.46	95	90	205
E08	H ₂ O	274.15	5.96	95	25	185
E09a	H ₂ O	274.15	6.46	105	195*	-
E09b	H ₂ O	274.15	6.46	105	105	160
E09c	H ₂ O	274.15	6.47	105	32	183
E10	H ₂ O	274.65	6.47	90	30	195
E11	H ₂ O	275.15	6.00	130	165	280
E12	H ₂ O	276.15	6.47	110	40	390
E13	NaCl (0.5)+H ₂ O	274.15	6.46	60	38	160
E14	NaCl (1.0)+H ₂ O	274.15	6.47	65	30	185
E15	NaCl (3.0)+H ₂ O	273.65	6.47	110	150*	-
E16	NaCl (5.0)+H ₂ O	274.15	6.45	110	325	150
E17	NaHCO ₃ (0.5)+H ₂ O	274.15	6.45	65	32	168
E18	NaHCO ₃ (1.0)+H ₂ O	274.15	6.46	65	30	200
E19a	NaHCO ₃ (3.0)+H ₂ O	274.15	6.47	115	210	195
E19b	NaHCO ₃ (3.0)+H ₂ O	274.15	6.48	115	200	200
E20	NaHCO ₃ (5.0)+H ₂ O	273.65	6.46	120	615*	-
E21	EG (0.5)+H ₂ O	274.15	6.47	110	340*	-
E22	EG (1.0)+H ₂ O	274.15	6.46	115	345*	-
E23	EG (5.0)+H ₂ O	273.65	6.47	115	25	185
E24	EG (10.0)+H ₂ O	273.65	6.47	120	505*	-
E25	NaCl (0.5)+ NaHCO ₃ (0.5)+H ₂ O	274.15	6.47	60	25	185
E26	NaCl (1.5)+ NaHCO ₃ (1.5)+H ₂ O	274.15	6.47	90	35	250
E27	NaCl (2.5)+ NaHCO ₃ (2.5)+H ₂ O	273.65	6.47	100	65	290
E28	NaCl (2.5)+ NaHCO ₃ (2.5)+H ₂ O	274.15	6.47	95	60	320
E29	NaCl (2.5)+ EG (2.5)+H ₂ O	273.65	6.47	90	55	235
E30	NaHCO ₃ (2.5) + EG (2.5)+H ₂ O	273.65	6.47	90	112	203

* Numbers in parentheses are mass percent of inhibitor; EG stands for ethylene glycol.

No hydrate crystal formed in this time period.

Table 2. Estimated kinetic parameter k_j values for various experiments on methane + water systems

Exp. No.	$k_1 \times 10^3$	$k_2 \times 10^2$	$k_{.2} \times 10$	$k_3 \times 10^3$	$k_{.3} \times 10^2$	$k_4 \times 10$	k_5
E02	33.99	135.1	45.37	0.3735	5.037	0.4297	6.626
E03	32.95	187.3	41.57	0.2669	8.527	0.1839	5.261
E04	19.46	12.13	28.48	1.470	5.386	4.097	10.93
E07	29.05	0.8026	6.543	6.374	9.195	10.94	4.976
E08	15.54	55.59	0.3661	0.01616	3.923	6.708	0.5876
E09b	14.15	0.03878	1.189	139.2	0.2266	0.7779	4.224
E09c	8.539	21.95	0.3699	0.03070	4.771	4.390	0.8824
E10	13.74	10.64	34.31	1.447	34.34	28.15	9.487
E11	21.28	0.9161	4.622	1.792	6.435	8.710	3.455
E12	10.22	94.46	3.016	0.02347	4.746	7.368	0.9024

Table 3. Comparison of the experimental and calculated gas phase pressure for the Experiments E09b and E16*

Experiment E09b				Experiment E16			
t (min)	P_{exp} (MPa)	P_{calc} (MPa)	Rel. Dev. (%)	t (min)	P_{exp} (MPa)	P_{calc} (MPa)	Rel. Dev. (%)
0.0	6.465	—	—	0.0	6.447	—	—
10.0	6.452	6.453	-0.018	15.0	6.430	6.431	-0.022
20.0	6.441	6.444	-0.040	30.0	6.417	6.422	-0.078
30.0	6.429	6.436	-0.110	40.0	6.412	6.418	-0.088
45.0	6.424	6.426	-0.034	55.0	6.405	6.414	-0.13
60.0	6.421	6.419	+0.036	75.0	6.401	6.410	-0.14
75.0	6.412	6.414	-0.034	95.0	6.400	6.408	-0.13
85.0	6.412	6.411	+0.013	110.0	6.399	6.407	-0.13
105.0	6.410	6.407	+0.049	135.0	6.399	6.406	-0.11
125.0	6.406	6.404	+0.028	150.0	6.399	6.405	-0.10
140.0	6.405	6.402	+0.040	170.0	6.398	6.405	-0.11
165.0	6.405	6.400	+0.082	200.0	6.398	6.403	-0.081
190.0	6.405	6.397	+0.120	230.0	6.397	6.401	-0.068
210.0	6.405	6.395	+0.150	260.0	6.397	6.399	-0.028
220.0	6.399	6.395	+0.065	290.0	6.396	6.396	+0.003
230.0	6.398	6.394	+0.066	350.0	6.395	6.392	+0.11
240.0	6.393	6.393	+0.004	410.0	6.394	6.378	+0.24
260.0	6.387	6.391	-0.066	445.0	6.392	6.372	+0.31
280.0	6.381	6.389	-0.120	480.0	6.382	6.367	+0.23
310.0	6.375	6.384	-0.140	515.0	6.376	6.361	+0.23
340.0	6.371	6.378	-0.120	540.0	6.372	6.356	+0.24
370.0	6.370	6.371	-0.022	575.0	6.368	6.350	+0.29

* Calculations for E16 were based on the parameter values determined from E09b.

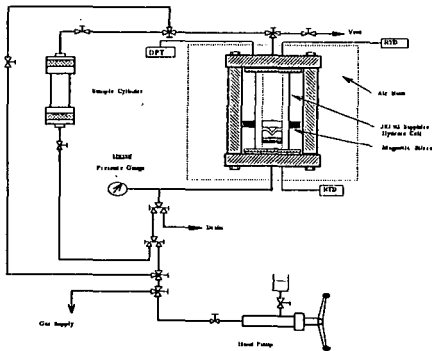


Fig. 1: Schematic diagram of the experimental system
 DPT—differential pressure transducer
 RTD—resistance thermocouple detector

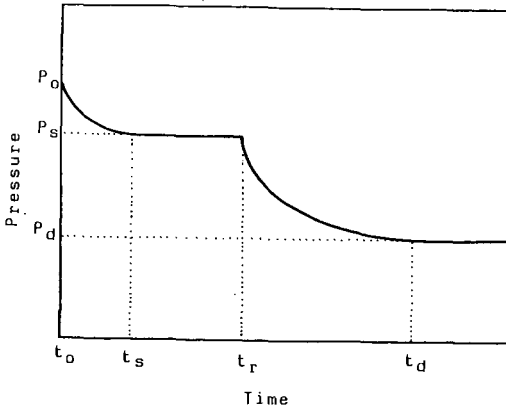


Fig. 2. A typical $P \sim t$ curve measured in this study

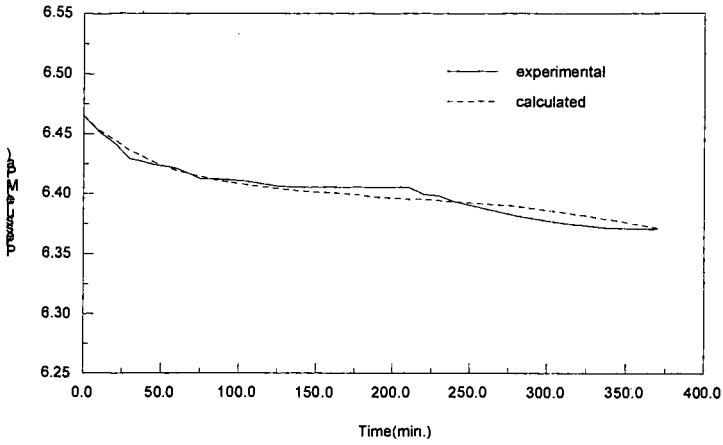


Fig. 3. The experimental and calculated $P \sim t$ curve for Experiment E09b

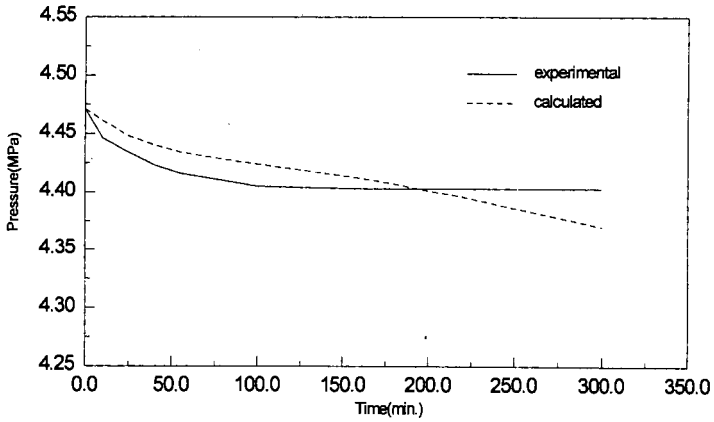


Fig. 4. The experimental and calculated $P \sim t$ curve for Experiment E01 (calculation based on the parameters determined for E04)

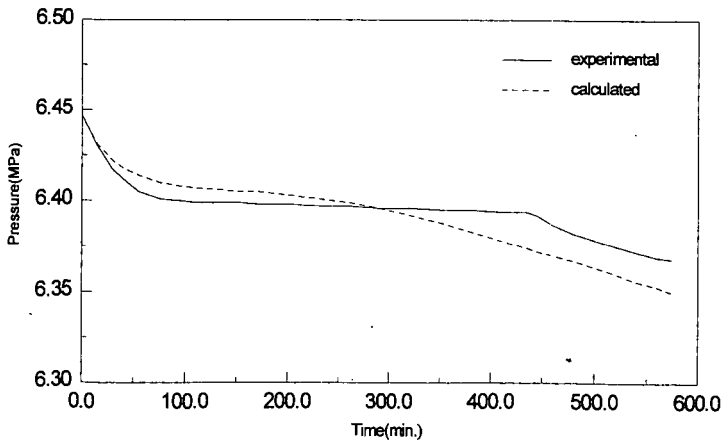


Fig. 5. The experimental and calculated $P \sim t$ curve for Experiment E16 (calculation based on the parameters determined for E09b)

"Experimental testing and evaluation of a kinetic gas hydrate inhibitor in different fluid systems"

Olav Urdahl¹, Are Lund², Lars Henrik Gjertsen¹ and Torstein Austvik¹

1 Statoil Research Centre, Field Development Technology, Postuttak, 7005 Trondheim, NORWAY

2 SINTEF, Applied Chemistry, 7000 Trondheim, NORWAY

*Corresponding author

Key words: hydrate inhibition, kinetic inhibitor, flowing system, performance

Introduction

The development of offshore mature basins such as the North Sea is increasingly characterized by marginal reservoirs. Feasible economic development of these reservoirs requires a shift towards total subsea production systems without fixed or floating production platforms. Unprocessed or minimum processed reservoir fluids will be transported to a central processing facility or ultimately to shore. One of the key issues of total subsea production systems is multiphase flow technology with particular emphasis on gas hydrate control technology.

Subsea transportation of unprocessed or minimum processed well fluids over long distances today requires the use of large amounts of methanol or glycols for hydrate inhibition. The effect of these additives is to decrease the water activity to an extent that markedly reduces its ability to participate in hydrate formation, and thereby in a lowering of the hydrate formation temperature. The amount of inhibitor necessary to obtain the desired lowering of the hydrate formation temperature is substantial, usually in the range of 20-40 weight% of the aqueous phase. This has prompted the search for new types of additives capable of inhibiting hydrate formation at far lower concentrations (1-5).

Statoil performs intensive research on hydrates; methods to prevent hydrate problems as well as studies on the formation and removal of hydrate plugs. This paper focuses on the robustness of a commercially available additive from T. R. Oil Services (Hytreat 525) with respect to degree of subcooling, pressure, salinity of the aqueous phase and the impact from having a defoamer or a corrosion inhibitor in the system. The inhibitor is tested both at continuous flow conditions and at re-starts after shut-ins. Results from tests on two different condensate systems as well as two crude oils are summarized.

Experimental

The experiments were carried out in a high pressure loop formed as a wheel. The system is illustrated in Figure 1. The test wheel was filled with the desired fluid at a specified temperature and pressure, and then set under rotation. The rotation creates a relative velocity between the pipe wall and the fluid thus simulating transport through a pipeline.

The high pressure wheel is made from stainless steel with an inner tube diameter of 52.5 mm and a wheel diameter of 2.0 m. The volume is 13.4 liters. The wheel includes two high pressure windows for visual inspection, and one of these is equipped with a video camera.

The flow simulator is placed in a temperature controlled chamber. The temperature is controlled using a programmable regulator, a heating fan and a refrigeration system. The temperature development in the chamber as a function of time is preset in the regulator.

The wheel is attached to a motor/gearbox system enabling a variation of the peripheral velocity of the wheel between 0.3 m/s and 5.0 m/s. A torque sensor is installed as a part of the rotational shaft enabling torque measurements to be performed during rotation. Pressure and temperature sensors on the wheel have ranges of 0-250 bara and -10 to +150 °C respectively. All signals are transferred through cables and slip rings to a real time PC-based data acquisition system.

The accuracy of the measurements is estimated to be ± 0.2 Nm for torque, ± 0.5 bar for pressure, ± 0.1 °C for fluid temperature in the wheel and ± 1.0 °C for temperature in the chamber.

Experimental procedure

1 Continuous flow

The wheel is rotated at a constant peripheral velocity (1.0 m/s) as the temperature is reduced from about 60°C to 4°C at a given cooling rate. In the following, these experiments are referred to as continuous flow experiments. In condensate systems without emulsifiers added, a velocity of 1.0 m/s creates separated liquid phases (prior to hydrate formation). The phases are generally mixed at this velocity when black oil systems are used.

2 Start-up

The system is cooled as the wheel is rotating (peripheral velocity of 1 m/s) to about 30 °C before the wheel is stopped. The wheel is then cooled to a temperature of 4°C and kept constant for a period of minimum 12 hours. The wheel do not move during this period. Then the wheel is restarted and rotated at a constant peripheral velocity of 1.0 m/s for the rest of the experiment. These experiments are referred to as start-up experiments.

In order to minimize the number of adjustable parameters for the experiments, only one given cooling rate is used both for the continuous flow experiments and the start-up experiments.

Results and discussion

The hydrate inhibitor tested in this work is a commercially available kinetic inhibitor consisting of a blend of different polymer/surfactants.

In this specific study the inhibitor was tested in the high-pressure system using two different crude oils and two gas condensates. Also the presence of a coorosion inhibitor or a defoamer on the performance was investigated for some of the fluid systems. Results from 27 experiments performed in the flow simulator with the different hydrocarbon fluids are presented. A summary of the experimental conditions and observations from these experiments is given in **Table 1**. It should be stressed that the subcoolings given in the **Table 1** have been corrected for the actual salinity of the systems. The results are discussed in more detail below.

Condensate A

Impact of corrosion inhibitor

Based on the visual information from the experiments the addition of the corrosion inhibitor changed the physical properties of the system with respect to foaming tendency. No significant change of performance of the hydrate inhibiting properties was observed. In all the inhibitor experiments there was a considerable kinetic effect but there was a decrease in transporability at hydrate formation compared to the pure system.

Impact of salinity

The salinity of the aqueous phase in these experiments was varied from 0-3,5 wt%. Increased salinity resulted in an increased delay of hydrate formation from 80 min to 20 hours. Previous studies (1,3,5) have shown that the optimal salinity for this inhibitor is approx. 3,5 wt%. The improved performance is due to conformational changes in the polymer systems in the inhibitor. A salinity of 0,25 wt% corresponds to the actual salinity of the produced water from the field.

Impact of subcooling

As seen from **Table 1** the subcooling in the experiments are varied from 9°C to 13°C. At continuous flow mode an addition of 0.5 wt% of the hydrate inhibitor prevented hydrate formation at a subcooling of approximately 9°C for the test period of 36 hours when the salinity was 0,25 wt%. Also restarts after a shut-in of 12 hours was successfully carried out at this temperature, although there were hydrates present in the system. However, at subcoolings above 9°C, the hydrate inhibitor tested was not able to fully prevent the hydrate formation during continuous flow. But in all the experiments hydrate formation was delayed compared to experiments on the blank Condensate A fluid.

Condensate B

Impact of subcooling

Experiments were here performed with a inhibitor concentration of 0.5 wt% of the aqueous phase . As seen from exp. 15, no hydrate formation were observed in this system at a subcooling of 11°C at a pressure of 70 bar within an experimental time of 80 hours. When the subcooling was increased to 13°C, hydrate formation was observed after 9 hours. When increasing the pressure to 140 bar (exp.16) keeping the subcooling constant at 11°C, hydrates were formed after 6 hours, and the flowloop plugged 1 hour after hydrate initiation. In these experiments the aqueous phase contained 3.5 wt% NaCl.

Crude oil A

The kinetic inhibitor was tested with and without the presence of a corrosion inhibitor both in continuous flow experiments and in shut-in experiments. In exp. 17-20 also a defoamer was present in the system.

Impact of defoamer and corrosion inhibitor

From **Table 1** one can observe from experiments 17-26 that the prescence of the defoamer reduces the performance of the hydrate inhibitor dramatically. For practical purposes it does not work at all.

During the continuous flow experiments without the defoamer present a significant delay of the hydrate formation was observed both with and without the presence of the corrosion inhibitor. At a subcooling of 11°C the presence of the corrosion inhibitor improved the performance compared to the system with only the hydrate inhibitor present. Hydrate formation was not initiated during a period of 60 hours.

In the start-up experiments, however, the induction time was reduced. Hydrates were formed during the stagnant period (12 hours), and the wheel was plugged shortly after restart.

The transportability of the hydrates formed was better in the presence of the corrosion inhibitor. This is opposite to what was observed for condensate A, and it illustrates the importance of fluid effects when this kind of technology is considered for use.

Impact of subcooling

The subcooling in the experiments was varied from 7°C to 13°C. The chemical was not capable of fully preventing the hydrate formation in any of the experiments. However, at subcoolings below 10°C the hydrates formed were transportable.

Crude oil A

Impact of subcooling

During continuous experiments at a subcooling of 7.3°C and 0.5wt% of hydrate inhibitor no hydrate formation was observed for almost 10 hours. The formation rate was then very slow for 2 hours before it increased rapidly resulting in a viscosity increase of the system. No hydrate plugging was observed.

In the start-up at a subcooling of 9.5°C, hydrates started to form very slowly after start-up. After approx. 4 hours the formation rate increased drastically and flow problems were observed due to the high viscosity of the system. However, no "solid" hydrate plug was observed in the experiment.

Fluid and flow dependency

The inhibitor were tested in 4 different fluids with different composition and physicochemical properties. The performance of the inhibitor is different for all these fluids. It is not possible to extrapolate the results from one condensate to another, or one black oil system to another. It is known the parameters like aliphatic/aromatic ratio, amount and state of asphaltenes and resins and also wax content will influence on the performance, and these factors will always vary between different fluids.

Regarding the influence of flow properties it has for all the systems investigated been shown that stagnant conditions are more difficult to handle than continuous flow. This aspect should be investigated further and will be addressed more thoroughly in a forthcoming paper.

Summary and conclusions

A commercially available kinetic hydrate inhibitor in a high pressure flowing system at various conditions and for different fluid systems. Also the presence of other production chemicals have been addressed. The conclusions can be summarized as follows:

- the defoamer has a negative effect. It reduces the performance to nearly zero.
- the corrosion inhibitor results in an increased mixing/emulsification of the system. This might be a benefit in some systems (black oils) but not in others (condensates).
- the salinity is crucial for the performance.
- the maximum subcooling to be handled is in the range 7-11°C depending on the fluid system.
- the effect of the inhibitor is reduced at stagnant conditions.

The results strengthen the knowledge that results from one fluid system should not be extrapolated to another. These kind of chemicals have to be qualified for each given fluid before they can be applied at real conditions.

Acknowledgements

The Statoil Multiphase Flow Program is acknowledged for giving permission to publish the results. T.R.Oil Services is acknowledged for supplying the kinetic hydrate inhibitor.

References

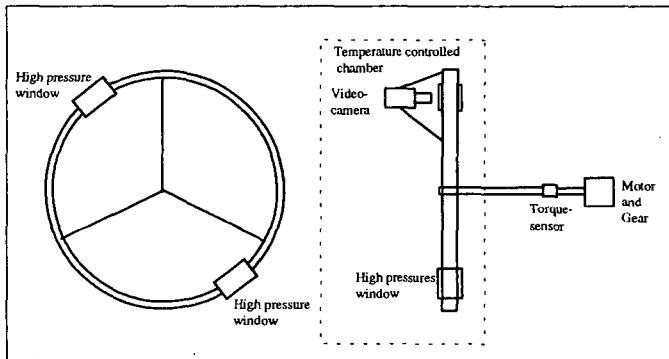
- (1) O Urdahl, A.Lund, P.Mørk and T.N.Nilsen. *Chem. Eng. Sci.*, **50** (5), 863-870, (1995).
- (2) A. Lund, O. Urdahl and S.S. Kirkhorn, *Chem. Eng. Sci.*, **51**(13), 3449-3458, (1996).
- (3) A. Lund, O. Urdahl, L.H. Gjertsen, S.S. Kirkhorn and F.H. Fadnes, Proceedings from the *2nd International Conference on Natural Gas Hydrates*", p. 407, Toulouse, France, July, (1996)
- (4) L.H. Gjertsen, T. Austvik and O. Urdahl, Proceedings from the *2nd International Conference on Natural Gas Hydrates*", p. 155, Toulouse, France, July, (1996).
- (5) A. Lund, O. Urdahl and S.S. Kirkhorn, *J. Pet. Sci. and Tech.*, Submitted.

Table 1: *Experimental conditions and observations from the experiments*

Exp.	Fluid	Inhibitor conc. (wt%)	Water cut (vol%)	Conc. of corr.inh. (ppm)	Salinity (wt%)	Mode	Sub cooling (°C)	Comments
1	Cond. A	0	20	-	0.25	Cont.	8.5	Hydrate formation started immediately and the pipe was plugged after 23 min.
2	Cond. A	0.50	20	800	0.25	Cont+start-up	13.0	Hydrate formation and plugging after 16 hours. Hydrate lumps and depositions at the window.
3	Cond. A	0.50	20	800	3.5	Cont+st.up	11.0	No hydrate formation observed during dynamic period. A hydrate plug formed during shut-in
4	Cond. A	0.50	20	800	3.50	Cont+start-up	11.0	A lot of foam in the condensate phase during dyn. conditions.. The foam broke down 5 hours after shut-in. Hydrate formation started after 9 hours. Plugged before restart.
5	Cond. A	0.50	20	-	0.25	Cont.	13.0	Foam observed in the condensate phase from start of experiment. Emulsification after 90 minutes and hydrate formation and plugging after 26 hours (dynamic conditions).
6	Cond. A	0.50	20	-	0.25	Cont+start-up	9.0	No hydrate formation observed during dynamic condition. 4 hours after shut-in hydrate formation started at interface growing into both condensate and aqueous phase. Loose hydrates. Smooth restart with minor depositions at the window.
7	Cond. A	0.50	20	-	0.25	Cont+start-up	11.0	Hydrate formation observed after 4 hours during dynamic conditions. Plugged before restart.
8	Cond. A	0.50	20	-	0	Cont.	10.5	No hydrate formation observed during the experimental time of 11 hours
9	Cond. A	0.50	20	-	0	Cont.	13.0	Hydrate formation and immediate plugging after 80 min.
10	Cond. A	0.50	20	-	3.5	Cont.	11	No hydrate formation observed for the experimental time of 25 hours.
11	Cond. A	0.50	20	-	3.5	Cont.	13	Hydrate formation and immediate plugging after 20 hours.
12	Cond. B	0	20	-	3.5	Start-up	14.5	Deposits and plugging within 11 min. after start of hydrate formation.
13	Cond. B	0.50	20	-	3.5	Start-up	13/15	No hydrate formation after 3 hours at 4°C. When temp. was lowered to 2°C rapid hydrate formation was initiated after 3.5 hours
14	Cond. B	0.50	20	-	3.5	Start-up	13	Rapid hydrate formation after 9.5 hours.
15	Cond. B	0.50	20	-	3.5	Cont.	11	No hydrate formation was observed within the experimental time of 80 hours
16	Cond. B	0.50	20	-	0	Start-up	11	Viscous emulsion after restart. Hydrate formation started 1.5 hours after restart.
17	Crude A	0	33	-	3	Start-up	13	Deposits at restart Plugging after 2 minutes.
18	Crude A	0.27	33	-	3	Start-up	13	Deposits at restart. Plugging after 1 minute
19	Crude A	0.27	33	-	3	Start-up	7	Hydrates formed 27 min. after restart Transportable hydrates but very viscous.
20	Crude A	0.50	33	-	3	Start-up	13	Hydrate deposits at restart. Plugging after 1 minute
21	Crude A	0	33	-	3	Start-up	10.5	Emulsion layer at the interface. Blocked 80 sec. after restart.

Exp.	Fluid	Inhibitor conc. (wt%)	Water cut (vol%)	Conc. of corr. inh. (ppm)	Salinity (wt%)	Mode	Sub cooling (°C)	Comments
23	Crude A	0.50	33	-	3	Cont.	11	Slow hydrate formation initiated after 7 hours. Formation rate increased later in the exp.
24	Crude A	0.50	33	-	3	Start-up	11.5	After stop of wheel the phases remained emulsified for 50 min. High formation rate 3 hours after start-up.
25	Crude A	33	0.50	800	3	Start-up	9	Droplets of water mixed in the oil phase. No hydrate formation for 68 hours. When subcooling was increased to 13°C the loop plugged.
26	Crude A	33	0.50	800	3	Start-up	11.2	Brown water phase during shut-in. Loop plugged 12 hours after restart.
27	Crude B	40	0	-	5	Start-up	7.6	Depositions and plugging 2 min. after start-up.
28	Crude B	40	0.5	-	5	Cont.	7.3	Slow hydrate formation initiated after 9.5 hours. More rapid formation after 11.5 hours and also large increase in viscosity.
29	Crude B	40	0.5	-	5	Start-up	9.5	No deposits observed at start-up, but slow hydrate formation observed. After 3.5 hours rapid hydrate formation occurs resulting in a very viscous system that nearly blocks the loop.

Figure 1: An illustration of the flow loop.



ENHANCED HYDRATE INHIBITORS: POWERFUL SYNERGISM WITH GLYCOL ETHERS

William D. Young, Jeff M. Cohen, and Philip F. Wolf
International Specialty Products
1361 Alps Rd., Wayne, NJ 07470

Keywords: Gas hydrates, hydrate inhibition, gas production

INTRODUCTION

Since natural gas hydrates frequently plug oil and gas production lines, various chemical and thermal methods have been developed to prevent hydrate formation. Conventional chemical treatment involves injecting 20-50 weight % methanol in the water phase at the wellhead or downhole to depress the freezing point of hydrates below the minimum fluid temperature in the line. However, high methanol injection rates are expensive and may exacerbate pipeline corrosion. Alternative chemical treatment methods are needed.

Recently Lederhos, et al¹ reported that certain water soluble polymers effectively inhibit hydrates at treatment levels of 0.1 to 1.0 wt% in the water phase, far less than required by methanol. At typical flowline conditions, these polymers slow the rates of hydrate nucleation and growth to such an extent that virtually no hydrates form in the wellstream during transport to processing facilities. Since the polymers slow hydrate formation rather than depress the freezing point, they are called 'kinetic inhibitors.' Under favorable conditions, kinetic inhibitors have prevented hydrates for more than 5 days. Industry field tests have demonstrated the viability of this technology.^{2,3}

The most successful of the kinetic inhibitors are vinylcaprolactam (VCL) and vinylpyrrolidone (VP) based polymers, including Gaffix VC-713, a terpolymer of VCL, VP, and dimethylaminoethylmethacrylate (DMAEMA), and PVCL homopolymer. In addition, PVP, although not as effective as VC-713 and PVCL, has been widely used because it costs less and provides adequate protection in less demanding applications.^{1,4}

ISP manufactures a full line of hydrate inhibitors including VC-713, PVCL, PVP and VCL/VP copolymers. These inhibitors are tested in the high pressure laboratory at realistic pipeline conditions. We have observed that several glycol ether solvents (for example, 2-butoxyethanol) significantly enhance the performance of the polymeric hydrate inhibitors. Better inhibitors provide lower polymer treatment levels and lower overall cost. This paper presents the results of our experimental study on hydrate inhibitors containing glycol ether solvents.

EXPERIMENTAL

The tests were conducted in a 300 ml stainless steel stirred reactor at high pressure and low temperature. A diagram of the apparatus is shown in Figure 1. Following the procedure of Long, et al,⁴ 30 stainless steel balls are placed in the bottom of the reactor to increase nucleation sites. The reactor is immersed in a refrigerated bath, which normally maintains temperature to within 0.5°F. The pressure in the reactor is controlled to within 5 psi by a programmable syringe pump. The pump displaces hydraulic oil into a piston cylinder which contains the hydrate-forming gas on one side and hydraulic oil on the other. The volume of oil displaced by the syringe pump to maintain constant pressure indicates gas consumption in the reactor.

The inhibitors were tested at 0.5 wt% dry polymer and 0.75 wt% glycol ether in the salt solution. In a typical experiment, 0.6 g dry polymer and 0.9 g glycol ether liquid were added to 120 g of a 3.5 wt%, filtered, synthetic sea salt solution and mixed for at least one hour. The resulting solution was transferred to the 300 ml reactor, sealed, and immersed in the temperature bath at 39.2°F (4°C). The pressure was then increased to 1000 psig with green canyon gas and held constant to within about 5 psi with the syringe pump. After the pressure reached 1000 psig, the reactor stirrer was turned on to 1000 rpm. The gas volume, as measured by the syringe pump, and the reactor pressure and temperature were recorded electronically at 1 minute intervals throughout the experiment.

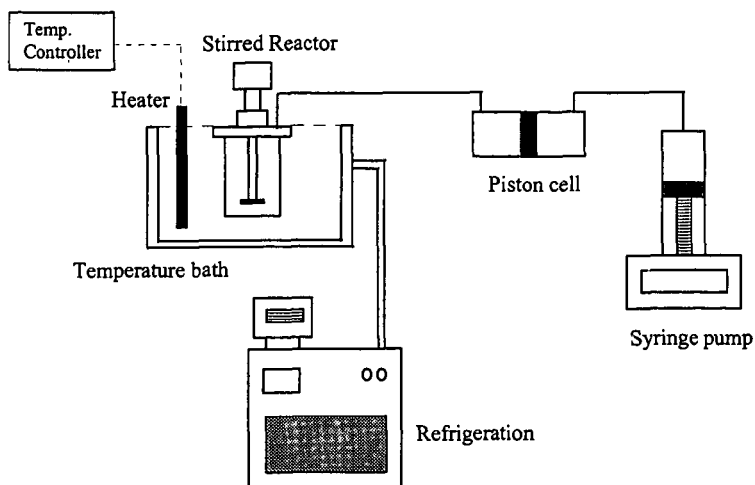


Figure 1: Gas hydrate test apparatus. The 300 ml reactor was charged with 120 g of sea salt solution containing 0.5% dissolved inhibitor. Tests were conducted at constant 39.2°F and 1000 psig for 20 hours. See text for more detail.

MATERIALS

Gaffix VC-713 is a terpolymer of VCL, VP, and DMAEMA. For consistency, all experiments reported here were conducted with the same manufacturing lot of VC-713.

Butyl Cellosolve, or 2-butoxyethanol, has the formula $n\text{-C}_4\text{H}_9\text{OC}_2\text{H}_4\text{OH}$. It is an industrial solvent with a boiling point of 171°C manufactured by Union Carbide. This material and the other glycol ethers listed in Table 2 were obtained from Aldrich and have a purity of about 99%.

The synthetic sea salt corresponds to ASTM 'Standard Specification for Substitute Ocean Water' and was purchased from Marine Enterprises of Baltimore, Maryland.

Green canyon gas is a typical natural gas mixture. It has the composition listed in Table 1.

Component	Mole %
nitrogen	0.4
methane	87.2
ethane	7.6
propane	3.1
isobutane	0.5
n-butane	0.8
i-pentane	0.2
n-pentane	0.2
total	100

Table 1: Green canyon gas composition

RESULTS AND DISCUSSION

Figure 2 shows the result of adding 0.75 wt% butyl Cellosolve to a mixture of 0.5 wt% VC-713 in sea salt solution. For comparison, the figure also shows the test results for 3.5 wt% sea salt solution with no inhibitor, 0.5 wt% VC-713 in sea salt solution, and butyl Cellosolve in sea salt solution. Each test was conducted at 39.2°F and 1000 psig. At these conditions green canyon gas has an equilibrium dissociation temperature of 64.7°F in deionized water, giving a total subcooling of 25.5°F. The gas consumption was calculated from measured volume change with the real gas law (compressibility factor = 0.83).

As the figure shows, this particular lot of VC-713 inhibits hydrates for only about 40 minutes at the test conditions. Adding 0.75 wt% butyl Cellosolve dramatically increases the performance of the inhibitor, to the extent that no detectable hydrates form for the duration of the 20 hour test. The figure also shows that butyl Cellosolve does not inhibit hydrates without polymer present.

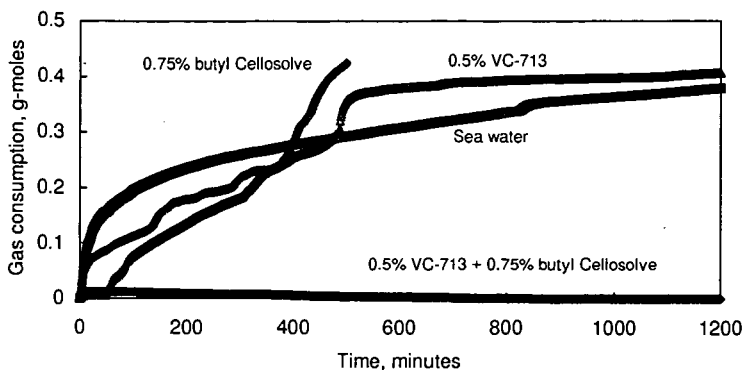


Figure 2: Hydrate inhibition test results at 39.2°F and 1000 psig (subcooling = 25.5°F). The aqueous phase is 3.5 wt% sea salt in all four tests. Concentrations are expressed as weight % in the aqueous phase.

Following up on the result with butyl Cellosolve, other glycol ethers with similar structures were tested at the same concentrations and conditions. Table 2 lists the observed induction times for each material, where induction time has been defined as the time at which detectable gas consumption begins, even if hydrate growth is slow beyond that point.

The data indicate that glycol ethers with 3 or 4 carbons in their alkoxy group significantly enhanced the performance of VC-713. Lower homologs did not appear to have any effect. Higher homologs were insoluble in the salt solution.

Glycol ether	Formula	Induction time (min)
2-butoxy ethanol	$n-C_4H_9OC_2H_4OH$	>1200
2-isopropoxy ethanol	$CH_3CH(CH_3)OC_2H_4OH$	800
1-propoxy-2-propanol	$C_3H_7OCH_2CH(CH_3)OH$	600
2-(2-butoxyethoxy) ethanol	$n-C_4H_9OC_2H_4OC_2H_4OH$	440
1-butoxy-2-propanol	$n-C_4H_9OCH_2CH(CH_3)OH$	450
2-propoxy ethanol	$n-C_3H_7OC_2H_4OH$	350
2-ethoxy ethanol	$C_2H_4OC_2H_4OH$	10
1-methoxy-2-propanol	$CH_3OCH_2CH(CH_3)OH$	10
none (sea water only)		0
none (VC-713 only)		40

Table 2: Induction times for 0.75 wt% glycol ether plus 0.5 wt% VC-713 in 120 g of sea salt water at 39.2°F and 1000 psig.

Butyl Cellosolve also showed strong synergism with other kinetic inhibitors. Table 3 compares the induction times for polyvinylcaprolactam homopolymer (PVCL) and 50/50 VCL/VP copolymer with and without butyl Cellosolve. Test conditions were identical to those described above.

Table 4 lists the surface tension of aqueous solutions of glycol ethers as reported in the manufacturer's literature.⁵ The data indicate that the higher homologs are surface active. If this hydrophobicity of the hydrocarbon chain also causes the chain to associate with the dissolved polymer, then the glycol ether may allow the polymer conformation to expand in solution. This could occur if the surfactant breaks the weak bonds between polymer segments which pull the coils together and tighten the conformation. An extended polymer would presumably have more of its length available for interaction with the crystal surface, which may account for its improved performance as a hydrate inhibitor.

Inhibitor (0.5%)	Induction times (minutes)	
	No additive	0.75% butyl Cellosolve
Gaffix VC-713	40	>1200
PVCL	0	>1200
50/50 VCL/VP	0	350

Table 3: Comparison of induction times for kinetic inhibitors with and without butyl Cellosolve added, at 39.2°F and 1000 psig in sea water solution.

Solvent	Mol. weight	Boiling point, °C	Surface tension at 25°C, for 25% aq. solution, by volume (dynes/cm)
methyl Cellosolve	76.1	124.5	54.3
Cellosolve	90.1	134.9	47.1
propyl Cellosolve	104.2	150.1	32.3
butyl Cellosolve	118.2	171.2	28.9

Table 4: Surface tension and other properties of the 2-alkoxy ethanol homologs. All data was obtained from manufacturer's literature.⁵

REFERENCES

- Lederhos, J. P.; Long, J. P.; Sum, A.; Christiansen, R. L.; Sloan, E. D., Jr., "Effective Kinetic Inhibitors for Natural Gas Hydrates," *Chemical Engineering Science*, 51 (8), (1996) 1221.
- Notz, K.; Bumgartner, S. B.; Schaneman, B. D.; Todd, J. L., "The Application of Kinetic Inhibitors to Gas Hydrate Problems," *27th Annual Offshore Technology Conference*, Houston, TX, 1-4 May 1995, 719.
- Bloys, B.; Lacey, C.; Lynch, P., "Laboratory Testing and Field Trial of a New Kinetic Hydrate Inhibitor," *27th Annual Offshore Technology Conference*, Houston, TX, 1-4 May 1995, 691.
- Long, J.; Lederhos, J.; Sum, A.; Christiansen, R.; Sloan, E. D., "Kinetic Inhibitors of Natural Gas Hydrates," *Proceedings of the Seventy-Third GPA Annual Convention*, New Orleans, LA, 7-9 March 1994, 85.
- Union Carbide, *Glycol Ethers*, (1993).

THE EFFECT OF IMPURITIES ON ETHANE HYDRATE INDUCTION TIMES

Martin Bylov
Calsep A/S
Gl.Lundtoftevej 7, 2800 Lyngby
Denmark

Peter Rasmussen
Department of Chemical Engineering, The Technical University of Denmark
Building 229, 2800 Lyngby
Denmark

Keywords: Hydrates, Induction Time, Growth Rate.

ABSTRACT

Three series of ethane hydrate formation experiments have been performed. The first series was carried out at 14 bar and 3 °C. Very scattered induction times (40,000 to 340,000 seconds) and less scattered growth rates were observed. Before the next series the cell was cleaned very thoroughly. With similar experimental conditions the induction time was longer than three weeks after which period of time the pressure was increased to 21 bar. Scattered induction times (10,000 to 150,000 seconds) and slightly higher growth rates were obtained. The third series was carried out at 20 bar and with 20 mg of impurities added. Short induction times and slightly lower growth rates were observed. All the experiments have been simulated using the hydrate kinetics model proposed by Skovborg (3). The experiments lead to the overall conclusion that impurities almost eliminate the induction time. This should be considered when transferring laboratory results to field conditions.

INTRODUCTION

The original scope of the presented experimental work was to establish an experimental procedure which would result in reproducible induction times. In the work by Skyum (1) and Andersen (2) numerous ethane hydrate experiments were carried out. Between each experiment the cell was opened, emptied and cleaned. Under seemingly identical conditions, large variations in the induction times were observed. It was assumed that a random amount of dust/dirt would be present in the cell in each experiment resulting in the observed variations in the induction times. Consequently it was decided to keep the cell closed between experiments thus having the same amount of dust/dirt in the cell throughout the measurement series.

EXPERIMENTAL SETUP AND PROCEDURE

The experimental setup is outlined in figure 1. The cell is a stainless steel container with a volume of 66.5 cm³. Sapphire windows are placed on two opposing sides. The cell is closed with a lid, through which the gas and water are lead to the cell. The pressure sensor is placed in the lid while the temperature sensor is placed in an oil filled pocket in the cell. The temperature in the cell is controlled by flowing a water/ethanol mixture through the cooling jacket. The cell is placed on top of a magnetic stirrer, that can rotate a teflon coated magnetic rod in the cell. The maximum working pressure of the cell is 60 bar.

Before the first experiment in a series, the cell is cleaned and then evacuated. The desired amount of water is introduced and the pressure is increased to the desired level using ethane gas. The cooling flow is started and gas hydrates will eventually form. When no further gas hydrate formation takes place, the cooling flow is stopped. The cell with content is left for 4-5 hours to dissociate all formed hydrates and to heat up the cell to ambient temperature. The cooling flow is then restarted, and a new experiment can start.

RESULTS - SERIES 1

Before the first series the cell was cleaned in the same way as used by Skyum (1) and Andersen (2). This means rinsing with distilled water and drying using compressed air. The cell was evacuated and loaded with 20 cm³ of distilled water and ethane at 21°C. Series 1 was started with a temperature setting of 3 °C. Figure 2 shows the pressure transient and part of the temperature transient of the first experiment (M6). The pressure initially drops from 15.3 bar to 14.0 bar due to the reduction in temperature from 21 °C to 3 °C. The pressure and the temperature then remain constant until the end of the induction time. As hydrates start to form the pressure drops dramatically due to gas consumption and there is a small increase in the temperature due to the heat evolved. The course of events in experiment M6 is representative for all the experiments in series 1 and 2.

A total of 11 experiments is included in series 1 and the results are shown in table 1 and in figure 3. The induction time is here defined as the time that elapses from the cooling flow is started and until the pressure starts to drop due to hydrate formation. To calculate the amounts of hydrate formed within 600 and 3600 seconds respectively after the induction period, the computer program HYLAB

has been used. The HYLAB program is essentially based on the gas hydrate kinetics model proposed by Skovborg (3):

$$\frac{dn}{dt} = k * A * c_{w0} * (x_{int} - x_b) \quad (1)$$

- dn/dt : Gas consumption rate.
k : Mass transfer coefficient.
A : Gas/water interfacial area.
 c_{w0} : Molar concentration of water in the water phase.
 x_{int} : Mole fraction of gas in water phase at the gas/water interface in equilibrium with the gas phase.
 x_b : Mole fraction of gas in the water phase in equilibrium with the gas hydrate.

In principle the model requires knowledge of the product $k * A$ to be able to calculate the gas consumption rate and the pressure drop with time.

When analysing experimental data as here the model is rearranged to allow a measured pressure drop to be converted into a gas consumption rate giving as the results the amount of hydrate formed and the product $k * A$.

The induction time varies between 38209 seconds and 341430 seconds whereas the growth rates are much more uniform.

RESULTS - SERIES 2

After discovering that simply keeping the cell closed between experiments thus keeping the composition constant did not yield reproducible induction times it was decided to try to eliminate the effect of presence of impurities. The cell was consequently cleaned much more thoroughly using only double distilled water and drying with dust free paper. Similar conditions to those used in series 1 were established. More than three weeks (~2,000,000 seconds) passed after pressurizing the cell and no hydrates were formed. The pressure was then increased to 21 bar. Approximately 38500 seconds later hydrates eventually formed. Series 2 comprises this and five more experiments at 3 °C and 21 bar. The results are shown in table 2 and in figure 3. Not surprisingly the growth rates were higher in series 2 than in series 1. The induction times were on the average lower (table 4) but still very scattered

RESULTS - SERIES 3

The results in series 1 and 2 showed that even minor amounts of impurities have some effect on the induction time. Consequently it was decided to add a large amount of impurities to the system to make it insensitive to addition of further impurities. It was decided that the "composition" of the added impurities should to some degree match the solid material found in multiphase pipelines. The impurities consist of equal amounts of $CaCO_3$, $BaSO_4$, rust and asphaltenes. Before addition of water and gas to the cell, 20 mg impurities was added and conditions similar to those of series 2 were established. The course of events in the experiments of series 3 differs drastically from that of the other experiments. In series 3 the pressure initially not only drops due to reduction in temperature but also because hydrates were formed shortly after the hydrate equilibrium temperature is reached. The observed induction time in table 3 is the time from the beginning of cooling until some hydrate particles were seen. In table 3 is also listed the time it takes before the conditions in the cell are favourable for hydrate formation from an equilibrium model (4) point of view. It can be seen that hydrates were often observed before the conditions for their formation were favourable. This cannot be contributed to low accuracy in the gas hydrate model used, but rather to the fact that there is some time delay in the temperature measurement. In all experiments performed in the cell the pressure start dropping for approximately 30 seconds before any change in the temperature is seen. For that reason it seems likely that gas hydrates start to form shortly after the actual conditions in cell are favourable for their formation.

DISCUSSION

The results in series 1 and 2 indicate that induction times are very hard to reproduce even under seemingly identical conditions. Series 3 indicates that addition of large amounts of impurities almost eliminates the induction time. It is however difficult from the present data to say whether the standard deviation on the induction times in series 3 is as large as for the other experiments. Comparison between the observed induction times in series 3 and the time after which the hydrate formation is favourable could indicate that the induction times also in this case are scattered, though very short.

The growth rates are for all series much less scattered than the induction times and thus easier to compare. It is no surprise that the growth rate in series 2 is larger than in series 1 since the driving

force for hydrate formation is considerably higher. Expressed in terms of the Skovborg model, the difference $x_{in} - x_b$ is larger in series 2 ($\sim 3.7 \cdot 10^{-4}$) than in series 1 ($\sim 1.8 \cdot 10^{-4}$).

When looking at the average $A \cdot k$ which is needed to describe the experiments in series 1 and 2, it is interesting to note that a smaller value applies for series 2. One must assume that the interfacial area is the same in both series, i.e. k must differ. This observation has two possible explanations. Either the mass transfer coefficient is pressure dependent or the mass transfer of ethane from the gas phase to the water phase is not the only significant kinetic step. If for example the building up of gas hydrate crystals is also a significant kinetic step, one must assume that x_b will be higher than predicted from a gas hydrate equilibrium point of view. If x_b is in fact higher than predicted by the model, an analysis of the data assuming equilibrium between the water phase and the hydrate phase will result in a higher value of $A \cdot k$ as it is the case in series 1 compared to series 2. This could suggest that when the driving force for hydrate formation is small, the building up of crystals is a significant step, whereas it becomes less significant for larger driving forces.

When analysing the amount of hydrate formed in series 3 it is seen that during the first 600 seconds it is even lower than the results obtained in series 1, whereas at later times the results are comparable to those of series 2 (table 4). The explanation is probably that the driving force for hydrate formation is small in the beginning of the series 3 experiments and the conditions of the experiments resemble those of series 2 at later stages. In series 3 the standard deviation on the amount of hydrates formed is higher compared to the previous series, indicating that impurities in some way make the growth rate more random.

One can also observe that the average $A \cdot k$ gets smaller as more hydrates are formed. This is most likely due to the reduction of the interfacial area caused by formation of a hydrate slurry layer between the two fluid phases.

CONCLUSIONS

Reproducing induction times in "clean" laboratory conditions seems very difficult if not impossible. Deliberate addition of impurities to the system seems to eliminate the induction time. Extreme caution should therefore be taken when operating a multiphase pipeline under conditions favourable for hydrate formation. Kinetic inhibitors that supposedly prolong the induction time should be evaluated also in the presence of considerable amounts of impurities.

The experiments reveal that the growth rate depend on the driving force. This may either be interpreted as a pressure dependence of the parameter k in the model by Skovborg or it may indicate that the building up of crystals is also a significant kinetic step. From the present experiments it is not possible to say which explanation is correct.

When analysing kinetic experiments one should consider that the system investigated may not be in thermal equilibrium at all times.

ACKNOWLEDGMENT

We are grateful to KSLA-ST/2, Amsterdam, The Netherlands for lending us the measurement cell, and to K.S. Pedersen, Calsep A/S for many productive discussions.

REFERENCES

- (1) Skyum L., 1995, "Hydrate Kinetics", M.Sc. Thesis, Department of Chemical Engineering, The Technical University of Denmark.
- (2) Andersen B.D., 1995, "Formation of Gas Hydrates", M.Sc. Thesis, Department of Chemical Engineering, The Technical University of Denmark.
- (3) Skovborg P. and Rasmussen P., 1994, "A Mass Transport Limited Model for the Growth of Methane and Ethane Gas Hydrates", Chem. Eng. Sci., **49**, 1131-1142.
- (4) Munck J., Skjold-Jørgensen S. and Rasmussen P., 1988, "Computations of the Formation of Gas Hydrates", Chem. Eng. Sci., **43**, 2661-2672.

Series 1 Experiment No.	Induction time /s	Moles of hydrate formed in 600 s.	Moles of hydrate formed in 3600 s.
M6	38209	0.0247	0.0804
M7	41827	0.0229	0.0792
M8	60066	0.0205	0.0768
M9	45509	0.0245	0.0802
M10	155361	0.0222	0.0786
M12	104444	0.0230	0.0797
M13	298416	0.0134	0.0631
M14	341430	0.0216	0.0785
M16	106390	0.0233	0.0804
M17	117085	0.0243	0.0807
M18	77961	0.0188	0.0733

Table 1. Results of series 1. T = 3 °C. Hydrate formation starts at 14 bar.

Series 2 Experiment No.	Induction time/s	Moles of hydrate formed in 600 s.	Moles of hydrate formed in 3600 s.
M20	38489	0.0294	0.1112
M21	147025	0.0262	0.1097
M22	67392	0.0275	0.1003
M23	122524	0.0313	0.1139
M24	47379	0.0222	0.1027
M25	10096	0.0269	0.0960

Table 2. Results of series 2. Thoroughly cleaned cell. T=3 °C. Hydrate formation starts at 21 bar.

Series 3 Experiment No.	Observed Induction time/s	Time for favourable hydrate conditions /s.	Moles of hydrate formed in 600 s.	Moles of hydrate formed in 3600 s.
M30	280	285	0.0183	0.0892
M31	239	290	0.0148	0.0822
M32	229	230	0.0248	0.1038
M33	174	205	0.0193	0.0990
M34	227	235	0.0168	0.0778
M35	220	215	0.0243	0.01095
M36	233	185	0.0239	0.01029

Table 3. Results of series 3. Initial conditions similar to those of series 2.

	Moles of hydrate formed in 600 s.	Moles of hydrate formed in 3600 s.	Induction time/s
Series 1 Average	0.0217	0.0774	126063
Series 1 Standard dev.	15.2%	6.7%	81.6%
Series 1 Average k^*A cm ³ /s	0.40	0.31	-
Series 2 Average	0.0273	0.1056	72151
Series 2 Standard dev.	11.3%	6.6%	72.7%
Series 2 Average k^*A cm ³	0.22	0.17	-
Series 3 Average	0.0203	0.0949	-
Series 3 Standard dev.	19.8%	12.6%	-
Series 3 Average k^*A cm ³	0.26	0.17	-

Table 4. Key results of the three measurements series.

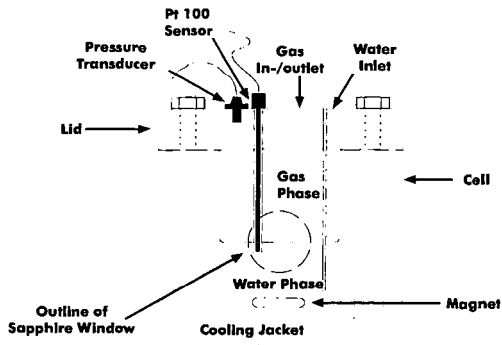


Figure 1. The Experimental Apparatus.

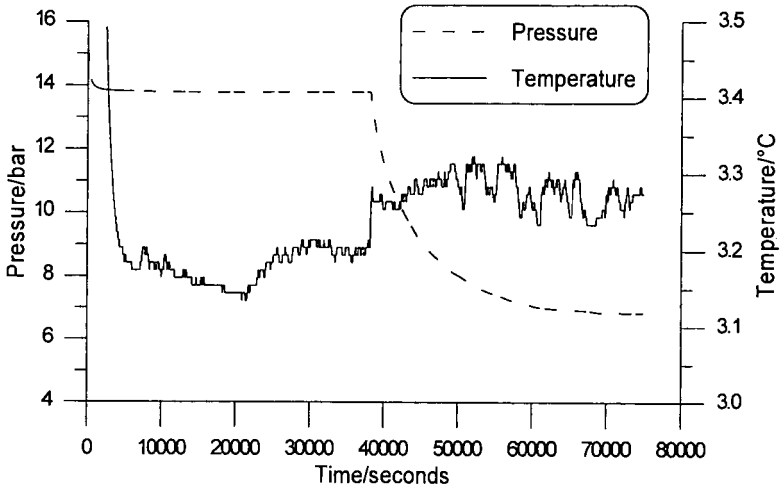


Figure 2. Pressure and temperature vs. time in a typical experiment (M6).

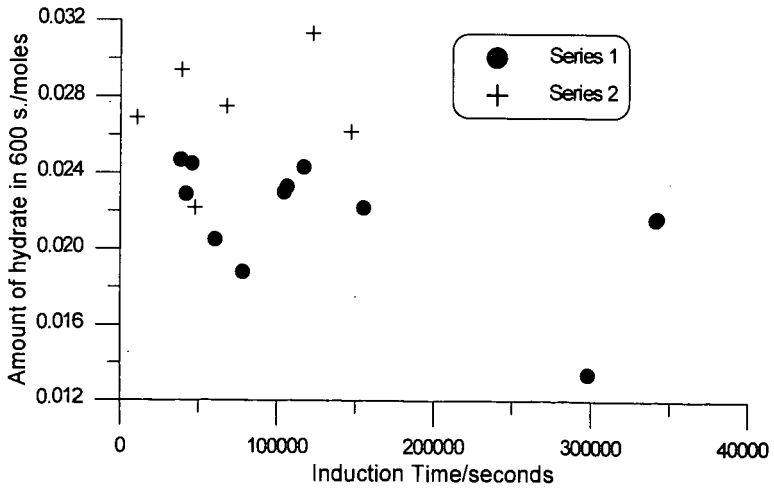


Figure 3. Growth rate vs. induction time for series 1 and 2.

AN EXPERIMENTAL STUDY OF HYDRATE CRYSTAL GROWTH FROM METHANE, CARBON DIOXIDE, AND METHANE+PROPANE MIXTURES

S.-Y. Lee, E. McGregor, and G. D. Holder
University of Pittsburgh
Chemical and Petroleum Engineering Department
Pittsburgh, PA 15261

Keyword: Gas Hydrates, Methane, Pipelines

Introduction and Background

Gas hydrates are crystalline inclusion compounds composed of water and natural gas in non-stoichiometric ratios varying from 5.67 to 17 water molecules per hydrated gas molecule (Holder, Zetts and Pradham, 1988; Sloan, 1990). Hydrate crystals represent one of the few phases and perhaps the only condensed phase where water and light non-polar gases exist together in significant proportions and are of particular interest to the petroleum and natural gas industries because of their potential as a separating agent, their potential as a storage vehicle and their undesired ability to plug gas transportation lines (Holder and Enick, 1995).

Gas-water mixtures will form crystals which coat the walls of and potentially plug gas transportation lines causing the cessation of gas or gas+oil flow (Lingelem, Majeed and Stange, 1994). When producing oil or gas, one goal of industry is to understand the conditions under which operation is possible without plugging. One such operating condition is where the hydrates are thermodynamically unstable. Such conditions are generally present when operating at temperatures above 25 C, although the temperature depends upon pressure, usually 50-200 Mpa, and gas composition, usually 95+% methane. Sufficiently high temperatures are generally not present when producing gas in offshore operations, because deep ocean waters are seldom warmer than 4-8 C. To prevent hydrate formation operators will generally inject methanol which acts as an antifreeze and destabilizes hydrates. Effective methanol concentrations are generally 10-50%, by weight, of the water+methanol liquid.

Sometimes, it is not desirable or possible to operate at conditions where hydrates are thermodynamically unstable. Such conditions may occur if methanol injection facilities fail or in cases where methanol injection and recovery are prohibitively expensive. In such cases it is desirable to understand for what duration, operation of a gas transportation line is possible without the complete plugging of the line by hydrates. To more completely understand this question, the rates at which hydrates form must be understood. The process includes the nucleation of hydrates on a heterogeneous surface, such as the pipewall, and the growth of these hydrates towards the center of the pipeline. This scenario for hydrate growth is deemed most likely for two reasons. First, the pipewall is generally the coldest part of the transportation line and hence the location where hydrates are most thermodynamically stable. Second, the formation of crystalline hydrates normally requires a solid nucleation site and the pipewall is generally the only source of such sites. Crystals can subsequently abraid from the pipewall and be transported down the pipeline, but such abraided crystals are not expected to be the primary cause of initial flow constriction.

In the present study, we determine the rates at which hydrates nucleate and grow on the surface of a cold pipewall over which gas is flowing at rates comparable to those which might exist in a pipeline.

Experimental

The apparatus for studying the precipitation and growth of solids is a variation of that described elsewhere (Figure 1 Holder and Enick, 1995). The apparatus consists of two coaxial cylinders. Hydrates form in the annular space by growing radially inward from the cooled outer wall. To form hydrates, the temperature controlled vessel is pressurized with the appropriate gas, 100-150 ml of water are injected and the inner cylinder rotated. The vessel can be operated in a vertical position as shown in Figure 1 or in a horizontal position. For these experiments a horizontal

position was used exclusively. The fundamental improvement of this apparatus relative to cells used in the past is that gas will flow in the annular space over the hydrate formation surface rather than remaining static. This will provide a means of investigating the effects of gas shear stress at the hydrate forming surface in pipelines.

Temperature gradients within this vessel are established by flowing methanol/water mixtures from separate isothermal baths through cooling coils on the outside of the vessel and the inner cooling chamber. The water in the vessel would coat the rotating inner cylinder, evaporate, and condense on the inside of the outer cylinder.

A temperature gradient was established across the annular gap. The surface of the water was then in direct contact with the flowing methane at 273K - 275K. Hydrates began to form inside the outer cylinder. Pressure decreased as the methane from the gas phase entered the hydrate phase and was used to deliver the amount of water converted to hydrate.

Experiments continued until either 1) the pressure of the methane remained constant, indicating that hydrate formation had ceased or 2) the rotation of the inner cylinder ceased because small amounts of hydrates clogged the bearings and friction surfaces. The system was then depressurized and the hydrate crystals examined before they had an opportunity to completely dissociate. The hydrates formed a relatively uniform layer of frost-like solid in the annular gap.

Results

We have measured the linear growth rate of hydrates formed from pure methane, pure carbon dioxide, two mixtures of methane+propane whose compositions were (95% methane and 5% propane) and (97% methane and 3% propane). The important variables in these studies were gas flow rate, gas composition, temperature, and pressure. Table 1 lists the results.

Gas flow rate: Higher gas flow rates (reported as RPM) tend to produce higher rates of hydrate formation. This is because the higher gas flow rates dissipate the considerable heat release generated during hydrate formation (50-100 kJ per mole of hydrated gas) and because the higher gas flow rates improve the mass transfer of water to the hydrate forming surface. It is still not clear which of these factors is most significant. However, the effect of gas flow rate appears to level off at the highest rates. This means that mass and heat transfer are no longer limiting and a true kinetic value for hydrate growth is obtained. The higher gas flow rates used here are comparable to pipeline Reynolds numbers in excess of 10,000 and thus these conditions are those that might be obtained in an actual gas pipeline.

Gas composition: It was observed that no clear difference in growth rates for the 95% methane and 97% methane mixtures were observed, but rates for gas mixtures and for carbon dioxide were faster than for pure methane. The methane hydrate is the least thermodynamically stable and it appears that the thermodynamic driving force (difference between the equilibrium temperature and the actual experimental temperature at the hydrate surface) affects the rate at which hydrates form. Another factor which may be important is the ability to stabilize the large cavity of the hydrate structure. Propane stabilizes the large cavity of structure II better than methane and carbon dioxide stabilizes the large cavity of structure I better than methane. The ability to stabilize the large cavity may play a role in the kinetics. The current experimental evidence is not conclusive on this issue.

Another variable of interest for the methane+propane mixtures is that the gas composition changes as the hydrates form since the propane concentration in the hydrates is much higher than in the gas phase. As more hydrates form a eutectic mixture of methane and propane containing less than 1% propane should be present. This mixture should result in the simultaneous formation of both structure I and structure II hydrate.

Temperature: In general, temperature is thought to increase the rate of any kinetic process. However, higher gas temperatures decrease the thermodynamic driving force and will tend to impede the rate.

Pressure: The range of pressures used was small, but the results indicate that higher pressures increased the rate of hydrate formation.

Inhibitors: Both WAX and PVP reduced the rate of hydrate formation to negligible values when present. Both were applied to the inside surface of the outer cylinder prior to hydrate formation.

The overall correlation for growth rate for both methane + propane mixture is

$$\text{linear rate} = 0.001535 (\text{RPM}) + 9.3 \times 10^{-6} (\text{P/KPA}) \\ - 0.0178 (\text{Cooling Coil (T/K)}).$$

This correlation has a R^2 of 0.75.

Conclusion

The rates of hydrate formation along pipe walls will likely be comparable to the rates measured in this study. Linear growth rates of 0.2 cm/hr are likely to represent the maximum growth rate that could be expected in gas transportation lines. As the hydrates thicken, they can serve as insulators of the line which will result in slower cooling of the produced fluids (which come out of the earth at higher temperatures than exist in the transportation line). The insulation will produce higher transportation temperatures and could either enhance or inhibit hydrate formation rates.

Based upon the rates measured here, transportation lines could be operated for hundreds or thousands of hours prior to their blockage by hydrates.

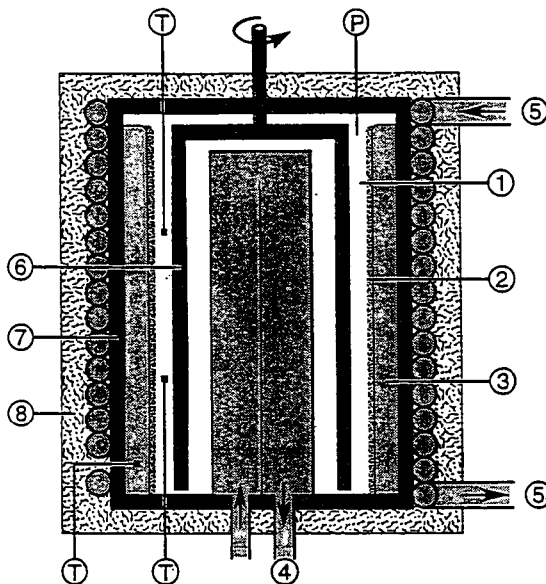
Acknowledgment

We would like to thank GRI for their partial support of the early stages of this research under contract GRI5091-260-2121.

References

- Holder, G.D. and R.M. Enick, "Solid Deposition in Hydrocarbon Systems-Kinetics of Waxes, Ashpaltenes and Diamondoids", Final Report, Gas Research Institute, GRI, 1995.
- Holder, G.D., S. Zetts, and N. Pradhan, *Reviews in Chemical Engineering*, 5(1), 1, 1988.
- Holder, G.D.; Zele, S.; Enick, R.; LeBlond, C. *Ann. N.Y. Acad. Sci.* 1994, 715, 344.
- M.N. Lingelem, A.I. Majeed, and E. Stange, "Industrial Experience in Evaluation of Hydrate Formation, Inhibition, and Dissociation in Pipeline Design and Operation", in *Natural Gas Hydrates*, Annals of the NY Academy of Science, E.D. Sloan et al, editors, New York, p75, 1994.
- Sloan, E.D., *Clathrate Hydrates of Natural Gas*, Marcel Dekker, New York, 1990.

Figure 1. High Pressure Tangential Annular Flow Apparatus



1. High Pressure Gas
 2. Gas Hydrate
 - 3.
 4. Gas Cooling Fluid Flowing in Cylinder
 5. Ice Cooling Fluid Flowing in Coils
 6. Rotating Cylinder
 7. High Pressure Cell
 8. Insulation
- T - Thermocouples
P - Pressure Transducer

Table 1: Growth Rate of Hydrates

Gas Composition	Bulk gas Temp (K)	Cooling coil Temp (K)	Initial Press (KPa)	RPM	Linear growth rate (cm/hr)
100% C ₁	283.7 +/- 0.4	273.7 +/- 0.3	6509	7	0.02
100% C ₁	283.5 +/- 0.5	271.4 +/- 0.1	6039	8	0.02
100% C ₁	282.9 +/- 0.4	272.0 +/- 0.3	6021	8	0.05
100% C ₁	282.1 +/- 0.4	271.9 +/- 0.1	6023	8	0.00
100% C ₁	281.9 +/- 0.3	272.1 +/- 0.1	5987	30	0.02
100% C ₁	283.0 +/- 0.5	271.8 +/- 0.1	6004	2	0.01
100% C ₁	282.3 +/- 0.7	271.9 +/- 0.2	6019	8	0.02
100% C ₁	279.7 +/- 0.6	271.5 +/- 0.2	6861	25	0.02
100% C ₁	276.5 +/- 0.2	271.5 +/- 0.2	6618	15	0.02
5% C ₂ :95% C ₁	291.1 +/- 0.3	272.9 +/- 0.1	7014	7	0.08
5% C ₂ :95% C ₁	288.9 +/- 0.4	273.6 +/- 0.2	7110	15	0.11
5% C ₂ :95% C ₁	288.7 +/- 0.6	270 +/- 0.1	6905	60	0.15
5% C ₂ :95% C ₁	288.4 +/- 0.7	271.1 +/- 0.1	6940	1	0.03
5% C ₂ :95% C ₁	287 +/- 0.9	270 +/- 0.1	7089	30	0.17
3% C ₂ :97% C ₁	284.7 +/- 0.7	271.6 +/- 0.1	6781	7	0.03
3% C ₂ :97% C ₁	288.1 +/- 0.1	273.2 +/- 0.1	7036	7	0.05
3% C ₂ :97% C ₁	284.5 +/- 0.1	271.7 +/- 0.1	6782	60	0.15
3% C ₂ :97% C ₁	286.8 +/- 0.2	274 +/- 0.1	7016	2	0.08
3% C ₂ :97% C ₁	287.5	271.5 +/- 0.1	6927	2	0.13
3% C ₂ :95% C ₁	286.4 +/- 0.1	273 +/- 0.1	7011	30	0.06
CO ₂	282 +/- 0.3	271.4 +/- 0.1	3555	8	0.10
CH ₄ /WAX	277.8 +/- 0.7	271.6 +/- 0.2	5296	15	0.002
CH ₄ /PVP	278.6 +/- 0.6	272.1 +/- 0.2	5482	15	0.000

METHANOL: CLATHRATE HYDRATE FORMER OR INHIBITOR ?*

Hirokazu Nakayama^{††}, Darren H. Brouwer[†], Y. Paul Handa[†], Dennis D. Klug[†], John S. Tse[†], Christopher I. Ratcliffe[†], Xu Zhu[†] and John A. Ripmeester^{††}

[†]Steeacie Institute for Molecular Sciences, ^{††}Institute for Chemical Processing and Environmental Technology, National Research Council of Canada, Ottawa, Ontario, Canada K1A 0R6

Keywords: methanol, hydrate, methanol monohydrate, hydrate inhibitor, clathrate hydrate

INTRODUCTION

Methanol has long been in use as an inhibitor of hydrate formation¹. It acts as a classical antifreeze, that is by lowering the activity of the water, and generally shifts the equilibrium lines for hydrate formation in the phase diagram to lower temperatures. It has been shown that in water - hydrate former - methanol systems the methanol is excluded from the clathrate hydrate when the material is frozen². From a molecular point of view, one may argue that methanol interacts strongly with water by hydrogen bonding, thus interfering with the structure formation required for the formation of solid ice and ice-like lattices. Thus, methanol is one of few small molecules that do not form clathrate hydrates at ordinary temperatures (~ 0°C). The propensity for small water-soluble molecules to form hydrates depends on a balance between hydrophobic and hydrophilic interactions, as many of the water soluble ethers readily form clathrate hydrates³. Ethanol is known to form two different hydrates⁴ at low temperatures which are probably semi-clathrates structurally related to Str.I and Str.II hydrates (Pm3m, a=11.88 Å, F4,32, a=17.25 Å respectively). Isopropanol, t-butanol and iso-amyl alcohol all are known to form double hydrates with small help-gas molecules⁵.

In 1991, a report appeared⁶ which suggested that methanol, when co-deposited with water in a vacuum at low temperatures, forms a clathrate hydrate of structure II with a lattice constant of 16.3 Å. This observation poses a number of questions regarding the ability of methanol to both inhibit and promote hydrate formation. If one is a high temperature property, and the other a low temperature property, at which temperature do they cross over and what are the responsible interactions ? On the other hand, there are some general questions regarding the interpretation of the results. For instance, the usual structure II lattice parameter is $17.1 \pm 0.1 \text{ \AA}$, so it isn't easy to see how the structure II lattice can adapt to a ~ 12% volume reduction.

Also, size considerations alone would suggest that methanol (an ethane-sized molecule) should form a structure I rather than a structure II hydrate. As noted above, the larger (propane-sized) ethanol molecule apparently forms semi-clathrates similar to both str. I and str. II. In this sense it is pertinent to note that calculations have been performed on a str. I hydrate lattice containing methanol guests⁶. A third point is that the report does not acknowledge the possible presence of methanol monohydrate, which was reported in a study of the methanol -water phase diagram in 1961⁹. These questions led us to have a close look at the low temperature behaviour of the methanol - water system.

EXPERIMENTAL

Methanol and water were co-deposited from metered amounts of the vapours on the cold plate (~ 20K) of a Displex closed cycle refrigerator. Sample stoichiometry was varied from 20:1 to 1:1. Pure amorphous ice and methanol phases were prepared as well. Samples were handled and stored under liquid nitrogen. Some samples of a 1:1 stoichiometry were prepared by direct mixing of the liquids followed by quenching to 77K and annealing above the eutectic temperature at ~ 150K.

Sample characterization was carried out by differential scanning calorimetry (DSC), powder X-ray diffraction (XRD) and NMR spectroscopy. Samples for NMR were isotopically enriched in ²H for either the water or methanol phases.

Thermal events were recorded by means of a Tian Calvet heat-flow calorimeter (Setaram, Model BT2.15). The details of the calorimeter and the operating procedure have been described previously¹⁰. A sample size of about 2 g was used, the sample temperature always remaining below 80K during loading. Samples were scanned from 78K to room temperature at 10 K°/h with nitrogen at 200 mbar as heat exchange gas. XRD measurements were performed on a Rigaku $\Theta - \Theta$ powder diffractometer equipped with a Paar temperature controller. Samples were loaded cold, and XRD

patterns were taken at 80K. Samples were annealed for 10 min. at the appropriate temperatures then cooled for the recording of the XRD pattern. The various phases which appear on crystallization of the amorphous deposits and mixtures were identified by comparison with data obtained for the pure crystalline materials or from literature data.

^2H NMR powder patterns were recorded at a frequency of 30 MHz on a Bruker MSL 200 NMR spectrometer equipped with a 5mm solenoid probe. Quadrupole echo sequences were used with a 90° pulse length of $\sim 2.5 \mu\text{sec}$ and an echo delay time of $30 \mu\text{sec}$. Samples of 1:1 stoichiometry were quenched and conditioned in the probe at temperatures somewhat above 150K. Quadrupole coupling parameters were determined by a fitting procedure using the Bruker Winfit package.

RESULTS AND DISCUSSION

Table 1 offers a summary of the calorimetric data which was obtained for a range of samples which reasonably well cover the methanol-water phase diagram. The column on the left is in good agreement with previously reported work on vapour-deposited ice. We note that all starting materials are amorphous, and that the first event to take place on warming is crystallization, or crystallization preceded by a glass transition. This is in agreement with the reported phase diagram, where devitrification is reported to take place between 110 and 120K. We note that it doesn't seem to matter much whether samples are produced by quenching the liquid mixture, or by vapour deposition.

A critically important component of the work is to identify the phases present in the low temperature region, that is after the glass transition/crystallization events. The XRD patterns of Ice Ih, Ice Ic and the clathrate hydrates are well documented. XRD patterns for the α and β phases of methanol were recorded in order to be able to recognize the presence of these phases.

In all of the experiments carried out, it was found that a number of reflections appeared which could not be assigned to one of the aforementioned crystal phases. These reflections appeared to be strongest for samples approaching a composition of 1:1 methanol/water. Another experiment showed that these reflections disappeared when the sample was warmed to 175K, leaving only the Ice Ih pattern, but reappeared on cooling. We can conclude that these reflections should be assigned to the methanol monohydrate which is known to melt incongruently at $\sim 171\text{K}$. Although methanol monohydrate has been known to exist for many years, so far no information is available on its structure. In order to facilitate further study, a good sample of methanol monohydrate was prepared by quenching a 1:1 mixture of methanol and water and annealing at 150K for 10 hrs. The sample still contained a significant quantity of hexagonal ice as impurity, however, the remaining 19 reflections could be indexed in terms of tetragonal Laue symmetry and a fit of the d spacings was obtained with unit cell dimensions of $a = 4.660(1)$, $c = 13.813(5) \text{ \AA}$.

With the identification of the methanol monohydrate phase, all of the reflections can be accounted for for all of the samples considered in this study. The crystallization processes which transform the lowest temperature amorphous phases are outlined below for a range of sample compositions.

Ice \Rightarrow Ice Ic

methanol/water (1:20, 1:10) \Rightarrow methanol monohydrate + Ice Ih + Ice Ic (trace)

methanol/water (1:2) \Rightarrow methanol monohydrate + Ice Ih + methanol

methanol \Rightarrow α -methanol

Perhaps the most unusual observation is the near disappearance of cubic ice as a distinct phase in the presence of methanol. Figure 1 shows a typical XRD run on a codeposit (1:2 methanol-water) initially annealed at 120K. The ice Ih reflections clearly are present for all temperatures. The calorimetric data is in agreement with this, as the only evidence for the crystallization of cubic ice is from a very weak exotherm near 148K in the 10:1 deposit (see table 1), and the subsequent transformation of ice Ic to ice Ih occurs near 179K; these events occur near 142K and 195K for pure ice. Methanol seems to act as a catalyst in the direct conversion of amorphous ice to ice Ih.

How do our results relate to those reported for the "methanol clathrate" 6 ? The material prepared was thought to be a clathrate mixed with some cubic ice based on the assignment of 10 reflections to a 16.3 \AA clathrate lattice plus 1 reflection due to cubic ice. By comparing the diffraction data for the two studies it becomes apparent that all of the observed reflections in both studies can be accounted for in terms of ice

Ih and methanol monohydrate. It should be noted that the small angle reflections ($hkl = 111, 220$ and 311 for str. II) which are essential for assigning the clathrate structures in mixed-phase systems were not observed. Certainly in light of our data there is no need to propose a structure II clathrate hydrate with an unusual lattice parameter.

Although the XRD powder data have given a good indication of the symmetry and size of the unit cell in the crystal, the detailed structure remains as yet unknown. Some additional information on the methanol monohydrate can be obtained from NMR spectroscopy. The ^2H NMR quadrupole coupling parameters obtained for the water lattice are useful, as these can be used to give information both on the strength of the hydrogen bonds and the dynamics of the water lattice. The ^2H NMR lineshape for a sample of $\text{CH}_3\text{OH} \cdot \text{D}_2\text{O}$ yielded a quadrupole coupling constant $\chi (= e^2\text{Qq}/h)$ of 206.9 kHz and an asymmetry parameter $\eta = 0.09$. These values are very near to those for ice Ih (215 kHz, 0.1¹¹), and are characteristic of a fully hydrogen-bonded network. The χ value is an average for the D_2O and CH_3OD deuterons, as exchange must produce the deuterium-substituted methanol. The small decrease in χ indicates that the O - O distances are, if anything, on average slightly shorter than those in ice Ih. The temperature dependence of the lineshape (fig. 2) gives a rough indication of the rate of the dynamic processes in which water molecules are involved. Above about 140K, the lineshape develops a central component which is a manifestation of slow reorientation of the water molecules within the lattice. A comparison with the lineshapes obtained for pure ice Ih indicates that the water molecules in the methanol hydrate at ~ 150K have the same motional correlation time as those in ice Ih at ~260K. Since the water reorientation in ice is defect-driven, the implied low activation energy for water reorientation in methanol monohydrate must reflect the ease with which defects can be generated. A more detailed analysis of D_2O dynamics is complicated by the fact that besides the water molecules there are two kinds of methanol O-D bonds that must be involved in restricted dynamic processes (see below). Examination of a corresponding $\text{CD}_3\text{OD} \cdot \text{H}_2\text{O}$ (fig. 2, below) sample showed that there are two dynamically inequivalent CD_3 groups, as there are two overlapping powder doublets. Both CD_3 groups show rapid rotation about their 3-fold axes, one of the two shows little or no additional motion, the second shows the presence of another process which formally can be explained by a jump between two positions with ~ 40° between the directions of the CD_3 group symmetry axes. The central line (fig. 2, right) arises from the more mobile OD and HOD deuterons. The NMR measurements show quite clearly that molecular motion is possible at much lower temperatures than in a pure ice lattice.

CONCLUSIONS

On the basis of results reported here it appears unnecessary to propose the existence of a clathrate hydrate of methanol. In vapour-deposited or quenched water - methanol mixtures the crystallization products include mainly methanol monohydrate and ice Ih on the water-rich side of the composition diagram. Methanol seems to act as a catalyst for the direct conversion of glassy ices to ice Ih. On the basis of XRD it is proposed that the methanol monohydrate is tetragonal with unit cell dimensions $a = 4.660$, $c = 13.813$ Å. NMR results indicate that both water and methanol are part of a fully hydrogen-bonded network, but that water reorientation takes place much more easily than in pure ice Ih and in most clathrate hydrates. Finally, one can say that methanol by all accounts remains an inhibitor of hydrate formation.

* Issued as NRCC no:39128

* Permanent address: Department of Chemistry, Osaka University, Osaka, Japan

† Author for correspondence

¹ Sloan, Jr., E. D. "Hydrates of Natural Gas", Marcel Dekker, New York, N. Y. 1991

² Davidson, D. W., Gough, S. R., Ripmeester, J. A., Nakayama, H., Canad. J. Chem. 1981 59, 2587

³ Davidson, D. W., in "Water a Comprehensive Treatise, Franks, F., Ed., Plenum, N. Y., 1973, Vol.2

⁴ Calvert, L. D., Srivastava, P., Acta Crystallogr. Sect. A 1969, 25, S131

⁵ Ripmeester, J. A., Ratcliffe, C. I., J. Phys. Chem. J. Phys. Chem. 1990 94, 8773

⁶ Blake, D., Allamandola, L., Sandford, S., Hudgins, D., Friedemann, F., Science 1991 254, 548

⁷ Davidson, D. W., Handa, Y. P., Ratcliffe, C. I., Ripmeester, J. A., Tse, J. S., Dahn, J. R., Leo, F., Calvert, L. D., Mol. Cryst. Liq. Cryst. 1986, 141, 141

⁸ Wallqvist, A., J. Chem. Phys. 1992 96, 5377

⁹ Vuillard, G., Sanchez, M., Bull. Chem. Soc. Fr. 1961, 1877

¹⁰ Handa, Y. P., Hawkins, R. E., Murray, J. J., J. Chem. Thermodyn. 1984, 16, 623; Y. P. Handa, J. Chem. Thermodyn. 1986, 18, 891

¹¹ Ripmeester, J. A., Ratcliffe, C. I., Klug, D. D., J. Chem. Phys. 1992, 96, 8503

Table 1. Summary of Calorimetric Data ; thermal events are shown in italics, phases present in bold type

Starting material			
ice (a)	10:1 mixture (a)	1:1 mixture (quenched)	methanol (a)
ice Ih		liquid mixture	liquid
195K(en)	179K(en; w)	183K(en; w)	178K(en)
	Ice Ih + liq 173K(en)	Ice Ih + liq 174K(en)	β phase + liq.
Ice Ic			
	MeOH.H₂O + Ice Ih	MeOH.H₂O + Ice Ih + eutectic mixture	168K(en)
		158K(en,w)	α phase + eutectic mixture 158K(en,w)
	148K(ex, w)		
142K(ex)		MeOH.H₂O + Ice Ih + eutectic mixture (s)	α phase + eutectic mixture (s)
136K(g)	131K(ex)	122K(ex)	
Ice (a)	amorphous mixture	112K(g)	
		amorphous mixture	102K(ex) methanol (a)

a = amorphous; ex = exotherm; en = endotherm; w = weak; g = glass transition, s = solid

Figure 1. X-ray powder diffraction patterns for a 1:2 methanol-water mixture obtained at 90K; the sample was annealed for 6 hours at 120K before the other patterns were obtained at the temperatures indicated. The crystalline phases present are: ice Ih (marked on the 180K pattern); methanol monohydrate (marked on the 160K pattern); α and β methanol (marked on the 140K pattern). the amorphous material shows up as broad background scattering especially at low temperatures, liquid as broad background at 180K.

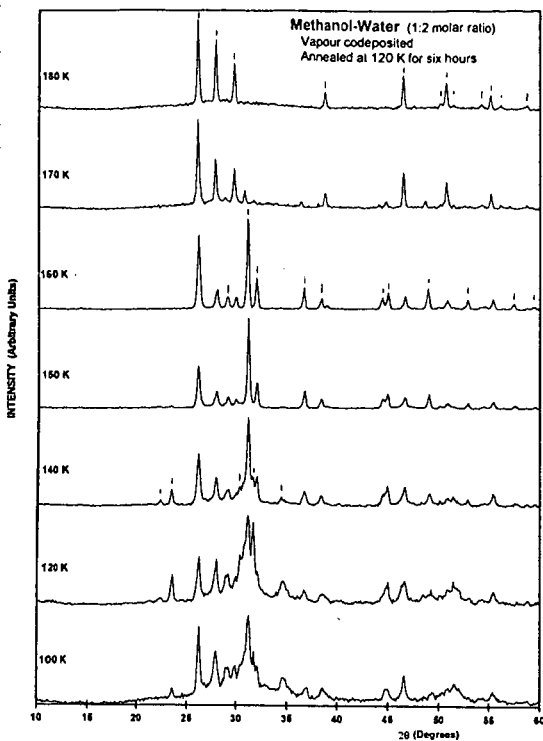
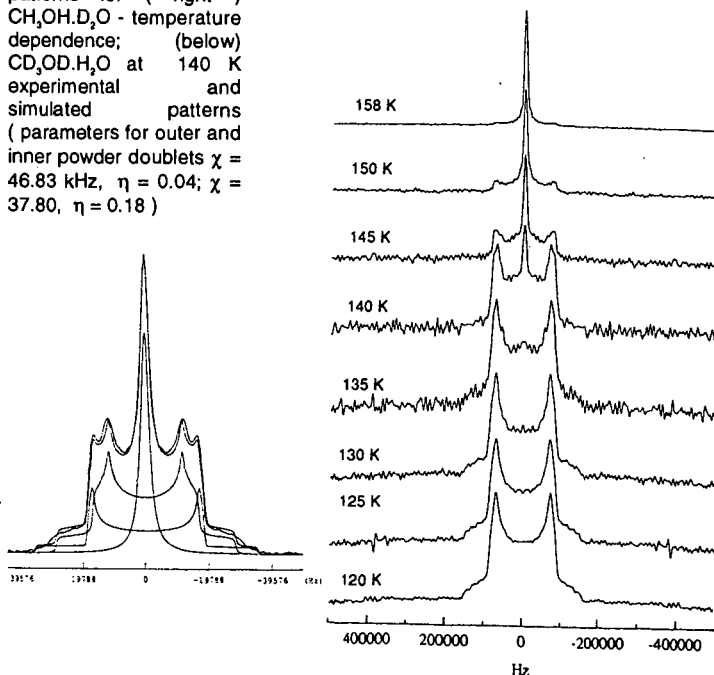


Figure 2. ^2H NMR powder patterns for (right) $\text{CH}_3\text{OH}\cdot\text{D}_2\text{O}$ - temperature dependence; (below) $\text{CD}_3\text{OD}\cdot\text{H}_2\text{O}$ at 140 K experimental and simulated patterns (parameters for outer and inner powder doublets $\chi = 46.83$ kHz, $\eta = 0.04$; $\chi = 37.80$, $\eta = 0.18$)



A SIMPLE METHOD FOR PREDICTING GAS HYDRATE FORMING CONDITIONS IN AQUEOUS MIXED ELECTROLYTE SOLUTIONS

Jafar Javanmardi and Mahmood Moshfeghian
Department of Chemical Engineering
Shiraz University, Shiraz, Iran
and
Robert N. Maddox
School of Chemical Engineering
Oklahoma State University, Stillwater, OK, USA

Key Words: Hydrate; Electrolyte; Gas

ABSTRACT:

A simple thermodynamic model is proposed for predicting hydrate forming conditions for natural gas components in the presence of single component or mixed electrolyte solutions. The parameters required for use of the model are developed and presented. The model is quite accurate with average deviations between calculated and experimental values of less than 0.5°C for systems not included in the model parameter determination.

INTRODUCTION:

Gas hydrates are a form of clathrate -- compounds in which guest molecules are entrapped in a cage lattice structure composed of host molecules. They were first discovered by Davy in 1810 who produced chlorine hydrate (24). Natural gas hydrates were first produced by Villard in 1888 (25). Hydrates of natural gas components are ice-like solid compounds that can form under temperature conditions 25°C (40°F) or more above the freezing point of water.

Several different hydrate structures are known. Most polar and some weakly polar gases form either a structure I or structure II hydrate. The hydrate formed depends primarily on the size of the guest molecule. Methane and ethane form structure I hydrates while propane and isobutane form structure II hydrates. Parrish and Prausnitz (18) reported the physical characteristics of structure I and II hydrates.

Gas hydrates are ice-like clathrate compounds that are solids. They can accumulate in low places or around valves and fittings causing gas gathering and flow lines to become clogged and shut off gas flow. This is a particular problem in cold weather when line temperatures are most likely to be in the hydrate forming range. Knowledge of hydrate forming conditions and ways of preventing hydrates from forming are important to the natural gas industry. These areas are well developed and reliable methods are available for both natural gas mixtures (Maddox, et al. 14) and gas mixtures with inhibitors present (Moshfeghian and Maddox, 16).

Salt solutions and brine are frequently produced along with natural gas. Also, hydrates have been suggested as one way of making sea water potable (Knox, et al., 12) and as a possible way of storing natural gas in salt pits (Miller and Strong, 15). Capabilities for predicting natural gas forming conditions in the presence of weak electrolytes need improvement. That is the justification for the work presented here.

APPROACH

The approach used to develop the procedure for estimating hydrate forming conditions for gases over electrolytes is similar to that used by Moshfeghian and Maddox (1990) for their work on inhibited water solutions. They predicted the conditions for hydrate formation over pure water and then calculated an adjustment, or change, in those conditions to account for the presence of the inhibitor.

In the present work the method of Holder, Corbin and Papadopoulos (1980) is used to calculate the conditions for hydrate formation over pure water, and equations are developed to adjust those conditions for the presence of electrolyte. Holder and co-workers used experimental measurements to generate chemical potential, enthalpy and heat capacity functions. No gas species dependent adjustable parameters are required.

THERMODYNAMIC MODEL

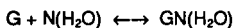
The equations used for predicting the influence of weak electrolyte solutions on natural gas hydrate forming conditions were developed from the work of van der Waals and Platteeuw, (23). The value of the Langmuir constant depends on temperature and potential energy function parameters and was evaluated using the mathematical expressions of Parrish and Prausnitz (18).

At equilibrium the chemical potential of water is equal in all phases present. If the free water is present as ice, none of the ice will be incorporated within the hydrate structure, and the chemical potential of the water in the hydrate will be equal to that of ice. If liquid water is present the free water and the water in the hydrate will have the same chemical potential.

The way in which the activity of water is evaluated depends on the components present in the system under consideration. If pure liquid water is present Holder, et al. (8) suggest that gas solubility in the water phase will be so slight that x_w , the mole fraction of water, may be used without creating significant error. If, on the other hand, water is present in an electrolyte solution with an appreciable concentration of salt present, the model suggested by Pitzer and Mayorga (22) can be used to estimate the activity of water in the electrolyte. Following Englezos and Bishnoi (5) and Tohidi, et al. (26) this work has used the Pitzer and Mayorga activity model for predicting conditions necessary for hydrate formation in the presence of electrolyte solutions.

In case there is more than one electrolyte present in the solution, the procedure proposed by Patwardhan and Kumar (19) is used to estimate the water activity.

Formation of hydrate from gas and liquid water molecules where G molecules of gas involve N molecules of water can be represented by the following chemical reaction:



For this representation Maddox, et al. (14) showed that the effect of a non electrolyte inhibitor on the hydrate temperature of a natural gas could be explained as:

$$\lambda_i(a_w) = \frac{-\Delta H}{NR} \left(\frac{1}{T} - \frac{1}{T_w} \right) \quad (1)$$

The derivation of equation (1) is discussed in detail by Pieroen (21). The electrolyte can be treated as an "inhibitor" if the procedure developed is used for estimating electrolyte activities and other parameters. In this work $(\Delta H/NR)$, the enthalpy of hydrate formation per water molecule in the hydrate lattice in equation (1) is assumed to be a function of pressure and the ionic strength of the electrolyte solution and to take the following form:

$$\frac{\Delta H}{NR} = \frac{e_1 I^2}{1 + e_2 P + e_3 (\lambda_i P)} \quad (2)$$

with e_1 , e_2 , e_3 and e_4 being adjustable parameters determined from experimental electrolyte solution hydrate data.

Experimental measurements of the hydrate temperature of methane (1, 2, 23) and ethane (6,26) in the presence of liquid water and electrolyte solutions and propane (8, 10, 13, 26) in the presence of ice, liquid water and electrolyte solution were used to evaluate the parameters in equation (2). The values are: $e_1 = 597.33$; $e_2 = -0.0409$; $e_3 = 0.0000227$; $e_4 = -0.0751$. These are global parameters that apply for any gas and any single or mixed electrolyte solution. They reproduce the measurements of Blanc and Tournier-Lasserre (1), Dholabhai, et al. (3), and Roo, et al. (23) for methane (CH_4) with an average absolute temperature deviation of 0.33°C; The experimental determinations by Englezos and Bishnoi (6) and Tohidi, et al. (26) for ethane are reproduced with an average absolute deviation of 0.56°C across all data points. Experimental data for propane by Englezos and Ngan (8), Holder and Godbole (10), Kubota, et al. (13), and Tohidi, et al. (26) are reproduced with an average absolute deviation for all propane data points of 0.35°C. A summary of these results is shown in Table 1.

CALCULATION PROCEDURE

Based on the discussion above a procedure for calculating the hydrate forming temperature and pressure for natural gas components in contact with water containing one or more electrolyte salts can be suggested. Assuming that the pressure is fixed and the hydrate forming temperature is required, the sequential steps in the procedure are:

1. Assume that the hydrate forming temperature in the presence of water with no electrolyte present is above 273.15K, the freezing point of water. If the hydrate temperature is lower than this, that fact will become evident and the assumed temperature can be changed. Use equations 3, 7 and 13 to evaluate T^0 .
2. Calculate the activity of water and $\Delta H/NR$.
3. Calculate the hydrate temperature in the presence of electrolyte.
4. If the temperature calculated in step 3 is greater than 273.15K, all is well; if it is lower than 273.15K return to step 1, assume the temperature is less than 273.15K, and repeat steps 2 and 3.

RESULTS

The procedure outlined has been used to predict hydrate forming conditions for carbon dioxide (CO₂) over electrolyte solutions. CO₂ is a different gas than light hydrocarbons in that it displays appreciable solubility in water, even at moderate pressures. There are cases in which gas solubility is high enough that the mole fraction of water in the water phase departs substantially from 1.0. The solubility of CO₂ in water can be expressed as:

$$x_{CO_2} = \left\{ \frac{f_{CO_2}^V}{(g_1 + g_2 T) \exp[(g_3 - P^{14}) / P^{14}]} \right\} \quad (3)$$

where:

$$\begin{aligned} g_1 &= -725919.22 \\ g_2 &= 2898.54 \\ g_3 &= 0.05127 \\ g_4 &= -0.11228 \end{aligned}$$

Calculations of CO₂ solubility using equation (3) match the experimental measurements of CO₂ solubility made by Stewart and Munjal (25) within an average absolute mole fraction CO₂ deviation of 0.00042 over temperatures from 259 to 281K and pressures from 1.0 to 4.25 MPa. Using equation (3) for CO₂ solubility in water and the hydrate prediction procedure developed here, the hydrate forming conditions for CO₂ over electrolyte solutions have been calculated and compared with experimental determinations made by Dholabhai, et al. (4), and Englezos (7). The results for CO₂ are summarized in Table 1. The 161 CO₂ data points show an average absolute temperature deviation of 0.46°C over the full temperature, electrolyte composition and pressure range of the data.

CONCLUSION

The model developed for predicting hydrate forming conditions in the presence of electrolyte solutions does an excellent job of reproducing experimental measurements. It also has the capability to make accurate predictions of hydrate formation in cases where the gas shows appreciable solubility in the water phase. It represents a significant step in predicting hydrate forming conditions for constituents of natural gas.

NOMENCLATURE

- a_w = activity of water
- a_w^0 = activity of water in the single salt solution defined by m_i^0
- A_ϕ = Debye-Hückel coefficient = 0.392 for water at 25°C
- β_0 = parameter in equation (10)
- β_1 = parameter in equation (10)
- β_2 = parameter in equation (10)
- C_{ml} = Langmuir constant
- C_p = specific heat, cal/g-mole-K
- f_λ = gas-phase fugacity of the λ th gas species
- h = molar enthalpy, cal/g-mole
- m = molality of electrolyte solution
- m_k = molality of electrolyte k in mixed electrolyte solution
- m_k^0 = molality of electrolyte k in a solution containing only electrolyte k and that has the same ionic strength as the mixed solution
- n = formula of electrolyte
- n_+ = number of positive ions in electrolyte formula
- n_- = number of negative ions in electrolyte formula
- nc = total number of components in gas phase
- R = gas constant, 1.987 cal/g-mole-K
- T = absolute temperature, K
- V = molar volume cm³/g-mole
- μ_w^H = chemical potential of water in the gas occupied lattice, cal/g-mole
- $\Delta\mu_w^H$ = change in chemical potential of water caused by hydrate formation, cal/g-mole
- μ_w^B = chemical potential of water in the unoccupied lattice, cal/g-mole
- μ_w^i = chemical potential of ice, cal/g-mole
- μ_w^λ = chemical potential of pure water, cal/g-mole
- θ_{mj} = fraction of the type m cavities which are occupied by a j-type gas molecule
- v_m = ratio of the number of type m cavities to the number of water molecules in the hydrate phase
- z = charge on ions in electrolyte formula

REFERENCES

1. Blanc, C., and J. Tourmier-Lasserve, World Oil, November (1990).
2. Carson, D. B. and D. L. Katz, "Trans. AIME," 146, (1942).
3. Dholabhai, P. D., P. Englezos, N. Kalogerakis and P. R. Bishnoi, "Can. J. Chem. Eng.," 69, 800, (1991).
4. Dholabhai, P. D., N. Kalogerakis and P. R. Bishnoi, "J. Chem. Eng. Data," 38, (4), 650 (1993).
5. Englezos, P. and P. R. Bishnoi, "AIChE J.," 34, (10), 1718, (1988).
6. Englezos, P. and P. R. Bishnoi, "Ind. Eng. Chem. Res.," 30, (7), 1655, (1991).
7. Englezos, P., "Ind. Eng. Chem. Res.," 31, (9), 2232, (1992).
8. Englezos, P. and Y. T. Ngan, "J. Chem. Eng. Data," 38, (2), 250, (1993).
9. Holder, G. D. and G. Gorbin, "Ind. Eng. Chem. Fund.," 19, (3), 282, (1980).
10. Holder, G. D. and S. P. Godbole, "AIChE J.," 28, 930, (1982)
11. Jeffrey, G. A. and R. R. McMullan, "Prog. Inorg. Chem.," 8, 43 (1967).
12. Knox, W. G., M. Hess, G. E. Jones and H. B. Smith, "Chem. Eng. Prog.," 57, (2), 66 (1961).
13. Kubota, H., K. Shimizu, Y. Tanaka and T. Makita, "J. Chem. Eng. Japan," 17, (4), 423, (1984).
14. Maddox, R. N., M. Moshfeghian, E. Lopez, C. H. Tu, A. Shariat and J. Flynn, Laurence Reid Gas Conditioning Conference, March 4-6, 1991.
15. Miller, B. and E. K. Strong, "Amer. Gas Assoc. Monthly," 28, (2), 63, (1946).
16. Moshfeghian, M. and R. N. Maddox, "Oil & Gas J.," 30, 78, (1993).
17. Moshfeghian, M. and R. N. Maddox, Annals of New York Academy of Science, 715, (1994)
18. Parrish, W. R. and J. M. Prausnitz, "Ind. Eng. Chem. Proc. Dev.," 11, 26 (1972).
19. Patwardhan, V. S. and A. Kumar, "AIChE J.," 32, (9), 1419, (1986).
20. Peng, D. Y. and D. B. Robinson, "Ind. Eng. Chem. Fund.," 59, (1976).
21. Pieroen, A. P., Recueil Trav. Chem., Vol. 74, 995-1002, (1955)
22. Pitzer, K. S. and G. Mayorga, "J. Phys. Chem.," 77, (19), 2300, (1973).
23. Roo, J. L., C. J. Peters, R. N. Lichenthaler and G. A. Diepen, "AIChE J.," 29, (4), 651, (1983).
24. Schroeder, W., Sammlung Chemischer & Chemisch-Technischer Vorträge, Ahren's, 1926.
25. Stewart, P. B. and P. Munjal, "J. Chem. Eng. Data," 15, (1), 67, (1970).
26. Tohidi, B., R. W. Burgass, A. Danesh and A. C. Todd, "SPE 26701," 255, (1993)
27. Van der Waals, J. H. and J. C. Platteeuw, "Advan. Chem. Phys.," 2, 1, (1959).
28. Villard, M., Comptes Rendus, 1888, 106, 1602.

Table 1

Component	Electrolyte Concentration mol/L			Temperature Range K	Pressure Range MPa	AATD* K
	NaCl	KCl	CaCl ₂			
CH ₄	0-5.43	0-1.57	0-1.07	261-281	2.39-92.0	0.33
C ₂ H ₆	0-4.28	0-1.88	0-1.59	265-283	0.50-2.0	0.56
C ₃ H ₈	0.4-2.7	0-3.35	0-1.61	248-278	0.1-0.54	0.35
CO ₂	0-4.29	0-2.36	0-2.24	259-281	1.0-4.23	0.46

* Average Absolute Temperature Deviation

MEASUREMENT OF GAS HYDRATE PHASE EQUILIBRIUM

Phillip Servio and Peter Englezos

Department of Chemical Engineering, The University of British Columbia
Vancouver BC, V6T 1Z4, CANADA

Keywords: hydrate equilibrium data, triethylene glycol, neohexane

ABSTRACT

Incipient equilibrium hydrate formation conditions for two systems are presented. The isothermal pressure search method was employed. First, structure II hydrate data for the propane-triethylene glycol water system at glycol concentrations of 0, 10 and 20 wt % are given. Triethylene glycol was shown to have considerable inhibiting effect on propane hydrate formation. The other data are hydrate formation conditions for the system methane-carbon dioxide-neohexane-water. The initial gas molar composition on a water-free basis was 80 % methane and 20 % carbon dioxide. At a given temperature, the incipient hydrate formation pressure was found to be within the range of the hydrate formation pressure for the methane-neohexane-water and the carbon dioxide-water systems. Thus, further analysis is required to elucidate the type of hydrate structure.

INTRODUCTION

During the past five years we have been measuring phase equilibrium data in gas hydrate forming systems in our laboratory. The broad objective of the work is to provide thermodynamic data which will be used either directly in process design of relevant operations in the oil and gas industry or can be used to test the validity of computational methods for phase equilibrium. We have studied the effect of glycols, water soluble polymers and electrolytes in hydrates from natural gas components. In the present work, we provide measurements for two systems: First, phase equilibrium data for the propane-water-triethylene glycol (TEG) system and second data for the methane-carbon dioxide-2,2-dimethyl butane (neohexane) system.

It has been known since the 1930s that natural gas and water can form a solid ice-like compound commonly called gas hydrate (Hammerschmidt, 1934). This may take place at temperatures above the normal freezing point of water. Because the formation of hydrates has severe economic consequences, in oil and gas operations, prevention of formation is major concern. The most common method to prevent hydrate formation is to inject methanol, glycol, or electrolytes (inhibiting substances). There is a growing interest to replace thermodynamic inhibitors with kinetic inhibitors i.e. chemicals which could perhaps prevent the agglomeration of gas hydrates after they have been formed (Muijs, 1991; Sloan et al. 1994; Englezos, 1996). In spite of this growing effort as well as the progress that has been made in hydrate thermodynamics, equilibrium data for gas hydrates are still needed not only for process design but also for the development and testing of predictive methods for hydrate equilibria (Sloan, 1990; Englezos, 1993; Sloan et al. 1994).

Triethylene glycol is an industrially used chemical to inhibit the formation of gas hydrates. Ross and Toczykin (1992) have presented data on the effect of TEG on methane and ethane gas hydrates. These are known to be structure I hydrates. Hence, one of the objectives of this work is to report incipient equilibrium data for propane hydrate in aqueous triethylene glycol solutions. Propane hydrate is known to form structure II type hydrate crystal lattice.

Following the report from the National Research Council (NRC) of Canada in 1987 on a new hydrate structure, Sloan and co-workers reported the first structure H hydrate phase equilibrium data in 1992 (Ripmeester et al. 1987; Ripmeester and Ratcliffe, 1990; Lederhos et al. 1992). The possibility of forming structure H hydrates in gas and oil reservoirs provides the motivation to obtain phase equilibrium data for structure H hydrates. Subsequently, additional data and a method to predict structure H equilibrium were reported from Sloan's laboratory (Lederhos et al. 1993; Mehta and Sloan, 1993; 1994a; Mehta and Sloan, 1994b; Makogon et al. 1996; Mehta and Sloan, 1996). Additional data were also reported by other laboratories (Danesh et al. 1994; Hutz and Englezos, 1996).

Thus far only methane, nitrogen and argon have been used as light components in the formation of structure H hydrates. Carbon dioxide in conjunction with neohexane and ice also forms structure H hydrates (Ripmeester, 1996). In our laboratory, we attempted to prepare such hydrate but in liquid water. However, we were not able to form hydrates which could be of structure H. At a given temperature, the hydrate that was formed was stable at the carbon dioxide structure I hydrate equilibrium pressure.

Hence, we decided to work with a gas mixture of 80 % methane and 20 % carbon dioxide on a molar basis in conjunction with neohexane which serves as the heavy component.

APPARATUS AND PROCEDURE

A schematic of the apparatus is shown in Figure 1. It consists of a high pressure 316 stainless steel vessel which is immersed in a temperature controlled bath. It has two circular viewing windows on to the front and back. The top of the vessel is held in place by six stainless steel bolts and is sealed with a neoprene O-ring. The temperature control bath contains 30 L of a solution consisting of approximately 50/50 mass percent water and ethylene glycol. A motor driven mechanism is used to stir the contents of the bath. The temperature of the bath is controlled by an external refrigerator/heater (Forma Scientific model 2095, Caltech Scientific, Richmond, BC) with a capacity of 28.5 L. The refrigerator/heater also uses a 50-50 mass percent glycol-water mixture. Mixing of the cell contents is accomplished using a magnetic stir bar that is magnetically coupled to a set of two rotating magnets (Tormag Engineering, Vancouver, B.C.) placed directly underneath the cell. The set of magnets is driven by an electric motor. The temperature at the top, middle and near the bottom inside the cell is measured by three Omega copper-constantan thermocouples. Their accuracy is believed to be ± 0.10 K. The pressure in the cell is measured by a Bourdon tube Heisse pressure gauge from Brian Controls (Burnaby, BC). The range of the gauge is 0-14 000 kPa and its accuracy is believed to be less than 0.25 percent of the span.

The objective of an experiment is to determine the minimum pressure, at a given temperature, where hydrate crystals can co-exist in equilibrium with a gas phase containing mostly propane and the aqueous liquid phase containing the triethylene glycol. In the structure H hydrate formation experiments, the equilibrium is among a gas phase rich in methane and carbon dioxide, an aqueous liquid phase, a liquid hydrocarbon phase rich in neohexane and the hydrate phase. The isothermal pressure search method is used for the determination of the hydrate formation conditions. We use this method because when a pressure change is imposed, the system can reach thermal equilibrium faster compared to the time required for an adjustment of the temperature. More detailed information on the equipment and the procedure to carry out the experiments is available elsewhere (Englezos and Ngan, 1994; Hutz and Englezos, 1996)

The solutions were prepared with deionized water. The purity of methane and propane was 99.9 and 99.5 % (by volume) respectively. These gases as well as the anaerobic grade carbon dioxide were supplied by Medigas. The neohexane (99%) was supplied from Aldrich. Triethylene glycol was also supplied by Aldrich and was 99% pure. The hydrate forming substances were used without any further purification. A Sartorius analytical balance with a readability of 0.05g was used to weigh the compounds used in the experiments.

RESULTS AND DISCUSSION

The propane-triethylene glycol-water system. The measured equilibrium hydrate formation conditions are shown in Figure 2 together with the vapour pressure of propane. As seen from the figure, the data indicate an inhibiting effect by TEG on propane hydrate equilibrium. One can read from the graph the hydrate point depression at a given pressure. For example at 300 kPa the hydrate point depression is 1.65 and 3.15 K for the 10 and 20 wt % TEG solutions respectively. At 400 kPa pressure, the hydrate point depressions are 1.70 and 3.25 K for the 10 and 20 wt % solutions respectively. It is noted that the freezing point depressions for these TEG solutions is 1.33 and 2.93 K. Comparing these values with our previous work with glycerol we note that, the inhibiting effectiveness of TEG is therefore comparable to glycerol but less than that of methanol and NaCl on the same weight % basis (Breland and Englezos, 1996). It is also noted that the difference in hydrate point depression for TEG solutions at different pressures are less than experimental uncertainty. Hence, it is assumed that the hydrate point depression values do not depend on pressure.

The methane-carbon dioxide-neohexane-water system. Experiments at NRC showed that carbon dioxide with neohexane forms structure H hydrate (Ripmeester, 1996). In spite of efforts to nucleate such hydrates but in liquid water and not in ice as was done at NRC, we were not able to obtain hydrates of structure H. The hydrate we obtained was stable within the carbon dioxide structure I hydrate equilibrium conditions. Since these experiments were inconclusive, we decided to work with an 80-20 % methane-carbon dioxide-neohexane-water system. Figure 3 shows the hydrate equilibrium measurements. The results indicate that the measured conditions are within the range of the methane-neohexane structure H and the carbon dioxide structure I hydrate formation conditions. At this stage, it is premature to decide upon the structure

of the hydrate. We plan to analyze the gas and the solid phase in order to elucidate the structure.

CONCLUSIONS

The effect of triethylene glycol (TEG) on the formation of propane hydrate was studied at 0, 10 and 20 wt % aqueous TEG solutions. TEG was found to have a significant inhibiting effect comparable to glycerol but weaker than methanol or NaCl. The experiments with a 80-20 % methane carbon dioxide mixture together with neohexane in liquid water were not conclusive with respect to the structure formed. However, the incipient equilibrium formation conditions for this system were determined.

REFERENCES

1. Breland, E., and P. Englezos 1996. Equilibrium Hydrate Formation Data for Carbon Dioxide in Aqueous Glycerol Solutions. *J. Chem. Eng. Data*, 41(1), 11-13.
2. Danesh, A., B. Tohidi, R.W. Burgass and A.C. Todd, 1994. Hydrate equilibrium data of methyl cyclo-pentane with methane or nitrogen. *Trans I Chem E (Chem. Eng. Res. Des.)*, 72, PartA: 197-200.
3. Englezos, P., 1993. Clathrate hydrates. *Ind. Eng. Chem. Res.*, 32(7): 1251-1274.
4. Englezos, P. 1996. Nucleation and Growth of Gas Hydrate Crystals in Relation to Kinetic Inhibition. *Revue de l'Institut français du pétrole*, (in press).
5. Englezos, P. and Ngan, Y. T., 1994. Effect of polyethylene oxide on gas hydrate phase equilibria. *Fluid Phase Equilibria*, 92: 271-288.
6. Hammerschmidt, E.G. 1934. Formation of Gas Hydrates in Natural Gas Transmission Lines. *Ind. Eng. Chem.* 26 (8), 851-855.
7. Hütz, U., and P. Englezos, 1996. Measurement of Structure H Hydrate Phase Equilibrium and the Effect of Electrolytes. *Fluid Phase Equilibria*, 117, 178-185.
8. Lederhos, J.P., Christiansen, R. L. and Sloan, E.D., 1993. A first order method of hydrate equilibrium estimation and its use with new structures. *Fluid Phase Equilibria*, 83: 445-454.
9. Lederhos, J.P., Metha, A.P., Nyberg, G.B., Warn, K.J. and Sloan, E.D., 1992. Structure H clathrate hydrate equilibria of methane and adamantane. *AIChE J.*, 38(7): 1045-1048.
10. Metha, A.P. and Sloan E.D.Jr., 1993. Structure H hydrate phase equilibria of methane + liquid hydrocarbon mixtures. *J. Chem. Eng. Data*, 38: 580-582.
11. Metha, A.P. and Sloan E.D.Jr., 1994a. A thermodynamic model for structure-H hydrates, *AIChE J.*, 40(2): 312-320.
12. Metha, A.P. and Sloan E.D.Jr., 1994b. Structure-H phase equilibria of paraffins, naphthenes, and olefins with methane. *J. Chem. Eng. Data*, 39, 887-888.
13. Metha, A.P. and Sloan E.D.Jr., 1996. Improved thermodynamic parameters for prediction of structure-H hydrate equilibria, *AIChE J.*, 42(7): 2036-2046.
14. Muijs, H.M. 1991. Surfactants in Oil Production, in *Chemicals in the Oil Industry: Developments and Applications*; Ogden, P.H., Ed., *Roy. Soc. Chem.* pp.277-297.
15. Ripmeester, J.A. 1996. Personal Communication.
16. Ripmeester, J.A., Tse, J.S., Ratcliffe, C.I. and Powell, B.M., 1987. A new clathrate hydrate structure. *Nature*, 325: 135-136.
17. Ripmeester, J.A. and Ratcliffe, C.I., 1990. ¹²⁹Xe NMR studies of clathrate hydrates: new guests for structure II and structure H. *J. Phys. Chem.*, 94: 8773-8776.
18. Ross, M.J. and L.S. Toczylkin, 1992. Hydrate Dissociation Pressures for Methane or Ethane in the Presence of Aqueous Solutions of Triethylene Glycol, *J. Chem. Eng. Data*, 37, 488-491.
19. Sloan, E. D. Jr., 1990. *Clathrates Hydrates of Natural Gases*. Marcel Dekker, New York.
20. Sloan, E.D.; Happel, J.; Hnatow, M.A. 1994. International Conference on Natural Gas Hydrates, *Annals of the New York Academy of Sciences*, Vol. 715, New York.

ACKNOWLEDGMENT

The financial support from the *Natural Sciences and Engineering Research Council of Canada (NSERC)* is greatly appreciated.

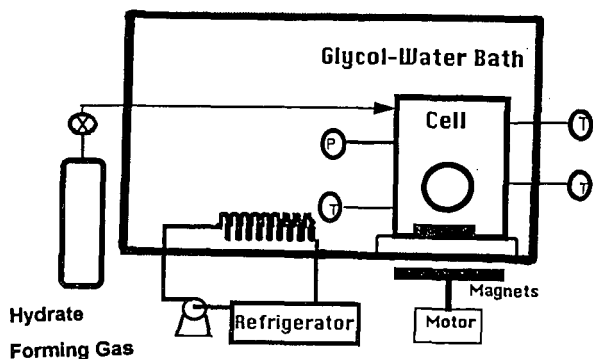


Figure 1. Experimental apparatus

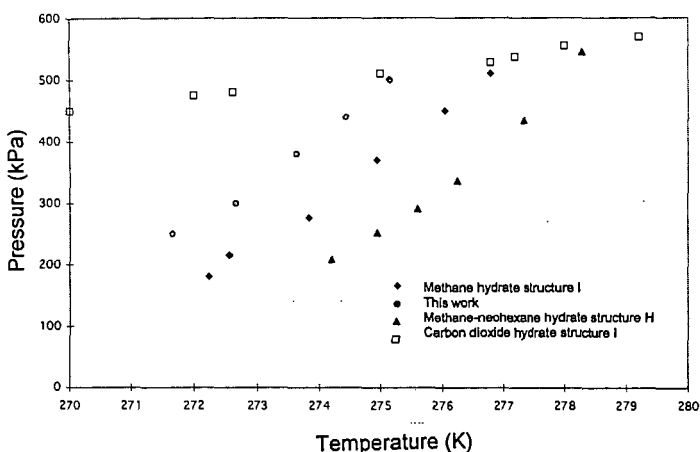


Figure 2. Incipient equilibrium propane hydrate formation conditions in aqueous triethylene glycol solutions.

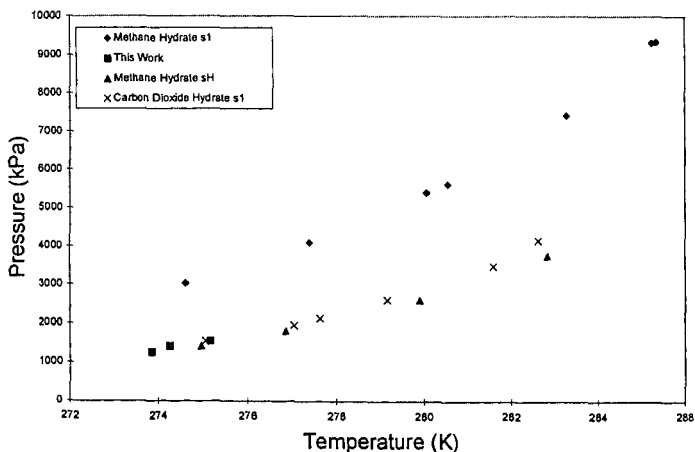


Figure 3. Incipient equilibrium hydrate formation conditions for the methane-carbon dioxide-neohexane-water system.

"MEASUREMENTS AND MODELING OF HYDRATE EQUILIBRIUM CONDITIONS OF SYSTEMS CONTAINING HEAVY HYDRATE FORMERS"

F.H. Fadnes¹, T. Jakobsen² and A. Lund³

1 Norsk Hydro A/S, N-5020 Bergen, Norway

2 Terra Environment A/S, N-5028 Bergen, Norway

3 Sintef Applied Chemistry, N-7034 Trondheim, Norway

* Corresponding author

Keywords: Gas Hydrates, equilibrium, cyclopentane

INTRODUCTION

Gas hydrates were, until recently, considered to be a phenomenon associated with small diameter hydrocarbon molecules. For systems relevant to the oil industry, the upper limit was set by n-butane.

In 1987, Ripmeester et al (1,2) discovered a new hydrate structure called structure H. This structure has cavities larger than those of the former known structures I and II and can therefore be stabilized by heavier guest molecules. Of components found in real hydrocarbon fluids, isopentane, methylcyclopentane, methylcyclohexane and 2,3-dimethylbutane were identified as potential structure H formers while benzene, cyclohexane and cyclopentane were identified as potential structure II formers.

Recently, Thoidi et. al (3) presented experimental and prediction results on the effect of isopentane, methylcyclopentane, cyclopentane and cyclohexane on the hydrate equilibrium properties of two natural gas mixtures. They concluded that structure II heavy hydrate formers increase the hydrate stability of the two hydrocarbon gas mixtures, where as structure H heavy hydrate formers do not have significant effect on the hydrate phase boundary.

In the oil industry the hydrate prevention strategy makes extensive use of hydrate prediction programs. To our knowledge, none of the present commercially available programs take account of the heavy hydrate formers. If some heavy hydrate formers, found in a real hydrocarbon fluid, have a significant effect on the hydrate equilibrium temperature these have to be included in the prediction programs.

In this work the hydrate equilibrium properties of isopentane, cyclopentane and cyclohexane in a synthetic hydrocarbon fluid have been determined. The vapor phase was simulated by either pure methane - a structure I former, or a synthetic gas mixture assuring formation of structure II. The hydrocarbon liquid phase was in all experiments Exxsol D60, which is a paraffinic C9 - C13 distillation cut.

Also presented is a survey of the content of cyclopentane in a selection of real hydrocarbon fluids from the North Sea area.

EXPERIMENTAL

All experiments were performed in a high pressure sapphire PVT-cell. The cell is placed in a temperature controlled air bath in which the temperature can be varied between -40 and +200 °C. The temperature stability is 0.1 °C and the resolution is 0.01°C. The cell has a maximum working pressure of 500 bara. The accuracy of the pressure measurement is estimated to be within 0.5 bar and the resolution is 0.1 bar. The cell volume is controlled and varied using a piston directly coupled to a computerized brushless motor. Volumes are read with a resolution of 0.0001 cm³. The estimated accuracy is 0.005 cm³. Maximum cell volume is 100 cm³.

Stirring is provided by a magnetically coupled stirrer, driven by a computer controlled, variable speed motor. Maximum speed is 1000 rpm. Rheology changes of the experimental fluids are continuously monitored by measurement of the effect required to keep the motor running at constant speed.

Experimental procedures. The sapphire cell was cleaned and evacuated prior to filling of the experimental fluids. All fluids were added gravimetrically in the following sequence: Water (purified by reversed osmosis), hydrocarbon liquid phase (D60 - added various amounts of heavy hydrate formers) and finally the hydrocarbon vapor phase (C1 or synthetic gas mixture). The water cut was, in all experiments, approximately 50%. The hydrocarbon phase were recombined and the saturation point, at ambient temperature, were determined.

Hydrate formation was initiated by cooling the system at a constant rate, 3 - 5 °C/hours, while continuously stirring the cell. After a period of time, allowing for equilibrium to be established, the system was reheated at a rate of 0.25 °C/hours until the hydrates were completely melted. The experiment gives information of the hydrate equilibrium temperature, the degree of sub cooling and the visual appearance of the formed hydrates. Hydrate formation and decomposition are indicated by deflections in a volume vs. temperature plot (the isobar) and by a change in the rheology of the system (the apparent viscosity). The experiments were performed at isobaric conditions, at 100, 200 and 300 bara.

All experiments were documented by video recordings.

Experimental fluids. The synthetic gas mixture were composed of C1, C2 and C3 in the ratio 74.89, 16.47 and 8.64 mole %, respectively. All components were minimum 99.9 % pure. Analysis of the mixture did not show significant contamination of any other components.

Methane were 99.95 % pure. Isopentane, cyclopentane and cyclohexane were all of analytical grade purity.

Exxsol D60 is a commercial paraffinic solvent. The composition of D60 is given in table 1.

The compositions of the different experimental systems are given in tables 2 and 3. The measured saturation pressure and the recombination gas/oil ratio are given along with the composition.

RESULTS AND DISCUSSION

The results from the experiments involving the potential heavy hydrate formers isopentane cyclopentane and cyclohexane, are presented in tables 2 and 3 and figures 1 to 4. Also included in these figures are predictions of the hydrate equilibrium conditions. These predictions were performed by use of PVTsim, a commercially available PVT and phase behavior simulation program.

Isopentane was expected to form structure H while cyclopentane and cyclohexane were expected to form structure II. As can be seen from the figures, only cyclopentane seems to have a significant effect on the hydrate equilibrium conditions for the tested systems. The effect of cyclopentane is, on the other hand, remarkable as hydrate equilibrium temperatures close to 30 °C were observed.

Isopentane: The effect of isopentane is demonstrated in figure 1. As can be seen from this figure, the hydrate equilibrium conditions for the C1/D60 system are not significantly altered by addition of isopentane at a concentration of 9.2 mole %. The C1/D60 system forms a structure I hydrate and our results indicates that, in this system, isopentane do not stabilize either structure II or structure H hydrate.

Cyclopentane: The effects of cyclopentane in a C1/D60 system are presented in figure 2. At concentrations of 9.4 and 4.6 mole % are the equilibrium temperature shifted to higher temperatures and it is reason to assume that the structure is shifted from I to II. At a concentration of 0.9 mole % are the hydrate equilibrium conditions for the C1/D60 system not significantly altered. It can thus be assumed that cyclopentane do not participate in the hydrate formation at this concentration.

The effects of cyclopentane in a synthetic gas/D60 system are presented in figure 3. This system forms structure II also when heavy hydrate formers are not added. The effect of adding 11 mole % cyclopentane to this system is seen by the significant increase in the hydrate equilibrium temperature.

Addition of 1.1 mole % cyclopentane to the synthetic gas system gives only a marginal increase (0.2 °C) of the hydrate equilibrium temperature.

Cyclohexane. The results from the experiments involving cyclohexane in a C1/D60 system are presented in figure 4. There were not observed any stabilizing effects in this system, which is expected to form structure I when no heavy hydrate formers are added. It seems therefore reasonable to conclude that cyclohexane, at this concentration, do not stabilize either structure II or structure H.

Significance for the hydrate prevention strategy. Figure 2 and 3 clearly states that cyclopentane at concentrations of 9.4 and 4.6 mole % significantly increases the hydrate equilibrium temperature. 1.0 mole % cyclopentane has, on the other hand, no significant impact on the hydrate equilibrium.

For the two systems tested, C1/D60 and synthetic gas/D60, our hydrate prediction program PVTsim predicts structure I and II, respectively. Cyclopentane is not included as a hydrate former in this program and the only predicted effect of adding cyclopentane to the test systems are a dilution of the hydrate formers and thus a slight reduction of the hydrate formation temperatures. At higher concentrations of cyclopentane will this clearly lead to a significant miscalculation of the hydrate equilibrium conditions.

Neither the concentration at which cyclopentane is able to switch from structure I to structure II, nor the concentration at which cyclopentane is able to significantly change the equilibrium temperature of structure II hydrate, are known. It seems, however, that 0.9 - 1.1 mole % is below the critical concentration where cyclopentane affect the hydrate equilibrium.

A survey of the content of cyclopentane in a selection of North Sea oil is given in table 4. As can be seen from this table the concentration seems, in general, to be below the critical concentration for having any significant impact on the hydrate equilibrium conditions.

CONCLUSIONS

- 1 The hydrate formation characteristics of two synthetic hydrocarbon system containing three heavy hydrate formers have been investigated.
- 2 9.2 mole % isopentane do not promote formation of structure II or structure H in a methane/D60 system. The hydrate equilibrium conditions are not significantly influenced.
- 3 9.4 and 4.6 mole % cyclopentane promotes formation of hydrate structure II in both the methane/D60 system and the synthetic gas/D60 system. The hydrate equilibrium conditions were shifted to higher temperatures.
- 4 1.0 mole % cyclopentane do not change the hydrate structure from I to II in the methane/D60 system and do not significantly increase hydrate the stability of structure II in the synthetic gas/D60 system.
- 5 8.0 mole % cyclohexane in a methane/D60 system do not promote formation of hydrate structure II or structure H and do not affect the hydrate equilibrium conditions.
- 6 In 13 different North Sea oil surveyed, are the concentrations of cyclopentane too low to affect the hydrate stability. We believe that the hydrate equilibrium conditions, for these oils, can be predicted with reasonable accuracy.

REFERENCES

- (1) Ripmeester, J.A., Tse, J.S., Ratcliffe, C.I. and Powell, B.M.: "A New Clathrate Hydrate Structure", *Nature* (1987) 325.
- (2) Ripmeester, J.A., Ratcliffe, C.I. and McLaurin, G.E.: "The role of heavier Hydrocarbons in Hydrate Formation", *AIChE Spring Meeting* (1991)
- (3) Thohidi, B., Danesh, A., Burgass, R.W. and Todd, A.C.: SPE35568 "Effects of Heavy Hydrate Formers on the Hydrate Free Zone of Real Reservoir Fluids", *European Production Operations Conference & Exhibition* (1996)

Table 1. Composition and properties of Exxsol D60.

Carbon no.	C9	C10	C11	C12	C13
N + iso paraffin (wt. %)	0	5	23	23	6
Naphtenes (wt. %)	1	13	18	8	3
Mw	126.2	140.8	155.4	169.8	183.7
Density (kg/m ³)	768	778	788	797	805

Table 2. The synthetic gas/D60 system. Composition and hydrate equilibrium data.

System	S.0	S.1	S.2
C1 (mole %)	41.16	38.02	39.9
C2 (mole %)	9.05	8.36	8.78
C3 (mole %)	4.75	4.39	4.60
Cy-C5 (mole %)		10.97	1.07
D60 (mole %)	45.03	38.26	45.66
GOR (Sm ³ /Sm ³)	144	139	132
Psat (Bara)	131 @23.1 °C	125 @23.9 °C	141@29°C
Hydrate equilibrium (°C):			
@ 100 Bara	19.7	25.3	19.9
@ 200 Bara	22.0	27.4	22.2

Table 3. The methane/D60 system. Composition and hydrate equilibrium data.

System	C.0	C.1	C.3
C1 (mole %)	60.87	57.69	57.67
i-C5 (mole %)		9.22	
Cy-C5 (mole %)			9.43
D60 (mole %)	39.13	33.09	32.90
GOR (Sm ³ /Sm ³)	182	182	183
Psat (Bara)	253 @24 °C	227 @23.6 °C	228 @24.5 °C
Hydrate equilibrium (°C):			
@ 100 Bara	13.7	12.9	25.7
@ 200 Bara			29.4
@ 300 Bara			29.8

Table 3 cont. The methane/D60 system. Composition and hydrate equilibrium data.

System		C.4	C.5	C.6
C1	(mole %)	59.02	59.75	58.47
C2	(mole %)			
Cy-C5	(mole %)	4.61	0.92	
Cy-C6	(mole %)			8.01
D60	(mole %)	36.37	39.33	33.52
GOR	(Sm ³ /Sm ³)	180	176	182
Psat	(Bara)	247 @25.4 °C	247 @21.7 °C	244 @24 °C
Hydrate equilibrium (°C):				
@ 100 Bara		22.4	13.1	13.6
@ 200 Bara			18.6	
@ 300 Bara			20.9	

Table 4. Content of cyclopentane in North sea oils.

Oil I.D.	Cyclopentane (mole %)	Cyclopentane (wt %)
1	0.04	0.01
2	0.03	0.01
3	0.07	0.05
4	0.07	0.05
5	0.12	0.11
6	0.04	0.04
7	0.05	0.04
8	0.06	0.05
9	0.05	0.04
10	0.09	0.09
11	0.08	0.08
12	0.04	0.02
13	0.07	0.03

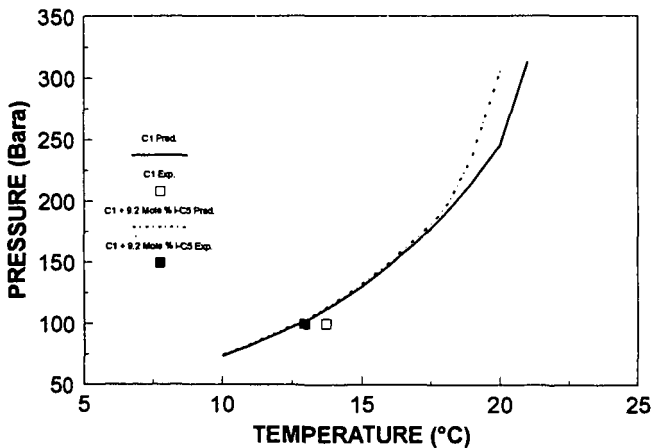


Figure 1. Experimental and predicted hydrate equilibrium conditions for a methane/D60 system containing isopentane.

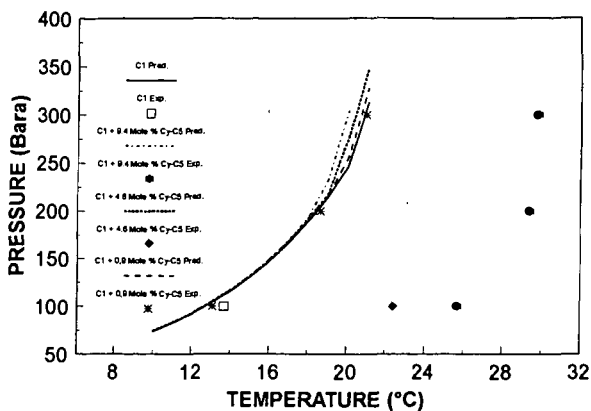


Figure 2. Experimental and predicted hydrate equilibrium conditions for a methane/D60 system containing cyclopentane.

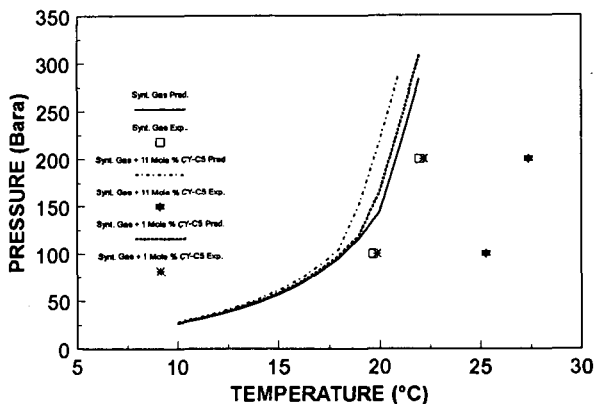


Figure 3. Experimental and predicted hydrate equilibrium conditions for a synthetic gas/D60 system containing cyclopentane.

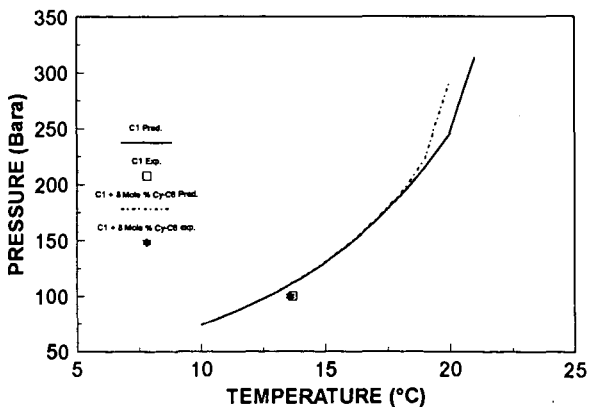


Figure 4. Experimental and predicted hydrate equilibrium conditions for a methane/D60 system containing cyclohexane.

ELECTRONIC AND VIBRATIONAL PROPERTIES OF GAS HYDRATES

J.S. Tse, Steacie Institute for Molecular Sciences, National Research Council of Canada, Ottawa, Ontario, Canada K1J 9B2, V. Shpakov and V. Belosludov, Institute for Inorganic Chemistry, Novosibirski, Russia 630090 and V.I. Murashov, Department of Chemistry, Dalhousie University, Halifax, Nova Scotia, Canada B3H 4J3.

Keywords : lattice vibration, thermal conductivity, clathrate hydrate

INTRODUCTION

The most unique physical property of gas hydrate is the anomalous low and unexpected glassy-like thermal conductivity [1,2]. This interesting behaviour has both significant practical and scientific consequences. Thermal conductivity is a vital parameter required for the computer modelling of the recovery of natural gas from the hydrate [3]. A knowledge on the variation of the thermal conductivity with pressure and temperature is a prerequisite to the exploitation of this important natural resource. Despite the well defined crystalline structures for gas hydrates [4,5], their thermal conductivities are characteristic of amorphous materials. The understanding of the causes responsible for this unusual phenomenon will shed light on the mechanism of thermal transport in the disorder system. In solid, the thermal energy is transported and dissipated by the acoustic lattice vibrations. These vibrations are normally too low in energy to be effectively studied by infrared and Raman spectroscopy. However, they can be conveniently probed by neutron incoherent inelastic spectroscopy. In the following, the results from such measurements will be presented and discussed with the aid of computer simulation of the guest and lattice vibrations with lattice dynamics and molecular dynamics methods.

EXPERIMENTAL AND THEORETICAL DETAILS

Methane hydrate in deuteriated water was prepared by condensation of the gas into a pressure vessel equipped with rolling rods at very low temperature. The vessel was then allowed to warm slowly to -30°C and annealed at this temperature with gentle rotation for 24 hours. The hydrate sample was carefully removed and stored under liquid nitrogen. The neutron incoherent inelastic experiments were performed at the C3 triple axis spectrometer at Chalk River Nuclear Laboratory [6]. Lattice dynamics [7] and molecular dynamics calculations [8] were performed on a single unit cell of 8 methane and 46 water molecules using the SPC [9] and TIP4P [10] water intermolecular potential, respectively.

RESULTS AND DISCUSSION

The experimental vibrational frequencies for the motions of the methane in the cavities of the hydrate can be obtained directly from the neutron scattering experiments. At 5 K, two peaks were observed at 32 , 57 and 72 cm^{-1} in the experimental spectrum which are in excellent agreement with the theoretical predicted values [11,6] at 35 , 54 and 78 cm^{-1} . These results reassured the reliability of the interaction potential models employed in the calculations. The motions of the enclathrated methane in the hydrate cages can be examined from the variation of the intensity of the $J = 0 \rightarrow 1$ rotational excitation peak with the neutron momentum transfer (Q) (fig. 1). If the methane is freely rotating the intensity of the excitation peak will be proportional to the first order Bessel function $J_1(Qr)$, where r is the C-H distance. A fit to the experimental data gives an effective C-H distance of 1.23 \AA

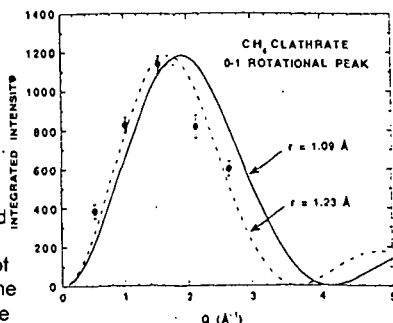


Fig. 1 Variation of the intensity (I) of the rotational peak with neutron momentum transfer (Q)

which is close to the correct value of 1.09 Å. This result indicates that the methane molecules rotate almost freely inside the hydrate cages and are in complete agreement with a previous NMR study [12]. Another important observation is the lack of energy dispersion in the rotational mode as the temperature is raised (fig.2). This effect is the consequence of a strong coupling between the low frequency acoustic lattice vibrations with the localized methane motions [13]. A clear picture of the interactions between the enclathrated methane with the host water lattice is now emerged from the neutron experiment. Although the methane molecule behaves like a free molecules, its motions are directly coupled with the lattice vibrations. This coupling provides a plausible mechanism for the transfer of thermal energy from the lattice to the methane. The heat transport can be dissipated via the thermal excitation of the methane thus reducing the thermal conductivity of the material

The interaction between the lattice acoustic vibrations with the localized motions of the guest has been proposed on the basis of molecular dynamics calculations [6] and experimental measurement of the lattice vibrational spectra of the gas hydrates [12]. This proposal can be quantified through the calculation of the cross time correlation function of the lattice and the guest motions by molecular dynamics techniques. The fourier transform of the correlation function gives the vibrational modes of the motions are correlated. If there is no correlation between the motions of the guest and the water lattice, time function will decay exponentially with time. Otherwise, the time decay will be modulated by the appropriate coupling frequencies. The results for such calculation for the structure I xenon hydrate and a hypothetical "light xenon" hydrate where the mass of the xenon has been set to 1 amu but retaining the interaction potentials as in the real xenon hydrate are shown in figs. 3 and 4. Inspection of the time correlation functions and their fourier transforms provide valuable information on the role of the guest-host coupling mechanism. In the case of the real xenon hydrate, it is evident that the correlation time extends to very long time (10 psec). The vibrational frequencies that couple the lattice and the guest vibrations occur at 23, 34 and 52 cm^{-1} . These frequencies are the same as the localized vibrations calculated for xenon [14] and fall within the acoustic region of the lattice vibrations [15]. Since the vibrational frequency of the rattling motion of the guest is inversely proportional to the square root of the reduced-mass [14], a "light xenon" should

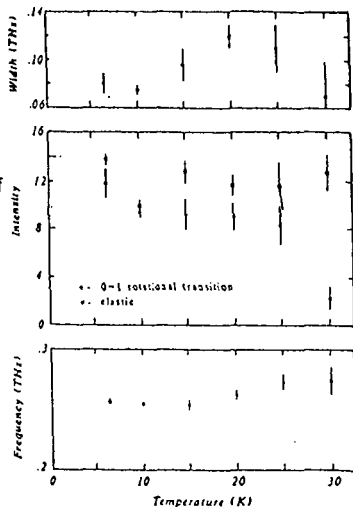


Fig. 2 The variation of the position, lineshape and intensity of the rotational peak with temperature.

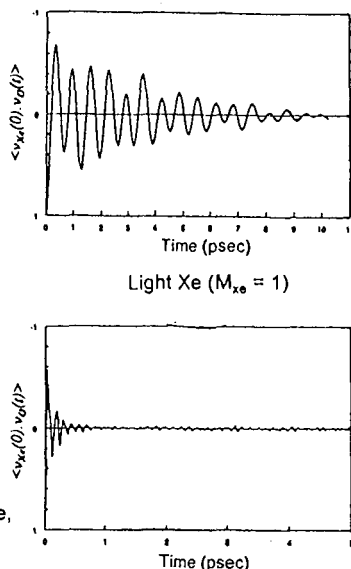


Fig. 3 The cross velocity correlation function for xenon and "light xenon" hydrate.

moves the guest vibrations out of the lattice acoustic region. This fact is shown in the calculations on the hypothetical hydrate. The correlation time between the "light xenon" and the lattice is extremely short and less than 1 psec. The corresponding "coupled" vibrations are located from 250 to 600 cm^{-1} , which are outside the translational region of the lattice vibrations. To summarize, it is shown from the present molecular dynamics calculations, the coupling between the guest and water lattice vibrations only occurs at the low frequency region. In practice, the hydrocarbons enclathrated in the hydrate structure all possess low frequency librational and rattling motions thus permitting the exchange of thermal energy with the host lattice.

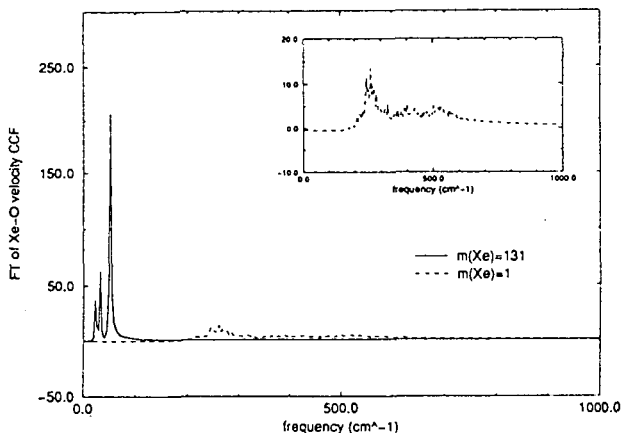


Fig. 4 The fourier transform of the cross velocity correlation function for xenon and "light xenon" hydrate.

Strong interactions between the guest and water lattice are also expected from a factor group analysis of the symmetry of the translational vibrational modes [13]. It can be easily shown that at the Brillouin zone center, both the guest and lattice translational vibrations possess the T_{1u} representation. However, the lattice acoustic lattice vibrations are strongly dispersive but the guest vibrations are largely localized and non-dispersive. A symmetry avoided crossing between the two vibrational branches must then occur along certain phonon wavevector between the zone center and the zone boundary. The resonance of two vibrational modes of the same symmetry can be a mechanism for energy transfer. A schematic representation of this interaction is shown in fig. 5. A lattice dynamics calculations on xenon hydrate indeed shows a considerable mixing of the positional displacements of the xenon and the water in the eigenvectors associated with the acoustic vibrations after the intersection of the phonon branches.

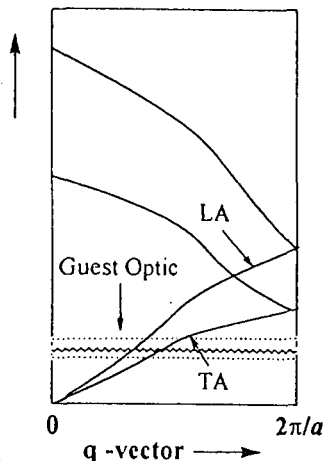


Fig. 5 Schematic diagram for the symmetry avoided crossing of the acoustic branch with the guest localized vibrations.

Realizing the basic mechanism for the coupling between the guest and host lattice, a simple model based on a modified Einstein model can be used to predict the thermal conductivity of gas hydrate [16, 17]. One important feature of this thermal conductivity

model is that only the molecular properties are needed as input parameters for the calculation of the thermal conductivity. In this model, the localized vibrations are assumed to be heavily damped with lifetimes of half a period of the oscillation and the distribution of the localized modes in a solid can be approximate by the Debye model. Using the equivalent of the gas kinetic equation, an expression for the minimum thermal conductivity Λ_{\min} can be derived.

$$\frac{\Lambda_{\min}}{\Lambda_{\infty}} = 2 \left(\frac{T}{\Theta_D} \right)^{2\Theta_D/T} \int_0^{\Theta_D/T} \frac{x^3 e^{-x}}{(e^x - 1)^2} dx$$

At high temperature when $T \gg \Theta_D$, the transport integral approaches unity and the limiting thermal conductivity Λ_{∞} is given by

$$\Lambda_{\infty} = \frac{1}{2} \left(\frac{\pi}{6} \right)^3 k_B n^3 (2v_t + v_l)$$

Where k_B is the Boltzman constant, n is the number density and v_t and v_l are the longitudinal and transverse sound velocity of the hydrate. Therefore, once the experimental density and acoustic sound velocities are known, the thermal conductivity at any temperature can be estimated. Previous calculations show that the calculated thermal conductivities for several gas hydrates employing these are in good accord with experiment [17].

The electrostatic field created by the water forming the cavities in a hydrate has important effects on the vibrations of the guest molecules. In view of the potential use of vibrational - infrared and Raman spectroscopies as an alternative means of the determination of the hydration number, it is imperative to understand these electrostatic effects. An electrostatic potential map (MEP) for the hydrate cavity can be computed from quantum mechanical method. We have computed the MEP for the small and large cage of a structure I hydrate. The MEP can be used to derive appropriate point charge model for the water molecules for the future simulation of the interactions between the guest and the cavities. Details of the computational results will be published elsewhere.

REFERENCES

1. Ross, R.G., P. Andersson, G. Backstrom, 1981, *Nature*, **290**, 322.
2. Tse, J.S., White, M.A., 1988, *J. Phys. Chem.*, **92**, 5006.
3. Holder, G., Angert, P.F., Pereira, 1983, "Natural Gas Hydrates", Cox, J.L. ed., Butterowrth Publishers.
4. McMullan, R.K., Jeffrey, G.A., 1965, *J. Chem. Phys.*, **42**, 2725.
5. Mak, T.C.W., McMullan, R.K., 1965, *J. Chem. Phys.*, **42**, 2732.
6. Tse, J.S., Powell, B.M., Sears, V.F., Handa, Y.P., 1993, *Chem. Phys. Lett.*, **215**, 383.
7. Shpakov, V.P., Tse, J.S., Belosludov, V.R., Belosludov, R.V., 1996, *J. Phys., Conden. Mat.*, (submitted).
8. Tse, J.S., Klein, M.L., McDonald, I.R., 1983, *J. Phys. Chem.*, **92**, 5006.
9. Berendsen, H.J.C., Postma, J.P.M., van Gunsteren, Hermans, J., 1981. "Intermolecular Forces", Pullman, B. ed., Reidel Dordrecht, the Netherlands.
10. Jorgenson, W. 79 L., Chandraskhar, J.D., Madura, J.D., Impey, R.E., Klein, M.L., 1983, *J. Chem. Phys.*, **79**, 926.
11. Tse, J.S., Klein, M.L., McDonald, I.R., 1987, *J. Chem. Phys.*, **91**, 5786.
12. Garg, S.K., Gough, S.R., Davidson, D.W., 1975, *J. Chem. Phys.*, **63**, 1646.

13. Tse, J.S., Ratcliffe, C.I., Powell, B.M., Sears, V.I., Handa, Y.P., 1997, *J. Phys. Chem.*, in press.
14. Tse, J.S., Klein, M.L., McDonald, I.R., 1983, *J. Chem. Phys.*, **78**, 2096.
15. Tse, J.S., Klein, M.L., McDonald, I.R., 1984, *J. Chem. Phys.*, **81**, 6124.
16. Cahill, D.G., Pohl, R.O., 1988, *Ann. Rev. Phys. Chem.*, **39**, 93.
17. Tse, J.S., 1994, *J. Incl. Phenom.*, **17**, 259.

DIRECT FREE ENERGY CALCULATIONS FOR GAS HYDRATES.

R.E. Westacott and P.M. Rodger

Chemistry Department, University of Reading, Whiteknights, Reading, Berks., RG6 2AD, UK.

Abstract.

In this work we present an efficient method for calculation of free energies for molecular crystals. This method is a generalization of the local harmonic approximation and allows full coordinate free energy minimization at finite temperatures and pressures. In terms of gas hydrates, this method provides a first principles route to the chemical potential of water in the hydrate lattice. This quantity has been calculated for different levels of cavity occupancy for the type I hydrate of methane. The values obtained indicate that the number of occupied cavities has a significant effect on the chemical potential of water. Further, we have used this method to calculate the total free energy of methane hydrate and ice. Using the integrated form of the equation of state for a Lennard-Jones fluid we have also calculated the free energy of the free guest species. With these three values the methane/ice/methane hydrate three-phase co-existence line can be obtained.

1. Introduction.

The ability to calculate free energy in an efficient manner is of paramount importance in the structural and thermodynamic study of gas hydrate systems. In principle, it is possible to fully characterize the structural and thermodynamic properties of the system from a knowledge of the free energy. In most cases, this involves calculating the structural or thermodynamic property as a function of temperature and pressure. If this is the case, the free energy must be calculated at many different state points. Thus the efficiency of the free energy calculation becomes the limiting factor and determines the scale of the calculations which can be undertaken.

The development of theories for free energy calculations on atomic solids based on local atomic vibrational behaviour has been an important contribution in this area¹. In the Local Harmonic Model (LHM) the atoms are modelled as Einstein oscillators which vibrate in the field created by the other atoms, but there is no interatomic vibrational coupling. The LHM is computationally inexpensive and has been shown to give a good description of the thermodynamic properties of atomic solids¹. It should be mentioned that analogous theories exist, notably the second moment model of Sutton², which is equivalent to the LHM only the nature of the approximation to the density of states differs. In this work we have further developed the LHM for complex molecular crystals and applied the theory to gas hydrates.

At present most attempts to explain the stability and properties of gas hydrates are based on the van der Waals and Platteeuw cell theory. According to this model the water molecules form a well-defined crystal lattice containing cavities into which the guest molecules may be absorbed. The theory also assumes that the free energy of the water lattice is independent of which molecules, if any, occupy the cavities. Thus the contribution of the water lattice to the total free energy of the system must be the same when all the cavities are empty as when all the cavities are occupied. Recent computer simulations by Rodger³ indicate some fundamental difficulties with the van der Waals and Platteeuw theory. His results indicate that the empty lattice is unstable rather than metastable. If this is the case, the guests must serve to dampen out the critical lattice vibrations that lead to the rearrangement of the host lattice. Tanaka⁴ has considered distortion of hydrate cages around xenon and carbon tetrafluoride guests. The work showed that the smaller xenon atoms did not distort the hydrate cages, while the carbon tetrafluoride caused significant distortion of the small cages. This deformation gave rise to a change in the water chemical potential and casts further doubt on the validity of the primary assumption of the cell theory.

In this paper we present the extension to the LHM for molecular crystals and its application to gas hydrates. The method provides a simple, computationally cheap tool for the investigation of the lattice relaxation in gas hydrates and their structural and thermodynamic properties. We present optimum cell lengths over a range of temperatures and pressures for methane hydrate obtained using a single co-ordinate free energy minimisation and a range of other properties. Also we present values of the free energy difference between ice and the β -hydrate, and between the β -hydrate and the water lattice of hydrates of various occupancies. We demonstrate how the three phase line (ice-hydrate-vapour) can be calculated using this method. Finally, we show the necessity for a full co-ordinate (*i.e.* all atomic co-ordinates) free energy minimisation rather than the single co-ordinate (*i.e.* unit cell length) calculation using the dissociation pressure calculated using each method compared to the experimental value.

Method.

The essence of the LHM is the ease of calculation of the vibrational partition function, q_{vib}

$$q_{vib} = \frac{1}{1 - e^{-\frac{h\nu}{k_B T}}} \quad (1)$$

which is simple to calculate from the vibrational frequency, ν

$$\nu^2 = \frac{\partial^2 U}{\partial r^2} \frac{1}{4\pi m^2} \quad (2)$$

The Helmholtz free energy can then be calculated from

$$A = -k_B T \ln q_{vib} \quad (3)$$

In the classical limit, where $k_B T$ is much greater than $h\nu$, equation (1) simplifies to

$$q_{vib} = \frac{k_B T}{h\nu} \quad (4)$$

For a perfect crystal with a unit cell of N atoms, the quasi-harmonic approximation gives the Helmholtz free energy as

$$A = U + kT \sum_i^{3N} \ln \left(2 \sinh \left(\frac{h\nu_i}{2kT} \right) \right) \quad (5)$$

where U is the potential energy and the vibrational frequency of atom i , ν_i , is obtained from the dynamical matrix with elements

$$D_{ij} = \frac{\partial^2 U}{\partial r_i \partial r_j} \quad (6)$$

as the square root of the eigenvalues of the matrix $M^{-1}D$, where M is the mass matrix. In the LHM, D_{ij} is set to zero unless i and j refer to co-ordinates of the same atom. Thus D is reduced from a $3N \times 3N$ matrix to N 3×3 matrices and the diagonalisation becomes substantially easier. Equation (5) is, therefore, a 3-dimensional, many-atom representation of equation (3).

However, for a molecular system, this neglect of interatomic coupling is only valid for atoms in different molecules. Within the same molecule the vibrations of the atoms are strongly coupled through the presence of covalent bonds. So, in the Molecular Local Harmonic Model (MLHM), the dynamical matrix can still be reduced to block diagonal form, except in this case each block represents a set of molecular co-ordinates rather than a set of atomic co-ordinates. Thus D is reduced to M 9×9 matrices. The expression for the Helmholtz free energy in the MLHM is

$$A = U + kT \sum_i^m \sum_j^{N_i} \ln \left(2 \sinh \left(\frac{h\omega_{ij}}{2kT} \right) \right) \quad (6)$$

where N_i is the number of atoms in molecule i , m is the number of molecules and $(\omega_{ij})^2$ are the eigenvalues of the molecular matrices $M_i^{-1}D_i$.

We have used the SPC model⁹ for water and a single Lennard-Jones site for the methane. Using a grid search method we have performed a single co-ordinate minimisation by calculating the free energy over a range of unit cell lengths. This is a simple application of the MLHM and provides optimum cell lengths and gradient properties such as thermal expansivity, isobaric compressibility and heat capacities. We have also performed full atomic co-ordinate free energy minimisation using a conjugate gradient-type approach, where the atoms are moved according to the free energy force. For the calculation of hydrate dissociation pressures we have used an equation of state for a Lennard-Jones fluid⁸ to describe the properties of the fluid guest.

III. Results.

In figure 1(a) we show the effect of temperature on the unit cell length of methane hydrate at 1 atmosphere. It is noticeable that the effect is linear and that the cell length values obtained are comparable with those of experiments⁷. In figure 1(b), we show the effect of pressure on the unit cell length of methane hydrate at 260 K. Again, the effect is linear and the cell length values are similar to experimental values⁷. The thermal expansivity calculated using the values shown in figure 1(a) is $1.78 \times 10^{-4} \text{ K}^{-1}$. This compares favourably with $0.77 \times 10^{-4} \text{ K}^{-1}$ obtained experimentally by Tse *et al.*⁹. The compressibility calculated from figure 1(b) is $3.3 \times 10^{-11} \text{ Pa}^{-1}$, which compares well with the estimate of $14 \times 10^{-11} \text{ Pa}^{-1}$ given by Sloan¹⁰. The heat capacities calculated from our work are of the order of 50 to 55 $\text{J mol}^{-1} \text{ K}^{-1}$, which is a factor of 4 to 5 smaller than the experimental values of Handa¹¹.

Initial observations of these results suggest that there is some effect of the guest molecules on the host lattice. The difference in Gibbs free energy between the β -hydrate and the water lattice of the occupied hydrates is approximately 1.1 kJ/mol. These differences are very similar to empirical estimates obtained by the cell theory for the free energy difference between the hydrate water lattice and ice (1.2-1.3 kJ/mol at 273 K¹²). There are also differences between the Gibbs free energies of the water lattices of the occupied systems. This difference is approximately 0.1 kJ/mol. On closer inspection, inclusion of guest molecules appears to stabilise the water lattice. However, it seems that enhanced stability and guest inclusion have a complex relationship. The fully occupied methane hydrate may have the lowest total Gibbs free energy, but it does not have the most stable water lattice. Occupation of the two 5¹² cavities has the greatest stabilising effect on the water lattice.

There seems to be some degree of variation of the effect of guest molecules on the host water lattice with temperature and pressure. The biggest differences, around 1.1 kJ/mol, are experienced at the higher temperatures and lower pressures that we have studied. These are precisely the conditions of interest in industrial applications. Given that the magnitude of these changes in the free energy of the water lattice, ΔG_{H} , is comparable with $\Delta\mu_{\text{w}}^{\text{B}}$, it must be expected that the accuracy of the cell theory predictions will vary with composition. At low temperatures and higher pressures the difference is considerably smaller, about 0.2 kJ/mol.

From the full atomic co-ordinate free energy minimisation we observe similar trends, such that the fully occupied hydrate is always the most stable hydrate, but the hydrates of intermediate occupancy have the more stable water lattice than either the β -hydrate or the fully occupied hydrate. The magnitude of ΔG_{H} seems to be temperature dependent, so that at higher temperatures the difference is larger. This is a reflection of the fact that the free energy minimisation is entropy driven. Our calculations show that ΔG_{H} can be as high as 2.3 kJ/mol at higher temperatures. Such differences in the thermodynamic properties are currently ignored in the cell theory, which assumes that the properties of the water lattice of occupied hydrates are the same as the β -hydrate. Thus $\Delta\mu^{\alpha-\beta}$ in the cell theory ignores any occupancy-dependent properties. Holder and Hand¹³, for example, used an optimum value for $\Delta\mu^{\alpha-\beta}$ of 1.115 kJ/mol. It is clear that occupancy-dependent changes in $\Delta\mu^{\alpha-\beta}$ of about 2.3 kJ/mol will be very significant and inclusion of such guest perturbation of the host lattice will be necessary to correct errors experienced when using the cell theory to determine hydrate dissociation pressures.

The MLHM, when coupled with an appropriate equation of state to describe the thermodynamics of the bulk guest phase, can be used to calculate hydrate dissociation pressures by calculating points on the ice/gas/hydrate phase line. We have used results from the unit cell optimisation and the full co-ordinate minimisation in order that we may determine whether the full co-ordinate minimisation is necessary to correctly describe gas hydrate properties, or whether the single co-ordinate minimisation is sufficient. In figure 2, we illustrate the dissociation pressure calculated using the unit cell optimisation. The point where the two lines cross indicates the dissociation pressure and in this case, methane hydrate at 270 K, it is approximately 40 MPa. In figure 3, we illustrate the case for full co-ordinate minimisation. Here we calculate the dissociation pressure to be 2.5 MPa. This is in excellent agreement with the experimental value⁸ of 2.32 MPa. The quality of this agreement must be contemplated given the errors within the SPC model¹⁴, although SPC water has been shown to yield the correct melting temperatures for methane hydrate¹⁵.

IV. Conclusions.

In this paper we have shown the development of a simple model for free energy minimisation of complex molecular crystals. We have applied this model to gas hydrates and shown that calculation of thermodynamic properties using this method yields values in good comparison to experiment. We have demonstrated the importance of lattice relaxation in the calculation

of some of these properties and illustrated this using the calculation of dissociation pressure as an example.

¹ LeSar, R., Najafabadi, R. and Srolovitz, D.J., *Phys. Rev. Lett.*, **63**, 624 (1989)
² Sutton, A.P., *Phil. Mag. A.*, **60**, 147 (1989)
³ Rodger, P.M., *J. Phys. Chem.*, **93**, 6850 (1989)
⁴ Tanaka, H., *Chem. Phys. Lett.*, **202**, 345 (1993)
⁵ Berendsen, H.J.C. *et al.*, in *Molecular Dynamics and Protein Structure*, ed. J. Hermans, Polycrystal Book Service, Illinois (1985)
⁶ Nicholas, J., Gubbins, K., Street, W.B., and Tildesley, D.J., *Mol. Phys.*, **37**, 1429 (1979)
⁷ Bertie, J.E. and Jacobs, S.M., *J. Chem. Phys.*, **77**, 3230 (1982)
⁸ Tse, J.S., McKinnon, W.R. and Marchi, M., *J. Chem. Phys.*, **91**, 4188 (1987)
⁹ Handa, Y.P. *et al.*, *J. Chem. Phys.*, **94**, 623 (1991)
¹⁰ Sloan, E.D., *Clathrate Hydrates of Natural Gases*, Dekker, New York (1990)
¹¹ Handa, Y.P., *J. Chem. Thermo.*, **18**, 891 (1986)
¹² Holder, G.D., Corbin, G. and Papadopolous, K., *Ind. Eng. Chem. Fundam.*, **19**, 282 (1980)
¹³ Holder, G.D. and Hand, J.H., *AIChE J.*, **28**, 440 (1982)
¹⁴ Karim, O.A., Kay, P.A. and Haymet, A.D.J., *J. Chem. Phys.*, **92**, 4634 (1990)
¹⁵ Rodger, P.M., Forrester, T.R. and Smith, W., *Fluid Phase Equilibria*, **116**, 326 (1996)

Figure 1(a) Effect of Temperature on Unit Cell Length.

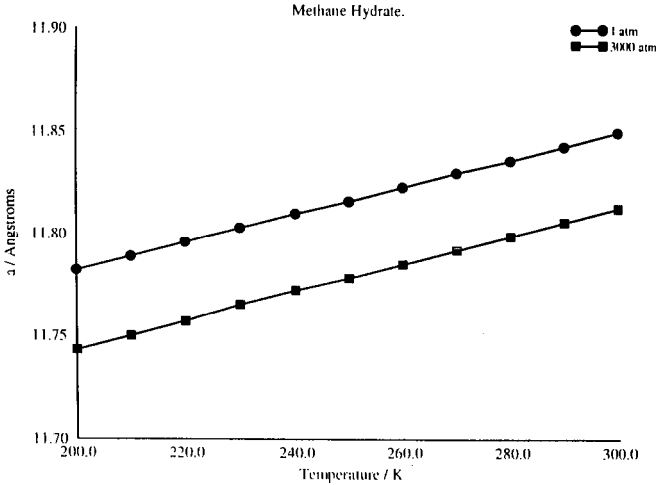


Figure 1(b) Effect of Pressure on Unit Cell Length.

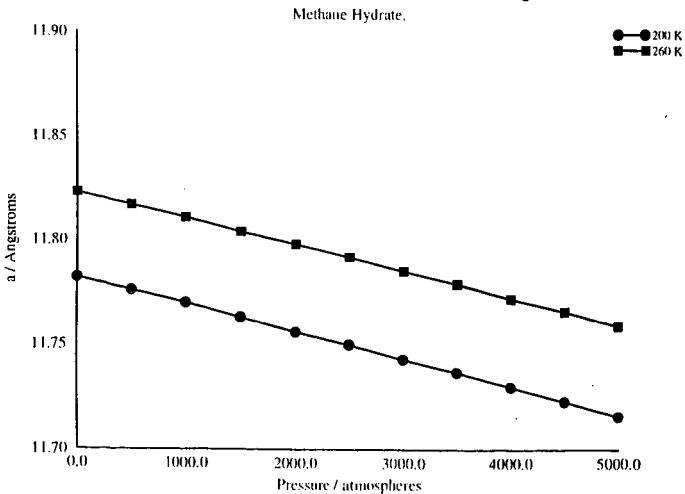


Figure 2. Dissociation Pressure of Methane Hydrate.

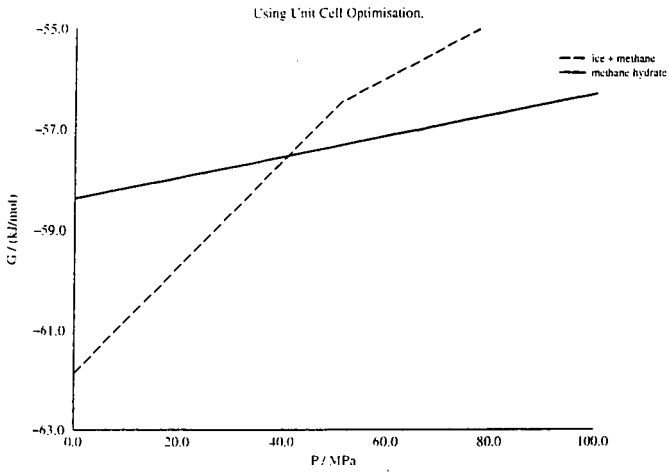
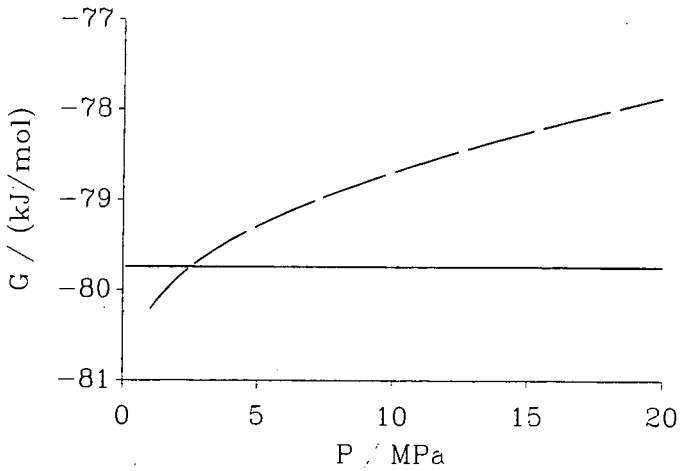


Figure 3. Dissociation Pressure of Methane Hydrate. Using full coordinate optimisation.



SYNTHESIS OF POLYCRYSTALLINE METHANE HYDRATE, AND ITS PHASE STABILITY AND MECHANICAL PROPERTIES AT ELEVATED PRESSURE

Laura A. Stern, Stephen H. Kirby (both at: USGS, Menlo Park, CA 94025)
and William B. Durham (UCLLNL, Livermore, California, 94550)

Key words: gas hydrate synthesis; reaction kinetics; mechanical properties

Abstract

Test specimens of methane hydrate were grown under static conditions by combining cold, pressurized CH_4 gas with H_2O ice grains, then warming the system to promote the reaction $\text{CH}_4(\text{g}) + 6\text{H}_2\text{O}(\text{s}) \rightarrow \text{CH}_4 \cdot 6\text{H}_2\text{O}$. Hydrate formation evidently occurs at the nascent ice/liquid water interface, and complete reaction was achieved by warming the system above 271.5 K and up to 289 K, at 25-30 MPa, for approximately 8 hours. The resulting material is pure methane hydrate with controlled grain size and random texture. Fabrication conditions placed the H_2O ice well above its melting temperature before reaction completed, yet samples and run records showed no evidence for bulk melting of the ice grains. Control experiments using Ne, a non-hydrate-forming gas, verified that under otherwise identical conditions, the pressure reduction and latent heat associated with ice melting is easily detectable in our fabrication apparatus. These results suggest that under hydrate-forming conditions, H_2O ice can persist metastably at temperatures well above its melting point.

Methane hydrate samples were then tested in constant-strain-rate deformation experiments at $T = 140\text{--}200\text{ K}$, $P_c = 50\text{--}100\text{ MPa}$, and $\dot{\epsilon} = 10^{-4}\text{--}10^{-6}\text{ s}^{-1}$. Measurements in both the brittle and ductile fields showed that methane hydrate has measurably different strength than H_2O ice, and work hardens to a higher degree compared to other ices as well as to most metals and ceramics at high homologous temperatures. This work hardening may be related to a changing stoichiometry under pressure during plastic deformation; x-ray analyses showed that methane hydrate undergoes a process of solid-state disproportionation or exsolution during deformation at conditions well within its conventional stability field.

INTRODUCTION

Methane hydrate is a nonstoichiometric compound consisting of a network of H_2O molecules that are hydrogen-bonded in a manner similar to ice and interstitially encaging CH_4 gas molecules (1). Distributed globally in shallow marine and permafrost environments, methane hydrate harbors a significant yet virtually untapped hydrocarbon source (2,3,4). Despite scientific interest in this compound and potential commercial importance, many of the physical and material properties of methane hydrate are as yet poorly constrained or unmeasured, and a full understanding of these properties will eventually be needed to turn potential energy projections into practical plans for its recovery. We have now established optimal growth parameters for efficient synthesis of methane hydrate suitable for such testing, and have measured these samples in deformation experiments to determine fracture and flow characteristics. The results revealed some anomalous behavior in the formation, plastic flow behavior, and stability of methane hydrate at elevated pressure (5).

SAMPLE SYNTHESIS

Our objective was to synthesize large-volume, cohesive, low-porosity, polycrystalline hydrate aggregates with controlled, fine grain size and random crystallographic grain orientation. Our technique differs from previous studies (6), most of which involve continuous agitation of reaction mixtures, resulting in strongly textured material unsuitable for materials testing. We produced samples of virtually pure methane hydrate by the general reaction $\text{CH}_4(\text{g}) + 6\text{H}_2\text{O}(\text{s}) \rightarrow \text{CH}_4 \cdot 6\text{H}_2\text{O}(\text{s})$, by the mixing and subsequent slow, regulated heating of sieved granular ice and cold, pressurized CH_4 gas in an approximately constant-volume reaction vessel (Figs. 1, 2, & 3A).

Sample fabrication details are as follows: CH_4 gas from a source bottle is initially boosted in pressure (P) by a gas intensifier and routed into sample molding vessels housed in a deep freezer. The sample assembly (Fig. 2) consists of two steel vessels immersed in an ethyl alcohol bath initially held at freezer temperature (T) of 250 K. One vessel serves as a reservoir to store and chill pressurized CH_4 gas, and the other houses the sample mold. The mold consists of a hollow split-cylinder that encases an indium sleeve filled with 26 g of H_2O ice "seed" grains, packed to 40% porosity. Seed material is made from a virtually gas-free, single-crystal block of triply distilled H_2O ice, ground and sieved to 180-250 μm grain size. Initially, the sample chamber with seed ice is closed off from the reservoir and is evacuated. A loosely fitting top disk inserted on top of the packed seed ice grains (Fig. 2) prevents displacement of the packed ice grains during evacuation.

The reservoir vessel is first charged with pressurized CH_4 gas to 34 MPa, and cools to 250 K. The reservoir is then opened to the pre-evacuated sample chamber, and CH_4 pressure drops to roughly 22 MPa. These steps serve to fill the porosity between the ice grains at a molar ratio of CH_4 to H_2O in the sample vessel well in excess of that required for full hydrate formation (7, 8). The bath T is then slowly raised by means of the hot plate situated beneath the alcohol bath (Fig. 2). As the sample and reservoir warm, they self-pressurize. Pressure increases steadily with increasing T until reaction initiates, at which point consumption of CH_4 gas by hydrate formation slows the rate of P increase. Data-acquisition software (LabVIEW, National Instruments) was used to monitor and record P and T conditions throughout each run, and the extent of reaction was determined by the measured P_{CH_4} offset from the reversible CH_4 expansion curve.

Following full reaction, the heat source is turned off and the system slowly cools back down to 250 K. The sample chamber is then quenched in liquid nitrogen, isolated from the reservoir, vented, disconnected from the apparatus, and opened. The inner, hollow split-cylinder containing the sample is pushed from the mold and pried off the jacketed sample. Samples are then stored in liquid nitrogen until mechanical testing.

THE HYDRATE-FORMING REACTION & POSSIBLE SUPERHEATED ICE

Representative pressure-temperature (P-T) and temperature-time (T-t) histories during a reaction run are shown in Figure 4. Up to at least 271.5 K, CH₄ pressure increases approximately linearly with T with a slope largely governed by the equilibrium thermal expansion of free CH₄ in the reservoir and sample reaction vessel. Progress of the hydrate-forming reaction was monitored by observing the deflection of P from this linear P-T curve, a deflection that accompanies the volume reduction associated with reaction. Completion of the reaction is marked by a P offset (ΔP_r) of 1.8 ± 0.1 MPa at a peak T of ~ 289 K, a state that is reached over a heating time interval of about 8 hours after the vessel crosses the 271.5 K isotherm (Fig. 4). After cooling to 77 K while venting unreacted CH₄, the resulting samples were shown by x-ray diffraction measurements to be virtually pure methane hydrate, with minor amounts of ice (0-3%) being the only additional phase (Fig. 3). That practically all the H₂O reacted to form hydrate was also consistent with both the calculated molar volume reduction of the reaction (9), and with the lack of a P-T anomaly associated with freezing of unreacted liquid water (Fig. 4A, cooling curve). Measurements of the mass uptake of CH₄ in fully reacted samples also were consistent with essentially complete reaction of the original H₂O to form hydrate of composition near CH₄·6.1H₂O (± 0.1 H₂O), which is the expected equilibrium stoichiometry for this compound at approximately 25-30 MPa methane pressure (9, 10). The resulting samples are translucent, white, cohesive aggregates of uniformly fine, equant grains with 250 ± 50 μ m grain size. The samples contain 28-30% porosity after full reaction (9). This porosity is eliminated by externally pressurizing sealed samples while venting the pore space gas, which we discuss later.

The detailed P-T-t curves (Fig. 4) and analyses of recovered samples revealed unexpected aspects of the reaction process. Figure 4 shows that deviation of the P-T record from the CH₄ self-pressurization curve first occurs just above the expected melting T of H₂O ice, 271.5 K at 28 MPa. As time proceeds, the rate of P increase slows as the hydrate-forming reaction consumes CH₄ gas (9). X-ray diffraction patterns of samples from runs with maximum temperatures below the ice melting curve showed no evidence of hydrate, and no deflections were observed in the P records to indicate any significant CH₄ mass uptake. Lack of appreciable reaction of CH₄ with ice below the H₂O liquidus was expected, in light of earlier investigations (6, 8).

After approximately 45% ΔP_r , the reaction rate decreases markedly. Full reaction was found to be most readily achieved by continuing to warm the system to conditions approaching the hydrate dissociation curve and well above the metastable extension of the H₂O melting curve (Figs. 1 & 4). To determine the rate of conversion of ice to hydrate at these conditions of T and P as a function of time, a series of partial-reaction experiments were quenched at various points along the full reaction curve, and subsequently weighed and x-rayed to determine hydrate content (Fig. 4, runs A - E). These partial-reaction tests indicate that during the early stages of reaction up to values of roughly 0.5 ΔP_r , the slow rate of seed ice melting still "outpaces" hydrate formation, as there is less hydrate in the samples than would be predicted by ΔP_r [see (5) for further discussion]. After this period, the rate of hydrate formation essentially keeps pace with incipient melting for the remainder of the 8 hours needed for full reaction at these conditions.

Figure 4 shows that there are no P-T discontinuities in the fabrication records to indicate bulk melting of the seed ice in the sample molds, even though full reaction to form hydrate at these conditions requires about 8 hours at temperatures well above the H₂O melting curve. The positive slope of the P-T curve within a few degrees above 271.5 K shows that there is not immediate and full melting of the ice as it is warmed above its liquidus, and there is a period of several tens of minutes after crossing the liquidus before there is any substantial indication of either ice melting or hydrate forming. These observations point to the conclusion that a large fraction of the seed ice exists in a superheated state for the many hours needed for full hydrate conversion.

This conclusion was verified by control experiments using neon (Ne, a non-hydrate-forming gas) in place of CH₄ gas, under the same environmental conditions and in the same apparatus as the methane hydrate samples (Fig. 5). We have previously described these results (5) and briefly outline them here. The Ne experiments confirmed that rapid, wholesale melting of the H₂O ice during the heating phase and refreezing of ice during the cooling phase of the tests (Fig. 5A) occurs in our apparatus when ice is not in the presence of a hydrate-forming gas, and that the associated P-T anomalies are easily detected. The T measured by the Ne sample thermocouple lags the rising T in the surrounding alcohol bath during the time interval over which the pressure drops (Fig. 5B), a phenomenon that we attribute to the absorption of heat by the expected endothermic melting of ice. In comparison, the T records of CH₄ runs displayed no such thermal anomalies, indicating that rapid, wholesale melting did not occur (Fig. 5B) (12). A prominent refreezing P-T anomaly occurred during the cooling phase of the Ne runs, and no P offset was detected after returning to the starting temperature (Fig. 5A). Visual inspection and x-ray identification of the final, quenched samples from the Ne experiments showed that they consist of clear cylinders of H₂O ice in the bottom of the mold, and that the loosely fitting top disk had sunk to the bottom, indicating full melting. In contrast, fully reacted methane hydrate samples have uniformly fine-grained granular textures and no displacement of the top disk. The Ne control experiments thus demonstrate that all the indicators of ice melting expected in our apparatus are actually observed when a non-hydrate-forming gas is used in the place of methane. The lack of such indicators in the methane experiments implies that such melting does not occur when hydrate is forming at our fabrication conditions.

The apparent suppression of macroscopic ice melting during methane hydrate synthesis raises several important questions; namely, why is full reaction achieved only after many hours at temperatures well above the the H₂O ice melting point, and why is there no evidence for wholesale melting of unreacted seed ice during this time? Probably of greatest influence is the availability of fresh ice surfaces to nucleate hydrate formation. For hydrate formation from either water or ice, the formation rate greatly diminishes once a surface layer of hydrate has formed, and vigorous shaking or stirring to crack the hydrate encasement and re-ew CH₄ access to ice/water surfaces is needed in order to continue the formation process at appreciable rates (13). Hwang and colleagues (8),

however, grew methane hydrate on disks of melting ice to measure hydrate growth rates at constant temperatures under static conditions. They observed two stages of methane hydrate formation, an initial "nucleation" period during which the formation rate increased with time, followed by a "growth" period, during which the formation rate decayed with time until no more ice remained on the disks. Hydrate growth rates were shown not only to be determined by the rate of the supply of the hydrate-forming species to the growth surface, but also by the rate of removal of the exothermic heat of formation from the forming surface (14). They concluded that the onset of melting ice along exposed surfaces not only promoted hydrate formation by providing a "template" for the formation of hydrates, but moreover, provided a heat sink for absorbing the heat of formation during hydrate growth. Once a rind of hydrate has encased an ice grain, the most likely process of continued hydrate formation involves solid-state diffusion of methane gas through the hydrate shell to the ice core (8, 15).

Our observations are in accord with the interpretations of Hwang et al. (8), and additionally we conclude from our sample textures and run records that this surface layer of hydrate encasing each seed ice grain not only rate limits reaction in the grain interior, but also serves to shield the ice grain from nucleating melt by removing the existence of a free external ice surface. A similar superheating effect has been measured in gold-plated silver single crystals, and results suggest that either a free external surface or internal defects or dislocations are critical for melting to take place at the normal "thermodynamic" melting point (16). In our experiments, methane hydrate may be producing a similar effect by shielding the ice cores from nucleating melt and from establishing a liquid-solid H₂O interface, by rapid reaction of incipient melt nuclei with CH₄ gas to form hydrate. We note that our method of seed ice preparation produces grains with few internal grain boundaries, and additionally, the ice grains are likely to anneal at the warm temperatures during fabrication, thus removing many of the internal defects for melt to nucleate on.

SOLID-STATE DEFORMATION TESTING & RESULTS

The strengths of methane hydrate specimens made by the above techniques were measured in constant-strain-rate tests in compression, at conditions ranging from T= 140 to 200 K, confining pressure (P_c) = 50 to 100 MPa, and strain rates ($\dot{\epsilon}$) = 3.5×10^{-4} to 10^{-6} s^{-1} (Table 1).

The testing apparatus is a 0.6 GPa gas deformation apparatus outfitted for cryogenic use, in which N₂ or He gas provides the P_c medium (17, 18) (Fig. 6). The thin, soft, indium jackets in which the samples were grown serve to encapsulate them during testing to exclude the P_c medium. Sample interiors were vented to room conditions by means of small-diameter tubing to allow initial compaction to eliminate porosity. The pressurized column within the apparatus consists of an internal force gauge, the jacketed sample, and a moving piston that compresses the sample axially against the internal force gauge at a fixed selected displacement rate (\dot{u}). Elastic distortion of the force gauge is measured outside the vessel and changes only with P_c and with the differential load that the piston exerts on the sample. In these experiments, differential force (F) and piston displacement (u) are recorded, corrected for changes from initial cross-sectional area and length (A_0, L_0) to instantaneous values (A, L), and converted to differential stress (σ), axial shortening strain (ϵ) and strain rate ($\dot{\epsilon}$) by the relationships: $\epsilon = u/L_0$; $\dot{\epsilon} = \dot{u}/L$; $A \cdot L = A_0 \cdot L_0$; $\sigma = F/A$. The force-time record (which we convert to stress-strain, as in Fig. 7B) usually reveals a transient response followed by a strength that ceases evolving with time, when various processes of work hardening and recovery have reached a steady-state condition.

Samples were subjected to a hydrostatic pressurization and compaction sequence at 170 K, prior to deformation. During this procedure, P_c was slowly "stepped" up to 100 MPa in increments of about 20 MPa. Following each P step, the piston was advanced to touch and square the bottom of the sample, then advanced just sufficiently to lightly compress the sample in order to compact it with minimal plastic deformation. Six of the samples were compacted using the internal vent line to eliminate the pore-space gas, and two of the samples were compacted without the venting capability. One sample (run 366, Table 1) was examined after compaction in the undeformed state. Volumetric measurements showed that virtually all porosity was eliminated, and that a cylindrical shape was largely maintained with only minor distortion of the sample. X-ray analysis showed evidence of a small fraction of H₂O ice in the sample ($\approx 7 \pm 3\%$), likely due to a disproportionation of hydrate as increasing P effects a stoichiometric change from CH₄·6.1H₂O to CH₄·5.8H₂O (10).

A suite of seven hydrostatically-compacted samples of methane hydrate were then tested by the methods described above and at the conditions shown in Table 1. Samples displayed measurably different steady-state strengths than H₂O ice, and results are summarized in Figure 7A. Moreover, the characteristics of transient deformation are markedly different. A typical stress-strain curve for methane hydrate is shown in Figure 7B; whereas H₂O ice ordinarily exhibits a strength maximum before leveling off to steady flow stress, usually within the first 5 - 10% of strain, methane hydrate exhibits monotonic work hardening (or strain hardening) that continues over more than 15% strain. This hardening effect persists to an extreme degree not only relative to other ices, but to most metals and ceramics as well.

Comparison of pre- and post-deformation x-ray diffraction analyses shows that samples underwent further structural changes while deforming within the nominal hydrate stability field. All deformed samples showed a significant volume fraction of ice in their final x-ray patterns ($25\% \pm 10\%$, Fig. 4B) compared with virtually no ice in their pre-test x-ray patterns ($<3\%$, Fig. 4A), and also showed larger fractions of ice than detected in the pressurized-only sample (run 366). It is possible, however, that either heterogeneous ice precipitation or deformation-enhanced textural and grain size changes in the precipitated ice increased the apparent ice peak intensities. No peaks were observed in post-deformation x-ray patterns to indicate growth of any other new phase besides ice and structure I hydrate. We note that the two non-vented samples (281 & 282), showed equally large fractions of ice in their post-deformation x-ray patterns as the vented samples. After first detecting this apparent solid-state disproportionation of the hydrate, a gas collection system was attached to the vent line for two of the runs to observe and collect possible CH₄ gas evolving during deformation. The only gas that appeared from the vent, however, was that squeezed from the pores

during initial pressurization before deformation. No gas evolved from the system during any portion of deformation testing or subsequent unloading. While collapse of the hydrate structure could occur if as-molded material were strongly nonstoichiometric and contained significant lattice vacancies, this is unlikely as we measured nearly full uptake of CH₄ gas into the as-molded material. Double occupancy in lattice cages also seems unlikely as a possible explanation due to special considerations. We therefore conclude that at the deformation conditions of this study, methane hydrate appears to undergo a form of stress-enhanced exsolution and/or precipitation process within its nominal stability field. Precipitating H₂O ice may likely be causing a dispersion hardening process during hydrate deformation, a process that will be targeted in further studies.

SUMMARY

Methane hydrate displays exceptional characteristics that merit further investigation into the nature and behavior of this important compound. In the course of establishing optimal growth parameters for synthesizing hydrate samples suitable for rheological testing, we demonstrated that under conditions favorable to hydrate formation, the rate of H₂O ice melting may be suppressed to allow short-lived superheating of ice to temperatures well above its melting point. Deformation tests showed that not only does methane hydrate have a measurably different rheology than H₂O ice, but that it also undergoes extensive work hardening accompanied by a process of solid-state disproportionation during deformation at conditions well within its equilibrium stability field. Such unexpected consequences of methane hydrate formation and deformation may affect the physical, mechanical, and geochemical properties of hydrate-bearing sediments in ways not previously appreciated. In particular, hydrate instability under nonhydrostatic stress may affect environments such as those underlying continental shelves or in associated accretionary prisms prone to regional tectonic influences, where the presence of hydrates influences the strength, stability, porosity, pore-fluid composition, and migration pathways of hydrate-cemented sediments.

REFERENCES & NOTES

- Natural gas hydrates belong to either of two crystal structures; methane hydrate (CH₄·6H₂O) is a structure I hydrate (1.2 nm cubic unit cell, space group *Pm3n*), constructed from 46 H₂O molecules and eight cavities available for CH₄ gas molecules.
- E. Sloan, *Clathrate Hydrates of Natural Gases*, Marcel Dekker, Inc., New York, 641 p., 1990.
- K. Kvenvolden, *Chemical Geology*, **71**, 41-51, 1988.
- Because hydrates concentrate methane by a factor of 170 with respect to STP gas and as little as 10% of the recovered energy is required for dissociation, hydrate reservoirs are considered a substantial future energy resource; it has been estimated that the total amount of gas in this solid form may surpass the energy content of the total fossil fuel reserves by as much as a factor of two (2), (3), also Claypool, G.E., and I. R. Kaplan, in: Kaplan, I. R., (ed), *Natural Gases in Marine Sediments*, Plenum Press, New York, 99-139, 1974).
- L. Stern, S. Kirby, and W. Durham, *Science*, **273**, 1843-1848, 1996.
- R. Barrer and D. Ruzicka, *Trans. Faraday Soc.*, **58**, 2253, 1962; R. Barrer and A. Edge, *Proc. Roy Soc. (London)*, **A300**, 1, 1967; B. Falabella and M. Vanpee *Ind. Eng. Chem. Fund.*, **13**, 228, 1974; K. Aoyogi, K. Song, R. Kobayashi, E. Sloan, and P. Dharmawardhana, *Gas Processors Assn. Research Report No. 45*, Tulsa, OK, 1980; see Sloan (2) for full review of fabrication techniques.
- Hwang et al (8) noted that for hydrate formation from melting ice, higher gas P yields higher formation rates. Makogon (15) had earlier suggested that as hydrate formation is an interfacial process, high concentrations of hydrate-forming species are required at the interface.
- Hwang, M.J., D.A. Wright, A. Kapur, and G. D. Holder, *J. Inclusion Phenom.*, **8**, 103-116, 1990.
- The volume of an empty structure I hydrate lattice is 16% greater than the equivalent mass of ice I [the empty structure I lattice has a density of 0.78, and stoichiometric methane hydrate has a density near ice (0.90 vs 0.92 for ice)], but there is a large ΔV associated with hydrate formation due to the volume reduction of the gas phase into the hydrate structure. Here, we start with 26 g of seed ice, and the actual molar reaction is: 1.4H₂O + 0.23 CH₄ (g) \rightarrow 0.23(CH₄·6 H₂O). The 3.8 g of CH₄ uptake measured after sample synthesis confirms this hydrate stoichiometry and is consistent with (10). Independent measurement of CH₄ collected from a dissociating sample also verified this stoichiometry (K. Kvenvolden and T. Lorenson, personal communication). While ΔV of the reaction is nearly 21%, we only measure a 6.4% associated drop from the starting P due to the large volume of the combined reservoir plus sample chamber.
- Gas hydrate number *n* varies with P; increasing P maximizes guest-molecule site occupancy. At sample synthesis conditions (~28 MPa) *n* for methane hydrate should be 6.1 \pm 0.1, and at 100 MPa *n* = 5.85 \pm 0.05 (S. Saito, D. Marshall, and R. Kobayashi, *AICE J.*, **10**, 734, 1964; also see (11), p.54.)
- Handbook of gas hydrate properties and occurrence*. U.S. DOE Publication DOE/MC/19239-1546, 234p., 1983.
- The reaction CH₄ (g) + 6H₂O (ice) \rightarrow CH₄·6H₂O liberates a small amount of latent heat (\approx 20 \pm 5 kJ/mol at 273 K and a CH₄ P of 28 MPa, determined from the Clapeyron slope (T. Makogon and E. Sloan, *J. Chem. and Eng. Data* **39**, 2, 351-353, 1994), the measured enthalpy of formation at standard conditions (Y. Handa, *Chem Thermodynamics* **18**, 915-921, 1986), ΔV_f (9), and its variation with P (11).) This heat is not reflected as a T anomaly (Fig. 5B), evidently because reaction occurs over a period of 8 hours and such heat would be small compared with the exchange of heat of the sample with its surroundings by conduction. (The standard enthalpy for melting of ice is -6.01 kJ/mol, or -36 kJ/6 moles for comparison with the hydrate-forming reaction).
- The importance of vigorous agitation to renew ice/water surfaces for hydrate formation was established by Villard (P. Villard, *Compt. Rend.*, **106**, 1602, 1888) and is also discussed by Sloan (2) and Hwang et al (8).
- Hwang et al. (8) note that as hydrate formation is an exothermic process, the heat released by the phase change increases the T at the formation interface. This effect is greater for hydrate formation from liquid water than from ice since the heat of formation is partially absorbed by the melting ice.
- Y. Makogon, *Hydrates of Natural Gases*, W.H. Cielewicz Translation, PennWell Publishing, Tulsa OK, 1981.
- J. Daeges, H. Gleiter, and J. Perepezko, *Phys. Lett.*, **119A**, 79, 1986. See also: S. Phillpot, J. Lutsko, D. Wolf, and S. Yip, *Phys. Rev. B*, **40** (5), 283-2840, 1989, and S. Phillpot, S. Yip, and D. Wolf, *Computers in Physics*, **3**, 20-31, 1989, for further discussion of results.
- H. Heard, W. Durham, C. Boro, and S. Kirby, in *The Brittle-Ductile Transition in Rocks, Geophysical Monograph* **56**, ed. by A. G. Duda et al., American Geophysical Union, Washington, D. C., 225-228, 1990.
- W. Durham, S. Kirby, and L. Stern, *J. Geophys. Res.* **97**, E12, 20,883-20,897, 1992; also S. Kirby, W. Durham, M. Beeman, H. Heard, and M. Daley, *J. Phys.*, **48**, suppl., 227-232, 1987.
- This work was supported under NASA order W-18927, and was performed in part under the auspices of the USGS and in part by the U. S. DOE by the Lawrence Livermore National Laboratory under contract W-7405-ENG-48.

Table 1. Mechanical test conditions and results.

Run# (step)	T (K)	P _c (MPa)	$\dot{\epsilon}$ (s ⁻¹)	ϵ_t	σ_y (MPa)	σ_{SS} (MPa)	Comments
281	160	50	3.5×10^{-4}	0.125	---	>85	Strain hardening.
2	160	50	3.5×10^{-6}	0.150	---	60	Strain hardening.
3	160	50	3.5×10^{-4}	0.160	100	---	Brittle failure. $\approx 25\%$ H ₂ O ice ^b .
282	140	50	3.5×10^{-6}	---	71	---	Failure, multiple events.
2	140	50	3.5×10^{-4}	0.160	94	---	Failure, multiple events. $\approx 25\%$ ice ^b .
366	168	100	---	---	---	---	Pressurization & compaction only;
367	185	100	3.5×10^{-5}	0.138	---	71	Strain hardening at 10^{-5} step.
2	185	100	3.5×10^{-4}	0.215	96	90	$\approx 30\%$ ice post-deformation.
368	168	100	3.5×10^{-5}	0.185	---	102	Strain hardening. 25% ice ^b .
369	168	100	3.5×10^{-5}	0.16	---	100	Identical run as 368 ^d . No evolved CH ₄ gas.
370	200	100	3.5×10^{-5}	0.120	---	62	Strain hardening at 10^{-5} . No evolved gas ^d .
2	200	100	3.5×10^{-4}	0.230	85	80	$\approx 30\%$ ice post-deformation.

^a P_c is confining pressure gas medium; ϵ_t is total strain; σ_y is yield strength; σ_{SS} is steady-state strength.

^b Post-deformation, determined by x-ray diffraction.

^c Samples 367, 368, 369, & 370 all underwent identical pressurization and compaction as 366 prior to testing.

^d Runs 369 & 370 had a gas collection system attached throughout testing to detect evolved CH₄ gas.

Figure 1: Phase diagram for the CH₄-H₂O system. Shaded region shows field of methane hydrate stability. At low pressures or high temperatures, methane hydrate dissociates to H₂O (ice or liquid) plus CH₄ gas. The metastable extension of the H₂O melting curve is shown by the grey curve. Dashed lines trace the sample fabrication reaction path (described in text.) Solid squares show pressure and temperature conditions of deformation tests (note change in pressure scale on y-axis from linear to log scale.) CH₄ cp designates methane critical point.

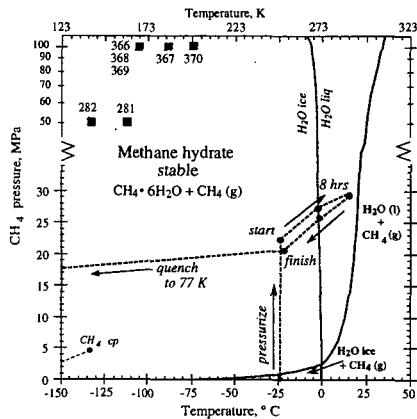


Figure 2: Apparatus for fabricating cylindrical test specimens of methane hydrate from CH₄ gas and melting ice. The sample assembly is housed in a freezer at 250 K, and consists of two steel vessels immersed in an ethyl alcohol bath. One vessel stores a reservoir of cold, pressurized CH₄ gas at 35 MPa and 250 K, and the second contains the sample mold with pre-jacketed and pre-evacuated H₂O "seed" ice. Two-way valves allow isolation of any component of the assembly, and a vacuum pump connected to the sample chamber permits evacuation of the system. The sample chamber is warmed by a hot plate situated beneath the alcohol bath and controlled remotely with a variable autotransformer. Temperature is monitored by thermocouples enplaced in the base of the sample mold and in the bath, and pressure is measured by the gauge and transducer, as shown. Procedures promoting methane hydrate crystallization are described in the text.

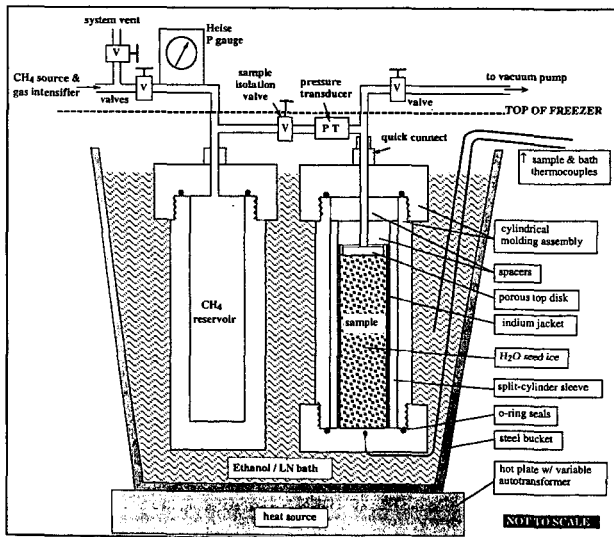


Figure 3:

X-ray powder diffraction patterns for methane hydrate as grown (A) and after mechanical testing (B). Methane hydrate deformed under nonhydrostatic stress undergoes a partial solid-state disproportionation, as evidenced by H₂O ice peaks (dotted lines) found in post-deformation x-ray diffraction patterns.

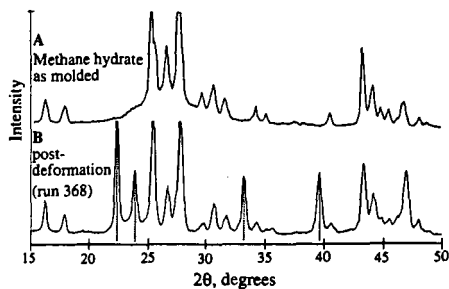


Figure 4:

(A) Temperature-pressure profile of sample fabrication conditions promoting the hydrate-forming reaction: CH₄ (g) + H₂O (ice) → CH₄·6H₂O. Warming the ice + gas mixture above the H₂O solidus (dot-dashed line, point A) initiates reaction. Increasing temperature slowly to 289 K, over an 8 hour span, accelerates full reaction. Complete reaction in our apparatus is marked by a 1.8 MPa pressure drop (ΔP_r) from start to finish. Squares A-E correspond to individual samples that were quenched at specific intervals during hydrate formation to determine hydrate content as a function of ΔP_r and time.

(B) Temperature-time profile during hydrate formation. Hydrate content (vol.%) of samples A-E given on top scale bar, and show how the rate of hydrate formation decays with time under static growth conditions.

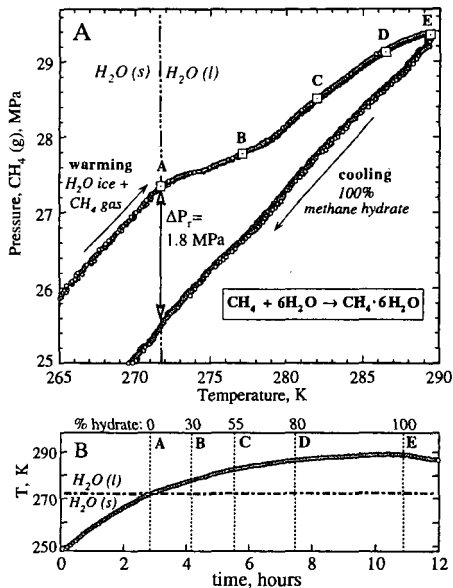


Figure 5:

(A) Temperature-pressure record of neon gas + H₂O ice experiment demonstrates full melting and refreezing of H₂O ice near its solidus when in the presence of non-hydrate-forming gas. The Ne + ice run shows no net pressure drop associated with melting and refreezing, so start-finish conditions are coincident.

(B) Detail of temperature-time history of Ne (g) + H₂O ice in the region of ice melting, showing the lag of the sample temperature compared to the bath temperature associated with the absorption of heat by the endothermic melting of ice. No such effect is displayed by the thermal history of the methane hydrate experiment, also shown (grey open circles).

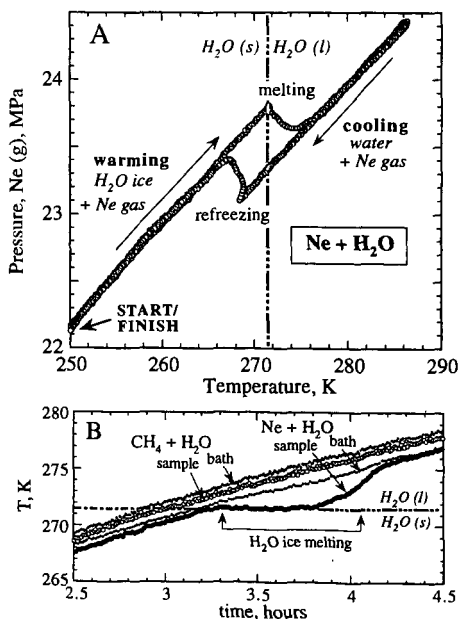


Figure 6:

Schematic of triaxial gas deformation apparatus set up for methane hydrate testing at cryogenic temperatures. The indium-jacketed sample sits within a cylindrical pressure vessel in which N_2 or He gas provides the confining medium. A sliding piston moves through dynamic seals from below to impose constant axial shortening. Samples are mounted on to a "venting" internal force gauge permitting sample communication with room conditions and allowing initial hydrostatic pressurization to eliminate residual porosity prior to deformation. The gas collection system (shown at top) was attached during several tests to monitor possible loss of methane gas during deformation.

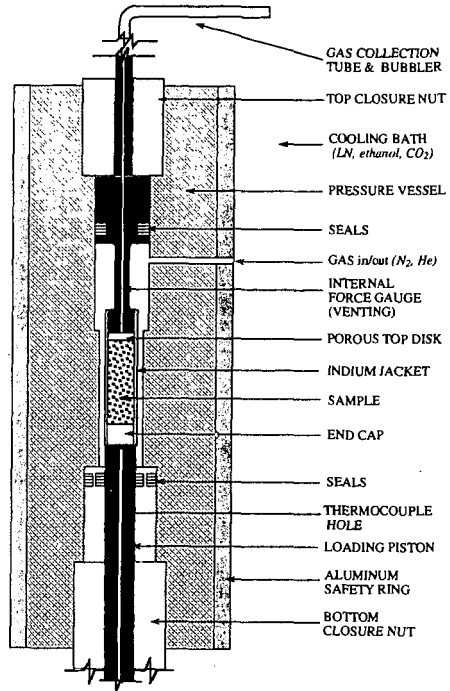
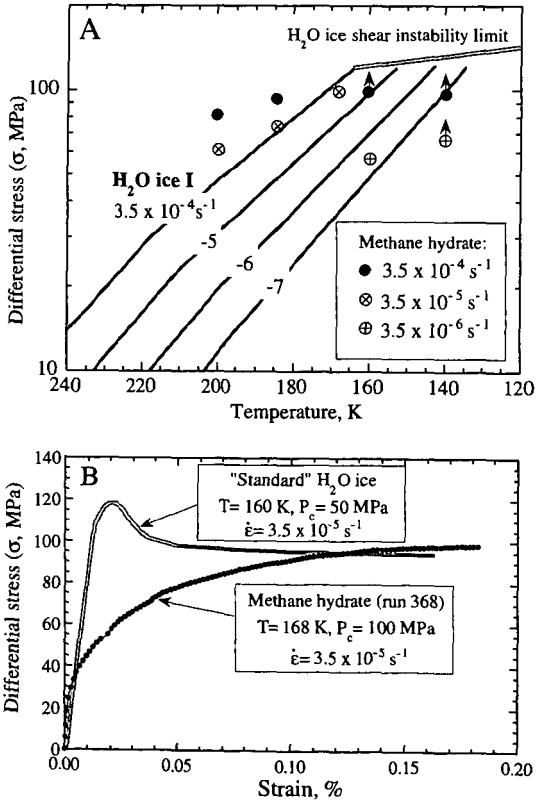


Figure 7:

(A) Strength measurements of methane hydrate show that it has measurably different strength than H_2O ice. Ice flow constants are from (18). Methane hydrate data points with arrows indicate faulting behavior.

(B) Stress-strain curves of deformed methane hydrate (run 368) compared to "standard" polycrystalline H_2O ice. While the strengths of the two compounds are comparable, methane hydrate undergoes systematic strain hardening to an extreme degree (over 18% strain) while H_2O ice typically displays an ultimate yield strength followed by relaxation to steady state behavior.



NEW METHOD OF TEMPERATURE-RAMPING, ISOBARIC EXPERIMENTS TO STUDY THE HYDRATE FORMATION AND DECOMPOSITION

Guillaume Besnard, Kyoo Y. Song, Joe W. Hightower, Riki Kobayashi, Doug Elliot*, and Roger Chen*, Department of Chemical Engineering, MS-362, Rice University, 6100 Main Street, Houston, Texas 77005-1892.

* International Process Services, Inc., a subsidiary company of the Bechtel Corp., P. O. Box 2166, Houston, Texas 77252-2166.

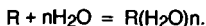
Key Words: Hydrate, Methane, Solubility, Enthalpy, Entropy

Gas hydrate formation and decomposition involving methane in water has been studied in a series of temperature-ramping, isobaric, variable-volume experiments. Results obtained have provided novel information on (1) gas solubility in the liquid phase at temperatures in the vicinity of hydrate formation, (2) derived thermo-physical properties such as enthalpy, entropy, etc., and (3) details of the mechanism of hydrate formation/decomposition. Also, heats of dissolution/formation may be obtained indirectly from these results. An attempt was made to overcome experimental difficulties which had been imposed by the appearance of the hydrate solid phase. Such detailed solubility information will add substantially to the scarce data currently available in the literature.

INTRODUCTION

Though the existence of hydrates was demonstrated by Davy (1) in the early part of the nineteenth century, current interest dates from 1934 when Hammerschmidt (2) discovered that hydrates were responsible for plugging natural gas lines. This discovery stimulated numerous studies to determine the hydrate structure and its formation and decomposition conditions. The authors have recently employed a temperature-ramped, isobaric (constant pressure), variable-volume technique that is capable of providing continuous details of hydrate formation and decomposition. Furthermore, the method enables a straightforward calculation of solubility of the hydrate former in the host phase which may be pure water or aqueous solutions.

Information on the solubility of gases like CH_4 in pure water is very useful for the calculation of some derived thermo-physical properties such as the enthalpy of solution, the enthalpy of formation, and the entropy change of the solution. Gas solubility has been extensively studied (5-12) and found to be extremely low. It has been generally reported for temperatures above ambient. However, the same information at the low temperatures and high pressures is very scarce. The solubility of hydrate formers, such as methane, ethane, carbon dioxide, etc., is not easily measurable due to the appearance of the hydrate solid phase, metastable phases, etc. The increase of the solubility with decreasing temperature can be explained by the formation of an ice-like structure (i.e. pentagonal dodecahedra) in the solvent (13-16). Another explanation is that displacement of solvation equilibrium occurs with changes in temperature ($\Delta H_{\text{solv}} < 0$) and that the solute introduces low entropy structures in water (15-17). The solvation of gas, R, is considered as a relaxation to the equilibrium process described as follows:



First introduced by Pauling (3) in 1957 and expanded in recent studies (12-18), a concept has developed that the hydrate structure has a geometry similar to basic water structure and the liquid forms its own "buckyballs". The "buckyball" includes 21 water molecules, 20 of which form a pentagonal dodecahedron with one molecule in the middle to add stability to the cage. At ambient temperature, it was proved that these structures are metastable and flicker in and out of existence (19). Sloan and Fleyfel (4) in 1991 proposed a kinetic model of gas hydrate formation from ice assuming that during the nucleation period considerable metastability occurs because of the forming and breaking of structures. Although many more detailed studies are required, our experiments have made it possible to detect the different steps suggested by Sloan et al. (4).

The solubilities of methane and ethane in water at low pressures (3.45 and 0.66 MPa, respectively) have been reported earlier (20). This paper reports results for methane obtained at higher pressures (10.48 and 13.93 MPa) in the temperature range 291.2 to 278.2 K, which includes the hydrate formation conditions, and divergence of these measurements from solubility predicted by Henry's law is presented.

EXPERIMENTAL SECTION

Experimental Apparatus

Calorimeter

A differential calorimeter, which is a variation of the common heat flux calorimeter (21), used in these studies consists of two symmetrical containment vessels, both thermally insulated from the surrounding aluminum block. One containment vessel serves as the sample cell while the other vessel serves as a reference. The surrounding block temperature is ramped at a fixed rate, (by using heating and/or refrigeration), allowing a steady-state heat flux between the sample vessel and the surroundings. But the calorimeter can also be used in an "isoperibolic" operation where the surrounding block is held at a constant temperature (22). The calorimeter is equipped with an internal electrical conductivity cell to track the amount of water in the hydrate and liquid phase by monitoring the conductivity of a dilute KCl solution during hydrate formation.

Moreover, any heat exchange between the containment vessel and the surrounding block occurs almost exclusively by conduction and is measured by two thermopiles. The resulting differences in voltage for the two thermopiles represent the differential heat flux for the two containment vessels. Integrating this voltage over time gives the total heat transfer associated with "the event." However, for this work, the heats of dissociation have been calculated from the solubility of methane since the thermopile values were not reliable enough to provide us with consistent data. Figure 1 shows the apparatus and the pressure-maintaining system.

Computer/data acquisition

Performance of the calorimeter strongly depends on the control and data acquisition program for the computer. Our program is capable of handling various data acquisitions while controlling the pressure and the temperature precisely. The program has been written in "Visual Basic" and can set heater load and pump position (i.e. volume of gas added to the cell during the ramping experiments). The pressure is controlled every four seconds, and the data are collected every minute, allowing precise control of the temperature-ramping, isobaric experiments. Measurements were made during the data acquisition from two pressure transducers, three PRTs, a thermopile, and an electrical conductivity device.

The stepping motor, Genrad RLC Digibridge, HP multimeter, and Keithley digital multimeter are controlled via an IEEE interface. Pressure transducers and a temperature controller are interfaced via an RS232. Figure 2 shows a block diagram of the control and data acquisition systems.

Experimental Procedure

The right cell of the calorimeter shown in Figure 1 is first charged with roughly 650 grams of the dilute aqueous potassium chloride solution (~0.004 normal) prepared with ultra-pure water (17.0 megaohm-cm resistance) and Baker Analyzed Reagent grade salt. This solution fills approximately two thirds of the cell, in order to insure that the electrical conductivity cell be immersed, and magnedrive propellers provide vigorous mixing of the cell contents. After the system has been evacuated to remove air, methane gas is introduced to the system comprising the calorimeter cell, the right pump, and the pressure lines.

The fundamental measurement is the change in volume of the digital pump during the temperature-ramping experiments while the pump is controlled by a stepping motor to maintain the pressure constant. The stepping motor is actuated by a digital-based driver which is controlled by a computer through the IEEE interface. The system consists of the stepping motor, Digidrive, transformer, and 2100 Indexer with an IEEE interface. Flow rates range from 5 to 96 cc/min has been achieved. The pump is able to add to or withdraw gas from the cell at very precise rates. But precise control of the isobaric operation strongly depends on the pressure transducer that closes the loop. They are rated at 10,000 psia with an accuracy of 0.07%. The displacement of the plunger of the pump gives us the volume of methane gas added to the cell, hence the solubility of methane in water-rich phase.

RESULTS AND DISCUSSION

Plots of changes in the system volume versus temperature, as shown in Figure 3, present typical experimental results in a way similar to that used previously (20). However, the current pressures (10.48 and 13.93 MPa) are much higher than the previous one, 3.45 MPa. Figure 3 shows different regions along the curve which are:

a) Cooling

- (1) An interstitial solubility where gas is dissolved into water according to

Henry's law.

- (2) Solubility of the gas begins to increase beyond that accounted for by Henry's law.
- (3) The gas intake by the water increases, and this point is commonly called a catastrophic temperature (T_c). The solubility continues to increase.
- (4) Catastrophic hydrate formation occurs, and the amount of solid present in the water has drastically increases.
- (5) Solidification starts but the magnetic stirrer is still running.

b) Heating

- (6) Dissociation of the hydrates begins. The hydrate crystals start melting and the volume maintains a constant value.
- (7) The volume drops very fast and the hydrates are almost completely decomposed. The volume returns to its initial value.

Figures 4 and 5 show calculated methane solubility of (\log [mole fraction CH_4 in water]) at 13.93 MPa (2020 psia) plotted vs. ($1/T$) and $\ln(T)$, respectively, while Figure 6 presents the solubility of methane ($1000 \cdot X_{\text{CH}_4}$) vs. temperature at 10.48 MPa (1520 psia). Table 1 provides the solubility of methane gas in pure water obtained during the temperature-ramping experiment at a rate of 1.2°C/hr , for both pressures of 10.48 and 13.93 MPa. Table 2 presents the changes of enthalpy and entropy obtained by plotting $\ln(x)$ versus $1/T$ (T in K) from the relation of

$$d \ln(x) / d (1/T) = - \Delta H/R$$

and $\ln(X)$ vs. $\ln(T)$ (again, T in K) by the relation:

$$d \ln(x) / d \ln(T) = + \Delta S/R$$

We had to extrapolate the available literature data of methane solubility in water far above hydrate formation condition (5) to establish a reference for the solubility of methane in pure water in the low temperature region.

Figures 3 and 4 demonstrate a sudden increase of the gas solubility from the extrapolated values. Below 17°C , the liquid solution becomes supersaturated with methane gas. Song et al. (20) attributed this increase to a "sorption" effect with the ordering of water molecules into an ice-like structure with the water molecules surrounding the hydrocarbon molecules. These ordered structures result from contact of the hydrocarbon with water which induces small dipole moments into the hydrocarbon molecules and allows some ordering through weak dipole-induced dipole interactions with the water. The number of water molecules affected by the interaction with the hydrocarbon solute is related to the size of the guest molecule, i.e. the contact surface of the guest molecule. Therefore, the size of the "ice-like" structures will increase with the size of the hydrocarbon (24).

At T_c , the catastrophic temperature at which hydrate crystals start to form, the solubility is increased by 78 % for 10.48 MPa and 51 % for 13.93 MPa. After hydrate crystals are formed, the solubility still increases, showing a high level of supersaturation of methane gas in liquid water, which started just before and just after T_c . These solubility measurements emphasize the crystallization-like process taking place during hydrate formation. The dissolved gas molecules form the nuclei which initiate the process of hydrate precipitation and crystal growth. One might state that around T_c , the nucleation occurs as a result of a fluctuation in free energy due to the local temperature and pressure fluctuations, of sufficient importance to surmount the free energy barrier (12).

From an energy point of view, the changes of enthalpies and entropies are negative and in agreement with reported values (20, 22, 25). The changes in enthalpy and entropy, as the temperature approaches T_c , could be compared with ice formation on one hand and experimental heats of dissociation on the other. The enthalpy of dissociation for the methane hydrate at 13.93 MPa is very close to the enthalpy of dissolution of the same gas when T_c is approached, as found previously (12). Moreover, the comparison of the entropies of solution derived here with corresponding values based on the same standard state for gases in non-polar solvents at 25°C shows that the entropies of solution in water are all negative by a large amount. The partial molal entropy of solution is influenced by the size of the cavity created by the gas molecules when the estimate of the cavity size is made by bond distances. Frank and Evans (15), and Song et al. (20) have demonstrated that the large negative values for partial molal entropies of solution of non-polar gases in water can be understood as the creation of a more highly ordered state in water or "icebergs". As the temperature is increased, these quasi-ice-like structures break up and ΔS becomes positive.

CONCLUSION

A fully automated calorimeter with some modifications has facilitated isobaric (constant pressure), variable-volume, and temperature-ramped experiments, and the experimental procedure has enabled us to elucidate discrete steps involved in the hydrate formation and decomposition for a high pressure methane-water system in a continuous manner.

Simultaneously, the measured volumes were utilized to determine directly methane gas solubility in the water phase in a way that minimizes uncertainties associated with the appearance of the solid hydrate phase.

Of importance, it has been confirmed that the solubility of methane gas in water in the vicinity of the incipient hydrate formation temperature is much greater than that would be predicted by Henry's law, a frequently-used conventional calculation procedure.

Finally, the obtained solubility was used to calculate derived thermo-physical properties, i.e. changes of enthalpy and entropy of the solution.

LITERATURE CITED

- (1) Davy, H. *Phil. Trans. Roy. Soc.*, London 1811, 101, 1.
- (2) Hammerschmidt, E. G. *Ind. Eng. Chem.* 1934, 26, 851.
- (3) Pauling, L. *The Structure of Water Hydrogen Bonding*. Hadzi, D. Pergamon Press, 1959.
- (4) Sloan, E. D.; Fleyfel, F., *J. AIChE* 1991, 37, 1281.
- (5) Culberson, L.; McKetta, J. *AIChE Trans* 1950, 189, 1.
- (6) Kobayashi, R. *Vapor-Liquid Equilibrium in Binary Hydrocarbon-Water systems*. Ph-D Dissertation, University of Michigan, 1951.
- (7) Katz, D.L.; Cornell, D.; Vary, J.; Kobayashi, R.; Elenbaas, J.R.; Poettman, F.H.; Weinang, C.F. *Handbook of Natural Gas Engineering* 1959.
- (8) Clever, H.L.; Han, C.H. *ACS Symp. Ser.* 1980, 133, 513.
- (9) Clever, H.L.; Battino, R. *Role. Data Sci. Prog.* 1986, 9, 209.
- (10) Battino, R. *Sol. Data Ser.* 1986, 24, 1.
- (11) Battino, R. *Sol. Data Ser.* 1987, 27, 1.
- (12) Feneyrou, G. *Elucidation of the Formation and Decomposition of Clathrate Hydrates of Natural Gases through Gas solubility Measurements*. M.S Dissertation, Rice University, 1996.
- (13) Klotz, I.M. *In Protein Structure and Function*, Brookhaven Symposia in biology 1960, 13, 25.
- (14) Patterson, D.; Barke, M. *J. Phys. chem.* 1976, 80, 2435.
- (15) Frank, H.S.; Evans, M.W. *J. Chem. Phys.* 1945, 13, 507.
- (16) Kauzmann, W. *Adv. Protein Chem.* 1959, 14, 1.
- (17) Nemety, G.; Scheraga, H.A. *J. Phys. Chem.* 1962, 36, 3401.
- (18) Fleyfel, F.; Song, K.Y.; Kook, A.; Martin, R.; Kobayashi, R. *J. Phys. Chem.* 1993, 25, 6722.
- (19) Bernal, J.D. *Royal Society on Physics of Water and Ice* published in Hydrogen Bonding, Pergamon Press 1957.
- (20) Song, K.Y.; Feneyrou, G.; Fleyfel, F.; Martin, R. Lievois, J.S.; Kobayashi, R. *Solubility Measurements of Methane and Ethane At and Near Hydrate Conditions, in press*, Fluid Phase Equilibria 1996.
- (21) Calvet, E.; Prat, H. *Recents Progres en Microcalorimetrie* Dunod Edition Paris 1958.
- (22) Lievois, J.S. *Development of an Automated, High Pressure Heat flux Calorimeter and its Application to Measure the Heat of Dissociation of Methane Hydrate*. Ph-D Dissertation, Rice University, 1987.
- (23) Frank, H.S.; Wen, W.Y. *Discussion Faraday Society* 1957, 24, 133.
- (24) Himmelblau, D.M. *Partial Molal Heats and Entropies of Solution for Gases Dissolved in Water from the Freezing Point to Near the Critical Point*. *J. Phys. Chem.* 1959, 63, 1803.
- (25) Rettich, T.R.; Handa, Y.P.; Battino, R.; Wilhem, E. *Solubility of Gases in Liquids. High-Precision Determination of Henry's Constants for Methane and Ethane in Liquid Water at 275 to 328 K*. *J. Phys. Chem.* 1981, 85, 3230.
- (26) CSMHYD - hydrate program developed by the Colorado School of Mines (Dendy E. Sloan), available through the Gas Processors Association (GPA), Tulsa, Ok.

Table I. Solubility of Methane Gas in Water (Obtained from Temperature-Ramping (1.2 °C/hr), Variable-Volume, Isobaric Experiments)

pressure, MPa a (psia)	temp., K (°C)	sol. of CH ₄ , X _{CH4} *1000	pressure, MPa a (psia)	temp., K (°C)	sol. of CH ₄ , X _{CH4} *1000
10.48 (1520)	291 (18.0)	2.04	13.93 (2020)	292 (19.0)	2.96
	289 (16.0)	2.41		290 (17.0)	3.22
	288 (15.0)	2.61		289 (16.0)	3.92
T ^a = 11.6 °C	285 (12.0)	3.62	T ^a = 14.6 °C	289 (15.5)	4.23
T ^b = 16.0 °C	285 (11.6)	4.09	T ^b = 18.0 °C	288 (14.6)	5.03
T* = 13.8 °C	284 (11.0)	4.45	T* = 16.24 °C	287 (14.0)	6.68
	283 (10.0)	5.17		286 (13.0)	11.29
	282 (9.0)	5.92		285 (12.0)	6.72
	280 (7.0)	7.54		283 (10.0)	25.70
	279 (6.0)	9.17		280 (7.0)	37.20
	278 (5.0)	11.41		279 (6.0)	44.95
				278 (5.2)	52.44
	298 (25.0) ^c	1.98		298 (25.0) ^c	2.62

a initial hydrate formation temperature,

b final decomposition temperature,

* predicted from hydrate program of Colorado School of Mines (22),

c obtained from Culberson and McKetta (1).

Table II. Derived Thermo-Physical Properties of a Methane-Water System (Obtained from Solubility Measurements)

pressure, MPa a (psia)	range of temp., °C	change of enthalpy, ΔH, KCal/mole of gas	change of entropy, ΔS, Cal/mole.K
10.483 (1520)	16.0 to 12.0	-16.8	-58.6
	12.0 to 11.6	-47.7	-170.5
T ^a = 11.6 °C	11.8 to 7.0	-21.1	-74.7
T ^b = 16.0 °C	7.0 to 5.0	-32.0	-115.9
T* = 13.8 °C			
13.931 (2020)	19.0 to 17.0	-7.1	-24.4
	16.0 to 14.6	-27.5	-95.2
T ^a = 14.6 °C	14.6 to 13.0	-87.8	-308.9
T ^b = 18.0 °C	12.0 to 6.0	-26.1	-92.3
T* = 16.24 °C			

a initial hydrate formation temperature,

b final decomposition temperature,

* predicted from hydrate program of Colorado School of Mines (22).

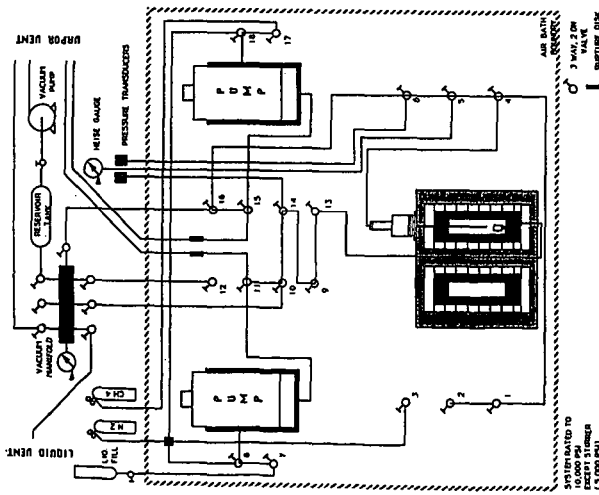


Figure 1. Calorimeter apparatus used for temp.-ramped, isobaric, and volume-variable experiments.

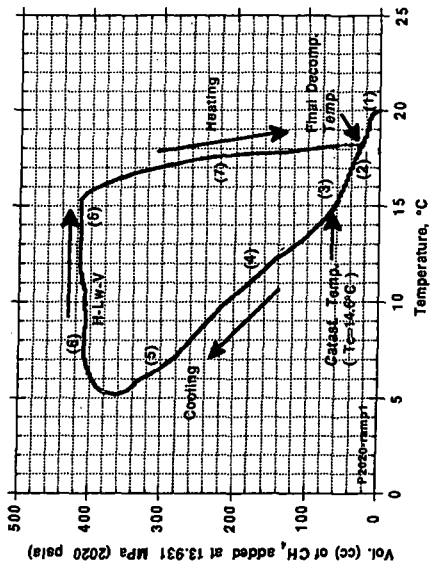


Figure 3. Change of system vol. vs. temp. for a methane and water system at 13.931 MPa (2020 psia) when the air bath temp. was ramped at 1.2°C/hr.

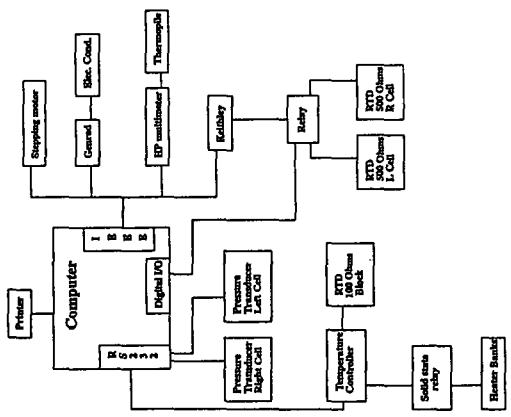


Figure 2. Block diagram of pressure and temperature controls and data logging system.

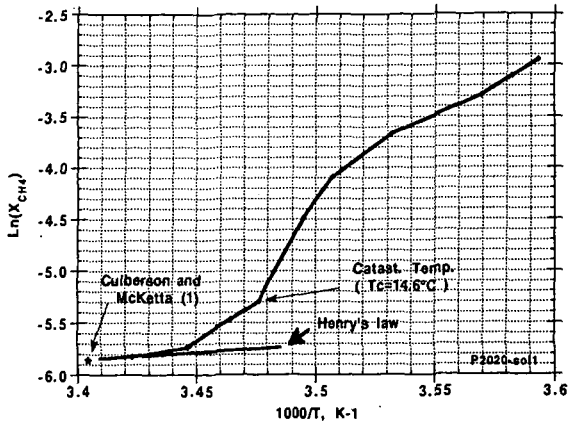


Figure 4. Logarithm of solubility (mole fraction) of methane in the water phase vs. reciprocal of the absolute temp. for a methane and water system at 13.931 MPa (2020 psia).

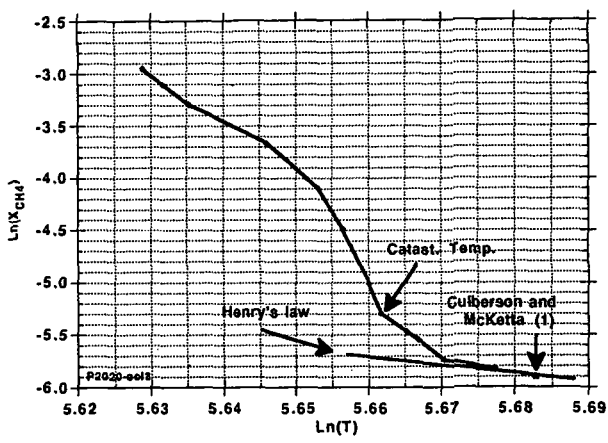


Figure 5. Logarithm of solubility (mole fraction) of methane in the water phase vs. logarithm of absolute temp. for a methane and water system at 13.931 MPa (2020 psia).

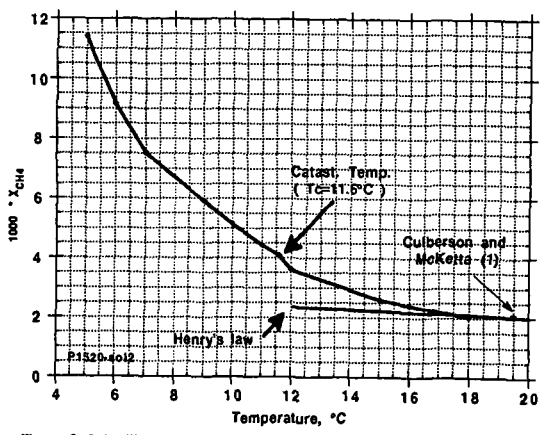


Figure 6. Solubility (mole fraction) of methane in the water phase vs. temp. for a methane and water system at 10.483 Mpa (1520 psia).

GROWTH AND INHIBITION PHENOMENA OF SINGLE HYDRATE CRYSTALS

Roar Larsen,
Norwegian University of Science and Technology, N-7034 Trondheim, Norway
Taras Y. Makogon,
Colorado School of Mines, Golden, CO, 80401
Charles A. Knight,
National Center for Atmospheric Research, Boulder, CO, 80307
E. Dendy Sloan, Jr.,
Colorado School of Mines, Golden, CO, 80401

Keywords: hydrate single crystals, crystal growth habit, hydrate inhibition

ABSTRACT

Single crystals of structure II (sII) and structure I (sI) hydrates were grown in aqueous tetrahydrofuran (THF) and ethylene oxide (EO) solutions. Normal growth habits from the melt are {111} crystallographic planes for sII, and {110} for sI. Addition of polymeric inhibitors in very small amounts changed the growth habit of sII to thin, 2-dimensional hexagonal {111} plates, and caused rapid small-scale branching of sI crystals. The highly branched sI crystals were found to still be single crystals. Higher concentrations of inhibitor were found to stop the growth of sII crystals completely. These concentrations were as low as 0.1 wt% at low supercooling. The minimum concentration needed to stop growth changed with temperature, polymer characteristics and solution agitation. Experiments showed the polymer adsorption to be practically irreversible, and an inhibition hypothesis was developed.

INTRODUCTION

Natural gas hydrates are of great interest from several different viewpoints. Historically, hydrates have been studied as a nuisance causing problems in the oil and gas industry (Englezos, 1993). Over the previous decade another motivation for study has been their role as deposits of immense energy resources in subsea sediments and subterranean permafrost (Kvenvolden, 1994). Just recently, the economics of using hydrates as a suitable storage and transport medium for natural gas have been addressed anew (Gudmundsson and Børrehaug, 1996). A comprehensive overview of hydrates is given by Sloan (1990).

This work uses model systems as an analogue to natural gas hydrates. To circumvent the need for high pressures or very low temperatures, tetrahydrofuran (THF) and ethylene oxide (EO) aqueous solutions are used to form structure II (sII) and structure I (sI) hydrates, respectively. THF and water mixed at the stoichiometric ratio for hydrates (17 water molecules per THF molecule) has a hydrate equilibrium melting point of about 4.4°C at 1 atm. pressure. For ethylene oxide at stoichiometry (23 water molecules per 3 EO molecules) the equilibrium melting temperature is about 11°C. In natural gas applications, sII is the predominant structure.

Over the past 50 years, the thermodynamics of hydrates have been studied extensively, to the point where commercially available simulation codes can predict equilibrium conditions with an accuracy good enough for most practical purposes. The kinetics of hydrate growth have not reached nearly the same level of resolution. Several groundbreaking studies have increased our understanding, but much work still remains to be done. This work takes a very basic approach, studying single crystals of the hydrate structures.

In addition to the basics of crystal growth, the main focus of this work is to study the effects of addition of inhibitors to the systems. Thermodynamic inhibitors like methanol have traditionally been used to alleviate or avoid problems with hydrates in the oil and gas industry, but the use of these can have severe implications for economy, logistics and product quality. There has therefore been a significant driving force towards finding better inhibitors which will work at much lower concentrations. There are two main classes of these inhibitors: anti-agglomerants (emulsifying agents) and kinetic inhibitors (chemicals that interfere with the growth process of the hydrate crystals). We have studied three of the best-known kinetic inhibitors in some detail. These are poly(vinylpyrrolidone) (PVP), poly(vinylcaprolactam) (PVCap) and a terpolymer of vinylpyrrolidone, vinyl caprolactam and dimethylaminoethylmethacrylate (VC-713) (Lederhos et al., 1996).

EXPERIMENTAL PROCEDURES

The growth cell used in our experiments is shown in Fig. 1. It consists of a transparent plexiglass cooling jacket for temperature control to within 0.1 K. Glass test tubes extend into this cooling chamber, and are filled with the experimental solution. The temperature is set to a predetermined level of supercooling and the solutions are left to equilibrate before proceeding. A rubber cap holds a thin glass pipette in the middle of the test tubes (open to the atmosphere at the top and to the experimental solution at the bottom). Crystal nucleation and initial growth is forced by inserting a cold wire into the pipette, creating a momentarily large local supercooling as well as a nucleation surface. The crystal growth then progresses inside the pipette, and, more often than not, nicely defined single crystals emerge into the test solution when the growth reaches the tip of the pipette. The cooling chamber has several test tubes, enabling quick transfer of crystals between uninhibited and inhibited solutions at the same temperature.

RESULTS

Uninhibited crystal growth

THF hydrate sII crystals grown from the melt (the stoichiometric solution) exhibit the {111} crystallographic planes, in the form of regular octahedra. One such crystal is shown in Fig. 2. Irregularities in form were sometimes observed, but at moderate supercooling (0-4 K) the {111} planes were always dominant. Higher supercooling resulted in skeletal crystals while still retaining the octahedral outline. Even higher supercooling (>8 K) resulted in dendritic growth of the crystals. Over the supercooling range of 0-5 K, the growth rate of these crystals was found to be exponential as a function of the supercooling.

Crystals of EO hydrate (sI) grown from the melt exhibit the {110} crystallographic planes, in the form of a dodecahedron with rhombic faces. This is the same shape as the common garnet. Fig. 3 shows one such crystal grown at a supercooling of 0.5 K. So far, no clear evidence of other crystallographic planes has been found for this system.

Crystal growth with inhibitors

For the THF hydrates, substantial changes in growth habit is observed already at very low concentrations of inhibitor in the system. For a supercooling of 1.4 K, concentrations lower than 0.1 wt% of PVP, PVCap or VC-713 all change the growth from octahedra to two-dimensional hexagonal plates. The large faces of these plates are still {111} planes, but some questions remain as to the orientation of their thin edges. The orientation of these planes is shown in Fig. 4, where an uninhibited octahedral crystal was transferred to a solution with inhibitor. The planes grow off the edges of the existing crystal, or sprout from its body, but are always parallel to the facets of the original crystal.

At slightly higher concentrations of the inhibitors PVCap and VC-713, further crystal growth is inhibited completely. At a magnification of 50x, no growth of the crystal faces could be measured over a period of more than 24 hours. This phenomenon is seen at concentrations from 0.1 wt% at 1.4 K supercooling for the best inhibitor polymers. The minimum concentration needed to achieve full inhibition depends strongly on the supercooling and to some degree also on the polymer type and molecular weight, as well as solution agitation. Fig. 5 shows one example of the dependence on supercooling. PVP does not produce complete inhibition, even at concentrations as high as 5.0 wt%.

To study the assumed adsorption of the polymers to the crystal surface, a set of experiments were conducted in which crystals which had been exposed to the no-growth solutions for periods ranging from 5 minutes to several hours were transferred back to uninhibited solutions. None of these crystals showed any further growth until at least 3 hours after being transferred back, and then only from the vertices of the original crystals, or from the interface between the crystals and the glass pipettes. The new growth quickly grew throughout the tubes and obscured any further investigation of the surface of the original crystals.

As control experiments, several tests with known non-inhibitors were performed. Polyvinyl alcohol, urea, hydroxyethylcellulose and polyacrylamide show no impact on the growth habits of the sII crystals at all. These chemicals were chosen because of their solubility in water, and in some cases for their similarity to the polymeric inhibitors in having a vinyl backbone and high hydrogen bonding capability.

EO hydrate crystals show an even more dramatic change of growth habit when a small amount of inhibitor is added to the melt. Low concentrations (0.1-0.2 wt%) produce rapid, small-scale branching of the crystals, producing spherical globules with flimsy branches. This effect was obtained only with PVCap and VC-713. Further experiments in flat capillaries on a cooled bed under a microscope revealed that the branching EO crystals are most likely still single crystals. At intermediate concentration of inhibitor, when the branching had clearly started but were still visibly faceted, the individual branches were seen to preserve a constant crystallographic orientation throughout (Fig. 6).

The EO hydrate system is still under investigation concerning the possibility of complete inhibition.

DISCUSSION

Crystal growth planes which are exhibited macroscopically are the slowest growing planes (faster-growing planes grow out of existence). Studying molecular models of the sII hydrate, it is evident that the 6-membered rings of the large cavities all lie in the {111} planes. This suggests a hypothesis for the normal growth habit, appealing to a presumed higher energy barrier against producing these rings compared to the 5-membered rings. The H-bonds between water molecules are strained more from their natural angle in forming 6-membered rings than in forming 5-membered ones. We therefore believe this process is slower, and may result in the planes containing these rings being the slowest growing. This hypothesis is strengthened when noting that 5-membered rings seem to be naturally occurring structures in water (Rahman and Stillinger, 1973). This contrasts with Smelik and King (1996) who describe a mechanism where forming of the S^{12} cages is viewed as the controlling factor. Our hypothesis does not transfer directly to the sI hydrate, but a similar argument can be made about specific {110} planes having a higher number of hexagonal rings per unit area (although not parallel to the plane) than e.g. the {100} or the {111} planes. No clear evidence for either of these hypotheses has been presented to date.

The exponential shape of the curve for growth rate vs. supercooling would indicate that the so-called Jackson α -factor is greater than 3 (Myerson, 1993), suggesting that the surface of the growing THF hydrate is molecularly smooth, and that the growth mechanism is creation and propagation of steps on the faces. We believe that surface nucleation is the most probable mechanism for this, as invoking screw dislocations as the dominating factor does not explain orientation preference and homogeneity. However, in the very few cases where other planes than {111} are seen, screw dislocations on {111} might be invoked as an explanation for speeding these planes up and exhibiting otherwise outgrown facets.

We have no completely satisfying explanation for the 2-dimensional growth at intermediate concentrations of inhibitor. The question is complicated by the fact that in some cases, the edges of these

plates have been identified as also being $\{111\}$, and this is puzzling, as it implies that some $\{111\}$ planes grow faster than others. Fundamentally there seems to be only two options to explain this, since just at an edge one expects the physical conditions in the liquid containing the crystal to be virtually identical on the two faces very close to their common edge. One possibility is an imperfection of some kind that stimulates growth on one of the faces (the thin edge), and the other is some kind of time-dependent adsorption effect for the inhibitor.

The first of these explanations has some precedent in the effect caused by stacking faults (van de Waal, 1996). Such faults would not be unexpected on the sII $\{111\}$ planes. We do not rule out this mechanism, but we are skeptical of it because of the complete lack of macroscopic morphological evidence of such faults. The second possible explanation appeals to a mechanism where a fast-growing plane pushes aside the inhibitor as it grows, quickly enough that the polymer can not reorient and find its structural fit and bond onto the leading surface. This phenomenon has some precedence also, in the effect of kinetic inhibitors on ice growth (Harrison et al., 1987). We do not feel confident in choosing one of these explanations over the other at present, and may eventually have to appeal to a combination of the two. The results indicate preferential adsorption on $\{111\}$, but this question is not completely resolved, as the crystals also only exhibit $\{111\}$ in their uninhibited state.

We believe that the complete growth inhibition is a result of polymer adsorption to the crystal surface, with the adsorbed molecules acting as barriers to further growth. When the concentration is high enough, polymer molecules will sit closer on the surface than twice the critical radius for crystal growth at the corresponding temperature, and the crystal will not be able to grow between the polymer strands. The adsorption process is fairly rapid, as no measurable growth takes place after a crystal is transferred to an inhibited solution, and the minimum no-growth concentration is probably close to the concentration needed at the surface, as the diffusivity of the polymer is much lower than any other component in the system. However, there has to be some time involved in diffusion and orientation of the inhibitor, if the latter of the above hypotheses for 2-dimensional growth is physically correct.

The tests with non-inhibitors show that it is not enough to have long molecules acting as diffusion barriers or molecules with a high capacity for H-bonding. We think that the pendant groups of our polymers are important in achieving strong adsorption. One possible explanation is that the pendants fit as pseudo-guest molecules in unfinished large cavities, with extra binding to the surface caused by H-bonds from the carbonyl groups on the pendants. There is some evidence from molecular simulations suggesting that this might happen (Makogon (1997), Carver et al. (1995)). The experiments where inhibited crystals were transferred back into uninhibited solutions, show that the adsorption is practically irreversible. Each pendant group or H-bonding site on its own probably shows equilibrium adsorption and desorption, but in the case where numerous sites along a polymer chain are engaged in this process, desorption of some of them would have little influence on the overall molecule, and these sites would be kept close to their adsorption area, and could easily re-adsorb. For the entire polymer to desorb, all the adsorption sites would have to "let loose" at the same time, an event which is statistically unlikely after a certain number of adsorption points has been achieved for each molecule. When desorption and further growth was found to occur, it happened in areas where it is easy to imagine the polymer fit to be less than perfect: at the vertices and at the interface between the crystal and the glass pipettes.

The EO hydrates grown with inhibitor have not yet been studied in as much detail as the THF system, but the preliminary results show some parallels to the sII hydrates. PVCap and VC-713 show different results than PVP, indicating that the difference in inhibition performance might be more fundamental than just a difference in degree of effectiveness. We believe that this is mainly due to the pendant group of PVP being smaller and not having the same stabilizing effect to provide strong adsorption. The dramatic small-scale branching of the EO hydrate crystals with inhibitor is somewhat similar to what is known in the crystallographic literature as spherulitic growth. However, our experiments indicate that these crystals are still single crystals with constant orientation throughout, whereas for spherulites, the orientation will be off by some degree for each new branch. We believe that this is a new phenomenon, as we have not been able to find reports of such growth in the literature, and remains a topic for further investigation.

ACKNOWLEDGMENTS

The following companies are gratefully acknowledged for their financial support of this work: Amoco, ARCO, Chevron, Conoco, Exxon, Mobil, Oryx, Petrobras, Phillips, Statoil and Texaco.

REFERENCES

- Carver, T.J., Drew, M.G.B., Rodger, P.M., *J. Chem. Soc. Faraday Trans.*, 91(19), pp 3449-3469 (1995)
Gudmundsson, J. and Børrehaug, A., Proc. 2nd Int. Conf. on Nat. Gas Hydrates, pp 415-422, Toulouse, France, June 2-6 (1996)
Harrison, K., Hallett, J., Burcham, T.S., Feeney, R.E., Kerr, W.L., Yeh, Y., *Nature*, 32, p 241 (1987)
Englezos, P., *J&EC Research*, vol. 32, pp 1251-1274 (1993)
Kvenvolden, K.A., *Ann. New York Acad. Sci.*, vol. 75, pp 232-246 (1994)
Lederhos, J.P., Long, J.P., Sum, A., Christiansen, R.L., Sloan, E.D., *Chem. Eng. Sci.*, 51, (1996)
Makogon, T.Y., Ph.D. thesis, Colorado School of Mines (1997).
Myerson, A.S., *Handbook of Industrial Crystallization*, Butterworth-Heinemann, Boston (1993)
Rahman, A., Stillinger, F.H., *J. Am. Chem. Soc.*, 95, pp 7943-7948 (1973)
Sloan, E.D., *Clathrate Hydrates of Natural Gases*, Marcel-Dekker, New York (1990)
Smelik, E.A. and King, H.E., *Am. Mineralogist*, accepted for publication (1996)
van de Waal, B.W., *J. of Crystal Growth*, vol. 158, pp 153-165 (1996)

FIGURES

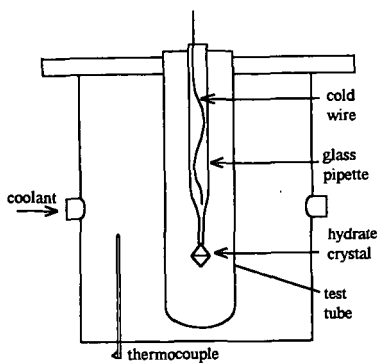


Figure 1 The experimental cell. Water or water-glycol mixtures are used as a coolant. The test tubes are ~2.5 cm outer diameter, screwcapped pyrex glass.

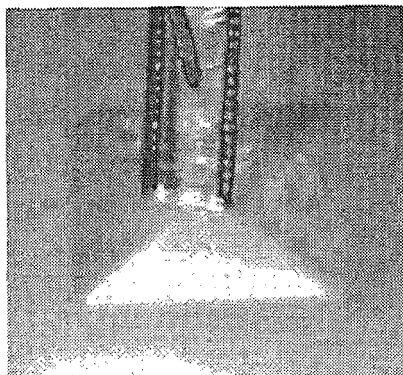


Figure 2 Octahedral s II {111} crystal of THF hydrate grown without any additives at $\Delta T = 3.4$ K. Pipette end is approximately 2 mm across.

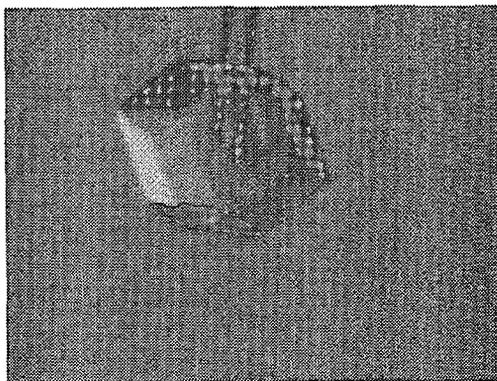


Figure 3 Dodecahedral s I {110} crystal of EO hydrate grown without any additives at $\Delta T = 0.5$ K. Pipette end is approximately 0.2 mm across.

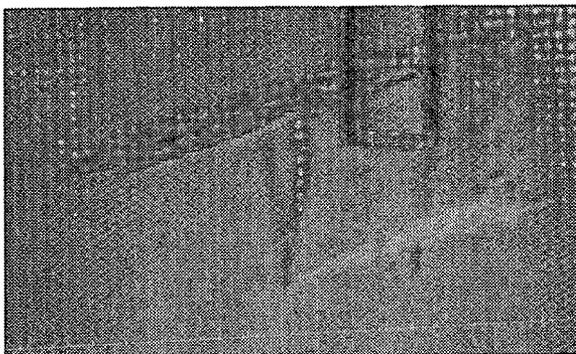


Figure 4 THF hydrate crystal growing in solution with 0.25 wt% VC-713 at $\Delta T=2$ K. Original crystal outline is seen, with the induced 2-d plates sprouting from it. Pipette end is approximately 2 mm across.

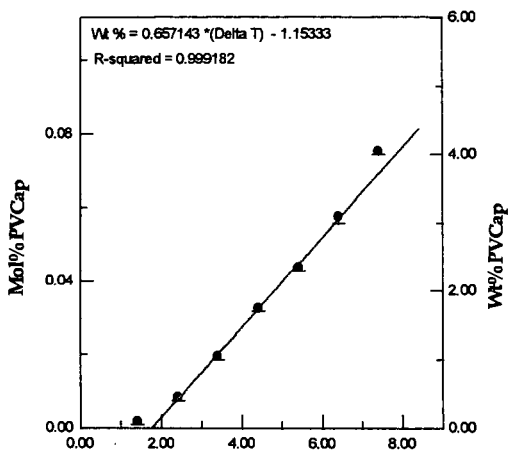


Figure 5 Complete inhibition and its dependence on supercooling. ΔT vs. concentration of inhibitor shows minimum concentration required to have complete inhibition of crystal growth. THF hydrates, sll. The inhibitor is a PVCap.

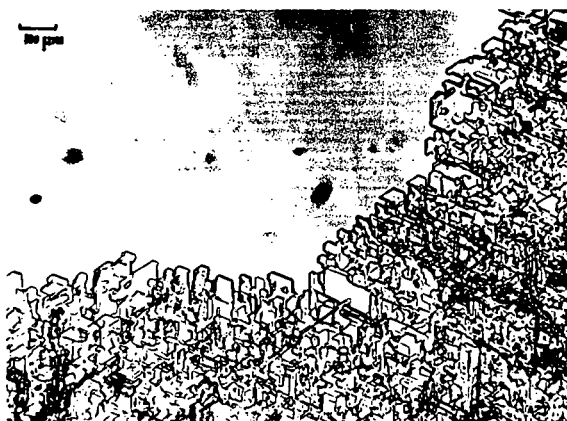


Figure 6 EO sI crystal grown in capillary at $\Delta T=0.5$ K. Intermediate concentration of inhibitor between unaffected and highly branched crystal, 0.08 wt % PVCap. Note preservation of crystallographic orientation throughout.

NEUTRON DIFFRACTION MEASUREMENTS OF THE NUCLEATION AND GROWTH MECHANISMS OF METHANE HYDRATE.

C.A. Koh[†], A.K. Soper[‡], R.E. Westacott[†], R.P. Wisbey[†], X.Wu[†], W. Zhang[†], and J.L. Savidge^{††}

[†] Chemistry Department, King's College, London, Strand, London WC2R 2LS, UK

[‡] ISIS, Rutherford-Appleton Laboratory, Chilton, Didcot, Oxon, OX11 0QX, UK

^{††} Gas Research Institute, West Bryn Mawr Drive, Chicago, Illinois, IL 60631, USA

Abstract

In this paper we present the results of our *in-situ* x-ray and neutron diffraction experiments during the formation of gas hydrates under industry operating conditions. We have performed energy dispersive x-ray diffraction to investigate the crystalline nature of species formed during the hydrate formation process. These experiments have been performed on carbon dioxide and propane hydrate. We show that Bragg peaks, indicating crystal structures, appear during the formation process. Some of these peaks appear in the final hydrate diffraction pattern and others do not. However, in the intermediate stages there is a lot of amorphous structure which could not be interpreted. In an effort to understand this part of the formation process we have performed neutron diffraction experiments on the Small Angle Neutron Diffraction for Amorphous and Liquid Samples (SANDALS) instrument at the Rutherford Appleton Laboratory. This instrument is designed to look at short range structure and provides information on the water structure around the guest molecules in the liquid phase. We present examples of the solvation sphere around methane molecules during the formation of methane hydrate, together with the average size and variance of the coordination sphere

Introduction

A substantial body of information is now available on the equilibrium properties of clathrate hydrates [1-5]. This data has been collected over several decades during which it has been used to support the development of fundamental models to explain chemical and engineering aspects of gas hydrate knowledge [6]. However, these properties and the information currently available fail to identify the mechanisms through which gas hydrates nucleate, grow or decompose, and in some cases fail to accurately determine the thermodynamic properties. Hydrate research has recently concentrated on the kinetics of gas hydrate formation. The methods for the prevention of hydrate formation have also concentrated on kinetic control rather than thermodynamic control.

The work described in this paper uses x-ray and neutron diffraction to investigate the structure in liquid water before and during hydrate formation. We have used the Energy Dispersive X-Ray Diffraction (EDXD) instrument at the Daresbury Laboratory to monitor the formation and decomposition of gas hydrates. We have also used the SANDALS (Small Angle Neutron Diffraction of Amorphous and Liquid Samples) at the Rutherford-Appleton Laboratory to monitor structure in the liquid phase before and during hydrate growth.

Methodology

Both types of experiment have been conducted in specially designed high pressure cells. Temperature, pressure and composition were selected and controlled throughout the experiments. The experiments were conducted *in-situ*, such that gas consumed during hydrate formation is replaced by gas from the cylinder and the pressure maintained.

The x-ray diffraction experiments were carried out over a 250 to 300 K temperature range and 0.1 to 3.5 MPa pressure range [7,8]. The detector angle was fixed at 5.042°. *In-situ* experiments were conducted for carbon dioxide/water and propane/water systems. Diffraction patterns were recorded every 200 second throughout the experiments. Data was collected as a series of intensity vs. energy spectra recorded with time throughout the experiments.

The neutron diffraction experiments on the methane/water system were carried out at constant pressure (2100 psi) and the temperature varied using a ramping procedure. Two scattering patterns were recorded at each temperature. The first stage of the experiment was carried out at a temperature in the water/gas region of the phase diagram (291 K). The scattering pattern was recorded over a 30 minute period. The temperature was reduced to a point within the hydrate region of the phase diagram (283 K). Further scattering patterns were obtained. The temperature was further reduced to 277 K and subsequently reduced to 263 K were the complete sample was frozen. Any ice obtained was melted by reheating to 277 K, where the final scattering patterns were obtained.

Spherical Harmonic Analyses were performed to obtain detailed views of the local intermolecular orientational correlation function [9-11]. Reverse Monte Carlo (RMC)

simulations were performed on one scattering pattern at each of the four temperature set points (291 K, 283 K, 277 K (cooling) and 277 K (heating)). The original simulation cell contained 12 methane molecules and 1500 water molecules arranged in a random configuration. The RMC simulation were carried out over 5 million trials, using an empirical water model. The results for the RMC simulations were deemed to be more realistic than our previous results using a Spherical Harmonic Reconstruction [9-11].

Results

The EDXD experiments lead to some interesting preliminary results. In figure 1, we show the diffraction patterns taken during an experiment. At time zero, the diffraction pattern indicates an amorphous sample, *i.e.* the liquid and gas mixture. As the experiment progresses, sharp peaks appear in the diffraction pattern. These peaks are due to Bragg reflections from a crystalline material. The final pattern is comparable with the diffraction pattern of the complete hydrate structure. That is, the calculated unit cell length is in agreement with literature values and the indexed peaks correspond to Bragg reflections obtained from the single crystal diffraction patterns.

The intermediate stages of this experiment are more difficult to interpret (see figure 2). These diffraction patterns contain a mixture of amorphous and crystalline species. At present, we cannot determine whether Bragg peaks in these intermediate stages which do not appear in the the final hydrate are due to a preferred orientation effect or a crystalline intermediate, which may or may not exist in some form in the product. Methods for interpreting these intermediate stages are currently under investigation.

The EDXD experiments are primarily designed to look at definite crystal structures, as the x-rays are diffracted by planes of electron density in the crystal. Neutrons, on the otherhand, are diffracted by atomic nuclei and therefore provides the possibility of investigating short-range order in liquids. The data shown here were subjected to a spherical harmonic analysis to assess the degree of orientational correlation of water around the methane. The first term in this series expansion of the data is simply the centres correlation function, methane carbon to water oxygen. This is shown in Figure 3 for the four cases. A pronounced co-ordination sphere is found in all instances, but changes quite abruptly for case (4) when a significant amount of methane hydrate is formed. It can be seen from cases (1) - (3), the co-ordination sphere peaks at an average distance of about 3.6 Å for case (1) and then gradually moves to larger radius values as the water/methane system is pushed towards the formation of hydrate by decreasing of temperature. The fits that were obtained are shown in figures 4 and 5.

The RMC simulations aim to reproduce the total corrected scattering pattern of the sample. In figure 3, we show the $\text{CH}_4\text{-O}$ pair correlation function obtained from the scattering patterns obtained at each of the four temperatures described above. The changing correlation function from (a) to (d) indicates an increase in the average number of water molecules in the co-ordination sphere around methane. This is taken from the area under the first peak in the pair correlation function in each case. The position of the peak also indicates that the co-ordination sphere contracts in radius as the experiment progresses. These distances have been used to extract examples of the co-ordination spheres from the final RMC structures. The regions extracted from these structures give some indication of the water structure around the methane molecules during each stage of the experiment. Firstly, we should point out that the number of water molecules within the required distance of the methane molecules is not the same for each methane at each stage of the experiment. The area under the first peak in the pair correlation function indicates the average number of water molecules in the first co-ordination sphere. In Table 1 we present the average and variance of the number of water molecules in the co-ordination spheres for each stage of the experiment. It is interesting to note that there are distorted ring tetramers, pentamers and hexamers in these structures. It is noticeable that the average number of water molecules in the co-ordination spheres increases from part (a) to part (d). This is a consequence of hydrate formation where the expected average number of water molecules in the co-ordination sphere is 23 assuming full conversion to hydrate.

Conclusions

We have demonstrated that the use of energy dispersive x-ray and small angle neutron diffraction techniques can provide complementary information on the formation of natural gas clathrate hydrates.

Acknowledgements

The authors would like to acknowledge the management and financial support of the GRI and funding from the Rutherford-Appleton Laboratory, ISIS Facility. Thanks are also due to C.C. Tang and A. Neild at the Daresbury Laboratory.

References

1. Van der Waals, J. H. & J. C. Platteeuw. *Adv. Chem. Phys.* **2**, 1, 1959
2. Makogan, Y. F. *Hydrates of natural gases*. Translated from Russian by W. J. Cieslesicz. Penn Well Books. Tulsa, Oklahoma, 1981.
3. Internl Conf. Natural Gas Hydrates, Toulouse, 1996.
4. Bishnoi, P. R., V. Natarajan & N. Kalogerakis. *Annals of the New York Academy of Sciences*. **715**. 311-321, 1994.
5. Bishnoi, P. R. & P. D. Dholabhai. *Fluid phase equilibria*. **83**. 455, 462, 1993.
6. *Annals of the New York Academy of Sciences*. **715**. 24-28, 1994.
7. C.A. Koh, J.L. Savidge, C.C. Tang, *J. Phys. Chem.* **100**, 6412-6414, 1996.
8. C.C. Tang, C.A. Koh, A.A. Neild, R.J. Cernick, R.E. Motie, R.I. Nooney, J. *Synchrotron Rad.* **3**, 220-224, 1996.
9. Finney, J. L. & A. K. Soper. *Chemical Society Review*. **23**, 1, 1994
10. Soper, A. K. 1993. *Physical Review E*, **47**, 2598, 1993.
11. Soper, A. K. *J Chem Phys* **101**, 6888, 1994.

Figure 1:
x-ray diffractogram for
carbon dioxide hydrate.

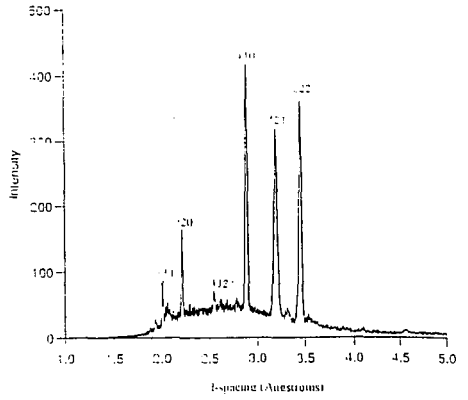


Figure 2:
x-ray diffractograms for
carbon dioxide hydrate growth.

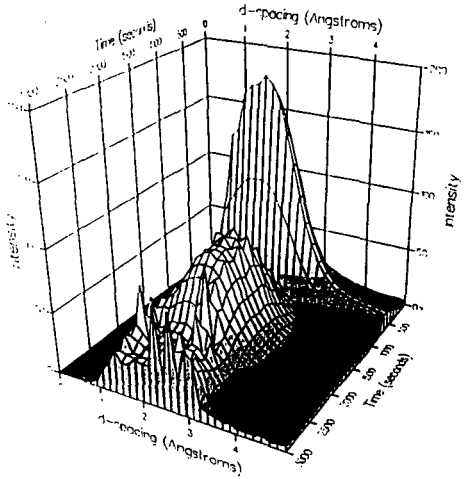
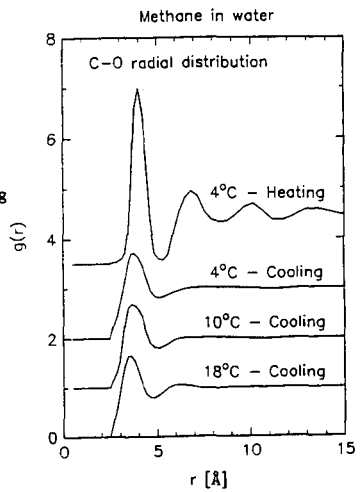


Figure 3:
radial distribution functions for
methane carbon and water oxygen during
methane hydrate growth.

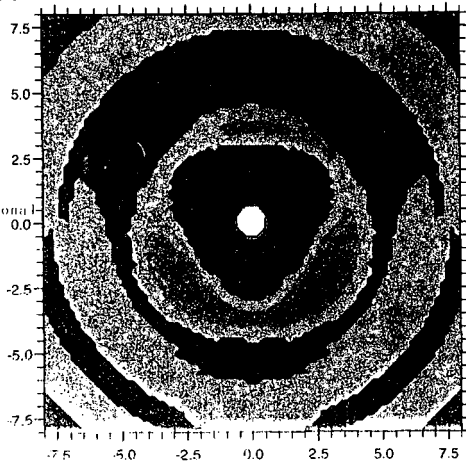
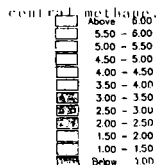


nvary = 4

y[A] koh3shmap1

Plot Date: 19-FEB-96 09:56

Figure 4 orientational diagram for H atoms of water around a central methane.

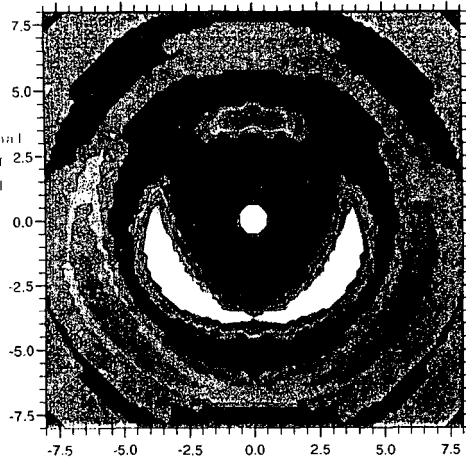
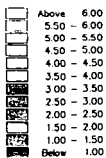


nvary = 4

y[A] koh4shmap1

Plot Date: 19-FEB-96 09:56

Figure 5 orientational diagram for H atoms of water around a central methane.



Equilibrium Properties and Kinetics of Methane and Carbon Dioxide Gas Hydrate Formation/Dissociation

Takeshi Komai, Yoshitaka Yamamoto and Sanshiro Ikegami
National Institute for Resources and Environment, MITI, Japan
16-3, Onogawa, Tsukuba, Ibaraki, 305 Japan
E-mail:koma@nire.go.jp

Keywords: Gas Hydrate, Methane Hydrate, Phase Equilibria, Formation and Dissociation

INTRODUCTION

Large quantities of gas hydrates, clathrate compounds of water and gases formed under high pressure and low temperature, are found in marine sediments and in cold regions. To produce large amount of methane gas from the reservoir with a reasonable way, it is necessary to obtain fundamentals on the mechanism of formation and dissociation and the properties under the practical situations, including phase equilibria and kinetics of gas hydrates. In addition, we have proposed the displacing method of gas hydrates, so that methane gas is extracted from the reservoir by displacing methane with carbon dioxide in molecular level. The main purposes of this research are to acquire the further understanding for the mechanism of hydrate formation/dissociation, and also to accumulate engineering data for completing the original concept of displacing method. We have carried out an experiment on the formation and dissociation of methane and carbon dioxide, using an apparatus consisting of extremely high pressure vessel and observation windows. This paper presents the experimental results on the properties of gas hydrates formation and dissociation under the condition of three phase equilibrium, and some discussion on kinetics and the mechanism of gas hydrate formation.

EXPERIMENTAL

The experimental apparatus, in which the formation and dissociation of gas hydrate could be observed, was designed and manufactured, so that the several conditions of pressure, temperature and concentration of gases could be precisely controlled. Fig.1 illustrates the schematic diagram of the apparatus and the measuring system of the experiment. The pressure cell (1), made of stainless steel and with 90 ml in internal volume, can be used under the pressure condition of up to 40 MPa. It contains three glass windows (2) for observation, a magnetic type mixing equipment (3), and some nozzles (4) for introducing gas and liquid component. The pressure cell is installed within a constant temperature bath (5) filled with cooling agent of ethylene glycol, where the temperature can be controlled with the accuracy of ± 0.2 °C. Gas and liquid fluids are introduced into the cell using a high pressure pump (6) and a fluid supplier system (7), and then are adjusted so that the pressure would be kept constant or free to change by means of two cylinder type controllers (8). The accuracy of controlled pressure is designed to be ± 0.05 MPa. Four transducer for detecting and controlling the pressures are equipped, and five thermocouples are installed for measuring the temperatures inside the cell as shown in Fig.1. The observation system including a optical fiber borescope (9) and a CCD camera (10) can be utilized for this apparatus.

The procedure of the experiment on the three phase equilibrium of gas hydrate are described in the following. First, a quantity of pure water is supplied by the high pressure pump into the pressure cell, and other portion of the volume is filled with pressurized gas component by the fluid supplier system. The quantities can be calculated as equivalent volume portions needed for hydrate structure. The internal pressure can be adjusted, using both the cylinder units in liquid phase and the supplier system in gas phase. The formation of gas hydrate is observed during the temperature of whole system going down, while the pressure is no longer controlled at this situation. The accumulation of hydrate would complete for about a couple of hours, after which the temperature is controlled to go up with the constant rate for getting the equilibrium data of dissociation. The optical cell and the spectrometric system are equipped at the glass window for detecting the nucleation and the change of liquid phase structure. A lot of experimental data, such as temperatures, pressures and gas concentrations, and other experimental conditions, are measured and analyzed using the data acquisition system.

RESULTS AND DISCUSSION

The solubility of gases and gas transport into liquid phase are important factors to promote the formation of gas hydrates in the three phase equilibrium condition. In this experiment, two types of mixing and bubbling operations were adopted for the promotion of nucleation. Fig.2 shows photographic figures for the formation of methane hydrate, observed through the glass window. These results were obtained under the same condition as the pressure was approximately 10 MPa and the temperature was 4.0 to 6.0 °C. As shown in the left figure, a lot of fine fragments of

methane hydrate were formed around the mixing blade and were accumulated in the liquid phase. On the contrary, as shown in the right figure, a lot of gas bubbles from the nozzle turned into solid phase droplets of methane hydrate at the interface of gas and liquid phase. The following experimental results are mainly related to the mixing operation, because it enables the equilibrium properties to become more favorable and reproductive. For keeping sufficient saturation or dissolved condition of gases into liquid phase, each experiment requires previous mixing operation for 30 minutes and enough mixing speed of no lower than 170 rpm.

Plenty of experiments using the gas hydrate formation apparatus have been conducted under the conditions, such as gas component, initial pressure and temperature, and restating hysteresis situation. Fig.3 shows the trend curves for temperature and pressure, obtained using the gas component of CH_4 (100%). TEMP1 represents the temperature measured by No.1 thermocouple at the center of the cell, and TEMP2 the controlled one outside the cell. PRES means the pressure of liquid phase inside the cell. This figure shows that the formation of gas hydrates eventually started during the process of temperature decreasing, because slight increases of temperature appeared after the nucleation point due to the heat of formation. The rapid decrease of pressure was observed around the formation point, while the pressure gradually decreased as the temperature became lower due to the change of solubility. On the other hand, the dissociation of gas hydrate was observed during the process of temperature increasing, from which the increase of temperature started to decline. Fig.4 shows the trend curve of differential temperature measured by No.1 and No.5 thermocouples as a heat balance in the experiment. The first peak on the curve indicates the exothermic heat of formation, and the last one the endothermic heat of dissociation. According to these relations and the observation, critical temperatures and pressures necessary for gas hydrate formation and dissociation can be determined as in Table 1. These results include the properties for the three phase equilibrium. Compared with data in experiments No.4 and No.9 for CO_2 and CH_4 hydrate, the critical temperatures of CH_4 hydrate formation and dissociation are much higher than those of CO_2 hydrate. Further, it is found that the critical temperatures of formation and dissociation increase as the initial pressures become higher in both cases of CO_2 and CH_4 hydrates.

Fig.5 shows the three phase equilibrium relation obtained through the series of experiment for CO_2 and CH_4 hydrate. Upper two lines are the formation and dissociation equilibrium curves for CH_4 gas hydrate, the relation between critical temperatures T and pressures P, and lower lines for CO_2 gas hydrate. In other words, gas hydrate can be present as solid phase with gas and liquid components at higher position from curves for formation, and it no longer exists at lower position from curves for dissociation. From the results it is clear that the relation between P and T is approximately linear in semi-log plotting, and that the critical pressures of CH_4 are relatively higher than those of CO_2 assuming the same temperature condition. This suggests that the formation of CH_4 hydrate requires much higher potential or activation energy rather than in the case of CO_2 hydrate. In addition, it is found that the equilibrium curves for the formation of hydrates are placed at upper position compared with those for the dissociation. Further, the equilibrium data measured in case of dissociation agree well with estimated values using theoretical methods of kinetics, but those in case of formation largely differ from the theoretical values. These large differences may include interesting phenomena and fundamentals on the mechanism of gas hydrate formation. Thus, further experiments were carried out on the behavior of history and hysteresis observed the process of formation and dissociation of gas hydrates.

Fig.6 illustrates the history curve of P and T obtained in the experiment No.39 for CH_4 hydrate. The formation process proceeds on the oscillated curve between A and D, and the dissociation process on the curve between E and F. The differences of temperature and pressure between formation and dissociation equilibria are approximately 3.5 °C and 0.5 MPa, respectively. The history of P and T is usually regarded to be the super cooling effect in the process of formation. The temperature differences obtained by the experiment using CO_2 were quite smaller than that in case of CH_4 . In addition, the super cooling effect clearly appeared in the case that the gas component was introduced by the way of bubbling. These results suggest that the super cooling effect in the history behavior might be largely related to the interface conditions, the way of gas introduction, and the component of gas and liquid.

Fig.7 shows the hysteresis curves for demonstrating the effect of restarting situations, obtained by continuous three experimental runs in the same conditions. The second and third runs were restarted immediately after completing the previous run. In the first run of experiment, the temperature of initiating formation was 15.2 °C at the pressure of 17.5 MPa. However, the formation temperature was shifted to 16.6 °C in the second run, and up to 16.8 °C in the third run. This means that the formation temperatures increase in case of restarting situations, so that they approach the dissociation temperatures or the theoretical temperature for three phase equilibrium. Another experimental run showed that the formation temperature of second run shifted by 2.5 to 3 °C compared with that of the first run, but that of third run recovered to the level of first run if the liquid with dissolved gas was left as the final condition of second run for 12 hours. These results

may suggest that the hysteresis behavior for gas hydrate formation largely depends on the presence of cluster structure in liquid phase, the promotion process of nucleation, and the saturation or dissolved condition of gases into liquid phase.

CONCLUSIONS

Experimental studies on the properties of three phase equilibrium and the process of formation and dissociation of gas hydrates have been carried out, using the specially designed experimental apparatus. As a result, it was found that measured equilibrium data in case of dissociation agree well with estimated values using theoretical methods, but those in case of formation largely depend on the interface conditions, the way of gas introduction, the structure of liquid phase, and the history and hysteresis process of hydrate formation. Thermodynamics properties of gas hydrates were also discussed on the basis of temperature and pressure data in formation and dissociation of gas hydrate. In order to make clear the effects of liquid structure and interface condition on the detail process of formation of gas hydrates, further experimental and theoretical approaches are necessary on the mechanism of nucleation and cluster structure.

ACKNOWLEDGMENT

The authors gratefully acknowledge Dr. T. Saito, Mr. F. Kiyono, Dr. R. Nagaosa and Dr. H. Nada in NIRE for their great assistance in developing the original concept of experimental method and the theoretical analysis of gas hydrates, and thank the New Energy and Industrial Technology Development Organization(NEDO) for the financial assistance in conducting the research project.

REFERENCES

- Burrus, R.C.: Crystallization of Natural Gas Hydrate: Video Microscopy and Mass Balance on Nucleation and Growth, Proc. Conf. Drilling Hydrates in Offshore, Japan, 182, (1995)
 Holder, G.D., Zett, S.P. and Pradhan, N.: Phase Behavior in Systems Containing Clathrate Hydrates: A Review, Reviews in Chemical Engineering, 5, 1-70, (1988)
 Uchida, T., Hondoh, T. and Mae, S.: Effects of Temperature and Pressure on the Transformation Rate from Air Bubbles to Hydrate Crystals, Ann. Glaciol., 20, 143-147, (1994)
 Matsumoto, R.: Feasibility of Methane Hydrate under the Sea as a Natural Gas Resource, J. Jap. Assoc. Petro. Tech., 60(2), 147-156, (1995)

Table 1 Experimental results of the formation and dissociation equilibrium data.

Exp.No.	Initial Pressure (MPa)	Formation Equilibrium		Dissociation Equilibrium			
		Pressure (MPa)	Temperature (°C)	Pressure (MPa)	Temperature (°C)		
EXMH09	5.80	5.4	4.4	4.2	5.0	CH ₄	
EXMH08	8.05	7.1	5.8	6.8	10.6		
EXMH24	10.20	9.4	8.1	8.6	11.7		
EXMH11	10.50	9.7	8.8	8.6	12.0		
EXMH07	11.90	10.8	8.8	9.9	13.2		
EXMH06	13.38	12.5	11.0	11.6	14.1		
EXMH29	17.97	17.0	12.9	16.8	17.1		
EXMH30	20.00	18.8	14.2	18.6	18.0		
EXMH12	3.1	2.4	4.0	1.9	5.0		CO ₂
EXMH13	4.0	3.4	6.0	2.6	6.9		
EXMH04	4.9	4.2	9.4	4.1	9.9		



Fig.2 The observation of methane gas hydrate formation.
 (Left figure) In case of mixing operation. (Right figure) In case of bubbling operation.
 P=10.0 MPa, T=8.0 °C P=10.0 MPa, T=4.0 °C

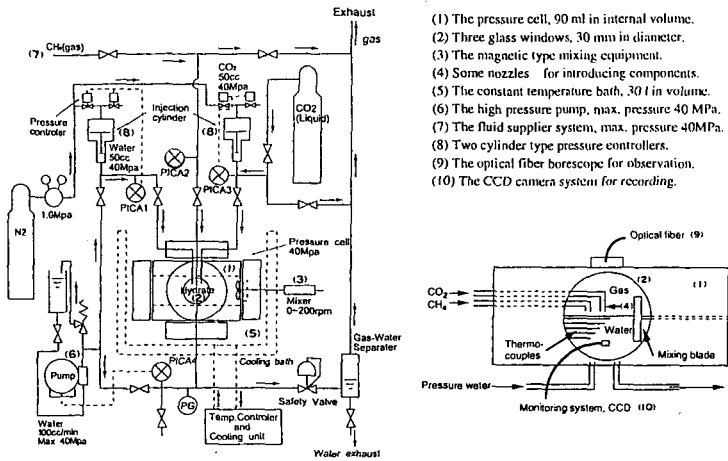


Fig.1 The schematic diagram of the experimental apparatus and the measuring system. (Upper figure) Main system. (Lower figure) Pressure cell and measuring sensors.

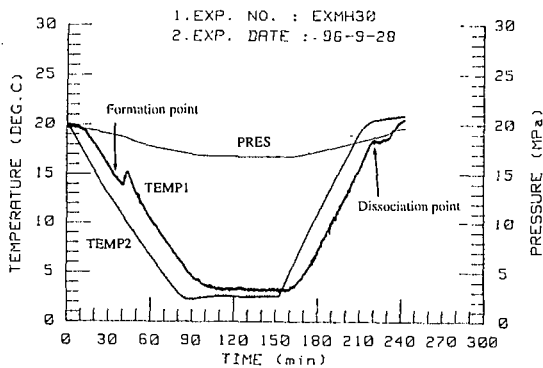


Fig.3 The trend curves of pressure and temperature obtained in the experiment for methane gas hydrate formation and dissociation.

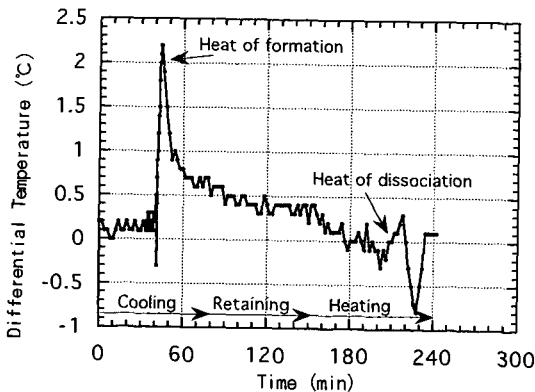


Fig.4 The change in differential temperature, and heat valance of gas hydrate formation and dissociation.

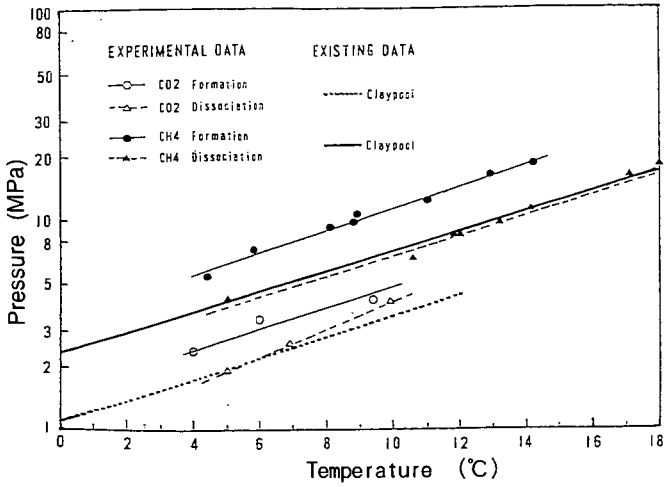


Fig.5 The relations between pressure and temperature in three phase equilibrium condition for CO₂ and CH₄ gas hydrates.

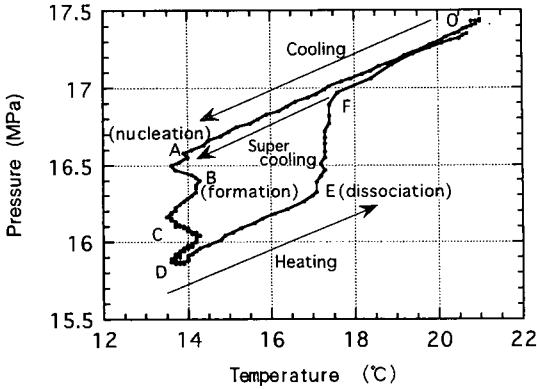


Fig.6 The history curve of pressure and temperature in the process of gas hydrate formation and dissociation.

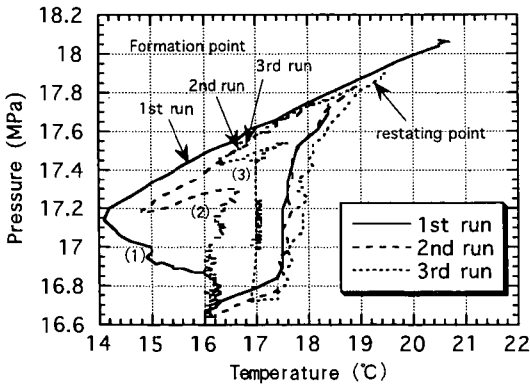


Fig.7 The hysteresis curves of pressure and temperature in the process of gas hydrate formation and dissociation.

STUDY ON FORMATION / DISSOCIATION MECHANISM OF GAS HYDRATES AND RECOVERY OF PURE HYDRATE CRYSTAL USING HIGH PRESSURE CRYSTALLIZATION TECHNIQUE

Yoshitaka Yamamoto*, Takeshi Komai*, Sanshiro Ikegami* and Akihiro Wakisaka**

*National Institute for Resources and Environment, 16-3, Onogawa, Tsukuba-shi, Ibaraki 305, Japan

**National Institute for Advanced Interdisciplinary Research, 1-1-4, Higashi, Tsukuba-shi, Ibaraki 305, Japan

Keywords: gas hydrate, high pressure crystallization, separation of pure crystal

INTRODUCTION

Gas hydrate is the species that guest molecules (CO_2 , CH_4 etc.) are included in the cage of hydrogen-bonding network of water molecules. Recently, it was found that there are great quantity of methane hydrate in the sediment below the sea bottom. Since Japan has no natural energy resources, we pay much attention to the natural gas hydrates as one of the hopeful energy source for the future. To establish elemental technologies for mining methane hydrate, we started fundamental and also practical study of gas hydrate.

The observation of real crystallization process is indispensable to study formation / dissociation mechanism precisely. On the other hand, it is important for establish methane hydrate recovering method to get pure hydrate crystals and measure accurate physical and chemical property of them.

To achieve these objects, we are constructing high pressure crystallization apparatus with optical window. In this presentation, we will report the resent result of hydrate crystal formation and recovery experiment with this apparatus.

As a fundamental research on the gas hydrate formation, we are interested in molecular clustering structure of aqueous solution. As for the interaction of magic numbered water cluster, $\text{H}^+(\text{H}_2\text{O})_{21}$, which has dodecahedral structure, with organic molecules, it was observed that tetrahydrofuran (THF) did not dissociate the hydrogen-bonding network of $\text{H}^+(\text{H}_2\text{O})_{21}$ cluster; however, methanol dissociated it. In the mass spectra of clusters generated from THF-water and methanol-water mixtures, $\text{H}^+(\text{H}_2\text{O})_{21}$ clusters contact with THF, $\text{H}^+(\text{H}_2\text{O})_{21}(\text{THF})_n$; $n=1,2,3,\dots$, and $\text{H}^+(\text{H}_2\text{O})_{21}$ clusters substituted by methanol, $\text{H}^+(\text{H}_2\text{O})_{21-n}(\text{CH}_3\text{OH})_n$; $n=1,2,3,\dots$, were observed, respectively¹⁾. Such molecular structures in aqueous solutions seem to be related with the nucleation mechanism of hydrate. That is, THF makes hydrates, but methanol works as gas hydrate inhibitor. We also intend to carry out methane hydrate formation experiment with any additives such as THF or CH_3OH , etc., and discuss nucleation mechanism of gas hydrate with the clustering structure of water molecules which were observed by cluster beam mass spectrometer.

EXPERIMENTAL

High pressure crystallization apparatus with optical vessel

Fig.1 shows the schematic diagram of the high pressure crystallization apparatus with optical vessel. Photographs of this apparatus and main vessel are also shown in Fig.2 and Fig.3 respectively. As shown in Fig.1, main vessel (C1) and sub vessel (C2) are piston-cylinder type high pressure vessels. Inner diameter and volume of these vessels are 15 mm and 20 ml respectively. The main vessel has a pair of sapphire windows to observe crystallization process on both side and stainless filter to separate liquid phase from solid phase on the bottom. Main vessel is soaked in a silicon oil bath [Temperature control range ; $-30^\circ\text{C} \sim +130^\circ\text{C}$]. This oil bath also has optical windows and crystallization process can be observed through these windows with microscope or multi channel spectrophotometer. Compression of vessels is carried out by using oil pressure equipment (19). Main vessel is connected with gas supplying system, which can supply host gases continuously under high pressure (max. under 400kg/cm^2). Control of gas flow rate is carried out by flow controller for high flow rate (3) [$0.5 \sim 5\text{N l/min}$] and low flow rate (4) [$0.01 \sim 0.1\text{N l/min}$]. Maximum pressure of crystallization unit is 4000kg/cm^2 .

Crystallization and separation procedure

Sample mixtures (pure water and THF, pure water and CH_4 etc.) are injected into the main vessel (C1) and compressed to form hydrate crystals. The excess liquid phase is removed from the crystals in the main vessel (C1) to the sub vessel (C2), keeping the pressure in the main vessel constant and slightly decreasing the pressure in the sub vessel. After separation process is finished, stop valve between two vessels (VH1) is shut and crystals are recovered.

To confirm performance of the apparatus, crystallization and separation of pure indole from indole/isoquinoline mixture was carried out. Then, we started hydrate formation experiment of THF/water system and CH_4 /water system. In case of methane/water system, to prevent dissociation of methane hydrate, the main vessel is cooled to about 80°C by dry ice/methanol bath before the decreasing of main vessel pressure and taking out of hydrate crystal.

RESULT AND DISCUSSION

Formation and separation of high purity indole crystal by high pressure crystallization method

Fig.4 shows the typical operation diagram of high pressure crystallization. Sample solution is indole-isoquinoline mixture (80mol%-indole). Separation process is as follows.

- 1) Inject sample mixture into main vessel (C1) and compressed to $1000\text{kg}/\text{cm}^2$ step wise under 50°C . In this process, pure indole crystal is formed and impurities concentrated into liquid phase
- 2) Hold the pressure of main vessel at $1000\text{kg}/\text{cm}^2$ until solid-liquid phase equilibrium is achieved.
- 3) Open the stop bulb (VH1) between main and sub vessel and remove liquid phase from the crystal. In this process, pressure in the main vessel is constant ($1000\text{kg}/\text{cm}^2$) all the way. However, as shown in Fig.4, after almost stop the piston displacement, the pressure which is indicated in pressure gauge (PH1) gradually decreased and finally reach almost atmospheric pressure. This means that almost all the liquid is removed and pressure in the main vessel can not be transmitted to pressure gauge (PH1). At that time, crystal in main vessel is squeezed under $1000\text{kg}/\text{cm}^2$ and remained liquid is perfectly separated.
- 4) Pressure of main vessel is decreased to atmospheric pressure and separated crystal is recovered.

The purity of recovered solid was measured by gas chromatography. Indole concentration of that crystal was 98mol% and it was known that high purity crystal can be separated by this high pressure crystallization apparatus.

Formation and separation of THF hydrate and methane hydrate

Generally, autoclave type high pressure vessels were used for hydrate formation experiment and it is said that stirring of the vessel is important to form hydrate crystal. However, it is difficult to stir sample in main vessel (C1) in our apparatus. As mechanical stirring is not performed at natural hydrate formation process, stirring seems to be not always necessary. To confirm if methane hydrate formation is occurred without stirring or not, we slowly injected methane gas into an autoclave type optical vessel which is filled with pure water. (details will be described in another presentation of our group in this meeting by Dr.Komai.) As a result, film like hydrate crystal was formed almost instantly with rising of methane gas bubble under the condition of 2°C , $100\text{kg}/\text{cm}^2$. Though it seemed to need fairly long time to make methane gas included in the hydrate film into crystal perfectly, it was confirmed that nucleation of hydrate can be occurred without mechanical stirring. According to this result, we tried hydrate formation experiment with the high pressure crystallization apparatus.

First, THF/water (THF : H_2O = 1 : 25 molar ratio) mixture was injected into the apparatus and examined efficiency of hydrate formation and separation. Temperature and separation pressure are 4°C and $200\text{kg}/\text{cm}^2$. After separation of excess water, main vessel was cooled to -10°C and THF hydrate was recovered. From the pressure which is indicated on pressure gauge (PH1), we confirmed that hydrate and excess water was perfectly separated as same as indole-isoquinoline mixture. Photograph of recovered THF hydrate is shown in Fig.5.

Next, methane hydrate formation and separation experiment was performed with this apparatus. 6ml of pure water and 4 ml of methane gas was injected into main vessel, and hydrate was formed under

4°C, 400kg/cm². After separation of methane hydrate from water phase was finished, hydrate crystal was cooled to about -80°C by methanol/dry ice bath. (Under -80°C, the dissociation pressure of methane hydrate become lower than atmospheric pressure.) Then, pressure of main vessel was decreased to atmospheric pressure and formed crystal was recovered. Photograph of recovered solid is shown in Fig.6. Recovered crystal is flammable white solid and dissolve with discharging babbles. Though It thought to be a methane hydrate, detailed analyses was still not performed and purity of crystal is not confirmed for the moment.

CONCLUSION

We constructed the gas hydrate formation/separation apparatus using high pressure crystallization method and confirmed a formation and recovery of gas hydrate by this equipment. For the present, adjustment of gas supplying unit was not finished perfectly and strict control of crystal formation is not achieved. Also, the system for observation of hydrate crystal formation is under adjustment.

From now on, we try to improve high pressure mass controller in gas supplying unit and structure of optical system and establish the technique for formation of pure hydrate and recover it. With the separated gas hydrate, we are going to measure physical and chemical property of it precisely.

We are also carrying out methane hydrate formation experiment with THF or CH₃OH. we will also make a discussion about influence of these additives to methane hydrate formation with the comparison of the clustering structure of water molecules which was observed by cluster beam mass spectrometer.

ACKNOWLEDGEMENT

This study is financially supported by NEDO (New Energy and Industrial Technology Development Organization).

REFERENCE

1. Yamamoto, Y. and Wakisaka, A., *Proc. Int. Conf. on Natural Gas Hydrate*, Toulouse, June, 1996, 355
2. Yamamoto, Y., Sato, Y., Ebina, T., Yokoyama, Ch., Takahashi, S., Nishiguchi, N. and Tanabe, H., *Nenryou kyokaiishi*, 1991, **70**, 533
3. Yamamoto, Y., Sato, Y., Mito, Y., Tanabe, H., Nishiguchi, N. and Nagaoka, K. *Proc. Int. Symp. on Prep. of Func. Mat.*, 1989, 195
4. Yamamoto, Y., Sato, Y., Ebina, T., Yokoyama, Ch., Takahashi, S., Mito, Y., Tanabe, H., Nishiguchi, N. and Nagaoka, K., *Fuel*, 1991, **70**, 565
5. Yamamoto, Y., Sato, Y. and Wakisaka, A., *J. Chem. Soc., Chem. Commun.*, 1994, 2727
6. Wakisaka, A., Shimizu, Y., Nishi, N., Tokumaru, K. and Sakuragi, H., *J. Chem. Soc., Faraday Trans.*, 1992, **88**, 1129
7. Christiansen, R. L. and E. D. Sloan, Jr., *Proc. Int. Conf. on Natural Gas Hydrate*, N. Y., April, 1994, **19**, 283

- 1: Pressure gauge 2: Flow meter
- 3: Flow controller for high flow rate
- 4: Flow controller for low flow rate
- 5: Stroke gauge 6: Thermocouple
- 7: Pressure gauge 8: Vacuum pump
- 9: Sampling tube 10: Relief valve
- 11: High pressure gas buster
- 12: Pressure control valve
- 13: Constant temperature oil bath
- 14: Optical window 15: Monitor
- 16: Video recorder
- 17: C.C.D camera 18: Microscope
- 19: Oil pressure equipment
- 20: halogen lump

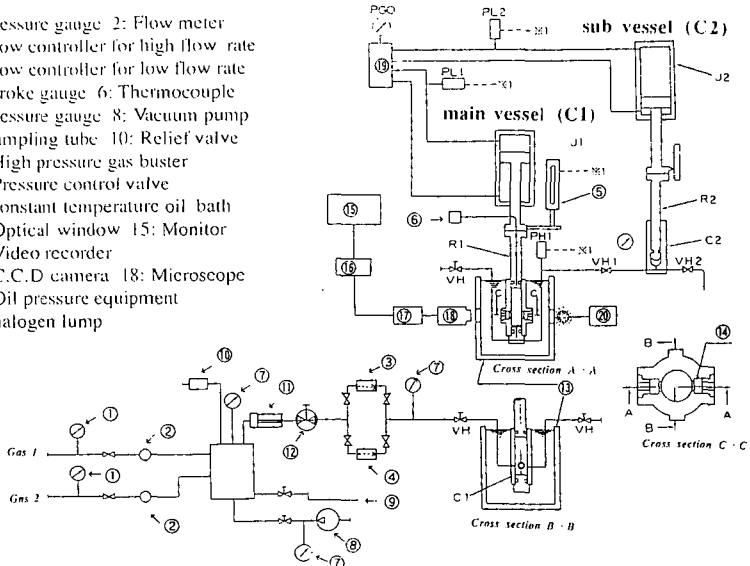


Fig.1 Schematic diagram of the high pressure crystallization apparatus with optical vessel

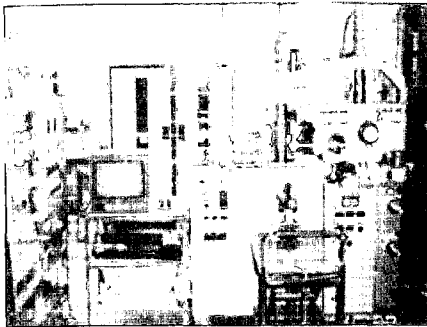


Fig.2 Photograph of the high pressure crystallization apparatus.



Fig.3 Photograph of the main vessel (C1)

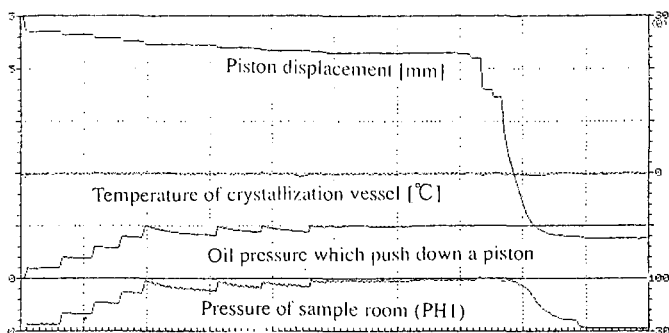


Fig.4 Operation diagram of crystallization and separation of pure indole from indole/isoquinoline mixture using high pressure crystallization technique (Indole concentration is 80mol%, separation temperature = 50°C, separation pressure = 1000kg/cm²)

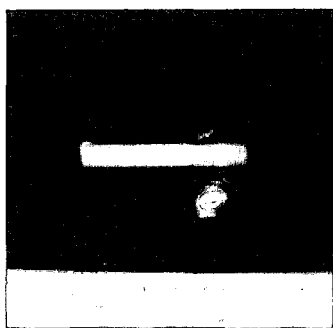


Fig.5 Photograph of recovered THF hydrate (separation temperature=1°C, separation pressure=200kg/cm²)

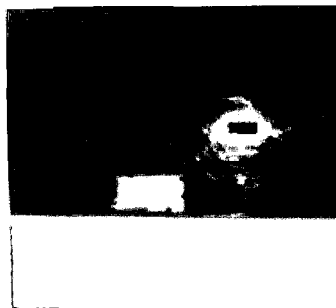


Fig.6 Photograph of recovered CH₄ hydrate (separation temperature=4°C, separation pressure=400kg/cm²)

THE EFFECT OF CO₂ CLATHRATE HYDRATE ON THE OCEAN DISPOSAL OF CO₂: A REVIEW OF DOE-SPONSORED RESEARCH

Robert P. Warzinski, Perry D. Bergman
U.S. Department of Energy, Federal Energy Technology Center, Pittsburgh, PA 15236

Stephen M. Masutani
University of Hawaii, Hawaii Natural Energy Institute, Honolulu, HI 96822

Gerald D. Holder
University of Pittsburgh, School of Engineering, Pittsburgh, PA 15261

Keywords: carbon dioxide, ocean disposal, clathrate hydrate

INTRODUCTION

Deep ocean disposal of CO₂ is an option to mitigate rises in atmospheric levels of CO₂ if other measures are ineffective and the worst global warming scenarios begin to occur. Through its Office of Fossil Energy, the U.S. Department of Energy (DOE) supports research directed at evaluating the feasibility of this option for long-term CO₂ disposal. Two projects, managed at the Federal Energy Technology Center (FETC) in Pittsburgh, Pennsylvania, are being conducted that specifically address the technical issues associated with deep-ocean disposal of CO₂. One of the projects is being conducted at FETC; the other at the University of Hawaii at Manoa (UHM) in Honolulu, Hawaii. The purpose of this paper is to describe the scope of these projects and summarize current experimental and theoretical results.

BACKGROUND

In 1993, a research needs assessment for capture, utilization, and disposal of CO₂ from fossil fuel-fired power plants was prepared for DOE by the Massachusetts Institute of Technology (1). This well-received report concluded that establishing the feasibility of large-scale disposal options should be assigned the highest research priority of all needs identified. Of the large-scale disposal options considered at that time, the principal ones were those using the deep ocean or deep confined aquifers for storage. With respect to ocean disposal, the key research recommendations focused on the impact of the CO₂ clathrate hydrate on the effectiveness of this disposal option.

Depth is a key factor in ocean disposal of CO₂. To avoid premature escape of the CO₂ from surface waters to the atmosphere, injection below a depth of about 500 m would be required. From approximately 500-m to 3000-m ocean depth, undissolved CO₂ would exist as a buoyant liquid. At greater depths, the liquid CO₂ would sink. In the absence of hydrate formation, the minimum depth for effective CO₂ sequestration would be around 700 m. Drops released at this depth would completely dissolve before reaching a depth of 500 m (1).

CO₂ clathrate hydrate (CO₂·nH₂O, 6 < n < 8) is a crystalline compound that can form under temperature and pressure conditions associated with CO₂ disposal in the ocean below a 500-m depth. The hydrate can form either as solid crystalline particles or as a coating on the surface of liquid CO₂ drops. The solid hydrate particles should sink in the ocean, facilitating sequestration; however, thin hydrate shells on liquid CO₂ drops would limit dissolution of the CO₂ and complicate sequestration attempts. During transport to depth and injection, hydrate formation may clog submerged conduits, erode and foul injector nozzles, and negatively impact CO₂ dispersion. The U.S. DOE supports experimental and theoretical research at FETC and at UHM to address these concerns. A small high-pressure viewcell at FETC and a large pressurized tank at UHM are being utilized in the experimental programs. Mathematical modeling of these phenomena is also being performed at both FETC and UHM.

RESEARCH AT FETC

The work at FETC was initiated in 1993. All of the experimental work has been performed in a high-pressure, variable-volume viewcell (HVVC) that has a maximum working volume of about 40 cm³. A description of the HVVC system and basic experimental procedures have been published (2,3). The HVVC system can operate at temperatures down to near 0°C and at pressures up to 69 MPa (10,000 psig). The HVVC system can therefore be used to simulate ocean depths down to 6900 m. This is more than adequate for studying the behavior of CO₂ at the depths currently being considered for unconfined release of CO₂ in the ocean (1000 m to 1500 m) (4).

To enable more accurate prediction of the fate of CO_2 injected into the ocean, experiments at FETC have focused on determining the relative density of the hydrate in water (2,5) and seawater and on the formation of hydrate shells on drops of CO_2 and their effect on drop dissolution (2,6). With respect to the relative density of the hydrate, observations in two-phase systems with water and either gaseous or liquid CO_2 showed that the hydrates which formed at the $\text{CO}_2/\text{H}_2\text{O}$ interface were initially snowlike in appearance and buoyant in the water-rich phase. With time, the hydrates became icelike (transparent) in appearance and sank. Trapped, unconverted CO_2 may have caused the bulk density of the initially formed hydrates to be less than that of the water-rich phase. Eventually, this trapped CO_2 either escaped or was converted to hydrate, causing the density to increase and the appearance to change. In contrast, when formed from dissolved CO_2 , the hydrates were initially icelike in appearance and sank. Buoyant hydrate particles would frustrate sequestration in the ocean by causing the CO_2 to rise to unacceptably shallow depths. On the other hand, sinking hydrate particles would facilitate sequestration by causing the CO_2 to descend to greater depths before dissolution and thus increase its residence time in the ocean.

Some of the above experiments with water and CO_2 have recently been repeated using General Purpose Seawater (GPS) from Ocean Scientific International Ltd. As in the fresh-water experiments, hydrates formed from CO_2 dissolved in the seawater were icelike in appearance and sank in the seawater-rich phase.

Observations of the rate of hydrate shell formation on CO_2 drops in water and seawater have also been performed at FETC. In these experiments, a CO_2 drop is introduced into the viewcell and comes in contact with either existing hydrate particles or the glass or stainless steel parts of the viewcell itself. In all such cases, hydrate shell formation began at the point where the bubble or drop contacted the crystalline hydrate or viewcell, then rapidly spread out along the bubble or drop surface. Others have also reported similar phenomena (7). Specific examples from our experimental work have been previously described (6). The rate of growth of the hydrate shell on CO_2 drops (0.5 cm to 1 cm in diameter) in water has been estimated at 0.5 to 1.0 cm^2/s . Recent observations in seawater gave similar results.

The rate of dissolution of hydrate-covered CO_2 drops has also been studied in water (2) and more recently in seawater. In these experiments, the rate of decrease in drop radius was measured. Rates in the range of 0.0045 to 0.02 cm/h have been observed for hydrate-covered drops. These rates are slower than those obtained by other workers (2). The differences between the results are likely due to dissimilar experimental conditions and equipment. Data from the recent experiments in the viewcell indicate that the rate of shrinkage of CO_2 drops in seawater appears to be slower than in fresh water for drops of similar size under similar conditions. The reason for the slower rate in seawater is the topic of current investigations.

To overcome the limitations of the viewcell and more realistically simulate the environment that a CO_2 drop encounters in the ocean, a high-pressure water tunnel facility has been planned. This device is patterned after a similar apparatus developed by others for the study of methane hydrates (8). A low-pressure model is currently under construction to verify the flow patterns in the proposed test section of the tunnel.

Recent mathematical modeling efforts at FETC have been directed at determining the thickness of the hydrate shell that forms on CO_2 drops under conditions expected for ocean disposal (6). The model was developed to estimate both the thickness of the initially-formed shell and the bounds on the ultimate thicknesses of shells after reaching steady state in saturated and unsaturated environments. The degree of saturation is determined relative to the equilibrium CO_2 concentration at the hydrate equilibrium pressure, C_H , at the temperature of the system. Under anticipated ocean disposal conditions, the system can actually be oversaturated owing to the induction period that often accompanies hydrate formation (6).

The model assumes that the ultimate thickness of the shell is governed by the diffusion of the CO_2 through the hydrate shell and diffusion or convection of dissolved CO_2 away from the hydrate-covered particle. It was demonstrated that a very thin hydrate shell (<0.1 cm) would initially form around drops of injected CO_2 . If injected into unsaturated water, a stable hydrate thickness on the order of 10^2 to 10^4 times the radius of the drop would form. The model therefore implies that the initially formed shell would become thinner in an unsaturated environment. The thinning of the hydrate shell after formation has been experimentally observed in the viewcell experiments and is reflected by changes in both the texture and transparency of

hydrate-covered drops. Initially, the shell has rough texture and is opaque. Within a few minutes the shell becomes smooth and relatively transparent.

For a CO_2 drop injected into saturated water, the model predicts that with time the hydrate shell would thicken, possibly approaching 10^{-1} cm in thickness for growth periods well in excess of 100 hours. Such conditions could occur in the vicinity of the injection. Since the water is saturated with respect to hydrate-forming conditions, the hydrate shell serves only to slow the diffusion of CO_2 and thus limit the formation of additional hydrate from the injected CO_2 . Results for this scenario are shown in Figure 1. The diffusivity values for CO_2 through the hydrate shell, D_H , used in Figure 1 are in the range of values for diffusivities in solids. Experimental determination of this value would be required for validation of this portion of the model.

In water oversaturated with CO_2 relative to C_H , the shell could also thicken by addition to the hydrate layer from the CO_2 dissolved in the water. This mode of growth was the subject of an earlier paper (9). The above model also did not take into consideration the effect of varying salt concentration at the surface of drop as hydrates form. Current modeling efforts at FETC are directed at incorporating this effect.

RESEARCH AT UHM

A 36-month research grant to investigate ocean disposal of CO_2 was awarded by DOE to the University of Hawaii at Manoa in August 1995. The laboratory study is being conducted by the Hawaii Natural Energy Institute of the School of Ocean and Earth Science and Technology. The principal objective of the study is to obtain data on liquid CO_2 discharge jet instability and on drop dispersion, interactions, and dissolution under conditions representative of the deep ocean. These data will be applied to the development and validation of predictive models to perform (ocean) environmental hazard assessments and to devise injection methods that ensure effective containment of the CO_2 from the atmosphere.

Experiments at UHM employ a unique High-Pressure CO_2 Mixing Facility (HCMF), designed specifically to investigate the oceanic CO_2 disposal process. The HCMF comprises a cylindrical pressure vessel, systems to hold and supply liquid CO_2 and chilled (ambient to 0°C) water, and diagnostics and data acquisition equipment. The insulated steel pressure vessel has an I.D. of 0.55 m and is 2.46-m tall. During experiments, it is partially filled with fresh or seawater and pressurized with an inert gas to simulate conditions in the ocean down to depths of approximately 600 m. A photograph of the pressurized test vessel is shown in Figure 2. Numerous viewports provide access for quantitative optical probes and for flow visualization. Details of the construction and operation of the HCMF have been reported (10).

Two types of tests will be conducted using the HCMF: (1) continuous discharging of liquid CO_2 through a variety of orifices over a range of conditions to study effluent breakup and injector performance; and (2) monitoring of single CO_2 droplets or droplet pairs as they dissolve and interact during simulated buoyant rise through the ocean. In the continuous discharge experiments, a non-intrusive, laser scattering diagnostic will be employed to map droplet size distribution spectra, velocity, and number density in the region immediately downstream from the injector. These data on initial CO_2 droplet size distributions and spatial dispersion are needed to model accurately the disposal process. The primary experimental variables include jet velocity, simulated depth of discharge, and injector orifice size and geometry.

In the droplet dissolution experiments, a transparent diffuser will be submerged in the pressure vessel aligned with its vertical axis. Water from the vessel is pumped downward through the diffuser to stabilize in space buoyant liquid CO_2 droplets that have been bled into the diffuser. By this means, the unrestrained rise through the ocean can be simulated in a facility of finite height. Close-up image acquisition and analysis will be employed to document droplet dissolution and interaction phenomena.

In both the continuous discharge and dissolution tests, experiments will be repeated under ambient water conditions that either foster or preclude the formation of the CO_2 clathrate hydrate. As of this writing, facility preparations and diagnostic development are being completed.

Complementary mathematical modeling to date has focused on theoretical analyses of CO_2 jet instabilities and the generation of the dispersed droplet phase. The effects of hydrate formation on these instabilities have been considered (11). Results suggest that if hydrate formation

kinetics proceed more rapidly than the amplification of the jet instability, then breakup may be modified and the dispersed droplet phase size distribution altered. At the extreme, a solid hydrate layer could grow and deposit around the injection orifice, encasing the jet and possibly closing it off. While calculations indicate that hydrate formation effects will be restricted to situations involving relatively large injector orifices (> 1-cm diameter) and low jet velocities (< 6 cm/s), the uncertainty in some parameters used in these calculations, notably the rate constant for hydrate formation, warrant experimental confirmation.

Recently, the DOE-funded experimental research at UHM has attracted international interest. Additional funds have been committed to the project by ABB Management, Ltd. in Switzerland and Statoil (Norway) has offered the use of instrumentation and the professional assistance of research personnel from the University of Bergen. Interest in collaborative studies has also been expressed by Japanese investigators.

SUMMARY

DOE-sponsored research at FETC and UHM is addressing important issues related to the effect of hydrates on the ocean disposal of CO₂. These issues include: 1) the relative density of hydrate particles and how to either preclude hydrate formation or form particles that would sink in the ocean and thus facilitate sequestration efforts; 2) the behavior of hydrates during formation either as particles or as shells around liquid CO₂ drops, and how their formation would impact CO₂ dissolution and jet dynamics; and 3) the dissolution behavior of hydrate-covered CO₂ drops and the fate of these drops in the ocean. Data are being sought to help develop and validate predictive models which can be employed to identify effective sequestration strategies and to evaluate impacts on the marine environment.

DISCLAIMER

Reference in this report to any specific product, process, or service is to facilitate understanding and does not imply its endorsement or favoring by the United States Department of Energy.

REFERENCES

1. A Research Needs Assessment for the Capture, Utilization and Disposal of Carbon Dioxide from Fossil Fuel-Fired Power Plants, DOE Report DOE/ER-30194, July 1993 (available NTIS).
2. Warzinski, R. P.; Cugini, A. V.; Holder, G. D. Proc. Int. Conf. Coal Sci. 1995, 2, 1931-1934.
3. Warzinski, R. P.; Lee, C.-H.; Holder, G. D. J. Supercrit. Fluids 1992, 5, 60-71.
4. Omerod, B.; Angel, M. Ocean Storage of Carbon Dioxide: Workshop 2 - Environmental Impact, IEA Greenhouse Gas R&D Programme Report, June 1996.
5. Holder, G. D.; Cugini, A. V.; Warzinski, R. P. Environ. Sci. Tech. 1995, 29, 276-278.
6. Holder, G. D.; Warzinski, R. P. Prepr. Pap. -Am. Chem. Soc., Div. Fuel Chem. 1996, 41(4), 1452-1457.
7. Burruss as reported by E.D. Sloan, Jr. in International Conference on Natural Gas Hydrates; E.D. Sloan, Jr.; J. Happe; M.A. Hnatow, Eds.; Annals of the New York Academy of Sciences; Vol. 715; p 17.
8. Maini, B. B.; Bishnoi, P. R. Chem. Engng. Sci. 1981, 36, 183-189.
9. Holder, G. D.; Cugini, A. V.; Warzinski, R. P. Environ. Sci. Tech. 1995, 29, 276-278.
10. Masutani, S. M.; Kinoshita, C. M.; Nihous, G. C.; Ho, T.; Vega, L. A. Energy Convers. Mgmt. 1993, 34(9-11), 865-872.
11. Teng, H.; Masutani, S. M.; Kinoshita, C. M.; Nihous, G. C. Prepr. Pap. -Am. Chem. Soc., Div. Fuel Chem. 1996, 41(4), 1447-1451.

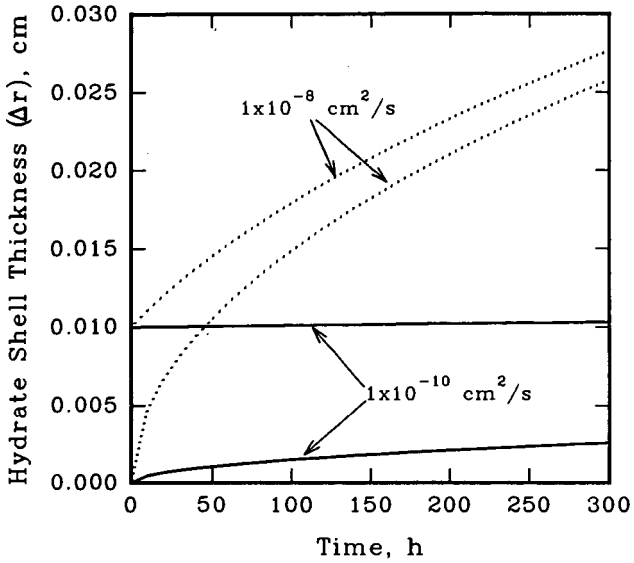


Figure 1. Thickening of the hydrate shell in a saturated reservoir as a function of time and solid-phase diffusivity, D_H (values shown in figure), and the initial thickness of the hydrate shell (indicated at time = 0).

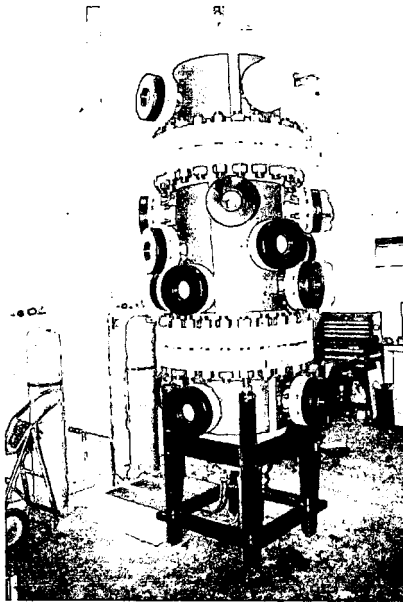


Figure 2. Photograph of the pressurized test vessel used in the High Pressure CO_2 Mixing Facility at the University of Hawaii at Manoa.